THE ROLE OF SKP1 GLYCOSYLATION IN SCF ASSEMBLY AND THE CHARACTERIZATION OF THE INTERACTION OF AN F-BOX PROTEIN AND ITS BINDING PARTNER

by

ANDREW WILLIAM BOLAND

(Under the Direction of Christopher Mark West)

ABSTRACT

Most eukaryotes depend on the SCF (Skp1/cullin-1/F-box protein) family of E3 ubiquitin ligases to regulate its proteome. The SCF binds to specific substrates and poly-ubiquitinates them as a signal for subsequent degradation by the 26S proteasome. The importance of proper regulation of the assembly and activity of this complex is evident in the cancers and other disease states that result from its dysregulation. Here we used *Dictyostelium discoideum* as a model to study how an oxygen dependent post-translational modification can influence Skp1 binding to F-box proteins (FBP) of both substrate receptor (SR) types and those lacking substrate receptor domains. This modification consists of prolyl hydroxylation by PhyA and subsequent glycosylation by a series of 5 glycosylation reactions. Immunoprecipitation of Skp1 from vegetative and slug cells revealed dramatic remodeling of Skp1's interactome between the two different stages of its life cycle. At both stages, Skp1 had higher levels of interaction with a number of FBPs when it was glycosylated that was not simply the result of differential abundance. Two of these FBPs, JcdI and FbxwD, were further characterized. JcdI, a JmjC non-heme dioxygenase and an FBP conserved throughout *Protista*, has been shown to serve as a putative oxygen-sensor in an SCF independent

manner. JcdI's F-box domain may serve to regulate its degradation as its levels are significantly increased in developing slugs that lack the Skp1 glycan. FbxwD, a WD40 SR-type FBP, negatively impacted *Dictyostelium*'s ability to successfully differentiate during development when overexpressed. Interestingly, this inhibition was dependent on FbxwD having an intact RING domain and an intact copy of the Vwa1 locus. Vwa1, a homologue to the tumor suppressor VWA5A/BCSC-1, has no effect on development when knocked-out or over-expressed but expression of individual domains of the protein cause dramatic arrests of development only when the endogenous copy was expressed. Vwa1 may engage in a form of auto-inhibition that prevents it from forming active complexes with FbxwD, a model that could be used to understand the role of its poorly understood human homolog.

INDEX WORDS: Cellular slime mold, Skp1, F-box protein, SCF, Ubiquitin, Glycosylation, Jumonji C, Prolyl hydroxylase, *Dictyostelium*, Oxygen sensing, Vwa1, RING, VWA5A, VIT, vFWA, Von Willebrand domain A

THE ROLE OF SKP1 GLYCOSYLATION IN SCF ASSEMBLY AND THE CHARACTERIZATION OF THE INTERACTION OF AN F-BOX PROTEINS AND ITS BINDING PARTNER

By

ANDREW WILLIAM BOLAND

B.A., Eckerd College 2011

B.S., Eckerd College 2014

A Dissertation Submitted to the Graduate Faculty of The University of Georgia in Partial Fulfillment of the Requirements for the Degree

DOCTOR OF PHILOSOPHY

ATHENS, GEORGIA

2022

THE ROLE OF SKP1 GLYCOSYLATION IN SCF ASSEMBLY AND THE CHARACTERIZATION OF THE INTERACTION OF AN F-BOX PROTEINS AND ITS BINDING PARTNER

By

ANDREW WILLIAM BOLAND

Major Professor: Christopher M. West

Committee: Maria Belen Cassera
David Garfinkel
Lance Wells

Electronic Version Approved:

Ron Walcott
Dean of the Graduate School
The University of Georgia
August 2022

DEDICATION

I would like to dedicate this dissertation to my parents. I am the person I am today because of them and certainly wouldn't be writing this dissertation if it weren't for their loving kindness. They have supported me through my education and through the toughest challenges in my life. I am very fortunate to have known them. I love you two so much.

ACKNOWLEDGEMENTS

I would like to thank my lab members that all helped me get here. Hanke showed me many methods from molecular work, Dictyostelium manipulations and most importantly where stuff is in the lab. She also contributed significantly to both Chapters 1 and 2. I would like to thank Msano Mandalasi for her endless patience, knowledge of all things molecular and moral support through tough days. Elisabet Gas-Pascual performed peptide cleanups, injected, and did the troubleshooting on the machine end of things for the majority of the LC-MS/MS data in this dissertation. Nitin Daniel purified the recombinant JcdI and teaching me how to use the NCG for isolating Vwa1. I thank Donavan Cantrell and Megna Tiwari for providing entertainment and moral support. Osman Sheikh's data formed the foundation that my dissertation is built on. I would like to acknowledge Chris West for mentoring me these seven years and supporting me financially. I have grown into a well-rounded and critical scientist in his lab and under his mentorship. He collaborated with me in the writing of these chapters.

I would also like to thank my committee members for guidance along the way and, in Belen Cassera and Lance Well's case, their lab space and reagents. Belen, David Garfinkel, Lance and Zac Wood, all of you helped keep me going when morale was low. In the Wells lab, I would like to thank Rob Bridger for helping me generate LC gradients and set up methods for the QE+ that are still in use in some shape or form today.

I would like to acknowledge my friends and family that brought me joy over the years

while in graduate school. All of you goons know who you are. Eulalie Geonzon's patience, food and sense of humor are what kept me going at the 11th hour of writing my dissertation when it was hard to see the end in sight.

TABLE OF CONTENTS

LIST OF TABLES

Page

LIST OF FIGURES

Page

ABBREVIATIONS

Ab	Antibody
ACN	Acetonitrile
αKG	α-ketoglutarate
AUC	Analytical ultra-centrifugation
BCSC-1	Breast cancer suppressor candidate-1
BSR	Blasticidin resistance cassette
cAMP	cyclic- adenosine monophosphate
CNS	COP9 Signalosome
co-IP	co-immunoprecipitation
Dd	*Dictyostelium discoideum*
DMSO	dimethyl sulfoxide
FA	Formic acid
FBP	F-box protein
FDR	False discovery rate
GT	Glycosyltransferase
HCD	Higher energy C trap dissociation
HFBA	Heptafluorobutyric acid
Hyp	4-(*trans*)-hydroxyproline
ITIH	inter-alpha-trypsin inhibitor heavy-chain

JmjC	Jumonji C
KO	Gene interruption or replacement with a resistance marker
LRR	Leucine-Rich-Repeat
MIDAS	Metal-ion-dependent association site
PARP4	Poly(ADP-Ribose) 4
RING	Really Interesting New Gene
SCF	Skp1-Cullin-F-box -Rbx1 complex
SR	Substrate receptor
TFA	Trifluoroacetic acid
Tg	*Toxoplasma gondii*
Ub	Ubiquitin
UPS	Ubiquitin proteasome system
VIT	vault protein inter-alpha-trypsin
vWFA	von Willebrand factor type A
VWA5A	Von Willebrand Factor A Domain Containing

CHAPTER 1

Introduction

The SCF and ubiquitination

All organisms both single and multi-cellular grow, change and adapt to dynamic needs and surroundings. Protein turnover is a necessary component of this adaptation to allow for damaged, misfolded, unused, and redundant proteins to be recycled. The Skp1-Cullin-F-box - Rbx1 (SCF) protein complex (Fig. 1.1A) serves an essential role in eukaryotic protein turnover through targeted degradation of proteins and regulation of proteostasis as a component of the ubiquitin proteasome system (1). The primary function of the SCF is to bind to specific protein substrates and poly-ubiquitinate them with lysine-48 (K48) linked poly-ubiquitin chains (2,3). These chains in turn target the substrates to the 26S proteasome where they are subsequently degraded. Ubiquitination via the SCF and other ubiquitin ligases are necessary for the survival of eukaryotic organisms and, as such, components such as Skp1, Cullin and Rbx1 are conserved across eukaryotes (4).

Cul1 type Cullins serve as a scaffold that brings the F-box protein/Skp1 dimers into proximity with ubiquitin-activated E2 ligases (5). Functional Cul1 exists as a heterodimer with Rbx1 (6), the protein that binds dynamically with activated E2 ligases via Rbx1's RING (Really Interesting New Gene) domain (7). Cul1's binding to Skp1 is highly regulated by the protein CAND1 (8,9). When complexed with CAND1, Cul1's binding site for Skp1 is rendered inaccessible. The inactivated CAND1/Cul1 complex dissociates when specialized E3 ligases covalently attach

the ubiquitin-like protein, NEDD8, to Cul1 in a process known as neddylation (10,11). The neddylation of Cullins is reversable and tightly regulated by the multi-protein metalloprotease complex known as the COP9 signalosome (CNS) (12). Structural studies have shown that the CSN's interaction with Cullin is competitive with substrate receptor assemblies and Cullins within active E3 ligase assemblies may be resistant to deneddylation (12,13).

The specificity of the SCF is conferred by a plethora of interchangeable F-box proteins (FBP), each with their own specific set of protein substrates. Common substrate receptors on F-box are WD40-repeat propellers, Leucine-Rich-Repeats (LRR), armadillo repeats, and kelch repeats (14). The repetitive and often hydrophobic nature of these domains facilitate the protein-protein interactions necessary to bring the substrate into proximity with the ubiquitin ligase (2,3). While the FBP's canonical role is to serve as a substrate receptor, some FBPs lack substrate receptors and have other specialized functions such kinase activity or single-ligand interactions (15). The 40-50 amino acid F-box domain for which F-box proteins gain their name, is typically located N-terminally of any substrate receptor domain and consists of three alpha helices that interact with Skp1 (16). This domain interfaces with the Skp1 adaptor's 3 C-terminal helices (17).

Contrary to the evolutionarily divergent and diverse FBPs, Skp1 is a highly conserved protein. It forms hetero-dimers with F-box proteins and serves as an adaptor between the divergent FPBs and a Cul1 (9). These Skp1-FBP heterodimers are dynamically interchanged via the previously mentioned CAND1 and neddylation (10-13). The mechanisms by which Skp1 selects specific FBPs to dimerize with is poorly understood but previous research proposes several mechanisms by which Skp1-FBP binding may be regulated in protists (18). One of these potential mechanisms, a post-translationally assembled pentasaccharide on a hydroxyproline has

been shown to alter levels of Skp1-FBP association in vitro and in *Dictyostelium discoideum* (19,20) and *Toxoplasma gondii* (unpublished), but it has been unclear whether this was due to differential abundance of the FBP or apparent affinity. Investigation of the role of this glycan and how it influences the proteome of the cell served as a basis for further investigation.

Dictyostelium discoideum, a model organism for studying the SCF

The soil-dwelling NIH model organism, *Dictyostelium discoideum*, lives as a unicellular amoeba for most of its life of as a free-living cell feeding on bacteria and in the case of the axenic mutants, soluble nutrient rich media. Upon nutrient depletion, *Dictyostelium* proceeds to extra cellularly signal to adjacent cells to aggregate with cyclic-adenosine monophosphate (cAMP). These aggregates polarize and organize into motile slugs that are comprised of differentiating pre-spore and pre-stalk cells. These slugs proceed to migrate to a suitable location to terminally differentiate into fruiting bodies (21). The motile slugs' movement is directed by oxygen gradients and light (18,21,22). Upon finding a suitable location to fruit, the motile slugs arrange themselves upright and the stalk cells elongate and produce a dense extracellular matrix of cellulose to serve as the structure of the stalk, sacrificing themselves in the process. Atop the elongating stalk, pre-spore cells with the differentiate into oblong, cellulose-coated spores (21). (Fig. 1.1B) The goal of this process is to distribute spores across long distances to potentially nutrient rich locales. *Dictyostelium*'s developmental process is marked by dramatic and concerted transcriptomic (23) and proteomic changes (24).

Dictyostelium has traditionally been used a model organism for studying chemotaxis, eukaryotic cell motility, and morphogenesis (25). Many genetic tools for gene expression are available and its genome readily undergoes homologous recombination (26) to aid in

endogenous epitope tagging and gene knockout (27). Axenically grown *Dictyostelium* has a replication time of 6-8 hours during its logarithmic growth phase (28) in manner that is scalable and relatively low in cost. Due to the synchronous and tightly controlled nature of *Dictyostelium* development, genetic disruptions of the SCF can be readily observed in development qualitatively through morphological observations and quantitatively through spore counts. Considering this, *Dictyostelium* serves as an excellent model for studying the SCF E3 ubiquitin ligases.

One of the first documented examples of ubiquitin-proteasome system (UPS) and SCF disruption resulting in a mutant fruiting phenotype was the knockout of the WD40 repeat containing FBP, FbxA (29). Cells deficient in FbxA fail to successfully differentiate into fruiting bodies. They either form undifferentiated aggregates on nitrocellulose, or long aerial slugs (30) that while resembling fruiting bodies, lack differentiated, cellulose coated spores or stalk cells after developing on bacterial lawns (29). When FbxA deficient cells develop mixed with wild-type cells, the *fbxA*$^{-}$ cells differentiate with the signaling assistance from the wild-type cells. The *fbxA*$^{-}$ cells preferentially occupy the spore forming sorus of the fruiting body rather than the stalk (29), which is referred to as cheating because only spores survive to the next generation. This F-box protein is enriched in pre-stalk cells compared to pre-spore cells and likely serves a role in stalk vs spore terminal cell fate. Its role has been tied to the PKA cyclic-AMP signaling pathway (31) which is essential for extracellular signaling (32) and successful development of *Dictyostelium*. While this example of FbxA emphasizes a potential role of the SCF in regulation of development, the whole picture is not fully understood as only a single substrate has been validated for FbxA (31).

Skp1 glycosylation and its biochemical and biological role

The West lab identified a unique fucose containing O-glycan on the Skp1 adaptor of the SFC E3 ligase (33). It was determined that the O-glycan is a pentasaccharide built upon a hydroxyproline. The prolyl hydroxylase responsible for initiating the Skp1 glycosylation, PhyA, is a HIFα-type enzyme (34) that serves a role in *Dictyostelium*'s ability to sense oxygen through the hydroxylation of proline 143 (35). PhyA has no other known substrates (36). Oxygen sensing had already been tied to *Dictyostelium*'s ability to differentiate (37) and successfully develop. The knockout of PhyA creates similar disruption of cells patterning as low oxygen (22). While a significant oxygen sensor in *Dictyostelium*, PhyA is not the only mechanism by which *Dictyostelium* senses environmental oxygen. Oxygen levels $\geq$40% do rescue the *phyA*$^-$ cells' ability to differentiate correctly and produce fruiting bodies. PhyA has also been shown to contribute to the fitness of *Toxoplasma gondii*. In addition to reduced cell fitness (38), plaque assays of *Toxoplasma* show that *phyA*$^-$ causes the cells to have a reduced capacity to multiply, lyse and reinfect host cells resulting in significantly reduced plaque area (39). Much like the soil dwelling *Dictyostelium*, *Toxoplasma* lives in environments with diverse concentrations of oxygen from the highly oxygenated lung tissues to the anoxic tissues of the gut. PhyA may serve a role to allow the cells to adapt to these differing host tissues.

The Skp1 glycan and its assembly are particularly unique. First, the assembly of the glycan takes place in the cytoplasm or nucleus. Most glycosylation takes place within the ER and Golgi apparatus on membrane associated or secreted proteins (40,41). Several cytoplasmic glycosyltransferases (GTs) act as an exception to this dogma. There is some speculation that cytoplasmic glycosylation may even be the ancestral mode compartmentalization of all

glycosylation events (42). *O*-GlcNAc transferase (43,44), the O-fucosyl transferase SpyA (45,46), the bacterial rhamnosyltransferase, EarP (47), in addition to a number of uncharacterized intracellular glycosyl transferases (48) contribute to the slowly increasing repertoire of recognized nucleocytoplasmic glycosyltransferases. What sets the Skp1's GTs apart from these examples is that each of the three, Gnt1(49), PgtA (50), and AgtA (51), processively assemble pentasaccharide on a single known substrate as opposed to the addition of a monosaccharide to a variety of substrates. This unique glycosylation pathway likely was present in the last eukaryotic common ancestor as homologues of PhyA, Gnt1, PgtA are predicted in the genomes of a diverse distribution of organisms (18) and have been validated in *Toxoplasma gondii* and *Pythium ultimum* (39,52,53). While the composition of the *Dd* and *Tg* Skp1 glycans differs at the penultimate sugar and *Tg* utilizes two GTs (52,53) instead of AgtA to terminally elongate the glycan, the pentasaccharide linkage structure and presumably the function is conserved (Fig 1.2). The role of the Skp1 glycan is derived from several of its biophysical characteristics. Molecular modeling of the *Dictyostelium* Skp1 informed by NMR suggests that the C-terminus has a disordered region in the F-box interface between helix 7 and helix 8 that has the capacity to open and close (53,54). This closed conformation is hypothetically unavailable for F-box domains to bind. When Skp1 is glycosylated at proline 143, the glycan is modeled to form van der Waals packing and hydrogen bonds along the disordered segment. This bestows rigidity to an otherwise dynamic portion of the protein and causes Skp1 to favor the open conformation to accept F-box proteins more readily or stabilize the interaction between Skp1 and the F-box proteins. As no structures of *Dictyostelium* F-box proteins have been determined experimentally, the human leucine-rich repeat protein (LRR) substrate receptor type FBP, Skp2 was used in docking models

to support the model that Skp1's availability to F-box interfacing is enhanced by the glycan. Skp1 has been previously reported to form homodimers in vitro (55). In *Dictyostelium*, the Skp1 glycan can affect Skp1's ability to form homodimers. Cross-linking studies, gel filtration and analytical ultra-centrifugation (AUC) has confirmed this (19). In its unmodified state, *Dictyostelium* Skp1 can for a homodimer in vitro with a K_D of 2.5 μM (56). Structural and experimental data have shown that this dimer masks the F-box binding site and potentially inhibits the initial formation of functional SCF complexes. Mutagenesis of the conserved F97 significantly destabilizes the Skp1 dimers in AUC studies (56), helping to confirm the dimer interface. It should be noted that while Skp1 dimerization blocks the F-box interface, The K_D of the Skp1/Skp1 dimer is a hundred-fold higher than published model Skp1/FBP dimers (55). Upon hydroxylation and glycosylation, the percent of Skp1 existing in a homodimer is reduced (19). This adds another dimension to the hypothesis that Skp1 is more accessible to FBPs upon glycosylation. Not only is its open conformation promoted upon glycosylation, its homodimerization that blocks the F-box binding region is reduced upon the addition of this oxygen dependent post translational modification.

Skp1's interactome and PhyA's role in SCF assembly

While only a fraction of targeted protein degradation takes place via the SCF, its importance in the UPS and protein turnover during development is apparent (22,29,31). In order to understand how the SCF and specifically Skp1 acts to remodel the proteome in developing slugs, Skp1's interactome was examined via endogenous immunoprecipitation (IP). Proteomic analysis of IP's of endogenous Skp1 revealed 18 putative interactors several of which were putative F-box proteins based on sequence analysis (20). In order to investigate the role of PhyA and by proxy, oxygen on Skp1's interactome, Skp1 was immunoprecipitated in the *phyA*$^-$ genetic

Fig. 1.1. The SCF complex and *Dictyostelium* development

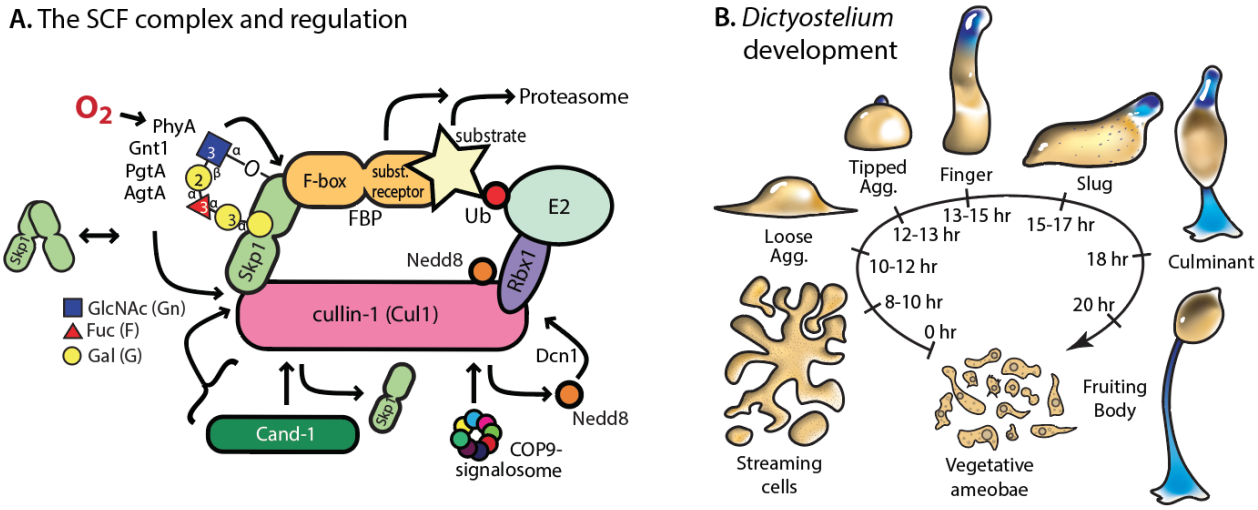

Fig. 1.1. The SCF complex and *Dictyostelium* development. *A,* schematic illustration of a generic SCF complex including modes of regulation and the posttranslational modification of Skp1. See text for explanation. *B*, schematic illustration of the starvation-induced developmental cycle of *Dictyostelium discoideum*. Pre-stalk cells and anterior-like cells are labeled blue (32). The life cycle is renewed when spores from a fruiting body germinate to become feeding amoebae.

Fig. 1.2. Assembly of the *Dd* Skp1 glycan.

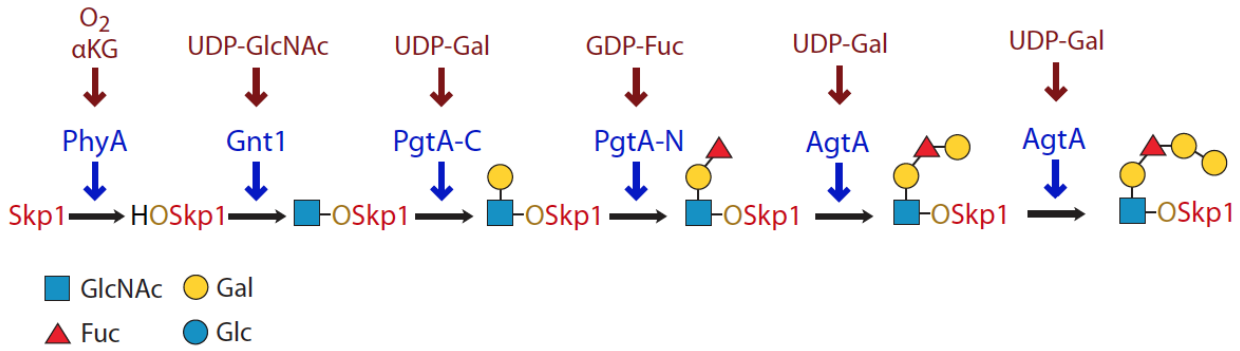

Fig. 1.2. Assembly of the *Dd* glycan. Oxygen dependent hydroxylation of Skp1 pro143 initiates the processive assembly of the pentasaccharide. Glycosyltransferases and their substrate nucleotide sugar for each step are presented as well as the transient, intermediate Skp1 glycan. The legend contains Symbol Nomenclature for Glycans for each sugar represented.

background alongside parental slugs. In line with the prediction that Skp1 glycosylation makes its F-box binding site more accessible (54), several F-box proteins co-precipitated at a higher level in the parental/*phyA*$^{+}$ background where Skp1 was >90% glycosylated (20). Of the two FBP's whose representation in the Skp1 interactome was enhanced by the presence of the glycan, both FbxA and FbxwD are WD40 substrate receptor (SR) type FBPs. This was particularly interesting because FbxA as previously mentioned plays an important role in proper organization of cellular differentiation in slugs and fruiting bodies. FbxwD's role in cells, on the other hand, was not well understood beyond noting that forced overexpression delayed development (Sheikh et al 2015). Characterization of this novel FBP is discussed later in this chapter. Counter to the trend seen with the SR-type FBPs, the Jumanji-C domain containing FBP, JcdI, exhibited higher apparent levels of interaction with Skp1 when Skp1 lacked the glycan (20). This phenomenon is investigated in Chapter 2 and hypothesized to be a consequence of higher levels of JcdI available to bind Skp1 during the slug stage of development.

Considering that the proteome and transcriptome of *Dictyostelium* differs significantly between its vegetatively growing stage and its development (23,57-59), the Skp1 interactome likely differs dramatically between the two different stages of life. In this dissertation the Skp1 interactome is probed and compared in both vegetative and slug cells to show how the interactome changes dynamically between life stages. Orthogonal co-immunoprepitation (co-IP) methods expanded upon the slug Skp1 interactome as well as illustrated a vegetative interactome with less than 50% overlap between the two life stages. In both life stages, PhyA and in effect Skp1 glycosylation enhanced interaction with certain candidate FBPs. With the knowledge that Skp1 glycosylation affects interaction with FBPs, it can be suggested that

individual substrates of those FBPs are degraded more efficiently in the cell capable of modifying Skp1. However, to this date, only one FBP substrate in *Dictyostelium* has been suggested (31) and has not had its degradation tied to Skp1 glycosylation.

The co-immunoprecipitations of Skp1 revealed that it interacts with two Cul1's, CulE by which *Dictyostelium* Skp1 interacts in addition to CulA (20). Glycosylation status had no effect on the levels in which CulE interacted known Skp1 independent interactors such as Cand1 and Rbx1 or with Skp1 itself. This was consistent with the NMR data on Skp1 glycosylation (54) that indicated that the glycan had no effect on the structure of the N-terminus of Skp1 that interacts with Cul1 homologues (60). Reciprocal pull down of CulE confirmed that the Skp1 glycan had no effect on the levels of co-precipitation of Skp1 or any other interactor with one exception: FbxwD's levels of interaction with CulE were reduced in the *phyA*$^{-}$ genetic background (20). This was consistent with Skp1 IP results where FbxwD exhibited lower levels of interaction with unmodified Skp1 and the interaction with CulE is presumed to be indirect. In addition, Skp1, Rbx1 and FbxwD, typical Cul1 regulatory components Cand1 and COP9 signalosome were identified as CulE interactors (20).

FbxwD, a substrate receptor type F-box protein influenced by the Skp1 glycan

Of the enhanced slug stage interactors, FbxwD was of particular interest. FbxwD was predicted to contain an F-box domain and it immunoprecipitated with Skp1. This made it a putative FBP. Mutagenesis of its LPXE (61-63) sequence in its predicted F-box to an AAXE abrogated Skp1 binding and thus validated it as a true FBP (20). FbxwD is a canonical WD40-domain containing substrate receptor F-box protein with a unique RING (Really Interesting New Gene) domain. RING domains such as the one found in Rbx1, are unique zinc-fingers that

predominantly mediate ubiquitin ligase activity by interacting with and perhaps activating a Ub-charged E2 subunit thereby facilitating access to its substrates (7,64). While uncommon there is precedent for an FBP to contain a RING domain (65-67). In the known examples of RING domain containing FBPs, the function of the domain is unclear. Reciprocal co-IP of FbxwD precipitated Skp1 and precipitated more Skp1 proportionately when Skp1 was modified (20). The reciprocal co-IPs of FbxwD validated its increased interaction with modified Skp1 observed in the Skp1 co-IPs. When immunoprecipitating the FbxwD with the LPXE F-box mutation, 12 proteins experienced a two-fold increase in their interaction with FbxwD-LPXE relative to wildtype FbxwD (20). As FBPs mark proteins for degradation, these increased interactors were noted as potential substrates for FbxwD. Although FbxwD is pre-stalk enriched during development (68), the immunoprecipitated FbxwD was over expressed from the *cotB* pre-spore promotor (69). As such, dependence of the interaction on the Skp1's glycosylation status, the potential confounding effect of dependence of levels on Skp1's glycosylation status, and the putative substrates, need to be further validated by immunoprecipitation of endogenously expressed FbxwD.

Vwa1 an FbxwD interactor

In this dissertation, an interactor found in the previously reported co-IPs of over-expressed FbxwD (20) and endogenous co-IPs reported here was investigated further. It was determined that a consistent interactor was identified that may be essential for the function of FbxwD as further elucidated in Chapter 3. This protein, called Vwa1/DDB_G0292016, is predicted to contain the vault protein inter-alpha- trypsin (VIT) (70), and the von Willebrand factor type A (vWFA) domains (71). The vWFA domain is a typical Rossmann fold (72) that contains a Metal Ion-Dependant Adhesion Site (MIDAS) motif potentially capable of mediating protein-protein

interactions (73). The vWFA domain is most commonly associated with the secreted von Willebrand factor but it thought to be a genetically mobile domain and thus is found in a wide variety of intra and extra-cellular proteins (74). The VIT domain in contrast to the vWFA is thought to be a 'passenger' always found in the presence of a 3' vWFA domain (70). Structurally it is a large β-sandwich atop the vWFA domain connected to the VWFA via an integrin-like hybrid domain (17). The hybrid domain is a smaller β-sandwich comprised of the amino acid sequences flanking the N and C-termini of the vWFA domain.

Similar hybrid+vWFA domain structures have been observed in integrins (75). Integrin-β lacks a VIT domain but contains a vWFA domain flanked N and C-terminally by a hybrid domain much like Vwa1. In this protein, binding of a ligand to the MIDAS shifts the positions of the vWFA's α-helices 1 and 7 to allosterically change the conformation of the hybrid domain (76). This conformational change upon ligand binding swings the hybrid domain away from the vWFA and dramatically alters the structure of Integrin-β (77). Similar mechanisms of MIDAS+ligand allosteric structural changes might exist in VWA5A like proteins and would likely affect the conformation of the VIT domain as it is predicted to be directly connected to both portions of the hybrid domain. An allosteric change to the VIT by the vWFA+hybrid may be a mechanism by which Vwa1 and VWA5A function.

This VIT-vWFA-hybrid domain organization occurs in the inter-alpha-trypsin inhibitor heavy-chain (ITIH) and Von Willebrand Factor A Domain Containing 5A (VWA5A)/ Breast cancer suppressor candidate-1 (BCSC-1) (78). ITIH has been characterized as an extracellular scaffold protein that complexes with a protease inhibitor to protect the extracellular matrix through localization of a protease inhibitor (79). On the other hand, VWA5A/BCSC-1's for which Vwa1 has

greater homology, is intracellular and implicated in reducing tumor metastasis (80) and downregulated in schizophrenia (81). Much like Vwa1, VWA5A has been found interacting with a SOCS-box E3 ubiquitin ligase component, SPRY (82,83) but its mechanism of action is yet unknown. Vwa1's potentially cooperative role with FbxwD may serve as a model for understanding the mechanism of action for VWA5A. Whereas human Vwa5 is a single copy gene that is, however, expressed as four spliceoforms, *Dictyostelium* Vwa1 belongs to a family of 6 highly related genes, with the intron-less Vwa1 possessing the greatest sequence homology with human Vwa5.

In regards for Vwa1 acting as an accessory protein/cofactor to Fbxwd, there is a precedent for accessory proteins assisting FBPs in recruiting specific biologically relevant substrates. While substrate receptor FBPs are typically thought act alone in recruiting substrates, there have been cofactors described that assist FBPs to assist in ubiquitinating other substrates. The leucine-rich repeat (LRR) FBP, Skp2, must be complexed with Cks1 to efficiently degrade the mitotic inhibitor, $p27^{Kip1}$ (84). SCF^{FBXL3} acts to ubiquitinate proteins as a traditional SCF complex, and it has been shown that SCF^{FBXL3} complexes with the circadian clock associated CRY1/2 specifically to recruit Tousled-like kinase 2 (TLK2) for ubiquitination and degradation (85). While the TLK2 substrate could interact with FbxL3 without the presence of CRY, induction of CRY significantly reduced TLK2 levels in a proteasome dependent manner. There is also precedent for FBPs complexing with other proteins to preform functions outside the scope of the SCF's role of ubiquitination. Rieu et al. 2022 report a the Kelch-type FBP, UFO, complexing with a transcription factor to bind DNA in a Skp1/SCF independent manner as its primary mode of action (86). With this in consideration, FbxwD may also have roles outside of that of a substrate receptor.

JcdI, a Jmjd6-like FbxO type F-box protein influenced by the Skp1 glycan

As previously mentioned, JcdI was identified as reduced in levels in the Skp1 slug interactome. It is a putative non-substrate receptor-type FBP with an enzymatic Jumanji-C (JmjC) domain. The JmjC domains are non-heme dioxygenases that utilize a coordinated Fe^{2+} atom, α-ketoglutarate, and oxygen to hydroxylate and/or de-methylate substrates (87). As such, JcdI is of particular interest because of its potential role as an oxygen sensing enzymatic FBP. JcdI's JmjC domain shares sequence homology with the well characterized JumanjiC domain containing protein Jmjd6. Jmjd6 acts as a lysyl-hydroxylase Jmjd6 has recently been shown to modify the tails of histones which could affect transcription (88). Additionally, it has been shown to affect alternative splicing in complex with the splicing factor, U2AF65. The activity of the Jmjd6/ U2AF65 complex is dependent on Jmjd6's ability to hydroxylate key lysines in U2AF65 (89). Jmjd6 is found to be enriched in a number of cancer types that are associated with high metastatic properties and poor prognosis (90).

While Jmjd6 lacks an F-box domain, there is evidence that it associates with an E3 ubiquitin ligase, TRAF6. It acts in competition with the methyltransferase, PRMT1, to regulate the activity of the E3 ligase. Where PRMT1 inhibits the E3 ubiquitin ligase through methylation, Jmjd6 removes the inhibitory methyl group to promote activation of NF-κB signaling (91). These JmjC proteins are well documented to serve as epigenetic modulators act in oxygen dependent manner (92). It is unclear what the role of a JcdI has in the context of the SCF or outside of it. Considering the many functions of Jmjd6, there may be multiple cellular processes regulated by JcdI. The role of JcdI's F-box domain may serve to not only help assemble functional SCFs for the purpose of targeted degradation but the F-box domain itself may serve to target JcdI itself to the

26S proteasome (93). Similar to Jmjd6, Jcdl's JmjC domain is proven in this dissertation to use oxygen as a substrate making it a candidate for a parallel or cooperative means by which *Dictyostelium* senses atmospheric oxygen.

CHAPTER 2

OXYGEN-DEPENDANT REGULATION OF E3(SCF)UBIQUITIN LIGASES AND A SKP1-ASSOCIATED JMJD6 HOMOLOG IN *DICTYOSTELIUM*

A. W. Boland, E. Gas-Pascual, B. L. Nottingham, H. van der Wel, M. O. Sheikh, C. M. Schafer, C. M. West. Accepted by *Journal of Biological Chemistry.*

Reprinted here with the permission of the publisher.

Abstract

E3-SCF (Skp1/cullin-1/F-box protein) polyubiquitin ligases activate the proteasomal degradation of thousands of proteins, but the evolutionary diversification of the F-box protein (FBP) family of substrate receptor subunits has challenged their elucidation in protists. Here we expand the FBP candidate list in the social amoeba *Dictyostelium* and show that the Skp1 interactome is highly remodeled as cells transition from solitary growth to multicellular development. Importantly, a subset of FBPs was less represented when the posttranslational hydroxylation and glycosylation of Skp1 was abrogated by deletion of the O_2-sensing Skp1 prolyl hydroxylase PhyA. A role of this Skp1 modification for SCF activity was indicated by partial rescue of development, which normally depends on high O_2 and PhyA, of *phyA* -knockout cells by proteasomal inhibitors. Further examination of two FBPs, FbxwD and the Jumonji C protein JcdI, suggested substitution of Skp1 by other factors in *phyA* -knockout cells. Although a double-knockout of *jcdI* and its paralog *jcdH* did not affect development, overexpression of JcdI increased sensitivity to O_2. JcdI, a non-heme dioxygenase shown to have physiological O_2-dependence, is conserved across protists with its F-box and other domains and related to the human oncogene JmjD6. Sensitization of JcdI-overexpression cells to O_2 depended on its dioxygenase activity and other domains, but not its F-box, which may however mediate its reduced levels in wild-type vs. Skp1 modification mutant cells. The findings suggest that activation of JcdI by O_2 is tempered by homeostatic down-regulation via PhyA and association with Skp1.

Introduction

For cells to adapt to their surroundings and proliferate or differentiate, their proteomes must be selectively modified. Protein degradation is largely mediated by autophagy and the

ubiquitin proteasome system. For the latter, the SCF (Skp1/cullin-1/F-box protein/Rbx1) family of E3 ubiquitin (Ub) ligases, conserved throughout eukaryotes, tags specific proteins with Lysine 48 (K48)-linked polyubiquitin chains for degradation by the 26S proteasome. These multi-protein complexes consist of a cullin-1 (Cul1) scaffold that brings Ub-charged E2 subunits into proximity with substrates that are typically presented by an F-box protein (FBP) that is linked to the other end of Cul1 via the Skp1 adaptor (1, 2) (Fig. 1.1A). Cul1 is a major target of regulation by CAND1 (Cullin-associated NEDD8-dissociated protein 1), which displaces Skp1 and its associated FBP. CAND1 binding is regulated by modification of Cul1 by the Ub homolog NEDD8 (3, 4), which also mobilizes the presentation of Ub-E2 via an effect on Rbx1. The linkage of NEDD8 is dynamically regulated by its own E3 subunit and the COP9 signalosome (5). FBPs comprise a large family of substrate receptors and proteins that may be substrates themselves (6), and are distinguished by the presence of a conserved 40 amino acid F-box domain that binds to the C-terminal region of Skp1 (7). Protein-protein interaction domains that are commonly found in substrate receptor FBPs include WD40-repeats and Leucine rich repeats (LRR), and are referred to as Fbxw# and Fbxl#, respectively. Other FBPs contain ankyrin-, kelch-, and armadillo-repeats as putative substrate receptor domains, and some of these Fbxo#-type FBPs lack archetypical protein-protein interaction domains (8). All of these regulatory features appear to be encoded in the genomes of examined protists. Contrary to the highly conserved Cul1, Skp1, Rbx1 and E2 proteins, FBPs can be challenging to predict owing to extensive diversification of their sequences across eukaryotic phylogeny (9), suggesting a tendency to assume organism specific roles. In humans, the 69 identified FBPs likely regulate the half-lives of over a thousand proteins.

Studies of the SCF complex in unicellular eukaryotes have revealed a novel post translational modification of the Skp1 adaptor (Fig. 1.1A). First described in the social amoeba *Dictyostelium discoideum* (10), it consists of a complex linear pentasaccharide assembled on Pro143 following its O_2-dependent hydroxylation by the prolyl 4-hydroxylase PhyA. A related modification is found in the apicomplexan parasite *Toxoplasma gondii* (11, 12), and phylogenetic and biochemical evidence suggests that the Skp1-glycan is present in diverse protists (13) including the crop plant parasite, *Pythium ultimum* (14).

Dictyostelium has been a favorable model organism to investigate mechanisms of O_2-sensing and the contribution of PhyA and glycosylation (13, 15). *Dictyostelium* proliferates by simple mitosis as single cells in the presence of nutritional sources but, when starved at an air-water interface, the amoebae aggregate to form multicellular slugs that culminate to form fruiting bodies each with a cellular stalk supporting a mass of spores (Fig. 1.1B). The process of morphological culmination involves major changes in the transcriptome and proteome, and O_2 is one of several known checkpoints for culmination both in the native soil environment and in laboratory settings. The dependence on PhyA is reminiscent of the role of its homolog in humans where it regulates the stability of HIFα and its availability to control the transcription of hypoxia responsive genes (16, 17). PhyA, like other non-heme dioxygenases, distributes O-atoms from O_2 to a target and αKG. Evidence indicates that *Dictyostelium* PhyA activity is regulated by O_2-availability both *in vitro* (18, 19) and *in vivo* (20, 21), and indeed the level of O_2 required for culmination varies inversely with the level of forced PhyA over-expression (13). Nevertheless, other O_2-sensing mechanisms must exist because the absence of PhyA can be overridden by hyperoxia. Based on related effects of varying the levels of Skp1 on O_2-regulation of culmination,

and ameliorating effects of mutating the target Pro143 or co-overexpression of Skp1, Skp1 appears to be the functional target of protist PhyA (22). We here present evidence that the mechanism by which PhyA mediates O_2-sensing involves protein turnover (13) based on the effects of proteasomal inhibitors. Other evidence indicates that the O_2-sensing role of Skp1 hydroxylation depends on further modification of the hydroxyproline (Hyp) by a pentasaccharide that is assembled by Skp1-specific glycosyltransferases in both *Dictyostelium* and *Toxoplasma* (23-25).

To explore the mechanism of PhyA's action on Skp1 we previously examined its influence on the interactome of slug Skp1 using co-immunoprecipitation (co-IP) and querying by mass spectrometry (20). The findings suggested that Skp1 glycosylation, enabled by its O_2-dependent hydroxylation, selectively promotes its interaction with certain FBPs whereas interaction with Cul1 remained unchanged, based on relative levels of FBPs that co-immunoprecipitated with Skp1 or Cul1 (20). The selective effect on FBP interaction was consistent with the proximity of the glycan's Hyp attachment site to the FBP combining site and evidence that the glycan affects local conformational preferences (24, 26). In addition, glycosylation also inhibits Skp1 dimerization which may be competitive with FBP association (25, 27). Here we introduce an orthogonal co-IP method to address the generality of the selective effect of glycosylation on specific FBP interactions. These results demonstrate that the Skp1 interactome is remarkably dynamic as cells develop from the single cell growth stage to the multicellular fruiting body.

To begin to understand the basis for altered representation of FBPs in the Skp1 interactome, two FBPs were epitope tagged for further study. One is FbxwD, and we show that increased representation in the Skp1 interactome of *phyA*$^-$ (*phyA*-knockout) cells is not simply

due to reduced expression, indicating preferential binding. The second is JcdI, which is evolutionarily related to human JmjD6, a JmjC (Jumonji C) domain containing non-heme dioxygenase that has been implicated in epigenetic regulation, RNA splicing and oncogenesis (29-31). We show that unlike JmjD6, JcdI is an FBP and, like PhyA, is an O_2-dependent dioxygenase whose enzyme activity is likely controlled by physiological variations in O_2. In addition, JcdI is to our knowledge the first FBP found to be conserved across the protist kingdom and higher plants. The previously reported decreased representation of JcdI in the interactome of Skp1 from wild-type (*phyA*$^+$) vs. *phyA*$^-$ cells (20) is attributable to a decreased level of JcdI that obscured increased interaction with Skp1. Significantly, overexpression of JcdI decreased the O_2 threshold for fruiting body formation. This effect depended on both its catalytic activity and non-catalytic domains, but not its F-box, suggesting that O_2 regulates endogenous JcdI both directly as a substrate and indirectly by controlling its level via PhyA and Skp1.

Results

Proteasome inhibitors bypass the dependence of culmination on PhyA

Dictyostelium is a social amoeba that normally proliferates in the presence of a bacterial food source or, for axenic mutants, in a rich liquid broth. In response to starvation, the amoebae, when deposited on a filter surface to ensure a high level of O_2, chemotactically aggregate via streams to form a multicellular slug that eventually, over the course of a few more hours, culminates into a fruiting body consisting of a ball of spores perched on top of a 1-2 mm long cellular stalk (Fig. 1.1B). In the absence of sufficient O_2, or in the absence of PhyA, slugs fail to culminate into fruiting bodies, which reflects the existence of an O_2-checkpoint that the slug uses to monitor its location in the vertical column of the soil that it normally inhabits (13).

In order to examine whether the failure of *phyA*$^-$ slugs to culminate into fruiting bodies is associated with dysregulation of protein degradation, as might be expected based on evidence that Skp1 is the only PhyA substrate, developing *Dictyostelium* were treated with inhibitors of the proteasome, which mediates the degradation of proteins that are polyubiquitinated by SCF complexes. As shown in Fig. 1.2A, under ambient O_2, *phyA*$^-$ cells exhibit a ~2-h delay through the early phases of multicellular development, as represented on the vertical axis, and fail to progress past the finger/slug stage or produce the normal number of spores, as shown by the examples in Fig. 1.2B. However, in the presence of MG132 at a concentration (80 µM) above that which inhibits the proteasome in single *Dictyostelium* cells (34), a substantial fraction of slugs was found to progress to the fruiting body stage and produce spores (Fig. 2.1A, B), despite a 4-6 h delay in moving through the earlier stages of development. In contrast, parental *phyA*$^+$ cells were simply delayed by 4-6 h and were modestly compromised in spore production. In some trials, a greater induction of *phyA*$^-$ spores was observed at the lower concentration of 40 µM, whereas 20 µM MG132 had no noticeable effect and 160 µM MG132 resulted in a developmental blockade at the early streaming stage in both strains (data not shown). Though considerable variation was observed over the 16 independent trials where matching pairs of *phyA*$^-$ and *phyA*$^+$ were analyzed (Fig. 2.1C), increased and usually substantial spore formation by *phyA*$^-$ cells was consistently found at either 40 µM (left panel) or 80 µM (right panel) MG132. To investigate the specificity of the effect, two proteasome inhibitors that have distinct mechanisms (35-38) were tested. Similar findings regarding selective induction of sporulation of *phyA*$^-$ cells were observed over the range of 0.5-1.0 µM Bortezomib (Fig. 2.1B, D), and for 80 µM Carfilzomib (Fig. 2.1B, E).

Fig. 2.1. Effects of proteasome inhibitors on developmental progression

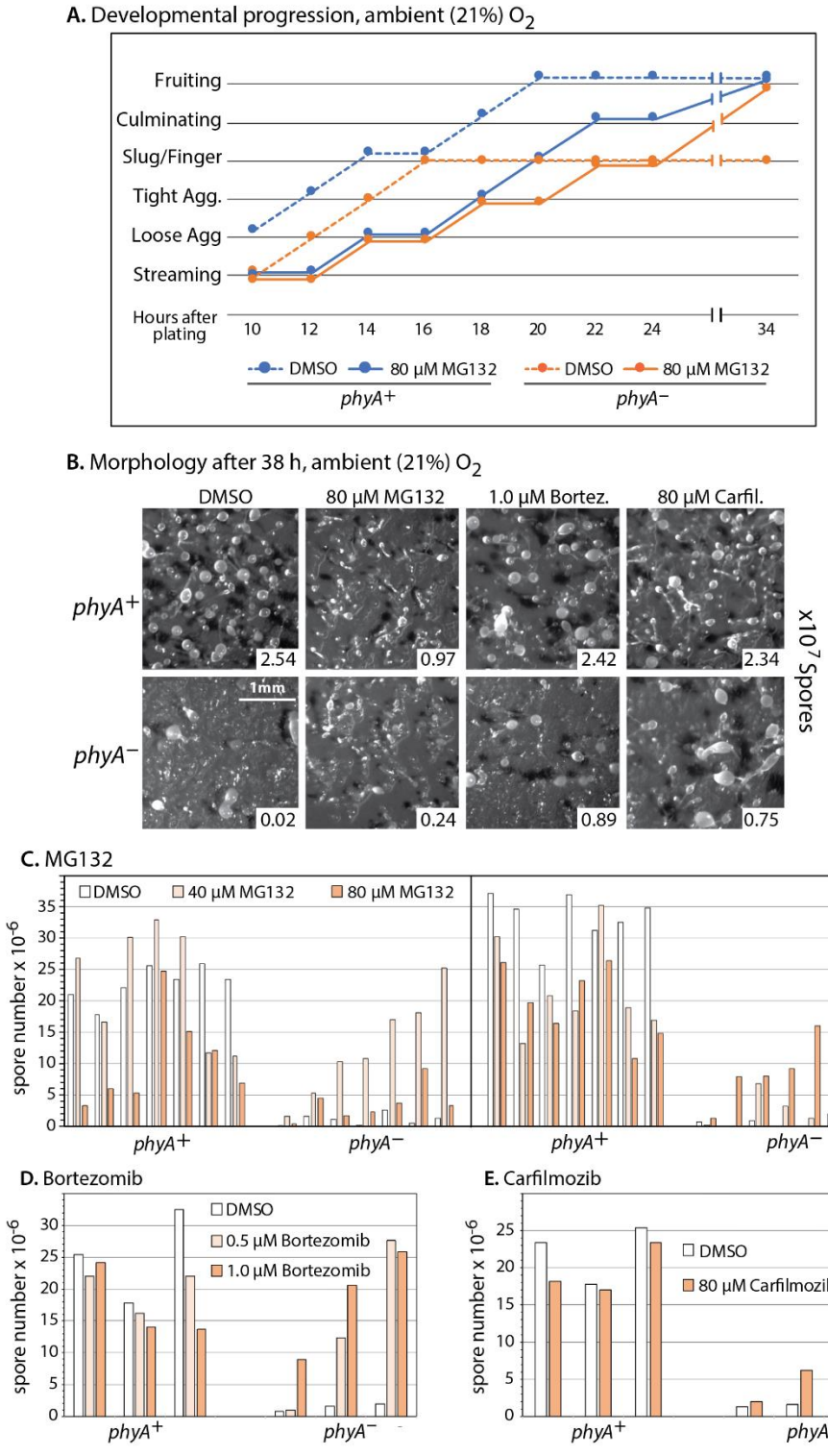

Fig. 2.1. Effects of proteasome inhibitors on developmental progression. Amoebae (*phyA*$^+$ or *phyA*$^-$) were spread on filters in the presence or absence of the indicated concentrations of inhibitors or an equivalent volume of the carrier solvent (DMSO), and allowed to develop. *A,* morphology, observed at 2 h intervals starting at 10 h, was graphed as a function of time. *B,* representative images of morphologies after 38 h in the presence of the indicated concentrations of inhibitors. The spherical structures represent the spore-containing sori of fruiting bodies. Spore counts from the represented trials are shown in the inset. *C-E,* quantitation of spore numbers from all trials. Results from all independent trials are shown, and graphed in increasing order of spore numbers produced by inhibitor-treated *phyA*$^-$ cells. *phyA*$^+$ cells from same trials are at the left in matching order. *C,* trials using 80 µM Carfilzomib. *D,* trials using 40 µM and 80 µM MG132. *E,* trials using 0.5 µM and 1.0 µM Bortezomib. Trials where maximal spore formation occurred at 40 µM or 80 µM MG132 are in separate panels.

Fig. 2.2. Effects of proteasome inhibitors on protein polyubiquitination

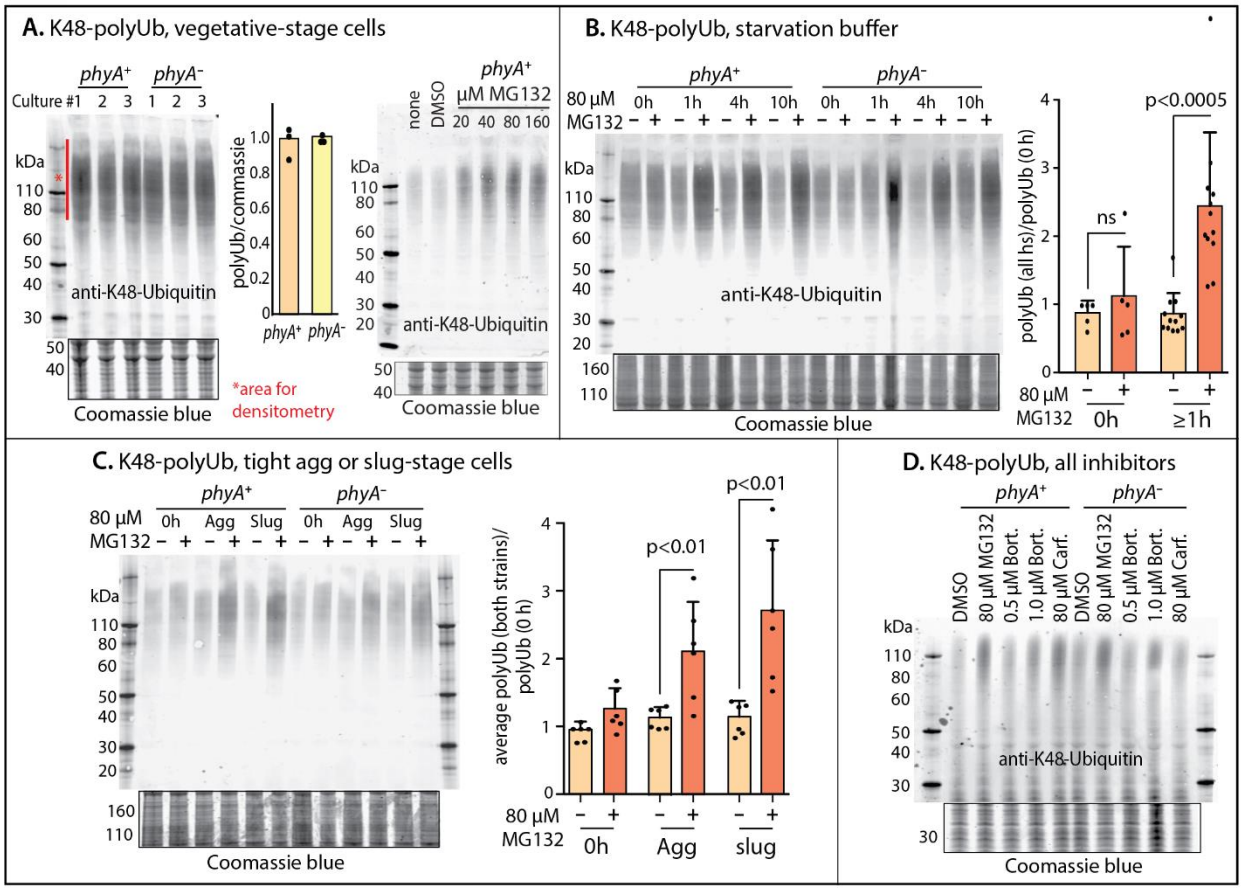

Fig. 2.2. Effects of proteasome inhibitors on protein polyubiquitination. Cells were treated with the indicated concentrations of proteasome inhibitors and analyzed by whole cell Western blotting using anti-K48-polyubiquitin (polyUb). Densitometry was performed on the indicated regions and normalized to the Coomassie blue stain intensity of the gel after electro-transfer. *A,* comparison of *phyA+* and *phyA*$^{-}$ vegetative cells. The quantitation shows the average ±S.D. of 3 independent trials. *B,* comparison of effects of 80 µM MG132 on cells shaken in starvation buffer over 10 h. For statistical analysis, time points ≥1 h were averaged. *C,* similar analysis of cells starved at an air-water interface, which allows development to the tight aggregate stage (10 h) or slugs (14-16 h, based on morphology). Paired t-tests were used to determine the significance of differences between pooled data from treated and untreated samples. *D,* comparison of the effects of three proteasome inhibitors, after incubation up to the slug stage of development.

The similar findings from all 3 compounds suggest that the rescue is the result of proteasome inhibition rather than off-target effects. To provide further evidence for this interpretation, extracts were evaluated for effects on protein polyubiquitination by Western blotting with antibodies against Ub, or specific for chains of Ub linked via K48 of the underlying Ub. These Abs revealed a relatively high level of binding to a higher apparent M_r region of the gel, which is elevated in cells treated with the inhibitors. The level of this labeling was similar between *phyA*$^+$ and *phyA*$^-$ cells grown vegetatively (Fig. 2.2A) or as slugs (data not shown). When cells were starved in non-nutrient buffer, 80 µM MG132 rapidly increased polyubiquitin levels in a fashion that plateaued by 1 h and was sustained for at least 10 h (Fig. 2.2B). A similar finding was observed in *phyA*$^+$ slug cells, and elevated poly-K48-Ub levels were also detected using 0.5 and 1.0 µM Bortezomib and 80 µM Carfilzomib (Fig. 2.2C-D). Lower concentrations (<40 µM for MG132) did not yield a detectable increase (not shown). Thus, the concentrations of inhibitors that caused increased steady state levels of poly-ubiquitinated proteins correlated approximately with concentrations that rescued development of *phyA*$^-$ cells. However, no reproducible differences in polyubiquitin levels were detected for untreated or treated *phyA*$^-$ and *phyA*$^+$ cells, suggesting that rescue might have resulted from effects on specific targets that were obscured at the level of the entire population.

The Skp1 interactome of vegetative (proliferating) amoebae

A previous mass spectrometry-based proteomics study of the Skp1 interactome in slugs (20) identified 18 candidate proteins and showed that the representation of several was influenced by PhyA (Table 2.1). These proteins are therefore candidates for mediating the role of PhyA, and for the rescue of *phyA*$^-$ cells by the proteasome inhibitors. However, that study did not

address the potentially dynamic nature of the Skp1 interactome, was limited to the use of a single method to immunoprecipitate Skp1, and did not address the basis for differential representation of proteins in *phyA*$^{+}$ vs. *phyA*$^{-}$ cells.

As a first step in expanding our understanding of the Skp1 interactome, we applied our previous co-IP method to vegetative cells. This method used an affinity-purified anti-Skp1 antiserum (pAb UOK77) and proteomic analysis of the captured material by nLC/MS-MS and quantitation by spectral counting (20). We analyzed three strains, the normal parental strain (Ax3), and two derivatives that overexpress either His_6AgtA or $FLAG_3$AgtA, the terminal Skp1 glycosyltransferase (38). Since the data profiles were indistinguishable, indicating negligible influence of AgtA-overexpression, the samples were analyzed together as biological replicates.

Thirty two proteins were confidently assigned to the Skp1 interactome of vegetative cells (summarized in Fig. 2.3-6 and Table 2.1 for details), based on the following criteria: i) ≥2 peptides from the protein were confidently assigned; ii) peptides and proteins were each detected at a false discovery rate set at 1%; iii) peptides were detected in the Skp1 co-IPs at a level that was ≥4-fold higher than in co-IPs using a non-immune rabbit IgG, based on analysis of 3 technical replicates from each of 3 independent biological replicates with a Wilcoxon p-value of <0.01. Candidates were further filtered to remove mitochondrial, ribosomal, and secretory proteins, and other common contaminants (see Methods).

To complement these findings, we developed an orthogonal capture method by expressing a C-terminally myc-tagged version of Skp1 under a semi-constitutive promoter (discoidin 1γ) and recovering complexes with an anti-myc murine monoclonal antibody covalently coupled to beads that were collected magnetically rather than centrifugally to reduce

non-specific binding. Western blotting showed that Skp1-myc was expressed at a level comparable to that of native Skp1 (39), thus doubling the total level of Skp1 in the cell. The anti-myc approach identified 42 high confidence candidates in vegetative cells, seven of which overlapped with those from the UOK77 co-IP (Fig. 2.7B; Table 2.1). The expected SCF subunits, CulE, CulA (Cul1 homologs) and Rbx1, were identified in the anti-myc but absent in the UOK77 co-IPs, suggesting that the myc-tag method was capturing a distinct though partially overlapping set of Skp1 subcomplexes. Combining the results, 67 interactors were identified in vegetative cells (Fig. 2.7B). Their mean relative abundances, summed from peptide counting (40), ranged over 500-fold (Fig. 2.4). This range might reflect their relative cellular levels, the fraction that interacts with Skp1, the number of tryptic peptides in the protein, and/or the stability of the interaction with Skp1, which may be direct or indirect. However, there was little overall correlation between transcript levels and representation in the Skp1 interactome (Fig. 2.4, Table 2.1).

The Skp1 interactome differs between vegetative and slug cells

Only six of the 32 vegetative stage proteins detected using UOK77 had been observed in the previously published slug stage interactome, which identified 18 interactors (20). This suggested that the interactome of Skp1 is dynamic with respect to developmental progression. To assess the generality of this interpretation, the interactome of slug stage Skp1-myc was examined. 35 interactors were identified at a threshold of 1% FDR (Table 2.1). Of the total of 35 candidate interactors, 6 were shared with the UOK77 slug Skp1 interactome (Fig. 2.7E). As for vegetative cells, the largely non-overlapping sets suggested separate subpopulations of slug Skp1 complexes captured by the orthogonal methods. This may reflect differential epitope

Fig. 2.3. Volcano plots of protein abundance ratios from experimental vs. control co-IPs, against statistical significance.

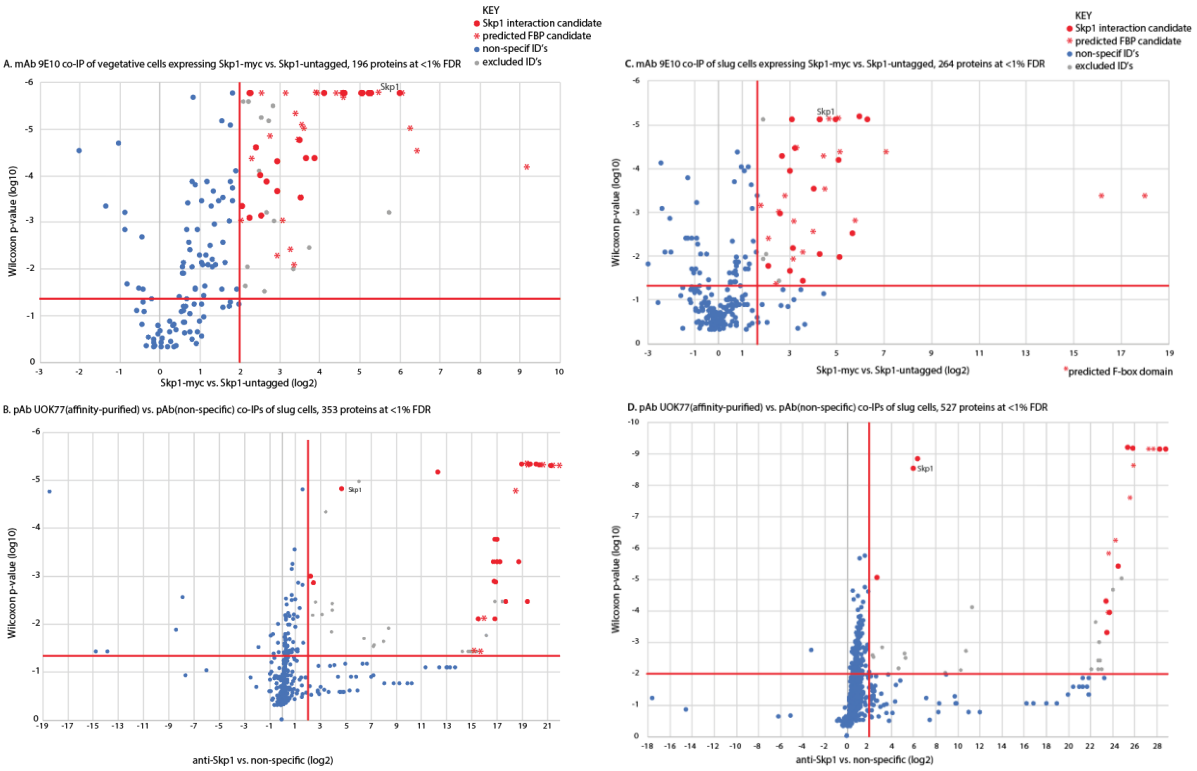

Fig. 2.3. Volcano plots of protein abundance ratios from experimental vs. control co-IPs, against statistical significance. *A,* average abundance values from reconstructed chromatograms from Proteome Discoverer 2.5 analyses of vegetative stage samples co-IPed with mAb 9E10 (anti-myc) from cells expressing Skp1-myc vs. controls were used to determine fold enhancement of proteins identified at an FDR <1%. These values were plotted vs. statistical significance based on pooled *phyA*$^{+}$ and *phyA*$^{-}$ samples (6 biological replicates × 3 technical replicates each) . Thresholds (red bars) were set at an enrichment ratio of 4 at t-test and Wilcoxon test p-values <0.05. Red symbols represent proteins that satisfy these criteria, and those with predicted F-box domains are represented as red asterisks. gray dots represent mitochondrial and ribosomal proteins, actin and actin binding proteins, secreted proteins and discoidins that were excluded from further analysis owing to their common high abundance in control pull-downs. 42 proteins were assigned as Skp1 interactors. *B,* same as in panel A, except comparing total spectral counts from co-IPs of control vegetative cells using pAb UOK77 (anti-Skp1) or non-immune rabbit IgG (3 biological replicates × 3 technical replicates each) were analyzed. 32 proteins were identified in this group. *C,* analysis of slug stage co-IPs using mAb 9E10 as in panel A. 35 proteins identified with an FDR <1% were detected in this group. D) Re-analysis of previously published (20) dataset of slug stage co-IP using pAb UOK77 at FDR <1%, collected as in panel B, with the current analysis protocol yielded 18 proteins. *UOK77 data was collected by Chris Schafer and Osman Sheikh.*

Fig. 2.4. Average abundances of Skp1 interactors.

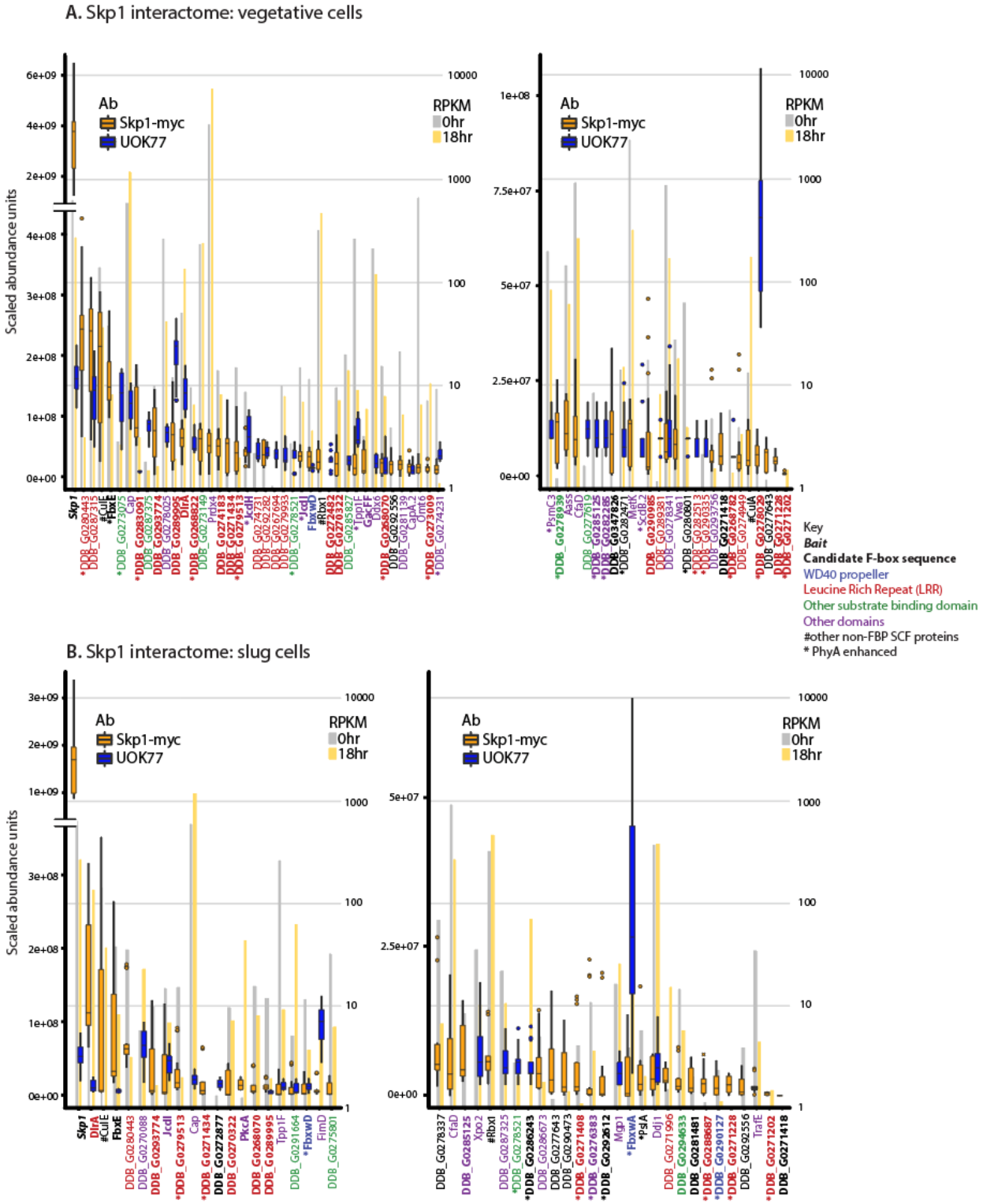

Fig. 2.4. Average abundances of Skp1 interactors. Proteins that satisfied criteria as Skp1 interactors (see Table 2.1 and Fig. 2.3) are quantified. *A,* average abundance values of proteins derived from reconstructed chromatograms of peptides from pooled *phyA*$^+$ and *phyA*$^-$ mAb 9E10 co-IPs from vegetative stage cells (6 biological replicates × 3 technical replicates each) are graphed in blue. Average scaled spectral counts pooled from *phyA*$^+$ and *phyA*$^-$ pAb UOK77 co-IPs from vegetative cells (3 biological replicates × 3 technical replicates each) were scaled to the mAb 9E10 values based on the average values for proteins detected in both samples, and are graphed in orange. Left and right panels show higher and lower abundance proteins. Protein candidate names are bolded, italicized or colored based on predicted characteristics as shown in the key. Candidates enhanced in *phyA*$^+$ samples are marked by an asterisk (see Fig. 2.3). RPKM values (58) at 0 h of development, equivalent to vegetative cells, are graphed in gray and 18 h or slug stage of development are graphed in yellow. *B,* same for slug-stage samples (6 biological replicates × 3 technical replicates each for mAb 9E10; data from (20) for UOK77). *UOK77 data was collected by Chris Schafer and Osman Sheikh.*

Table 2.1A Summary of Skp1 interactors

Accession (dictybase.org)	MW [kDa]	Veg. Score Sequest HT	Slug Score Sequest HT	Scaffold FDR	Description (dictybase.org)	Skp1 interactome – Vegetative (proliferating stage): Specificity anti-myc	p-value	Wilcoxon p-value	Specificity anti-Skp1	p-value	Wilcoxon p-value	Skp1 interactome – Slug stage: Specificity anti-myc	p-value	Wilcoxon p-value	Specificity anti-Skp1	p-value	Wilcoxon p-value
DDB0191107	18.7	13404	7308	<1%	Skp1	65.0	1.50E-09	1.78E-06	27.0	0.00E+00	1.55E-05	31.8	4.83E-07	7.88E-06	67.0	#######	3.24E-09
DDB0307223	65.0	195	163	<1%	DDB_G0274231	6.4	1.60E-02	6.37E-04	>100	3.84E-04	3.52E-03	22.3	4.84E-01	7.41E-02			
DDB0231647	22.9	976		<1%	Prdx4	15.1	1.19E-04	1.78E-06	0.3	4.17E-04	3.17E-02				1.8	1.25E-01	2.42E-03
DDB0302551	61.6	853			DDB_G0273149	11.4	4.47E-04	1.77E-05									
DDB0346673	68.5	548	326		DDB_G0292282	17.5	1.57E-04	1.78E-06				2.8	1.39E-01	4.79E-03			
DDB0230070	41.7	319	164	<1%	MetK	4.9	8.06E-04	1.78E-06	0.8	6.66E-02	1.03E-02	1.6	2.94E-01	2.56E-02	1.6	1.79E-01	3.20E-02
DDB0306747	102.3	263			Vwa1	24.4	3.66E-06	1.78E-06									
DDB0229909	25.8	193	319	<1%	Omt6	37.5	5.20E-07	1.78E-06				2.7	1.85E-02	2.52E-04	1.7	8.67E-01	1.65E-01
DDB0266498	35.3	182	1387		CapA-2	4.8	5.63E-04	8.49E-04				1.5	1.73E-01	4.79E-03			
DDB0237522	102.9	181	817	<1%	Aass	7.7	2.88E-03	5.08E-05	1.1	3.38E-01	4.88E-01	0.5	1.34E-01	6.14E-04	2.1	3.05E-01	5.12E-02
DDB0306982	36.0	140			DDB_G0281139	33.6	2.97E-07	1.78E-06									
DDB0185191	89.3	120	508		CulA	4.2	3.93E-03	4.75E-04				1.2	9.45E-01	3.20E-01			
DDB0307560	76.0	86			DDB_G0274949	5.8	7.21E-06	9.94E-05									
DDB0235385	125.6	81			DDB_G0293756	7.7	4.24E-06	2.22E-04									
DDB0235361	50.2	75		<1%	DDB_G0278341	14.7	1.67E-05	4.28E-05	1.4	3.46E-02	6.07E-03				2.6	7.84E-01	8.77E-03
DDB0232967	46.9	100	386	<1%	PsmC3	2.2	1.40E-01	3.86E-02	5.6	4.87E-03	1.44E-03	1.0	9.85E-01	4.31E-01	2.0	5.80E-02	1.12E-02
DDB0306383	31.2			<1%	DDB_G0285827				>100	1.00E-10	4.83E-06						
DDB0232249	23.7			<1%	DDB_G0278025				>100	1.14E-13	4.76E-06						
DDB0346933	116.3			<1%	DDB_G0287375				>100	1.00E-10	4.91E-06						
DDB0347953	65.7			<1%	DDB_G0274731				>100	1.00E-10	4.98E-06						
DDB0308330	66.7			<1%	DDB_G0267694				>100	1.00E-10	4.88E-06						
DDB0308012	66.9			<1%	DDB_G0279933				>100	1.00E-10	4.93E-06						
DDB0238336	90.1			<1%	ScdB-2				4.9	4.51E-03	1.03E-03						
DDB0346604	41.8			<1%	DDB_G0290335				>100	8.60E-03	1.77E-04						
DDB0305518	164.0			<1%	DDB_G0277619				>100	1.82E-02	1.77E-04						
DDB0349103	70.1			<1%	DDB_G0282513				>100	2.15E-02	5.27E-04						
DDB0306363	146.5			<1%	DDB_G0282471				>100	7.96E-02	5.16E-04						
DDB0349035	148.5			<1%	DDB_G0280801				>100	4.83E-02	5.21E-04						
DDB0237880	96.5			<1%	DDB_G0289381				>100	6.74E-01	8.01E-03						
DDB0234196	48.2			<1%	Ddx6				>100	2.18E-01	1.34E-03				1.9	7.30E-01	5.06E-02
DDB0302592	162.9			<1%	DDB_G0273075				>100	1.04E-01	3.51E-03						
DDB0306469	177.1			<1%	DDB_G0287315				>100	1.00E-10	5.11E-06						
DDB0214912	75.7	284	167	<1%	Tpp1F	3.6	6.28E-03	1.90E-04	>100	7.65E-01	8.14E-03	35.2	1.74E-01	1.08E-02	>100	1.27E-12	7.48E-10
DDB0266744	87.1	2007	1968		CulE	24.6	7.89E-06	1.78E-06				34.8	2.08E-02	6.56E-05			
DDB0306197	60.0	1757	1061		DDB_G0280443	24.0	6.67E-07	1.78E-06				8.7	5.98E-04	7.88E-06			
DDB0185174	177.7	244	72		DDB_G0292556	11.8	1.53E-03	8.44E-06				16.0	4.97E-02	2.87E-03			
DDB0229857	58.6	224	260		CfaD	39.0	1.83E-11	1.78E-06				12.0	3.32E-01	3.94E-02			
DDB0231276	12.1	130	84		Rbx1	5.3	1.06E-04	2.53E-05				8.4	3.12E-03	1.18E-04			
DDB0305490	154.0	74	84		DDB_G0277643	11.6	8.32E-04	3.02E-04				6.1	3.99E-02	1.02E-03			
DDB0191139	49.6			<1%	Cap				>100	1.00E-10	7.03E-06				88.6	1.78E-15	1.64E-09
DDB0230019	102.4			<1%	DDB_G0278521				>100	4.67E-05	5.21E-04				>100	5.80E-01	1.21E-04
DDB0232222	195.4		370	<1%	FimD							8.3	2.71E-02	1.18E-04	>100	1.00E-10	7.86E-10
DDB0229339	111.2		197	<1%	DDB_G0291664							9.1	2.03E-01	1.24E-02	>100	2.10E-09	6.93E-10
DDB0233279	44.3	230	252		DDB_G0275801	2.5	1.01E-01	6.69E-03				8.3	1.54E-01	2.28E-02			
DDB0309096	127.5		187		DDB_G0286673							9.5	3.27E-02	3.56E-05			

Accession (dictybase.org)	PhyA-dependence – Vegetative (proliferating stage): Enrichment in PhyA+ anti-myc	Simplify 1.5 fold enhanced Wilcoxon	PhyA enhnaced in all replicates	Enrichment in PhyA+ anti-Skp1	p-value	Wilcoxon p-value	PhyA enhnaced in all replicates	PhyA-dependence – Slug stage: Enrichment in PhyA+ anti-myc	Simplify 1.5 fold enhanced	PhyA enhnaced in all replicates	Enrichment in PhyA+ anti-Skp1	p-value	Wilcoxo n p-value	PhyA enhnaced in all replicates	FBP?: Substrate binding domain	Fbox	Other Domains: Predicted	RNAseq RPKM (ref. 58): 0hr	18hr
DDB0191107	1.3	3.2E-01	no	1.3	2.1E-01	7.6E-03	no	1.0	7.6E-01	no	1.4	3.7E-01	1.3E-01	no	NA	NA		630.0	267.9
DDB0307223	8.2	5.4E-04	yes	>100	0.0E+00	1.1E-03	yes								no*	no	PHD	9.4	1.1
DDB0231647	1.2	0.3227	no												no	no	thioredoxin peroxi	3324.0	7318.8
DDB0302551	3.0	5.2E-01	no												ARM*	no	importin α A	231.0	241.7
DDB0346673	1.7	1.4E-01	no												FNIP*	no		2.1	0.2
DDB0230070	1.1	0.3992	no												no	no	S-adenosylmethio	2367.8	314.1
DDB0306747	1.6	8.0E-02	no												no	no	VIT/VWFA	27.5	18.0
DDB0229909	1.0	4.8E-01	no												no*	no	Me-xferase	654.8	6.7
DDB0266498	2.5	8.0E-02	no												no	no	cAMP-BP	0.0	0.0
DDB0237522	0.8	0.2869	no												no	no	Lysine ketoglutara	145.5	61.3
DDB0306982	1.0	0.5204	no												no	no	lectin like	21.1	5.3
DDB0185191	0.6	8.0E-02	no												no	no	Cullin-1	13.1	172.5
DDB0307560	1.0	3.6E-01	no												FNIP	no		3.9	3.4
DDB0235385	0.4	1.9E-02	no												no	no	Zn finger	4.9	1.6
DDB0235361	1.4	0.4392	no												no	no	ATP citrate syntha	860.7	170.1
DDB0232967				4.0	1.9E-03	2.2E-03	yes								no	no	proteasome	200.8	85.0
DDB0306383				0.8	4.8E-01	1.5E-01	no								TPR	no		19.9	14.0
DDB0232249				1.1	5.2E-01	3.5E-01	no								no	no	villin headpiece	265.2	41.2
DDB0346933				1.3	2.1E-01	1.3E-02	no								no	no		1.8	1.5
DDB0347953				1.2	3.4E-01	1.2E-01	no								FNIP	no		2.2	0.1
DDB0308330				0.9	9.8E-01	4.1E-01	no								FNIP	no		1.1	0.1
DDB0308012				1.0	7.8E-01	4.7E-01	no								FNIP	no		10.1	7.9
DDB0238336				2.6	1.3E-03	1.1E-03	yes								no	no	FA desaturase	0.0	0.0
DDB0346604				4.5	3.8E-03	3.2E-02	yes								FNIP	no		2.2	0.2
DDB0305518				1.6	1.5E-01	2.4E-01	no								Ankyrin*	no		1.7	0.6
DDB0349103				2.8	1.5E-02	6.6E-02	yes								LRR*	no		0.3	0.2
DDB0306363				2.5	1.9E-02	6.6E-02	yes								no	no		14.0	15.2
DDB0349035				3.0	6.3E-02	1.2E-01	yes								no	no		62.9	4.0
DDB0237880				5.8	1.3E-01	2.9E-01	no								FNIP	no		1.2	8.3
DDB0234196				1.8	2.1E-01	3.5E-01	no								no	no	DEAD	213.3	117.5
DDB0302592				>100	3.2E-09	1.1E-03	yes								ARM	no		2.9	2.7
DDB0306469				1.9	2.4E-02	4.3E-03	no								LRR	no		20.0	5.5
DDB0214912				>100	9.2E-06	7.6E-03	yes	2.1	0.2464	no	0.68	7.3E-01	2.2E-01	no	no	no	Peptidase	262.8	9.2
DDB0266744	1.6	4.8E-01	no					1.4	3.4E-01	no					no	no	Cullin	140.6	37.0
DDB0306197	1.8	4.1E-02	no					1.5	3.2E-01	no					LRR/fNip	no		35.5	3.2
DDB0185174	0.5	4.1E-02	no					1.3	4.8E-01	no					no*	no		3.9	0.2
DDB0229857	0.9	2.5E-01	no					2.1	3.6E-01	no					no*	no	Counting Factor-A	913.4	265.8
DDB0231276	0.9	3.2E-01	no					0.9	5.7E-01	no					no	no	RING	320.9	464.6
DDB0305490	0.9	3.2E-01	no					1.5	6.5E-01	no					no*	no		1.2	0.5
DDB0191139				1.0	9.7E-01	4.7E-01	no				0.98	7.7E-01	4.9E-01	no	no	no	cyclin associated	591.2	1182.2
DDB0230019				>100	1.0E-10	1.1E-03	yes				>100	3.4E-09	1.8E-05	yes	Ankyrin	no		2.8	2.1
DDB0232222								2.0	5.0E-01	no	1.0	6.1E-01	1.6E-01	no	no*	no	actin binding	0.1	8.7
DDB0229339								7.4	1.0E+00	no	1.4	2.2E-01	1.7E-01	no	Ankyrin	no	kinase	5.2	63.1
DDB0233279								1.1	4.4E-01	no					WWE	no	E3 function	32.4	6.3
DDB0309096								3.9	7.2E-02	no					no	no	Ub biosysnthesis	5.0	1.8

Table 2.1B Summary of Skp1 interactors

						Skp1 interactome										PhyA-dependence										FBP?		Other Domains	RNAseq RPKM (ref. 58)	
						Vegetative (proliferating stage)						Slug stage				Vegetative (proliferating stage)				Slug stage											
Accession (dictybase.org)	MW [kDa]	Veg. Score Sequest HT	Slug Score Sequest HT	Scaffold FDR	Description (dictybase.org)	Specificity anti-myc	p-value	Wilcoxon p-value	Specificity anti-Skp1	p-value	Wilcoxon p-value	Specificity anti-myc	p-value	Wilcoxon p-value	Specificity anti-Skp1	p-value	Wilcoxon p-value	Enrichment in PhyA+ anti-myc	Simplify 1.5 fold enhanced Wilcoxon	PhyA enhnaced in all replicates	Enrichment in PhyA+ anti-Skp1	p-value	Wilcoxon p-value	PhyA enhnaced in all replicates	Enrichment in PhyA+ anti-myc	Simplify 1.5 fold enhanced	PhyA enhnaced in all replicates	Enrichment in PhyA+ anti-Skp1	p-value	Wilcoxo n p-value	PhyA enhnaced in all replicates	Substrate binding domain	Fbox	Predicted	0hr	18hr
DDB0233520	16.4		145		DDB_G0278337							4.4	5.12E-01	1.79E-02											2.3	5.2E-02	no					no	no		68.1	6.7
DDB0308155	76.8		136		DDB_G0290473							9.0	1.44E-01	6.87E-03											4.0	1.8E-01	no					no	no		2.3	1.5
DDB0238607	105.8		94		DDB_G0271996							63.5	1.43E-05	6.65E-06											1.9	9.8E-01	no					LRR	no		1.5	15.2
DDB0191506	148.8		94		PsiA							51.3	5.55E-02	3.13E-03											16.6	3.0E-02	yes					no	no		5.7	2.1
DDB0306711	51.6	100	76		TrafE	3.5	1.10E-01	3.52E-04				6.5	3.14E-02	5.35E-05											1.7	3.2E-01	no					no	no	RING,TNF receptor	34.8	4.5
DDB0306611	61.2			<1%	DDB_G0270088										>100	1.00E-10	7.78E-10											0.94	7.0E-01	3.1E-01	no	no	no	ATPase	5.8	23.1
DDB0305914	108.1			<1%	Xpo2										>100	2.13E-02	4.15E-06											0.79	2.6E-01	3.3E-01	no	no	no	CSE1	35.2	10.3
DDB0238505	131.4			<1%	DDB_G0287325										>100	8.95E-01	5.38E-04											0.59	6.8E-01	3.3E-01	no	no	no	EGFR substrate	21.8	10.7
DDB0233877	102.3			<1%	Mgp1										>100	4.71E-01	5.41E-05											1.1	6.1E-01	3.8E-01	no	no	no	RhoGAP	16.2	25.5
DDB0215016	45.7	257	167	<1%	Ddj1	1.0	9.58E-01	3.16E-01	1.5	8.95E-01	2.24E-01	0.8	4.32E-01	2.85E-01	6.7	2.56E-03	9.42E-06											1.2	4.4E-01	2.7E-01	no	no	no	HSP	370.4	379.0
DDB0347150	49.5			<1%	DDB_G0268782				>100	1.66E-01	1.40E-03										>100	1.7E-05	1.1E-03	yes								LLR*	partial		5.8	1.4
DDB0238368	63.0	439	119	<1%	JcdH	5.9	1.73E-04	1.78E-06	>100	1.00E-10	5.06E-06	3.1	2.10E-01	8.35E-03				1.7	1.4E-02	no	2.9	2.4E-03	1.1E-03	yes								no	yes	JmjC	8.7	0.1
DDB0302572	52.5	138		<1%	DDB_G0283091	67.5	1.11E-07	1.78E-06	>100	1.00E-10	4.88E-06							2.5	1.0E-02	yes	1.1	7.5E-01	4.1E-01	no									FNiP	yes	coiled coil	14.6	3.2
DDB0238868	98.0	640	633		DDB_G0274183	11.2	1.09E-03	1.77E-05				2.5	8.02E-01	3.93E-01				1.8	4.0E-01	no													LRR	yes		14.2	8.2
DDB0233844	99.5	272	457		GacFF	12.3	1.01E-04	1.02E-05				2.5	1.85E-01	1.59E-02				1.3	9.7E-02	no													no*	yes	PH Rho-GAP	3.3	6.0
DDB0347829	77.5	219	379		DDB_G0347826	6.7	1.57E-03	1.47E-05				3.8	1.91E-01	1.24E-02				0.8	2.5E-01	no													no	yes		3.7	0.6
DDB0218123	59.6	210	206		DDB_G0278939	10.4	2.66E-02	8.42E-03				2.8	6.54E-01	3.53E-01				68.4	7.8E-05	yes													β-sheet*	yes		1.3	0.0
DDB0349441	65.8	200	366		DDB_G0273009	4.1	2.00E-03	9.77E-04				1.4	8.68E-02	4.42E-02				6.1	3.1E-04	no													LRR*	yes		7.3	10.5
DDB0347166	89.6	189			DDB_G0290985	5.0	1.03E-03	4.28E-05										1.1	4.0E-01	no													LRR*	yes		17.7	3.5
DDB0347759	56.7	77			DDB_G0278029	7.7	2.72E-01	5.29E-03										3.7	1.9E-02	yes													LRR*	yes		3.0	0.1
DDB0308175	115.1			<1%	DDB_G0268822				>100	1.63E-01	3.93E-02										>100	2.5E-03	9.0E-02	yes								LRR	yes		9.7	6.5
DDB0308449	72.6			<1%	DDB_G0272482				>100	2.22E-16	4.86E-06										0.8	7.5E-01	2.9E-01	no								FNiP	yes		0.8	0.1
DDB0237866	61.8			<1%	DDB_G0282285				>100	7.95E-01	8.01E-03										>100	1.8E-04	7.6E-03	yes								no	yes	ApaG	2.5	7..82
DDB0306343	89.1	2460	2320	<1%	FbxE	15.2	1.57E-06	1.78E-06	>100	1.00E-10	5.13E-06	20.0	4.38E-04	7.88E-06	>100	5.77E-01	1.21E-04	1.4	1.2E-01	no	2.0	1.6E-02	2.2E-03	yes	1.5	2.6E-01	no					no	yes		38.1	8.3
DDB0220015	89.5	1982	2920	<1%	DirA	8.9	4.82E-06	1.78E-06				79.3	1.86E-04	7.88E-06	>100	6.89E-11	2.58E-09	0.9	3.2E-01	no					1.2	8.9E-01	no	0.9	4.1E-01	5.6E-02	no	LRR	yes	PHD	51.2	134.0
DDB0306685	51.0	803	339	<1%	DDB_G0289995	44.9	2.71E-04	1.78E-06	>100	1.00E-10	5.11E-06	3.5	1.10E-02	7.28E-04	>100	3.26E-02	1.55E-06	1.5	2.5E-01	no								1.0	4.4E-01	4.9E-01	no	FNiP	yes		12.0	2.0
DDB0238369	115.8	734	625	<1%	JcdI	24.1	1.84E-04	1.78E-06	>100	1.00E-10	5.08E-06	11.5	2.09E-01	6.00E-02	>100	1.00E-10	7.78E-10	1.9	4.1E-02	no	1.2	2.7E-01	9.0E-02	no				0.67	1.9E-01	5.6E-02	no	no	yes	JmjC	14.8	7.0
DDB0306754	60.5	375	235	<1%	FbxwD	21.2	4.67E-05	1.78E-06				22.4	3.87E-02	5.36E-05	>100	4.41E-08	2.68E-08	1.3	3.6E-01	no					11.1	2.0E-03	yes	2.6	1.2E-03	4.3E-03	yes	WD40	yes	RING	11.6	3.7
DDB0307389	54.3	154	217	<1%	DDB_G0268070	9.7	9.47E-04	4.15E-03	>100	2.93E-07	1.76E-05	34.9	1.15E-05	7.42E-06				0.7	1.9E-01	no	7.0	3.6E-04	2.2E-03	yes	1.8	3.6E-01	no					LRR	yes		15.7	8.1
DDB0347879	56.7	642	657		DDB_G0293774	12.8	2.01E-03	4.28E-05				19.8	1.66E-01	9.54E-03				3.3	4.0E-01	no					1.2	1.5E-01	no					LRR/TNip	yes		9.9	1.7
DDB0306918	67.4	557	585		DDB_G0279513	24.4	9.17E-04	2.18E-06				7.2	1.28E-02	4.33E-04				6.7	7.8E-05	yes					5.2	2.8E-03	yes					LRR	yes		15.1	2.0
DDB0348534	75.0	469	449		DDB_G0271434	8.5	1.59E-02	9.77E-04				35.3	3.10E-02	4.37E-05				2.2	8.0E-02	no					4.2	7.2E-02	yes					LRR	yes		1.6	0.1
DDB0307778	77.4	271	92		DDB_G0271418	10.5	1.81E-03	4.77E-06				>100	2.38E-01	4.41E-04				0.9	0.3992	no					1.8	0.3299	no					no	yes		0.0	0.0
DDB0348450	73.9	260	236		DDB_G0271228	77.1	5.67E-09	1.02E-05				12.0	2.27E-01	8.47E-03				1.3	2.2E-01	no					7.3	1.5E-01	yes					LRR*	yes		0.8	0.7
DDB0238672	81.7	210	273		DDB_G0270322	86.7	1.59E-05	3.02E-05				138.7	2.03E-02	4.36E-05				1.3	4.0E-01	no					1.4	4.0E-01	no					LRR	yes		9.8	7.2
DDB0346829	72.7	99	95		DDB_G0271202	586.2	1.39E-04	7.12E-05				>100	1.47E-01	4.41E-04				2.0	0.09744	yes					7.1	0.05465	yes					LRR	yes		0.9	1.5
DDB0237864	62.4		71	<1%	DDB_G0285125				>100	1.39E-01	3.94E-02	25.9	5.38E-04	7.79E-06							>100	4.3E-03	9.0E-02	yes	2.6	5.6E-02	no					no*	yes	xmembrane	8.5	0.9
DDB0231197	152.4		406		PkcA							9.8	7.70E-03	3.56E-05											1.8	6.3E-01	no					no	yes	kinase	1.3	43.6
DDB0348609	75.6	187	293		DDB_G0271408	2.1	3.15E-01	8.42E-03				9.3	1.79E-02	1.65E-03											2.7	2.0E-01	yes					LRR*	yes		4.1	1.1
DDB0346681	59.5		153		DDB_G0292612							56.0	7.40E-03	1.59E-03											34.4	4.4E-03	no					no*	yes		0.9	0.1
DDB0306232	231.0		142		DDB_G0276383							5.5	3.22E-01	4.65E-02											44.2	9.3E-04	yes					no	yes	vWFA, RNA bindin	10.8	3.6
DDB0347353	69.2		84		DDB_G0288687							23.0	1.28E-02	3.09E-04											11.3	5.5E-02	yes					LRR	yes		1.2	0.7
DDB0234172	112.2		79		DDB_G0294633							6.2	3.12E-02	1.09E-03											1.5	9.4E-01	no					Ankyrin	yes		14.7	5.8
DDB0308058	61.4		71		DDB_G0281481							4.4	7.37E-03	4.05E-03											4.1	4.4E-01	no					no	yes		2.1	0.6
DDB0185042	142.3		99	<1%	FbxwA							12.7	8.19E-01	3.84E-01	>100	1.00E-10	7.81E-10											2.4	3.9E-03	9.7E-03	yes	WD40	yes		3.9	48.4
DDB0306262	61.7			<1%	DDB_G0272877										>100	2.85E-01	8.06E-03											0.20	3.8E-01	4.7E-01	no	no	yes		1.3	0.7
DDB0305126	116.8			<1%	DDB_G0286243										>100	4.53E-03	5.94E-07											3.2	3.7E-04	9.7E-03	no	no	yes		0.8	69.6
DDB0237770	73.6		76		DDB_G0290127							16.6	4.36E-04	1.08E-03											4.0	0.5377	yes					WD40	yes		2.4	1.2

Indicates identification below interactor threshold

reliably detected in one experiment

Indicates significant enrichment in PhyA+

Indicates inconsistent enrichment in PhyA+ between Abs

*assessed by Swiss Model homology modeling

Table 2.1. Summary of Skp1 interactors. The average fold-enrichment of proteins, based on the sum of their peptides quantitated in co-IPs with Skp1 or Skp1-myc, relative to control co-IPs, are listed for all identified proteins. Those with an enrichment ratio of greater than 4 at p-values (t-test and Wilcoxon) of <0.05 and are classified as Skp1 interactors. Statistical significance is based on 3 biological replicates with up to three technical replicates each. Sequest scores and FDR values (depending on data processing method) indicate confidence of protein assignments. Interactors that satisfied the above criteria, but fell under the category of common background/IP artifact proteins were excluded from the list of interactors. The common background proteins are as follows; mitochondrial and ribosomal proteins, actin and actin binding proteins, secreted proteins, and discoidins. Data where the two co-IP methods yield inconsistent results regarding candidate identification for the same stage are shaded in gray. Skp1 interactor candidates are grouped from top to bottom according to their detection at the vegetative stage, both stages, or slug stage only. Within groups, candidates are clustered according to method of detection and generally from highest to lowest confidence (top to bottom). The relative enrichment of proteins in w/t (*phyA*$^{+}$) vs. *phyA*$^{-}$ strains is indicated in the middle columns, and those whose enrichment is ≥1.5 with statistical significance of p<0.05 are shaded in green. Additionally, candidates enriched 1.5 fold in w/t co-IPs in pairwise comparisons of w/t vs. *phyA*$^{-}$ in all three biological reps are shaded in green. Columns to the right-hand indicate the predicted presence of F-box, substrate receptor, and other domains based on sequence analysis and structure modeling. The right-hand columns indicate transcript abundance at the vegetative and slug stages from ref. 58. See Fig. 2.3 for 2-D volcano plots illustrating the distribution of enrichment ratios and statistical significance relative to control co-IPs, Fig. 2.7 for

volcano plots for enrichment in *phyA*$^{+}$ vs. *phyA*$^{-}$ cells, and Fig. 2.4 for graphing of statistically significant interactors according to relative abundance.

Fig. 2.5. Alignment of predicted F-box domain sequences found in Skp1 interactors.

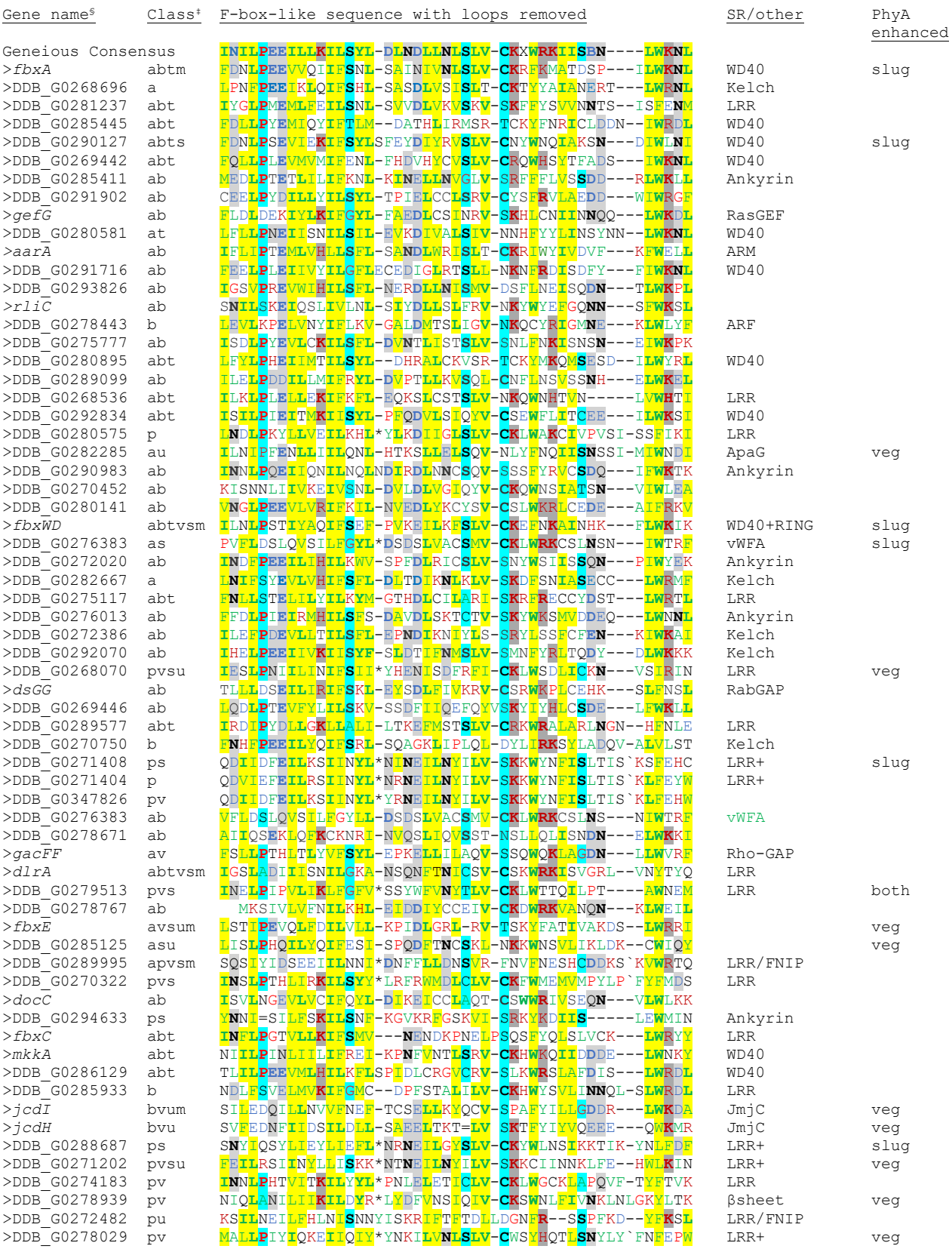

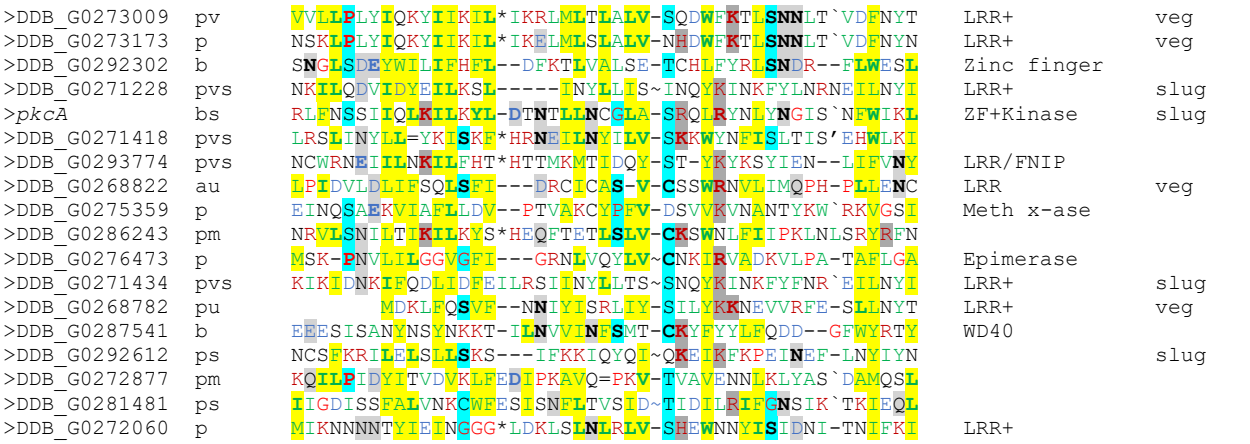

§ dictybAse.org
+ Domain determined by Swiss Model

†Key
a F-box annotated in Uniprot (December 2021)
b F-box sequence predicted by BLASTp searches in dictyBase.org
p F-box sequence predicted in Skp1 interactors using Geneious
t F-box training set
v Found in mAb 9E10 vegetative co-IP
s Found in mAb 9E10 slug co-IP
u Found in pAb UOK77 veg co-IP
m Found in pAb UOK77 slug co-IP (20)

SR = substrate receptor-like

Loop between helix 1 & 2
*DDB_G0280575-pv
(NDEYSSCSGVANTKPQNPFFHNNCYSDQMTNGKDGQDKKQKQCLKNSSSIVNNKPIPASAEPVAATTNNSNNNNNNNQPIIVSQTSSTCV)
*DDB_G0276383-s (L)
*DDB_G0268070-pv (SDE)
*DDB_G0271408-pv (LINKKNNNNNNNTSNQYKINKFYF)
*DDB_G0271404-p (LISKKKKKNNNYNTSSQYKINKFYL)
*DDB_G0347826-pv (LTSKKNKNKNNNLNNNTINIYKINKFYF)
*DDB_G0279513-pvs (NKINS)
*DDB_G0289995-pvs (VI)
*DDB_G0270322-pv (YNHCLSMYEYIEKSKGSQFSGYK)
*DDB_G0288687-ps (LVNKKLKKINKKTLLK)
*DDB_G0274183-pv
(IENKVDLEKSEIRFSGSPEGESASNNGSNNNGQLSMSGGSSGSDGGSPLGSSLLNSLNNSGSNSGNGIIVKKN)
*DDB_G0271202-pvsu (NKNNNN)
*DDB_G0278029-pv (CLHYFNVKKILNHKEKRR)
*DDB_G0273009-pv (CRYID---KNNKSINCVIDDYRGNESQ)
*DDB_G0273173-pv (CKHIDRNNKLIDSIRYMDIDYRDNEKL)
*DDB_G0278939-pv (LKSLSHNE)
*DDB_G0293774-pv (RLFNV)
*DDB_G0286243-m (IKLSLLDNT)
*DDB_G0271418-pvs (YL)
*DDB_G0272060-pv (EIDFI)

Loop between helix 2 & 3
~DDB_G0271228-pv (KNNK----TNYNNT)
~DDB_G0276473-ps (EQKC)
~DDB_G0271434-pv (KKNKKKNSTNNSNT)
~DDB_G0292612-pv (SNQ)
~DDB_G0281481-ps (LDPPKQRT)

Loop between helix 3 & C-terminus
`DDB_G0271408-pv (NNIINN)
`DDB_G0271404-pv (NNIINN)
`DDB_G0347826-pv (NNIINN)

```
`DDB_G0289995-pvs      (NIFY)
`DDB_G0270322-pv       (NT)
`DDB_G0278029-pv       (YCIQ---D)
`DDB_G0273009-pv       (VS)
`DDB_G0273173-pv       (VS)
`pkcA-s                (MEKKTFS)
`DDB_G0275359-pv       (TMQE)
`DDB_G0271418-pvs      (NNIINNKSF)
`DDB_G0271434-pv       (NE)
`DDB_G0268782-pv       (DRE)
`DDB_G0272877-m        (ISVS)
`DDB_G0281481-ps       (NNN)

Extra residues in helix
=DDB_G0294633-ps       (NNNNNNNNNNNENDDKN)
=jcdH-vu               (MN)
=DDB_G0271418-pvs      (INKTNNNNNNNN)
=DDB_G0272877-m        (SS)
```

Fig. 2.5. Alignment of predicted F-box domain sequences found in Skp1 interactors. An alignment of 83 F-box sequences predicted based on global BLASTp studies (class b) or from sequences of Skp1 interactors (this study) searched using a Geneious pair-wise alignment algorithm relative to a training set of 17 confident F-box domain sequences (class p or t) (See Methods for details). Loops and inserts were removed in the alignment shown but are noted below. To facilitate visualization of relatedness, acidic residues are in blue, basic in dark red, Gly and Pro in red, and hydrophobic in green, as previously described (86). Positions possessing related chemical characteristics are highlighted in yellow (hydrophobic), gray (acidic), dark grey (basic), or teal (small). Residues identical to the consensus sequences are bolded. Sequences are ordered from high to low similarity to FbxwA. See Fig. 2.6 for a similarity matrix.

Fig. 2.6. Similarity of *Dictyostelium* F-box-like sequences

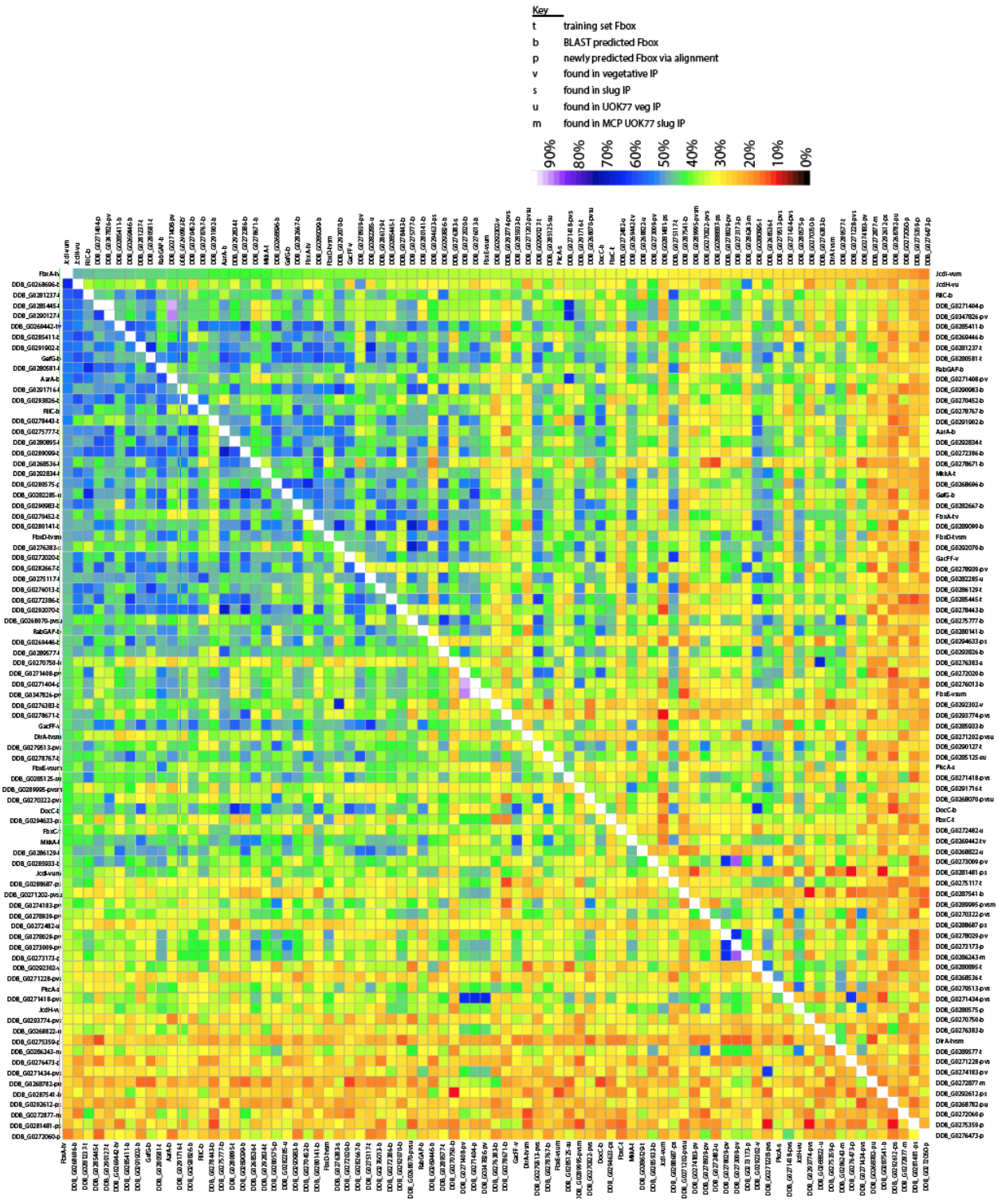

Fig. 2.6. Similarity of *Dictyostelium* F-box-like sequences. *A*, the similarity of F-box-like sequences found in the Skp1 interactome from this study, and an additional group obtained by BLASTp-based searches of the *D. discoideum* genome, are rendered as heat maps as implemented in Geneious. The map to the lower left of the diagonal compares sequences to FbxwA, and the map to the upper right shows their similarity to the divergent F-box sequence of the FBP JcdI (Fbxo13). *B*, a graphical comparison of relative similarity of the F-box-like sequences to F-box sequences from FbxwA and JcdI. The sequences are ordered from most to least similar from top to bottom, and the lines connect the same sequence from each list.

Fig. 2.7. Dependence of the Skp1 interactome on cell differentiation and Skp1 modification

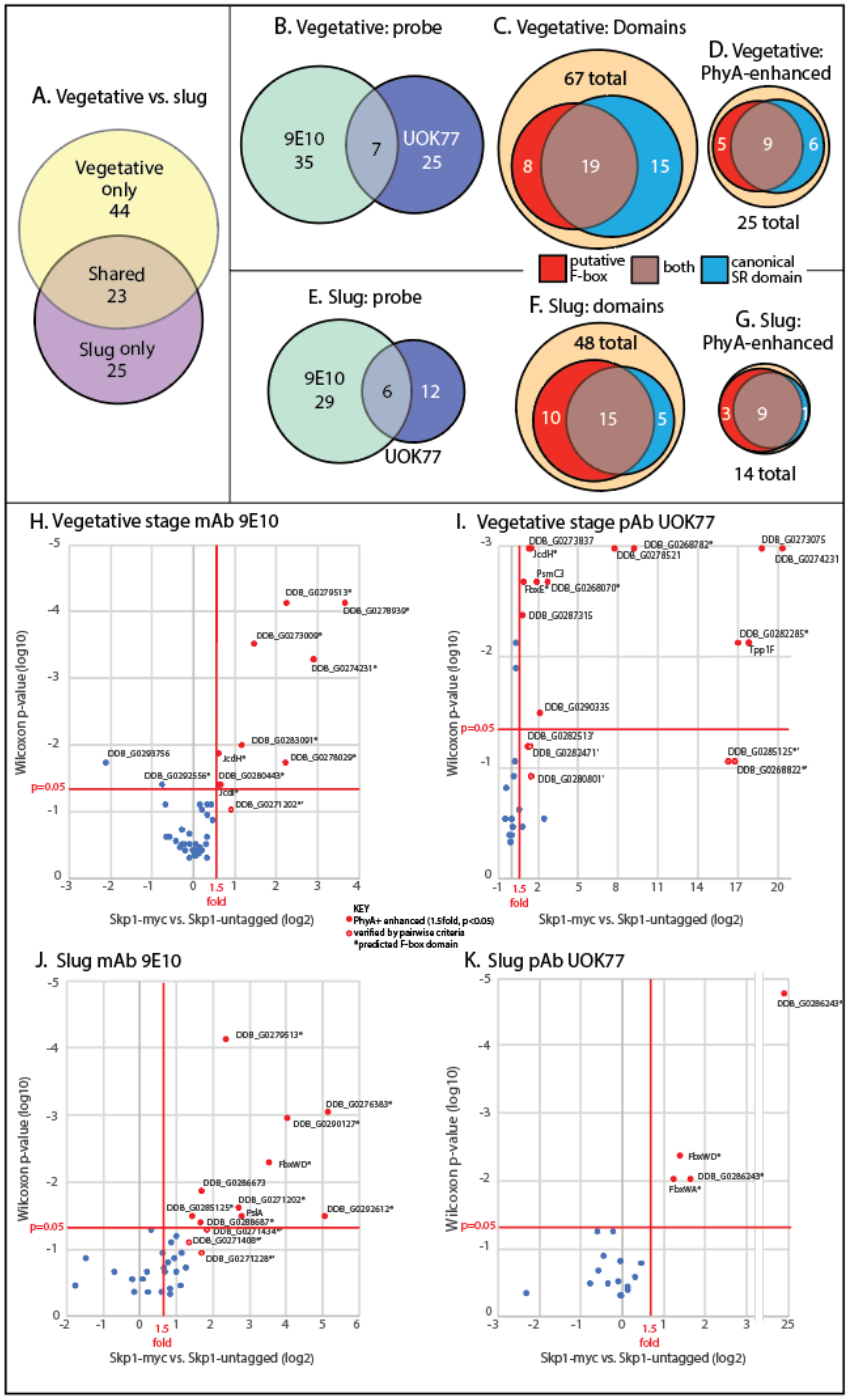

Fig. 2.7. Dependence of the Skp1 interactome on cell differentiation and Skp1 modification. The Skp1 interactome was assessed by co-IP with anti-myc (mAb 9E10) from cells expressing Skp1-myc, or with anti-Skp1 (affinity-purified pAb UOK77) from strains lacking a tagged Skp1, and captured proteins were detected and quantified by label-free proteomic analysis. Proteins that were enriched relative to a statistically significant extent over control co-IPs (un-tagged Skp1 for mAb 9E10, and non-specific IgG for pAb UOK77), as summarized in Table 2.1 and Figs. 2.3 and 2.4, are classified according to life cycle stage, the detection method, properties, and dependence on PhyA. *A*-*G*, Venn diagrams illustrate the overlap of results between the two life cycle stages (panel A), overlaps between the two antibodies (panel B for vegetative stage cells; E for slugs), fraction of interactors possessing predicted F-box and substrate receptor domains (panel C for vegetative cells; F for slugs), and fraction of the interactors shown in panels C and F that are enriched in *phyA*$^{+}$ vs. *phyA*$^{-}$ cells (panel D for vegetative stage; G for slug). *H*, Skp1-myc interaction candidates in vegetative cells were plotted according to fold-enrichment in *phyA*$^{+}$ vs. *phyA*$^{-}$ cells and statistical significance. Red data points represent interactors that were found at a 1.5-fold higher levels at t-test and Wilcoxon test p-values ≤ 0.05. Open red circles represent candidates determined to be *phyA*$^{+}$ enhanced by pairwise comparison criteria (Table 2.1). *I*, same for results from anti-Skp1 and vegetative cells. *J*, same as panel *H*, using slug cells. *K*, same as panel I, using slug cells. *UOK77 data were collected by Chris Schafer and Osman Sheikh.*

accessibility owing to structural differences among Skp1 complexes, and is consistent with the finding that 20-40% of all Skp1 was uncaptured by either method.

Of the 35 slug Skp1-myc interactors, only 17 were also detected in the vegetative cell Skp1-myc interactome (Table 2.1), paralleling the dynamic developmental regulation observed for the UOK77-captured subpopulation. Combining the anti-myc and UOK77 slug datasets, a total of 48 Skp1 interactors were described in slug cells at the single time point analyzed, and their relative representation inferred from peptides detected are summarized in Fig. 2.4B. Overall, the co-IP approaches together predict 92 Skp1 interactors. The majority of interactors were exclusive to one stage or the other (Fig. 2.7A). Given the long half-life (14 h) of *Dictyostelium* Skp1 during development (44), these changes likely involve exchange of Skp1 partners, potentially facilitated by chaperone-based mechanisms.

Sequence characteristics of Skp1 interactors

The interacting proteins included the formerly validated FBPs FbxwD (20) and FbxwA (41), which contain WD40 repeats that likely serve as substrate receptors, and the SCF subunits CulE, CulA, and Rbx1. The remaining hits were compared against a list of 54 proteins predicted to possess F-box like sequences based on reiterative unbiased BLASTp searches of the *D. discoideum* genome. Although these sequences were conserved in 5 other cellular slime molds, only 7 of them appeared in the current interactome of 92 proteins. The remaining hits were then examined for potential F-box sequences using an algorithm in Geneious guided by a training set of 17 predicted F-box sequences that were supported by the downstream presence of WD40- or LRR-like substrate receptor sequences (see Methods). Using these methods, 38 of the interaction candidates were predicted to possess an F-box-like sequence, if allowing for insertions between

the 3 predicted α-helices. A heat map of the similarity among these candidates reveals a high degree of variation relative to the sequence of the F-box of FbxwA (Fig. 2.6). To assess the significance of these differences, the heat map was recalculated using the relatively divergent F-box sequence of JcdI, validated below. Many of the predicted F-box sequences that were distantly related to the FbxwA F-box sequence were more closely related to the JcdI F-box sequence, and *vice versa*. However, some sequences were distantly related to both, so are more speculative. The interactor sequences were also searched for canonical substrate receptor domains, including Leucine-Rich-Repeat (LRR), WD40 β-propeller, and ankyrin repeats, using the NCBI Conserved Domain Database and Swiss Model (see Methods). Of the 38 interactors predicted to have F-box sequences, 24 possessed substrate receptor-like domains (Figs. 2.7C, F). An additional 18 interactors possessed substrate receptor-like sequences. Most predicted substrate receptor domains were LRRs, including the FNIP subclass common to *Dictyostelium* and Mimiviruses (43). Given the degeneracy of F-box domain sequences, we do not exclude the possibility that these 18 candidates may be divergent FBPs. Thus, more than 60% of the vegetative and slug Skp1 interactors show sequence features of FBPs. Significantly, as tabulated in Table 2.1, many of the 14 FBP-like proteins appear to have domains that lack substrate-receptor characteristics, consistent with the concept that some FBPs are actually independent proteins that possess F-boxes merely for regulating their turnover. 31 of the remaining proteins that lack any FBP features possess sequences indicative of other functions. Whether any of these proteins possess cryptic F-box sequences or are indirectly associated with Skp1 will require future study.

Dependence of the Skp1 interactome on PhyA

In the previous study of the interactome of slug Skp1, the representation of 3 of the 18 interactors was enhanced by the mutational deletion of enzymes that modify Skp1 (20). To address the generality of this effect, samples of *phyA*$^{-}$ cells, which are unable to glycosylate Skp1, were examined in parallel with the new Skp1 interactomes described above. After normalization of abundances to the total peptide signal, proteins with an average abundance ratio for *phyA*$^{+}$:*phyA*$^{-}$ of >1.5, at a Wilcoxon p-value < 0.05, or with pairwise averages of *phyA*$^{+}$:*phyA*$^{-}$ within all biological replicates of >1.5, were considered enriched in the Skp1 interactome when Skp1 could be glycosylated. Of the 67 vegetative Skp1 interactors, 25 showed enhanced representation in wild-type vs. mutant cells (Fig. 2.7D), and 14 of the 48 slug Skp1 interactors were similarly enhanced (Fig. 2.7G). In contrast, only two interactors were significantly enhanced (>1.5) in mutant cells, and only in the anti-myc vegetative cell co-IP (Table 2.1). Overall, 29-37% of Skp1 interactors from either co-IP methods (mAb 9E10 or pAb UOK77) and from either developmental stage exhibited increased representation when Skp1 was modified. A high proportion (80-93%), in both stages, possessed putative F-box or candidate substrate binding domains (Figs. 2.7D,G), suggesting a selective enrichment of FBPs. Two candidates, a WD40 domain containing F-box protein (FbxwD) whose representation was enhanced by Skp1 glycosylation in slug cells, and the JmjC-containing FBP JcdI, whose representation was enhanced in vegetative cells, were selected for further analysis.

Glycosylation dependence of the FbxwD/Skp1 interaction

FbxwD is an example of substrate receptor type of FBP whose representation in the Skp1 interactome was enhanced by PhyA in slug stage cells (Fig. 2.8, Table 2.1). Since increased

representation did not achieve significance in vegetative cells, it was unclear whether this was due to differential binding or to increased levels of FbxwD. A previous study suggested differential binding (20), but this was based on overexpression in prespore cells, which is not the cell type in which FbxwD is normally expressed. To verify this finding, FbxwD was epitope-tagged via modification of its genetic locus to examine the interaction of endogenous FbxwD with Skp1.

A double-crossover homologous recombination strategy was employed to insert cDNA for a C-terminal peptide extension that contains a triple-FLAG epitope followed by a floxed blasticidin-resistance cassette, which was subsequently excised by transient expression of Cre-recombinase, and confirmed by PCR. To examine the role of Skp1 modification, the *phyA* locus was subsequently disrupted as previously described (18). Western blotting with anti-FLAG Ab detected a novel band with an apparent M_r 70,000 in both strains, consistent with an expected M_r 68,430 (including the appended peptide). Tagging of the *fbxwD* locus did not have an apparent effect on growth rates in axenic medium or the morphology and timing of the developmental program.

Densitometry analysis of Western blots of whole cells indicated that FbxwD-FLAG was expressed at similar levels in *phyA*$^+$ (Ax3) and *phyA*$^-$ cells of either vegetative (Fig. 2.8A) or slug cells (Fig. 2.8B). This showed that increased representation in the Skp1 interactome of *phyA*$^+$ cells was not simply due to higher levels of FbxwD. Consistent with a previous study (44), the absence of PhyA also did not affect levels of Skp1 (Fig. 28). To verify the increased interaction between Skp1 and FbxwD in Skp1 co-IPs, the reciprocal co-IP was performed using anti-FLAG under conditions where essentially all FbxwD-FLAG was captured. Four-fold greater levels of Skp1 were recovered in *phyA*$^+$ vs. *phyA*$^-$ slug cells (Fig. 2.8B), consistent with previous findings

Fig. 2.8. Interactions of FbxwD with Skp1

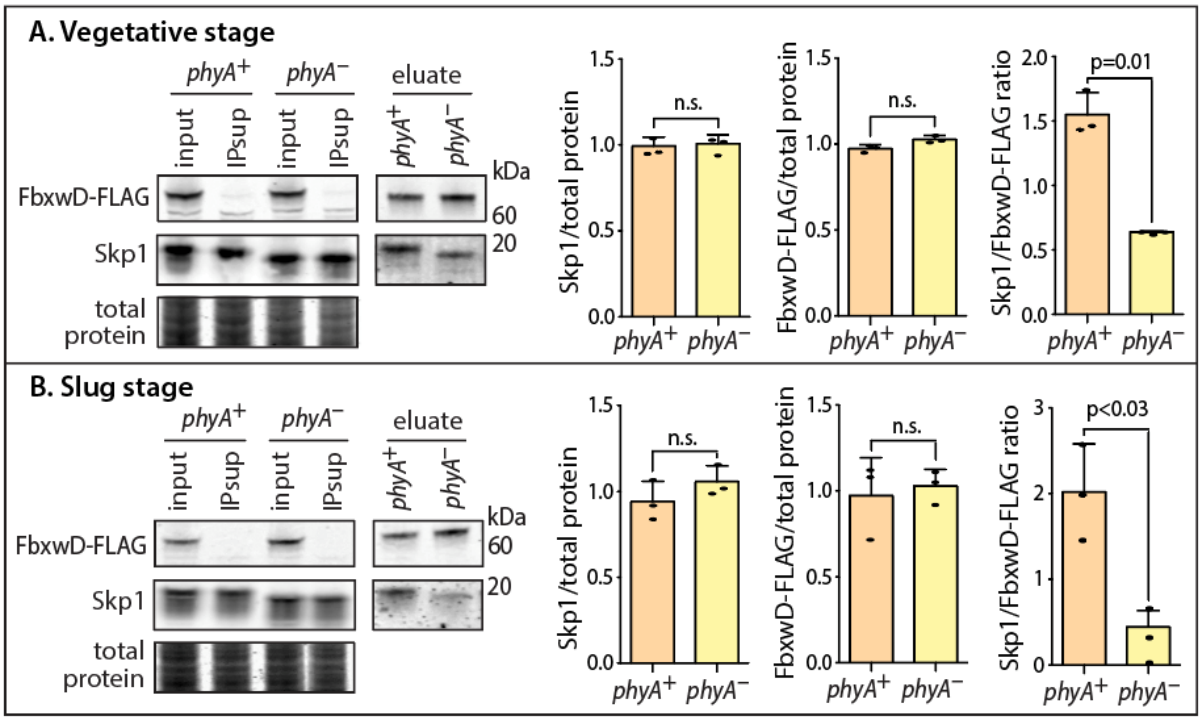

Fig. 2.8. Interactions of FbxwD with Skp1. The *fbxwD* locus was modified in *phyA*$^{+}$ and *phyA*$^{-}$ cells to append a C-terminal FLAG tag to the protein. *A,* FbxwD and Skp1 abundance were analyzed by Western blot analysis of whole cells solubilized in SDS using anti-FLAG for FbxwD-FLAG and pAb UOK77 for Skp1. Levels were quantitated by densitometry and normalized to Coomassie blue staining of the blotted gel. Note the more rapid gel migration of Skp1 from *phyA*$^{-}$ cells owing to absence of glycosylation. The average ratio of 3 independent trials ±S.D. are graphed. FbxwD-FLAG was IPed with mAb M2 under conditions where >90% of FbxwD-FLAG was captured, and analyzed similarly by Western blotting. The average ratio of co-IPed Skp1 relative to FbxwD-FLAG is graphed from 3 independent trials, ±S.D. *B,* similar analysis of FbxwD-FLAG and Skp1 from slug cells.

when FLAG-FbxwD was overexpressed in prespore cells (20). Unexpectedly, a lesser 2.5-fold increased representation of Skp1 was also observed in vegetative cells. The discrepancy between anti-Skp1 and anti-FbxwD co-IPs may be due to the differential efficiency of target capture. Since anti-FbxwD capture was greater than 90% vs. ~60% efficiency for anti-Skp1, the results suggest that differential representation resided in the subpopulation of Skp1 that was not captured by anti-Skp1. Given that recombinantly expressed FBPs are generally insoluble in the absence of Skp1, these findings suggest that, in *phyA*$^-$ cells, FbxwD is partially associated with alternative protein and unable to enter an SCF complex.

Glycosylation dependence of the JcdI interaction with Skp1

JcdI is an example of a potential FBP whose representation in the Skp1 interactome is not apparently affected by PhyA (Table 2.1), and in fact based on previous data (20) was suspected of having enhanced representation in *phyA*$^-$ slug cells. JcdI is a highly abundant interactor of Skp1 based on Skp1 co-IPs (Fig. 2.4), and the interaction is predicted to be direct, due to the presence of an F-box like sequence near its N-terminus (Fig. 2.9A, B). To confirm this, the JcdI coding sequence was modified to append an N-terminal 3×FLAG tag and with point mutations that abrogated binding of the FBP Ctf13, a yeast centrosomal protein, to yeast Skp1 (45). FLAG-JcdI and FLAG-JcdI(ARA), in which the motif VFxxF was changed to ARxxA, were overexpressed in *phyA*$^+$ and *phyA*$^-$ cells using an integrating plasmid. Clones expressed a novel FLAG-tagged protein that migrated as a closely spaced doublet with an apparent M_r of 120,000 based on SDS-PAGE (Fig. 2.9E), consistent with the predicted M_r of 122,000 of FLAG-JcdI. The biochemical basis for the doublet and minor anti-FLAG reactive lower M_r species (Fig. 2.12A) is not known. Clones that stably expressed similar levels of normal or mutant FLAG-JcdI were examined using non-ionic

detergent lysates in which JcdI was fully solubilized. As shown in Fig. 2.9C, substantial co-IP of FLAG-JcdI was observed in anti-Skp1 pulldowns, and of Skp1 in anti-FLAG pulldowns. In contrast, negligible interactions of Skp1 were observed with FLAG-JcdI(ARA). Furthermore, as described below, recombinant expression of a soluble form of JcdI in *E. coli* required co-expression with Skp1, and the two proteins formed a stable complex during chromatographic purification. Thus, the JcdI/Skp1 interaction appears to be directly mediated by the predicted F-box domain in JcdI, which is now also annotated as Fbxo13 owing to its lack of an obvious substrate receptor domain.

To further analyze the interaction of JcdI with Skp1, its locus was modified to encode a C-terminal FLAG tag as above for FbxwD, in *gnt1*$^+$ (Ax3) and *gnt1*$^-$ cells (44). *gnt1*$^-$ cells were used in place of *phyA*$^-$ cells owing to an incompatibility in selection markers. Though the *gnt1*$^-$ strain allows for 4(*trans*)-hydroxylation of its Pro143 residue, it does not allow for glycosylation thought to be important for affecting FBP interactions (20). These tagged clones grew and developed normally, and expressed a novel FLAG-tagged protein at the expected M_r position of 120,000 (Fig. 2.9E) that did not, however, migrate as a doublet as occurred for the overexpressed version.

The interaction between JcdI-FLAG and Skp1 was revisited using Western blot analysis of co-IP experiments, which allowed for a larger number of replicates. Based on densitometry of Western blots, analysis of unbound fractions showed that essentially all JcdI-FLAG was captured, compared to ~75% of Skp1 that was captured by anti-Skp1 beads. In JcdI co-IPs from vegetative cells, a 2-fold greater amount of Skp1 (Skp1:JcdI ratio) was captured in *gnt1*$^+$ relative to *gnt1*$^-$ cells (Fig. 2.9E, F). A similar though lesser difference was observed in reciprocal anti-Skp1 co-IPs, despite similar JcdI-FLAG protein levels. A similar analysis of slug cell extracts using anti-FLAG also indicated preferential (2-fold) interaction of JcdI in *gnt1*$^+$ vs. *gnt1*$^-$ cells (Fig. 2.9H, I). Remarkably,

Fig. 2.9. Effect of Skp1 glycosylation on endogenous levels of JcdI and its interaction with Skp1

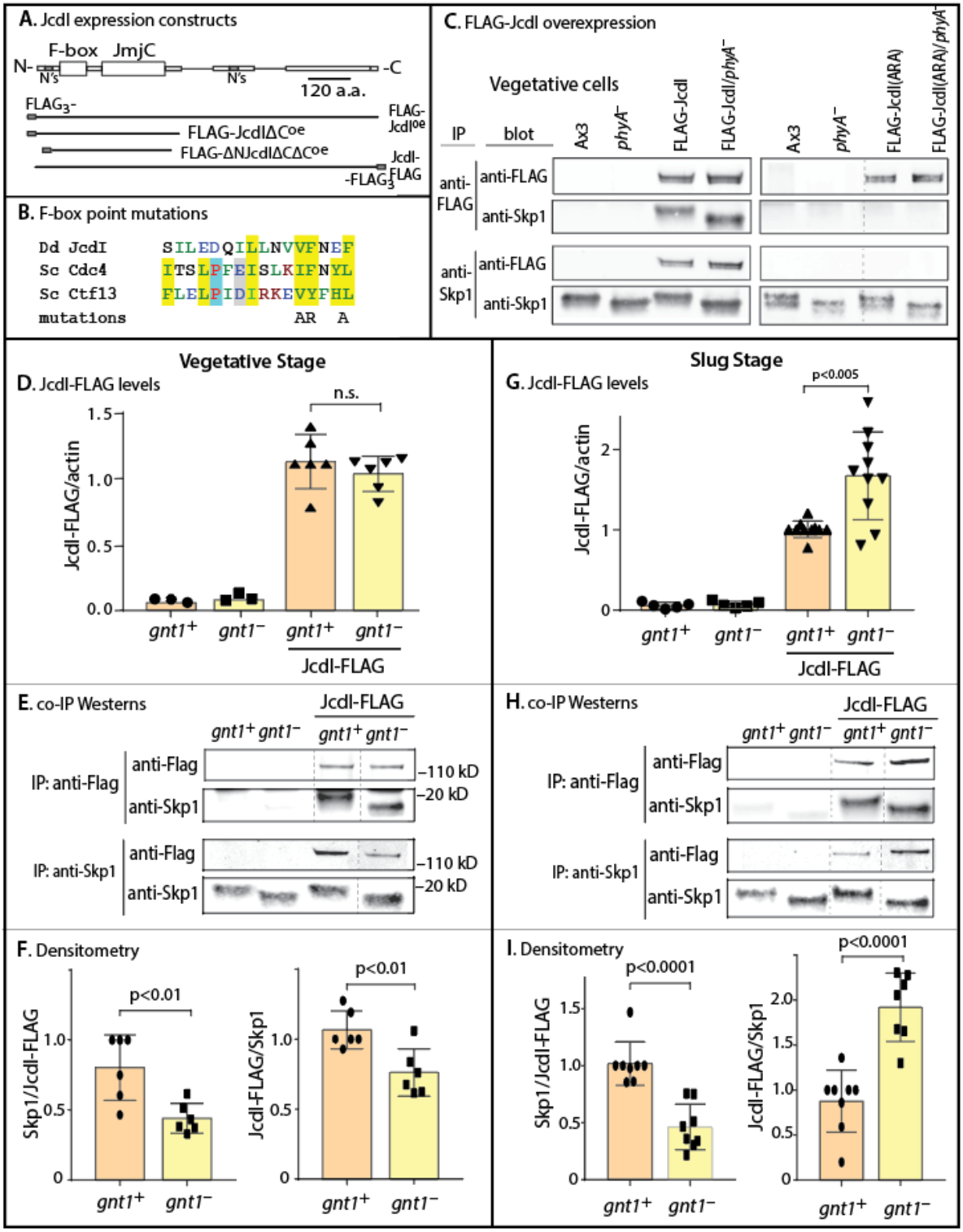

Fig. 2.9. Effect of Skp1 glycosylation on endogenous levels of JcdI and its interaction with Skp1. *A,* schematic diagrams illustrating ectopic expression of full-length FLAG-JcdI (FLAG-Fbxo13) and truncated and mutated derivatives, and tagging of the endogenous gene with a C-terminal FLAG tag (JcdI-FLAG). *B,* point mutations in the predicted F-box domain, based on mutations used for yeast Ctf13. *C,* strains ectopically expressing FLAG-JcdI and FLAG-JcdI(ARA) were subjected to co-IP with mAb M2 (for FLAG-JcdI) or pAb UOK77 (for Skp1) and analyzed by Western blotting and probing with the respective Abs. *D-F,* endogenous JcdI-FLAG was compared between *gnt1*$^{+}$ and *gnt1*$^{-}$ vegetative cells. *D,* the total level of JcdI-FLAG relative to actin in NP40-solubilized whole cells (panel D) was determined on two independent clones from three biological replicates (each represented by a triangle) using an unpaired t-test. *E,* the interaction of JcdI-FLAG with Skp1 was assessed in reciprocal co-IPs. *F,* ratios were quantified by densitometry and the average ±S.D. for the indicated number of independent trials (represented by separate symbols). *G-I,* similar analyses of slug stage cells. Tooled vertical lines mark where irrelevant lanes were deleted from the same Western blot or gel. *Braxton Nottingham generated all data for the above figure.*

the opposite result was observed in the anti-Skp1 co-IPs. However, this can be explained by the 50% reduction in JcdI-FLAG levels in the *gnt1*$^{+}$ slug cells (Fig. 2.9G). Thus JcdI-FLAG appears to bind glycosylated Skp1 better than unglycosylated Skp1 at both stages, as best revealed by the Skp1:JcdI-FLAG ratio in the anti-FLAG co-IPs. Since recombinant JcdI is insoluble in the absence of Skp1 (see below), JcdI appears to partially replace Skp1 with another unknown protein in *gnt1*$^{-}$ cells, as concluded for FbxwD above. Unlike FbxwD, however, this is associated with increased relative levels of JcdI-FLAG though only in slug cells, inviting speculation that reduced involvement in SCF complexes protects it from degradation.

JcdI is a non-heme dioxygenase

JcdI/Fbxo13 contains a JmjC-like sequence C-terminal to its F-box domain (Fig. 2.10A). JmjC domains are a subgroup of the family of non-heme dioxygenase domains, and generally hydroxylate the side chains of proteins, or their methylated derivatives resulting in demethylation. To verify its enzyme activity, a C-terminally truncated isoform that retained the JmjC sequence was expressed in *E. coli* with or without coexpressed *Dictyostelium* Skp1A. Initial studies showed that co-expression with Skp1 was necessary to recover soluble protein, and further truncations of a poorly conserved N-terminal region and additional C-terminal regions were necessary to prevent degradation during expression. Purification using Ni^{++}-Sepharose and gel filtration generated a nearly homogenous preparation of a complex of the truncated His_6-ΔNJcdIΔCΔC with Skp1 (Fig. 2.10B). Since the target of JcdI is unknown, a luminescence assay for free-wheeling conversion of the co-substrate αKG to succinate and CO_2, as commonly occurs for this enzyme class, was employed. Pilot studies indicated a pH optimum of 6.0 to 7.0, with markedly decreased activity at pH 7.5 and above, and maximal activity at 10 μM αKG. Thus, the

Fig. 2.10. JcdI/Fbxo13 is an O_2-dependent non-heme dioxygenase

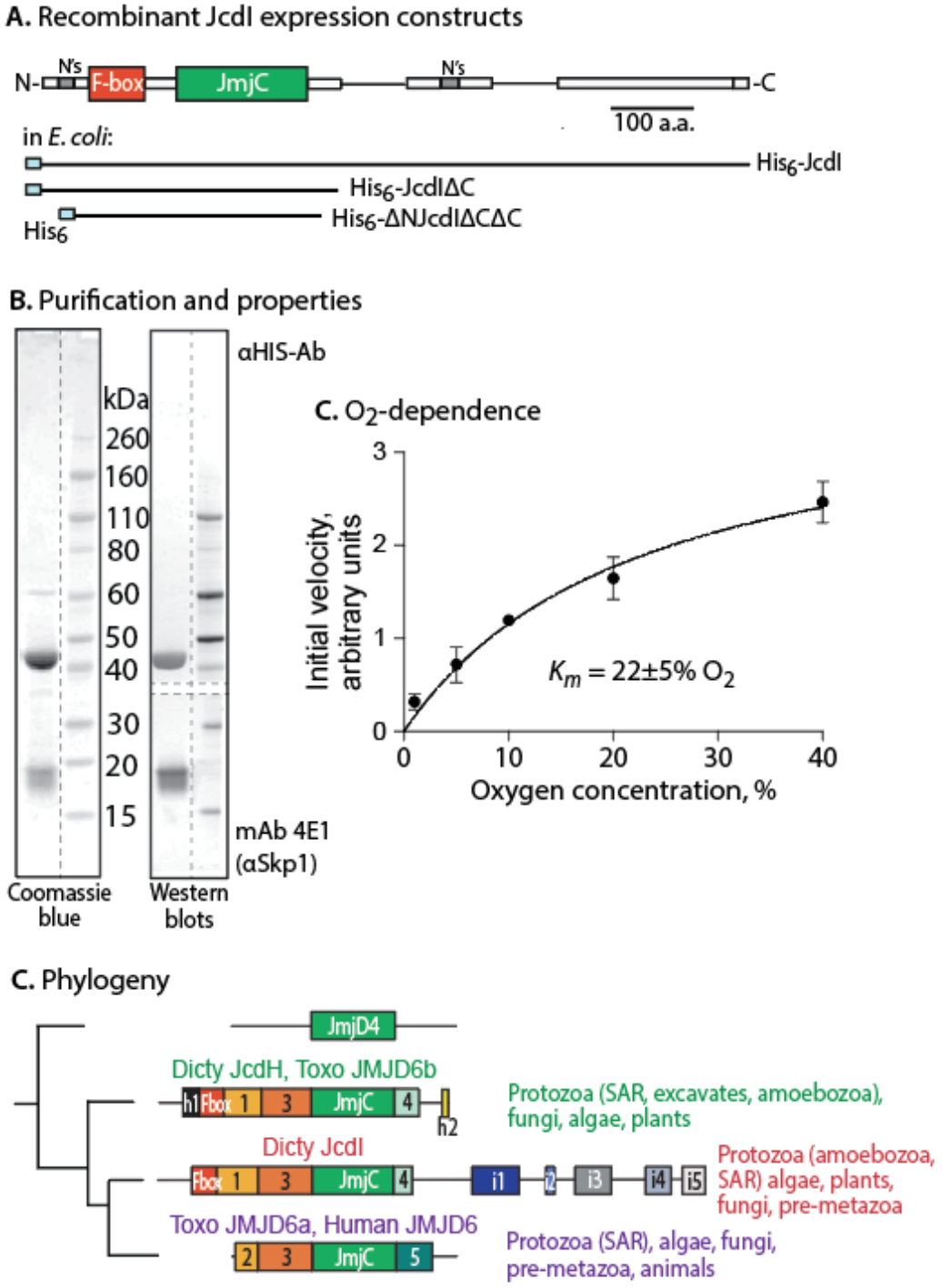

Fig. 2.10. JcdI/Fbxo13 is an O_2-dependent non-heme dioxygenase. *A,* domain analysis of the predicted JcdI protein and summary of expression constructs in *E. coli*. *B,* SDS-PAGE and Western blot analysis of the purified ΔNJcdIΔCΔC/Skp1 complex expressed in *E. coli*. Vertical dashed lines refer to irrelevant lanes removed from the same gel, and horizontal dashed lines indicate the division of the same blot for probing with different Abs. *C,* non-heme dioxygenase activity was measured based on the conversion of αKG to succinate, as is typical of this enzyme class even in the absence of an acceptor substrate, in the presence of various levels of O_2. Succinate was detected using a commercial luminescence-based Succinate-Glo assay. Initial velocities were calculated from three technical replicates of a single trial that was replicated with similar results in an independent trial. *Protein was purified by Nitin Daniels. Hanke van der Wel performed Succinate-Glo assays and generated the evolutionary tree for JcdI.*

peripheral domains were not required for this core activity. Under optimized conditions (see Methods) where activity was linearly dependent on time and enzyme concentration, the K_m for O_2 was estimated at 22 ± 5% O_2 (Fig. 2.10C), suggesting that, in addition to regulating JcdI via PhyA, O_2 may also directly control JcdI's enzymatic activity.

JcdI/Fbxo13 is evolutionarily related to human JMJD6

BLASTp searches at NCBI for sequences similar to the JcdI catalytic domain yielded JmjD6 as the most related group of proteins, and JmjD4 as the second most related. A manually curated alignment of the amino acid sequences of the 71 most similar JmjC domains across phylogeny (Fig.2.11) was analyzed by a maximum likelihood method to explore the diversity within this group. As indicated by the unrooted tree shown in Fig. 2.10C,11, JmjD6-like sequences are found throughout protists, plants, fungi and animals, and resolved into 3 major groups that were well resolved from the JmjD4-like sequences. Human JmjD6 and all the animal sequences are clustered in a subclade of a larger group (at bottom, in violet) that also includes representatives from major protist groups, including the stramenopile-alveolate-rhizaria (SAR) cluster, algae, and fungi. These sequences are related approximately according to the phylogeny of the organisms consistent with a common function. This is supported by the presence of two characteristic sequence motifs, referred to as homology domains H2 and H5, that flank the JmjC domain and the adjacent H3 homology domain that is found with all JmjD6 and JmjD4 JmjC domains (see domain diagrams in Fig. 2.10C,11). The other two groups each contain representatives from a diverse array of protists, higher plants, and some fungi, but not metazoa. They are distinctive from the animal JmjD6-like sequences in that their H3/JmjC domain pair is flanked by homology domains H1 and H4. Strikingly, they are each in possession of an F-box like sequence near their

Fig. 2.11. Evolution of JmjD6-related sequences

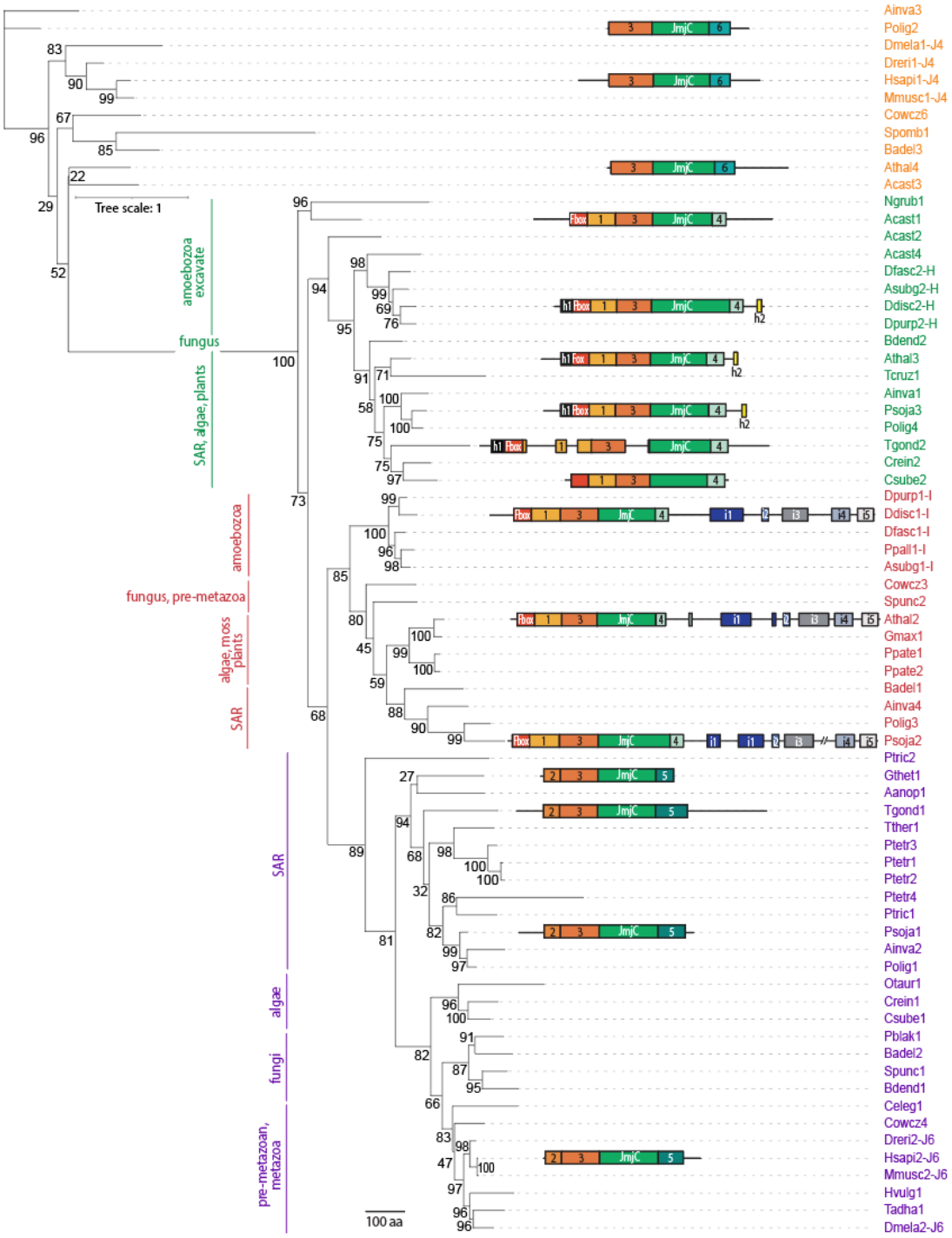

Fig. 2.11. Evolution of JmjD6-related sequences. A BLASTp search for sequences was performed to identify proteins whose JmjC domains were most closely related to that of *Dictyostelium* JcdI. *A,* the JmjC domains of the 71 most closely related were aligned, and their evolutionary relationships were examined using a maximum likelihood method implemented in IQ-tree. The tree with the highest log likelihood value is shown and is unrooted. The percentage of trees in which the associated taxa clustered together is shown at each branch. Branch lengths are measured by the number of substitutions per site. Red and green labels indicate proteins with JcdI-like or JcdH-like JmjC domains, violet labels are assigned to proteins most closely related to human JMJD6, and orange-labeled proteins are JMJD4-like. An alignment of the full-length sequences of select examples were searched for similarities, which are represented by boxes in the domain diagrams and referred to as homology domains. Only the JmjC and F-box domains have known functions. *Hanke generated the evolutionary tree for JcdI.*

N-termini, a position that is typical for FBPs. JcdI lies in the second group (in middle, red), whereas the closely related *Dictyostelium* paralog, JcdH, lies in the third group (green). The members of each of these two groups are related approximately according to the phylogenies of their parent organisms, consistent with a common function, which is supported by their additional shared domains. Members of the JcdI group have characteristic homology sequences i1-i5 at their C-termini, which are lacking from the JcdH group. Many but not all members of the JcdH group have sequence homologies referred to as Hh1 and Hh2 (Fig. 2.11). The alignment of JmjC domains also reveals sequence motifs that are distinctive among the three groups (asterisks in Fig. 2.11). The topology of the tree suggests that modern day human JmjD6 originated and diversified in protists via two successive gene duplications. In this scenario, the JcdI and JcdH groups evolved from the duplication of an ancestral JmjD6-like gene containing H1 and H4. Then a second gene duplication spawned the animal and human JmjD6 sequences and was associated with the replacement of H1 and H4 by H2 and H5, respectively. Some members of the JcdH and JcdI groups subsequently acquired additional characteristic domains. Thus, it is unclear whether JcdI and JcdH, with their distinctive F-box domains, have the lysyl hydroxylase or arginine demethylase activities that have been controversially ascribed to JmjD6 (17, 29, 30). To our knowledge, Fbxo13/JcdI represents the first FBP found to be conserved across the protist kingdom, which includes many animal and plant pathogens.

Developmental role of JcdI in O_2-sensing

The finding that JcdI's *in vitro* enzyme activity is limited by physiological levels of O_2 led us to genetically test its contribution to O_2-sensing in cells. We previously found that overexpression of PhyA reduces the O_2-threshold required for culmination, as assayed

morphologically and by quantifying the number of spores that differentiate in the resulting fruiting bodies (46). Here we analyzed a strain that was genetically altered to constitutively overexpress FLAG-JcdI (Fig. 2.12A). In these trials and based on spore numbers generated, parental cells (strain Ax3) required more than 15% O_2 to fully culminate, and negligible culmination occurred at 12% O_2 (Fig. 2.12C). In contrast, approximately 50% of FLAG-JcdI overexpressing cells still culminated at 12% O_2, and 10% culminated at 10% O_2. Similar results were obtained for 2 independent FLAG-JcdI overexpression clones. Representative images of the morphology of the terminal structures confirm the failure of Ax3 to culminate into fruiting bodies at 12% O_2, whereas the FLAG-JcdI overexpression strain exhibited substantial fruiting body formation (Fig. 2.12B). To assess whether this effect depended on JcdI enzymatic activity, an inactivating point mutant, in which the highly conserved His319 residue critical for binding the co-substrate αKG (47-49) was changed to Ala, was overexpressed at similar levels (Fig. 2.12A).

This strain required 15% O_2 for efficient culmination, and exhibited minimal culmination at 12% O_2. To examine the significance of the modestly conserved C-terminal region of the JcdI clade of JmjD6-like sequences, a truncated version, FLAG-ΔNJcdIΔCΔC (Fig. 2.10A) was analyzed in a clone that over expressed the protein. This strain was similar to the parental Ax3 strain (Fig. 2.12B, C), suggesting that the C-terminal domain contributes to O_2-dependent JcdI functionality; however, clones expressing the same high level of expression were not found (Fig. 2.12A). Finally, the importance of the F-box domain was tested using FLAG-JcdI(ARA). Interestingly, this overexpression strain, which does not bind Skp1 to a significant extent in co-IPs (Fig. 2.9C), also required less O_2 to culminate, like native JcdI. Since JcdI required co-expression with Skp1 for solubility when expressed in *E. coli*, the FLAG-JcdI overexpression strains were subjected to gentle

Fig. 2.12. JcdI overexpression reduces O_2-threshold for development

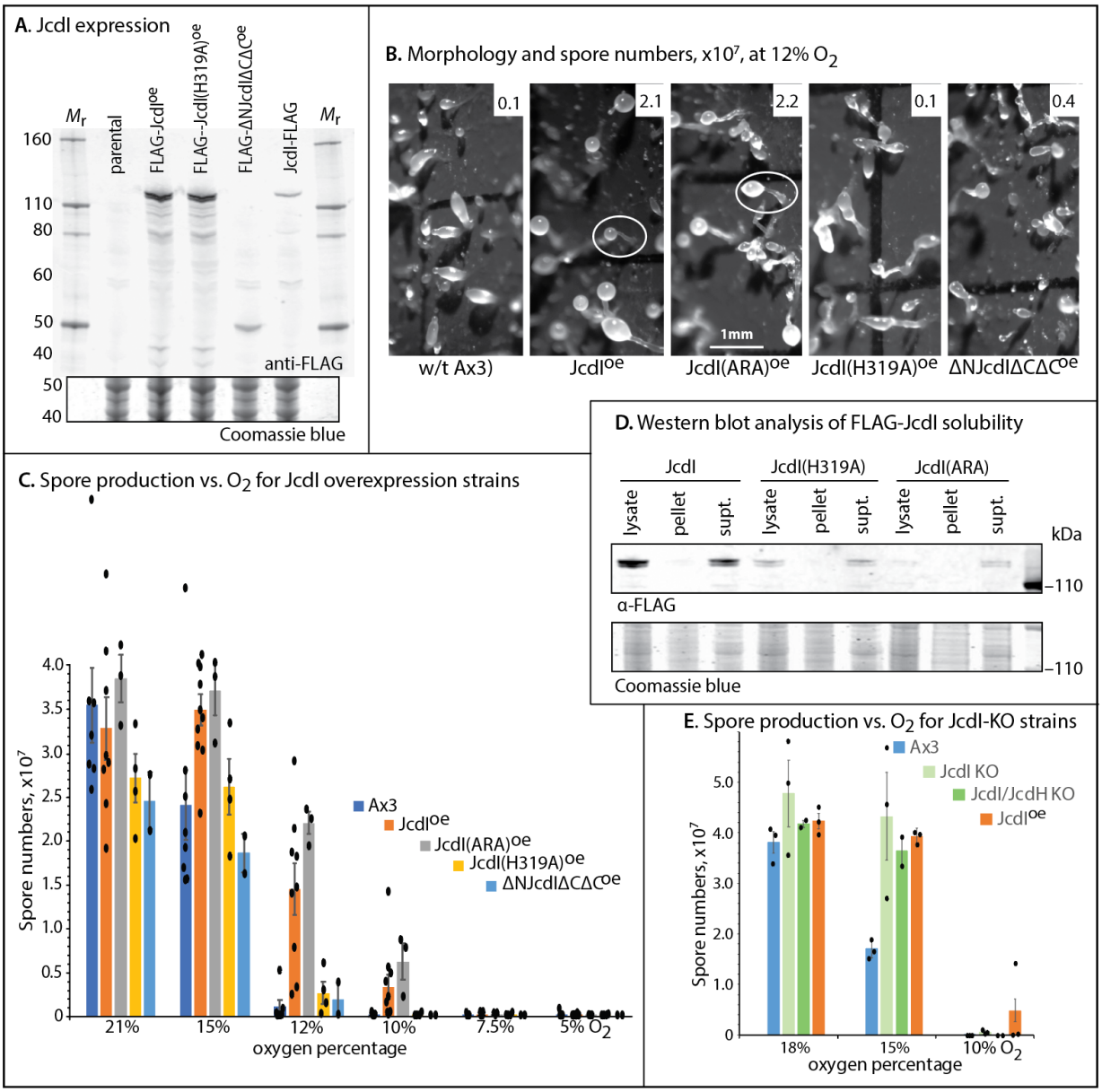

Fig. 2.12. JcdI overexpression reduces O_2-threshold for development. *Dictyostelium* was transformed with plasmids directing the overexpression of normal or mutant FLAG-JcdI isoforms under control of the constitutive discoidin-1γ promoter. *A,* clones were screened for expression level in vegetative cells, as assessed by Western blotting of whole cell extracts probed with anti-FLAG (mAb M2). Cells were induced to develop by spreading at high density on moist filters in starvation buffer as in Fig. 2.1B, and maintained under controlled flow of different O_2 levels. *B,* representative terminal morphologies at 12% O_2. Typical fruiting bodies are encircled in white. *C,* mean spore counts from 3 independent trials of FLAG-JcdI overexpression development, which included data from 3 independent FLAG-JcdI-overexpression strains, after 36 h, ±SEM. *D,* Western blot analysis of the distribution of FLAG-JcdI isoforms between particulate and cytosolic fractions after gentle filter-lysis of vegetative stage cells in the absence of detergent, and centrifugation at 200,000 × g for 30 min. *E,* mean spore counts from 3 independent trials of *jcdI*$^-$ and *jcdI*$^-$/*jcdH*$^-$ cells after 36 h, ±SEM.

filter lysis under conditions that preserve organelles, and centrifuged at high *g* force to generate particulate and cytosolic fractions. Unexpectedly, FLAG-JcdI(ARA), like the wild-type isoform, was primarily soluble (Fig. 2.12D) and, thus, potentially functional as an enzyme.

The contribution of JcdI to O_2-sensing was also examined in a strain in which its coding region was replaced with a *bsr* cassette. This *jcdI*$^-$ strain did not exhibit statistically significant effects of O_2 levels on spore production (Fig. 2.12E). Since the genome expresses a related JmjC-containing FBP, JcdH (Fig. 2.11), we examined a strain whose *jcdH* locus was disrupted. This strain also exhibited no effect on O_2-dependent spore production (data not shown). Finally, we generated a *jcdI*$^-$/*jcdH*$^-$ strain, which also exhibited normal O_2-dependence. These findings suggest that genetic redundancy, possibly by another of the 12 annotated JmjC proteins encoded by the *Dictyostelium* genome, may compensate for the absence of these proteins. In contrast, the dominant effect of JcdI's overexpression suggests a functional role in O_2-sensing that would be expected to be concealed by redundant functions.

Discussion

Cells have a need to sense and respond to changing levels of O_2 in their environments, and this is especially important for single-celled protists that are not buffered by multicellularity. Here we find that a relative of human JmjD6 contributes to O_2 sensing in *Dictyostelium*, a protist that uses gradients of O_2 for aerotaxis (15) and, during development, to polarize its slug (21, 50) and to know to culminate near the soil surface (46). *Dictyostelium* JcdI is a non-heme dioxygenase that uses O_2 as the source of O-atoms to hydroxylate residues on currently undefined target proteins. JcdI is also an FBP, which renders it subject to regulation by another non-heme dioxygenase, the prolyl hydroxylase PhyA, via its action on the Skp1 subunit of the SCF class of

E3(SCF)Ub-ligases. Prolyl hydroxylation of Skp1 leads to an increased fraction of JcdI that is bound to Skp1, which is associated with decreased cellular levels of JcdI during development. Our finding that the Skp1 association of another FBP, FbxwD, is also increased by PhyA suggests that a similar mechanism may operate for others of the 90 additional and largely dynamic Skp1 interactors suggested by this study. The role of PhyA in regulating Skp1 appears to involve protein degradation owing to rescue of the culmination defect of *phyA*$^-$ cells by proteasomal inhibitors.

JcdI has properties of an oxygen sensor during development

The act of culmination, which involves reorganization of the multicellular *Dictyostelium* slug into a fruiting body with aerial spores, is exquisitely O_2 sensitive, which helps ensure that the process occurs where O_2 levels are highest, at the soil surface to maximize potential dispersal of the spores. Thus, this model system offers a favorable opportunity to examine the contributions of additional O_2-sensing factors. JcdI was selected for analysis not only because of its presence in the interactome of Skp1, which is regulated by the PhyA O_2-sensor, but also because its possession of a putative JmjC domain suggests that it too directly depends on O_2. We found that recombinantly expressed JcdI is indeed a non-heme dioxygenase, and its apparent K_m (O_2) of 22% (Fig. 2.10) indicates that its enzymatic activity would be directly limited by O_2 availability in cells. Genetically induced overexpression of JcdI modestly reduced the O_2-requirement for culmination (Fig. 2.12), as expected if its activity was rate-limited by O_2 and this was overcome by the presence of more enzyme. The inability of a similarly expressed inactive mutant confirmed that JcdI acted via its enzymatic activity to render this effect. A truncated version of JcdI that retained its JmjC and flanking domains was also not active, suggesting that the missing domains contribute in some way to JcdI function. Thus, JcdI is similar to PhyA in the sense that its overexpression

reduced the O_2-requirement for culmination; however, its removal by gene replacement did not increase the O_2-requirement as occurs in *phyA*$^-$ strains (46). *Dictyostelium* expresses a closely related homolog, JcdH, but neither its disruption nor the double-knockout of *jcdI* and *jcdH* had any effect on the O_2-dependence of culmination (Fig. 2.12). Thus, JcdI may function as a go-signal to coordinate a parallel aspect of O_2-sensing, whose absence might therefore lie beyond the sensitivity of our analyses. Alternatively, JcdI might function redundantly with another of the 12 predicted JmjC-containing proteins encoded by *Dictyostelium*. The expression pattern of JcdI, which according to a global transcriptomic analysis is expressed at a 2.7-fold higher level in prestalk over prespore cells (65), is consistent with action in the apical end of the slug thought to signal culmination (46).

Evolution of JcdI

Based on sequence similarities, JcdI is predicted to be a lysyl hydroxylase as directly demonstrated for human JmjD6, and/or possibly an arginine demethylase which has also been proposed (30, 51). However, an analysis of the evolution of the JmjC-domains of JmjD6-like sequences suggests that JcdI evolved separately from JmjD6 after a gene duplication early in eukaryotic evolution (Fig. 2.11), followed by diversification of domains that flank the JmjC domain and persist today in extant versions in protists, fungi, and metazoans. Thus these paralogs may have a distinct catalytic function. *Dictyostelium* JcdH is found in another lineage of JmjD6-like proteins that appears to have derived from a yet earlier gene duplication, and this group lacks the C-terminal sequences that characterize the JcdI group. The JcdI and JcdH families are distributed widely in protists, algae, and fungi, but are conspicuously absent from metazoa. They

also all contain a predicted F-box domain, rendering them potentially subject to another level of regulation via the SCF complex and PhyA.

Effect of PhyA on JcdI and FbxwD

The potential for regulation of JcdI by the SCF was suggested by its presence in the Skp1 interactome and its predicted F-box domain. JcdI is confirmed to be an FBP because point mutations in its predicted F-box domain inhibited its interaction with Skp1 (Fig. 2.9C). Furthermore, co-expression with Skp1 in *E. coli* was required for its solubility (Fig. 2.10). The original co-IP studies suggested a modestly greater representation in the Skp1 interactome of *phyA*$^-$ slugs, in contrast with other interactors. A similar result was obtained by Western blot analysis of strains in which endogenous JcdI was FLAG-tagged in *gnt1*$^+$ and *gnt1*$^-$ cells (Fig. 2.9I), though this difference was not observed in vegetative cells (Fig. 2.9F). More telling was that in reciprocal co-IPs captured with anti-FLAG, approximately 2-fold more Skp1 was captured from *gnt1*$^+$ compared to *gnt1*$^-$ cells in both slug and vegetative cells. The discrepancy is explained by the finding that endogenous JcdI-FLAG was reduced 2-fold in *gnt1*$^+$compared to *gnt1*$^-$ slug but not vegetative cells. The result from the anti-FLAG co-IP is considered more reliable owing to is capture of >95% of JcdI-FLAG from extracts, compared to the <75% of Skp1 captured by anti-Skp1 which would allow for bias if subpopulations vary in epitope accessibility. Since recombinant JcdI is insoluble in the absence of Skp1, it is likely that in *gnt1*$^-$ cells, JcdI is bound to an alternative protein, as has been observed for other FBPs (52, 54), and would not be accessible to the SCF and possible autoubiquitination and degradation. An example of this is scenario was described for the FBP Tir1 in *Arabidopsis* (55). This explanation for why JcdI-FLAG levels are reduced in *gnt1*$^+$ cells is consistent with the ability of overexpressed mutant FLAG-JcdI(ARA) to affect O_2-sensing,

if the substitution of the very hydrophobic Val and two Phe residues with an Arg and two Ala residues were sufficient to render it soluble, as suggested by the cell fractionation results (Fig. 2.12D). While the physiological role of PhyA-dependent reduction of JcdI levels is not known, one possibility is that it is a slow homeostatic process to regulate the rapid stimulatory effect of O_2 on JcdI enzymatic activity.

A second FBP, FbxwD, also exhibited preferential binding to Skp1 when it was glycosylated, though no statistically significant effects on its levels were observed (Fig. 2.8). Unlike FbxwD, JcdI is an enzyme and potentially not a traditional substrate receptor, which might subject it to differential outcomes.

Regulation of FBP/Skp1 interactions has also been described in yeast, in response to stress (e.g., heavy metals) or Skp1 phosphorylation (56, 57). Skp1 glycosylation represents a novel mechanism. Previous studies showed that glycosylation inhibits Skp1 dimerization (25) and, since dimerization interferes with FBP binding (27), glycosylation could increase the availability of Skp1 for FBP interactions. In addition, glycosylation also modifies the conformational profile of the F-box binding region of Skp1 in a manner that is predicted to increase accessibility to F-box domains (24), which was supported by size exclusion chromatography of Skp1 complexes from normal compared to mutant extracts (20), and enhanced binding to mammalian Fbs1 *in vitro* (25). Evidence exists for this mechanism in other protists including *Toxoplasma gondii* and *Pythium ultimum* (13, 23, 14).

How general is the effect of Skp1 modification on FBPs?

The current study expands our knowledge of the putative Skp1 interactome by use of an epitope-tagged Skp1 in addition to an affinity purified Skp1 antiserum, and by analyzing its

developmental regulation (Fig. 2.7, Table 2.1). In addition to 3 known non-FBP SCF subunits, 89 proteins were specifically associated with Skp1 at a high confidence level, which is a 5-fold increase over our previous study of slug stage cells using anti-Skp1 (20). The proteins in the interactome range in abundance by over 500-fold (Fig. 2.4). 16% lack known substrate receptor or other domains (Table 2.1). Only 14% of the proteins were detected by both pull-down methods, suggesting that epitope accessibility varied among complexes and confirming the value of orthogonal capture agents for these complexes. 73% of the interactors were observed in vegetative cells, and 52% were in slug cells, with only 25% apparently present throughout the life cycle. To address the possibility that presence simply reflected the availability of interactors at the two stages, we queried the transcriptomes of vegetative and slug cells as reported (58). Superimposing Reads Per Kilobase of transcript per Million mapped reads (RPKM) values above protein abundance values interpreted from the proteomics data showed no systematic correlations (Fig. 2.4), suggesting that presence in the interactome is based on selectivity rather than simple availability. Using a 4-fold reduction in transcript level as an approximate prediction of what difference might on average result in loss of detection in one stage relative to the other, we found that less than 40% of the vegetative-only interactors, and less than 30% of the slug-only interactors, met this criterion (Table 2.1). Furthermore, two vegetative-only proteins had higher transcript expression in slug cells and vice-versa for 16% of the slug-only proteins. Given the long half-life of Skp1 in cells (44), which undergo minimal proliferation during development, it is thus likely that changes in the Skp1 interactome involve some developmental reassortment of Skp1 interactors.

Many of the Skp1 interactors appear to be FBPs and may bind Skp1 directly. 38 possess F-box-like sequences in their N-terminal regions based on sequence and/or structural homology. 24 of those possess C-terminally oriented sequences that represent known substrate receptor domains, and 18 additional proteins possess potential substrate receptor domains, raising the possibility that they also possess cryptic F-box domains that explain their association with Skp1. These approaches likely underestimate the number of FBPs, given the extensive variation within known F-box sequences including insertions that make the motif difficult to detect. In addition, a BLASTp search for F-box-like sequences that are conserved among social amoebae yielded 38 additional candidates that were not detected in this study, which might have been due to epitope inaccessibility, low expression level, or expression at other life cycle stages. The remaining proteins that are not predicted to be FBPs might be FBP substrates or cofactors that contribute to substrate interactions (59), or possibly reflect unknown functions of Skp1 in this protist. Skp1 interactors described in other organisms, such as Sgt1 (60), were not observed despite the presence of a highly conserved homolog in the *Dictyostelium* genome.

The representation of ~39% of the interactors were increased when Skp1 was glycosylated in either of the two biological states investigated whereas, strikingly, only two were decreased (in vegetative cells). The affected proteins were enriched in FBPs relative to all interactors (80% vs. 92%) (Figs. 2.7A-G). Possible explanations for increased representation are increased absolute levels available for co-IP, co-localization of interactor and Skp1 pools in cells, different interaction stability, or an increased fraction of the FBP pool that is stably bound to Skp1 as shown for FbxwD and Skp1 (Figs. 2.8,9). This latter effect may be more common than inferred based on the example of JcdI where decreased levels concealed increased interaction (Fig. 2.9).

Analysis of an alignment of F-box-like sequences of interactors did not reveal obvious correlations with PhyA-dependence, but a role for Skp1 interacting sequences outside of the canonical F-box domain cannot be excluded.

The role of protein degradation

The dynamic nature of the Skp1 interactome suggests that the specificity of protein degradation changes over the life cycle, a concept that has been previously proposed (41). O_2-sensing occurs not only for regulating slug migration and polarization (50), culmination (46), and sporulation (21), but also for aerotaxis at the single cell vegetative stage (15). The role of Skp1 modification in vegetative cells is unknown. The very low conservation of FBP sequences across phylogeny makes it difficult to predict substrates so experimental approaches will be key to confirming this prediction. Nevertheless, the ability of proteasomal inhibitors to partially rescue the development of *phyA*$^-$ cells (Fig. 2.1) indicates that PhyA senses O_2 via an effect on E3(SCF)Ub ligase activity, which is consistent with its evident specificity for Skp1 (22, 14, 19). A possible explanation is that proteasomal inhibition raises the level of FBPs, which would have the effect of driving increased interactions with Skp1 toward levels normally achieved via Skp1 glycosylation. Although proteasomal inhibition would also be expected to interfere with the action of substrate receptor type FBPs, FBPs like JcdI and JcdH with SCF independent activities might experience increased levels and promote developmental progression. However, which FBP(s) is responsible for mediating PhyA's role in culmination remains to be determined. Overall, the findings support the general model that, for the soil dwelling *Dictyostelium*, Skp1 modification is a mechanism that links the pace of protein turnover required for developmental progression to favorable environmental factors like optimal O_2 levels. This phenomenon is

reminiscent of the role of protein turnover in regulation of developmental timing during mammalian development (61).

Table 2.2. Strains used in this study

Strains	parental	genotype	resistance	ref.
Ax3	NC-4	*axeA/B/C*	none	60
Ax4	Ax3	*axeA/B/C*	none	61
HW288	Ax3	*phyA*$^-$	blasticidin-S	34
HW302	Ax3	*dscC*::Skp1B-myc	G418	29
HW304	HW302	*dscC*::Skp1B-myc; *phyA*$^-$	G418, blasticidin-S	this report
HW503	Ax3	*gnt1*$^-$	hygromycin	31
HW418	Ax3	*dscC*::His_6AgtA	G418	27
HW535	Ax3	*dscC*::FLAG-AgtA	G418	this report
HW536	HW288	*dscC*::FLAG-AgtA; *phyA*$^-$	G418, blasticidin-S	this report
HW540	Ax3	FbxwD-FLAG	blasticidin-S	14
HW544	HW288	FbxwD-FLAG; *phyA*$^-$	blasticidin-S	14
HW559	Ax3	*dscC*::FLAG-JcdI (Fbxo13)	G418	this report
HW560	Ax3	*dscC*::FLAG-JcdI	G418	this report
HW561	Ax3	*dscC*::FLAG-JcdI	G418	this report
HW562	Ax3	*dscC*::FLAG-JcdI(ARA)	G418	this report
HW564	Ax3	*dscC*::FLAG-JcdI(H319A)	G418	this report
HW566	Ax3	*dscC*::FLAG-JcdI(ΔNΔCΔC)	G418	this report
HW568	HW288	*dscC*::FLAG-JcdI; *phyA*$^-$	G418, blasticidin-S	this report
HW570	Ax3	JcdI-FLAG	blasticidin-S	this report
HW572	HW503	JcdI-FLAG; *gnt1*$^-$	blasticidin-S, hygromycin	this report
HW574	Ax3	*jcdI*$^-$	blasticidin-S	this report
HW576	Ax3	*jcdI*$^-$	none	this report
HW578	HW576	*jcdI*$^-$/*jcdH*$^-$	blasticidin-S	this report
37_C_10	Ax4	*jcdH*$^-$	blasticidin-S	62 (GWDI)

Methods

Cell culture

Dictyostelium discoideum strains Ax3, Ax4, and their genetically modified derivatives, were routinely grown vegetatively in shaking axenic HL-5 media at 22°C, and passaged by 1000-fold dilution every third or fourth day. Strains Ax3 and Ax4 are considered normal but are mutant derivatives of a wild-type strain. Vegetative stage cells were collected by centrifugation during logarithmic growth for experimental studies. Starvation-induced development was induced on at an air-water interface on filters or in suspension as previously described (21). Slug stage cells were typically scraped at 14 h unless otherwise indicated. Cell density was determined using a hemacytometer.

The dependence of culmination on O_2-levels was performed by incubating filter dishes in air-tight translucent containers through which was continuously passed humidified premixed gasses consisting of the indicated O_2-level with the balance made up of N_2, as described (44). Plates were illuminated by overhead fluorescent (daylight) room lighting at 22°C. Morphology was qualitatively assessed by direct visualization during development and after 38 h. Culmination was quantitated by direct spore counting in a hemacytometer. Over the years and possibly the seasons, the O_2 requirement for culmination of the parental strain Ax3 in the laboratory varies from 7.5-15% O_2, suggesting sensing of unknown factors. For the trials conducted for this project, the average O_2 requirement was 15%. Each trial included all experimental and reference strains to control for this variation, and were carried out over a period of several months.

Proteasome inhibitor treatments

Proteasome inhibitors (Ubiquitin-Proteasome Biotechnologies, Dallas, Texas) were

dissolved in anhydrous DMSO and used fresh or from frozen aliquots stored at -80° C. Stock solutions were 30 mM MG132, 30 mM Bortezomib, and 50 mM Carfilzomib. For suspension development, cells were resuspended in Agg Buffer (0.01 M sodium phosphate, pH 6.0, 0.01 M KCl, 0.005 M $MgCl_2$) containing the indicated concentration of inhibitor or the equivalent concentration of DMSO and, after shaking for the indicated times, were recovered by centrifugation and flash frozen. For development at an air-water interface, cells were resuspended in PDF, deposited on filters wetted in the same inhibitor solution or the equivalent volume of DMSO and, after incubation for the indicated times, scraped and flash frozen. Because the occasional breakthrough culmination of *phyA*$^-$ cells at ambient (21%) O_2, as previously reported (10), would confound interpretation of inhibitor effects, only data from the trials (16/20) that failed to culminate at 21% O_2 were analyzed.

SDS-PAGE and Western blotting

For whole cell analysis, fresh or frozen cell pellets were diluted with Laemmli Sample Buffer and boiled for 5 min. For analysis of cytosolic fractions, cells were filter-lysed (62) in 0.25 M sucrose in 50 mM Tris-HCl (pH 8.0) plus protease inhibitors, and centrifuged at 200,000 × *g* for 30 min. Supernatants were diluted 1:1 and boiled in 2× Laemmli buffer, and pellets resuspended in Laemmli buffer as above. Samples (2-10×10^5 cell equivalents) were separated on precast 4-12% Bis/Tris NuPage polyacrylamide SDS page gels (Invitrogen) for 45 min in MOPS or MES running buffer (for Skp1 analysis). Proteins were transferred to nitrocellulose using an iBlot 2 (Invitrogen) dry blotting system. Blots were blocked in 5% (w/v) nonfat dry milk in Tris-buffered saline (TBS; 100 mM NaCl, 50 mM Tris-HCl, pH 7.5), probed with the indicated primary antibody in blocking buffer overnight at 22°C, washed in TBS, probed again with a corresponding Alexa

Fluor-680 or Alexa Fluor-800 secondary Ab (1:10,000 dilution) in blocking buffer, and quantitated for fluorescence in a Li-Cor Odyssey infrared scanner. Blotted gels were stained with Coomassie blue and scanned for use as a protein loading control. Blots were alternatively post-incubated with anti-actin (Sigma) as a loading control. Digital image files were processed uniformly in Adobe Photoshop by expanding to use the full 8-bit range without altering contrast. Scans were densitometrically analyzed in ImageJ with appropriate background subtraction.

For detection of polyubiquitinated proteins, blots were probed with 1:700 mouse anti-ubiquitin antibody (P4D1, Cell Signaling Technology) or 1:1000 rabbit K48-ubiquitin specific antibody (D9D5, Cell Signaling Technology), and processed as above. mAb M2 (Sigma) was used at 1:1000 for probing FLAG-tagged proteins, and mAb 4E1 or pAb UOK77 (20) were used for Skp1.

Co-immunoprecipitations

For mass spectrometry, co-IPs of Skp1 using affinity purified pAb UOK77 and a non-immune rabbit IgG were performed as described (20). For co-IPs of Skp1-myc and corresponding untagged strains, cell pellets were solubilized in Lysis buffer (250 mM NaCl, 50 mM Tris-HCl (pH 8.0), 0.2% v/v NP-40, 10 µg/ml leupeptin, 10 µg/ml aprotinin) at a final concentration of 1.2-1.5 × 10^5 cells/µl for vegetative cells and 2.4×10^5 cells/µl for slugs for 15 min on ice. Cell lysates were spun at 21,000 × *g* for 15 min to produce an S21 supernatant. 83 µl was incubated with a 100 µl slurry of Pierce™ anti-c-myc magnetic polystyrene beads (#88842), a ratio that was optimized for the minimal amount that achieved maximal (>60%) depletion of Skp1-myc from lysates. After rotation at 4°C for 1 h, beads were magnetically captured and the supernatant removed. The beads were successively rinsed 1× in lysis buffer, 2× in lysis buffer without protease inhibitors, 3× in detergent buffer (250 mM NaCl, 50 mM Tris-HCl (pH 8.0)), and finally in detergent and buffer

free solution (50 mM NaCl). Proteins were eluted in 133 mM triethanolamine for 15 min, neutralized immediately with acetic acid, and dried in a vacuum centrifuge for mass spectrometry.

For Western blot analysis of JcdI/Skp1 interactions, 3×10^7 slugs or exponentially growing vegetative cells were lysed as above. Skp1 was immunoprecipitated using 5 µl of packed affinity purified UOK77 conjugated to Sepharose beads (20). FLAG-JcdI and JcdI-FLAG were immunoprecipitated using 2.5 µl of packed anti-FLAG M2 beads (Sigma). After rotation for 1 h at 4°C, beads were collected by centrifugation at 2000 × *g* for 30 sec, resuspended and washed 3× with 1 ml of IP buffer (50 mM Tris-HCl, pH 8.0, 150 mM NaCl, 0.2% NP-40), and transferred to a fresh tube after the first centrifugation. The preparation was boiled in 1×Laemmli buffer for 3 min, and 1×10^6 cells were analyzed by SDS−PAGE and Western blotting.

For Western blot analysis of FbxwD co-IPs, endogenously tagged FbxwD-FLAG and untagged control strains were lysed as above to produce S21 fractions. 100 µl was incubated with 10 µl packed M2 magnetic beads (Sigma) by rotation at 4°C for 1 h. Beads were washed as above and eluted with Laemmli buffer for SDS-PAGE and Western blotting.

Proteomic analyses

Eluted proteins were solubilized in 8 M urea in 50 mM Tris-HCl (pH 7.8), reduced with 10 mM DTT at 22° C, and alkylated with 50 mM chloroacetamide (63). After 1:1 dilution with 50 mM Tris-HCl (pH 7.8), 1 µg of endo-LysC/trypsin (Pierce cat#A40009) was added and rotated at 22°C for 2 h, and then subsequently diluted with the same buffer to a final concentration of 2 M urea for continued overnight digestion.

The peptide samples were amended with heptafluorobutyric acid to a final concentration of 0.1% (v/v) and aspirated 5 times through a pre-equilibrated C18 Zip-Tip (Agilent Bond Elut Omix), which was then rinsed twice with 0.1% heptafluorobutyric acid. Peptides were eluted with 50% (v/v) acetonitrile, 0.1% formic acid, followed by 75% acetonitrile, 0.1% formic acid. The eluants were pooled, dried in a vacuum centrifuge, and dissolved in 5% ACN, 0.05% trifluoroacetic acid.

The peptide solution was loaded onto a C18 trap column (Thermo Acclaim™ PepMap™ 100 C18 series) in a Thermo Fisher UltiMate 3000 nano-HPLC, and eluted from the trap column onto a C18 nano-column (Thermo Acclaim™ PepMap™ 100 C18 series) in a 5%-90% ACN gradient in 0.1% formic acid over 3 h. The eluent was directly introduced via a nano-electrospray source into a Thermo-Fisher Q Exactive Plus and analyzed by MS and MS/MS. Full MS scans were acquired from *m*/*z* 350 to 2000 at 70,000 resolution. Peptides were selected for fragmentation in the C-trap via higher energy collision-induced dissociation for MS/MS analysis using a Top 10 method and a 30 sec fragmentation exclusion window.

Samples were analyzed in Proteome Discoverer 2.5, using its two step Protein Search method with label free quantification and Consensus workflow with parameters specific to the MS1 and MS2 fragmentation and mass tolerances of the Thermo-Fisher Q Exactive Plus. A modified *D. discoideum* protein database containing 12,428 unique proteins (64), modified to include a 179-protein exclusion list of common ectopic contaminants (65), was used for peptide identification. Sequest HT search parameters were 10 ppm precursor ion mass tolerance, 0.02 Da fragment ion tolerance, and up to 2 missed tryptic cleavages; variable modifications: oxidation of Met, formylation or acetylation of the protein N terminus; fixed modification:

carbamidomethylation of Cys. False Discovery Rate (FDR) was determined via Target/Decoy in the Proteome Discoverer Processing Workflow. Protein identifications were ranked by protein FDR confidence intervals of High (X<1%), Medium (1%<X<5%) and Low (5%<X<10%). Candidates assigned as mitochondrial, ribosomal or secretory proteins (see listing in database referenced below) were filtered as before (20). Protein quantifications were derived from reconstructed ion chromatograms of all peptides assigned to a protein at the MS1 level. Comparisons of protein abundance were done after setting total abundance of each sample within a single analysis equal to the highest value within the experiment in Proteome Discoverer. Normalized abundance values of proteins were analyzed for statistically significant differences between groups using the SimpliFi algorithm (https://simplifi.protifi.com/) (66). Since SimpliFi can use nonparametric statistics that assume only that data model themselves, we used this to perform tests on normalized abundances, with 1 added to all spectral counts to avoid zero values, rather than on logarithmic transformations. Proteins whose abundances were >4-fold higher in experimental vs. control samples with a Wilcoxon test p-value <0.05 were classified as Skp1 interactors. Proteins whose values were ≥1.5-fold higher in *phyA*$^+$ vs. *phyA*$^-$ samples, with t-test and Wilcoxon test p-values <0.05, were classified as enriched in the *phyA*$^+$ Skp1 interactome. The mass spectrometry proteomics data are deposited in the ProteomeXchange Consortium via the PRIDE (67) partner repository with the dataset identifier PXD033864 and 10.6019/PXD033864.

Sequence motif searches

To predict the FBP repertoire of *D. discoideum*, BLASTp studies (68) were conducted at dictybase.org using multiple validated human and yeast (9) F-box sequences to generate a candidate list. This list was expanded by additional BLASTp searches seeded with candidate

Dictyostelium F-box sequences to ensure maximal coverage. Additional inclusion criteria were evidence for expression based on RNAseq data (69), predicted targeting to the cytoplasm or nucleus, positioning of the F-box motif N-terminal to other domains of interest, and manual confirmation of conservation of hydrophobic residues and helical motifs with proven F-box motifs. This yielded 52 confident candidates, almost all of which were conserved in the genome sequences of other cellular slime molds.

In addition, the sequences of new Skp1 interactors (Table 2.1) were searched using the Geneious (42) pair-wise alignment algorithm against a training set of 17 predicted F-box domains from FBPs found above that also contained a canonical substrate receptor domain. Parameters included a PAM250 cost matrix, a gap open penalty of 20, a gap extension penalty of 10, and 2 refinement iterations. In some examples of F-boxes, such as Ctf13, Amn1, Ylr352w, and Ydr306c of *S. cerevisiae* (e.g., 70), intervening sequences occur between α-helices. Thus manual refinement of the alignments tolerated loops between α-helix 1 and α-helix 2, sequence extensions between the C-terminus of α-helix 3 and the final 4-5 amino acids of the F-box domains, but not gaps/extensions within α-helices or between α-helix 2 and 3. All predicted F-box sequences were aligned with the training set using the same parameters (excluding inserts), and % pairwise similarity was used to generate heat maps (Fig. 2.5).

To search for potential substrate receptor domains, the full-length amino acid sequences of Skp1 interactors were input into Swiss Model's (70-75) web interface for homology modeling. Proteins containing more than 500 amino acids were divided into multiple amino acid segments to reduce complexity.

FLAG-AgtA overexpression strains

AgtA cDNA was excised from the previously described pVS(His)spy-AgtA (76) using BamHI, and ligated into the BamHI site of the previously described (20) pVS3 (pV3D) expression plasmid, which derives from pVS4 and contains a sequence downstream of the semi-constitutive discoidin 1γ promoter encoding the following motifs: ATG/BclI/His_6/BglII/3×FLAG/EcoRI/BirA recognition/NcoI/TEV protease site/BamHI/TAA. A clone containing the desired forward orientation of AgtA, termed pVS3-FLAGAgtA, was confirmed by DNA sequencing. pVS3-FLAGAgtA was electroporated into Ax3 and *phyA*$^{-}$ strains, and stable transformants were selected in the presence of 20 or 120 µg/ml G418, as described (77). Clones from each transformation were grown and screened for FLAG-AgtA expression levels using anti-FLAG (M2) and anti-AgtA (pAb UOK101), enabling selection of clones with equivalent levels of overexpression in growth stage cells.

Tagging the fbxwD and jcdI loci

C-terminal tagging of the FbxwD gene product was based on double crossover homologous recombination (78). The *fbwxD* 5'-targeting sequence was amplified from *D. discoideum* genomic DNA (Ax3 strain) by a polymerase chain reaction (PCR) using primers FbxwD-5'-S and FbxwD-5'-AS and ligated into pCR4-TOPO (Invitrogen). The *fbxwD* 3'-targeting sequence was amplified and ligated in a similar manner using FbxwD-3'-S and FbxwD-3'-AS. The *fbxwD* 5'-targeting sequence was excised using BssHII and BglII and cloned into similarly digested pVSCulE-BsR, which was used previously for tagging the *culE* locus (20). The *fbwxD* 3'-targeting sequence was similarly transferred using PstI and PvuII. The *fbwxD*-tagging construct was excised using *PvuII* and *BssHII*, briefly treated with BAL-31 exonuclease (78), and gel purified. Wild-type strain

Ax3 cells were transformed by electroporation as previously described (77), selected in 10 µg/mL Blasticidin S (MP Biomedicals) in HL-5+ medium, and cloned on *Klebsiella aerogenes* on SM-agar. Cell lysates from clones were initially analyzed for modification of the *fbxwD* locus by western blotting using the M2 anti-FLAG mAb (Sigma) and verified by PCR. To examine the role of Skp1 modification, the floxed *bsr* cassette used to select for tagged *fbxwD* transformants was excised by transient transfection with the puts-NLS Cre plasmid encoding Cre recombinase as before (79). Successfully deleted clones were screened based on sensitivity to blasticidin, and confirmed by PCR). The *phyA*-locus was subsequently disrupted as previously described (17).

JcdI was tagged in a similar manner. The primer pair JET-5'-S and JET-5'-AS was used to amplify the 3'-region (996 bp) of *jcdI* from gDNA by PCR, and a 915 bp stretch downstream of the JcdI stop codon was amplified using JET-3'-S and JET-3'-AS. The PCR products were separately cloned into pCR4-TOPO, and sequences confirmed using M13F and M13R primers. The 5'-targeting insert was recovered from pCR4-TOPO-JET-5' by digestion with BssHII and BglII and cloned into similarly digested pVSCulE-BsR. pCR4-TOPO-JET-3' was then digested with PstI and PvuII and the insert cloned into similarly digested pVSCulE3'-JET5'-BsR. The 4-kb tagging cassette was excised using BssHII and PvuII and electroporated into strains Ax3 (*gnt1*$^{+}$) and HW503 (*gnt1*$^{-}$). Cells were selected in the presence of 10 µg/ml blasticidin-S and clones recovered from bacterial plates were extracted for gDNA and screened by PCR, using JET-UP-S, designed to anneal just upstream of the 5'-targeting sequence, and the reverse primer JET-BSR-AS designed to anneal in the bsr cassette of the construct. PCR was performed as above with a denaturation temperature of 94° for 45 sec, annealing temperature of 56°C for 1 min, and extension temperature of 68°C for 2 min, repeated for 30 cycles.

Table 2.3. Oligonucleotides employed in this study.

Primer Name	**Sequence** - restriction sites used are italicized.
FbxwD tagging	
FbxwD-5'-S	5'-AA*GCGCGC*GAAAAGAATGAGAATAAAGGAGCAGCA (*BssH1*)
FbxwD-5'-AS	5'-AA*CCATGG*ATCTAAATTAAAATTATATAATCTAACTAAATTATTGAAAACAC (*NcoI*)
FbxwD-3'-S	5'-AT*CTGCAG*TTGTTAAGATCAAATTACTGTGGATTTAATTG (*PstI*)
FbxwD-3'-AS	5'-TT*CAGCTG*GATGTTTTAATGGTAATTTTTTAATTGTTTCTC (*PvuII*)
FbxD3Tar-AS	5'-ATCCACAGTAATTTGATCTTAACAACTGC
BsR-AS (SKPK/O2U-AS)	5'-GAGTGGAATGAGTTCTTCAATCGTAG
BirATAG-S	5'-AGCACAAAAAATTGAATGGCATGG
JcdI expression and tagging	
JcdI-Ex1-S	5'-TAT*CCATGG*TATGGTAGTTCTTAAAAACACAT (*NcoI*)
JcdI-Ex1-AS	5'-GAA*TCCGGA*AAAATGTAATGGAATATATG (*BspEI*)
JcdI-Ex2-S	5'-CATTT*TCCGGA*TTTCTATTCACATGA (*BspEI*)
JcdI-Ex2-AS	5'-*GAGCTC*TTATACATCTAAATTCCAAATTGAATT (*SacI*)
J-ET-5'S	5'-*GCGCGC*TACCAGATTCATTACCTTA (*BssH1*)
J-ET-5'AS	5'-*AGATCT*TGAGCCTGATCCTACATCTAAA (*BglII*)
J-ET-3'S	5'-*CTGCAG*ATCGCATTGCAATCTACTG (*PstI*)
J-ET-3'AS	5'-*CAGCTG*TCACTTTTTTACCAGTTTTAACTCC (*PvuII*)
JET-OUT-S (JET-UP-S)	5'-GTCATGGTCAACAGAGTTATTCTTATATTCAA
JET-BSR-AS	5'-TTCGTATAATGTATGCTATACGAAGTTATCCGT
JcdI-disruption	
JCDI-5'-S-Stop	5'-*GCGCGC*ATGGTAGTTCTTTAAAACA (*BssH1*)
JCDI-5'-AS	5'-*GGATCC*TGATGGCACTTTCTCGC (*BamHI*)
JCDI-3'-S-Stop	5'-*CTGCAG*TGTAATTCTTAAAATTTCGATGAAGT (*PstI*)
JCDI-3'-AS	5'-*CAGCTG*CAACTAAGAAATCAACTAAATTGTC (*PvuII*)
JcdI-disruption Screening	
JcdI-KO-5'UpS	5'-TGTGCATACATCATAATAATCGGTTGGAA
JET-BSR-AS	5'-TTCGTATAATGTATGCTATACGAAGTTATCCGT
JcdI-KO-BSR3'Scr-S	5'-ATATGCATTAGATGTAAAACAGCCAAAGAGTATGAA
JcdI-KO-Dwn3'Scr-AS	5'-TATCATCAATTTCAATTGAATGAATTAATGATA
JcdI-KO-BSR-AS	5'-ACAATTGATGGACGACCCGAGCT
JcdI-F-box point mutation	
JCDI-SDM-FboxARA-S	5'-ATCAATTTTAGAGGATCAAATTTTATTGAACGTTGCTAGAAATGAAGCAACATGTAGTGAACTATTGA
JCDI-SDM-FboxARA-AS	5'-AACACATTGATATTTCAATAGTTCACTACATGTTGCTTCATTTCTAGCAACGTTCAATAAAATTTGAT

JcdI-H319A point mutation	
JcdI-H319A-S	5'-CTTCGTGGGCGATCGACCCTGCCG
JcdI-H319A-AS	5'-GGGTCGATCGCCCACGAAGCACCG
ΔN-JcdI Nshort Dicty expression	
JcdI-ΔN-S	5'-CATGGTATGTCAAAAGGTGTCAAAGTTGTAATTGGAGAAAC
JcdI-ΔN-AS	5'-ACCTTTTGACATACCATGGATATGCCATTCAATTTTTTGTG
JcdI-ΔC-S	5'-TCTCAAAATTAAGAGCTCGGGTCgtccatcaattg
JcdI-ΔC-AS	5'-GAGCTCTTAATTTTGAGAATTACAAAAGTTTTGAGTTACTGCAATC
JcdH-disruption	
JcdH-5'-KO-S	5'-*GCGCGC*GCTAATGAACCATCAAAATGTGAAAT (*BssHI*)
JcdH-5'-KO-AS	5'-*GGATCC*CACCAAATGGATGTGGAATATATAATTCAAC (*BamHI*)
JcdH-3'-KO-S	5'-*CTGCAG*CCACCACATGTTGTACCACCAGG (*PstI*)
JcdH-3'-KO-AS	5'-*GTCGAC*CTTAAATCATCACCAAAAGAGAATGAAAATG (*PvuII*)
JcdH-disruption validation	
JcdH-del-S1	5'-ATAATTGATTCAATTTTAGATTTATTAAGTGCAGAAGAATTAAC
JcdH-del-S2	5'-CAATGAATTTAGTTAGTAAAACATTTTATATTTATGTTCAAGAGG
JcdH-del-AS1	5'-AATACATTGAATAAATCCTCTTTGAAATAAGCATCTG
JcdH-del-AS2	5'-GTTTGGATCTTTATGAAATGAAGCACCTG
BSR_pVS_conf_v3	5'-GACCCGAGCTCTGATCATTAGGAT
pVS_tag_non-c_seq_F-v2	5'-CCGAAAGCTCGGATCTGATATCATAACTTC
JcdH3'ext-AS	5'-AGTCGTACTTACTGCTGCCGC

Fig. 2.13. Tagging the *fbxwD* gene locus.

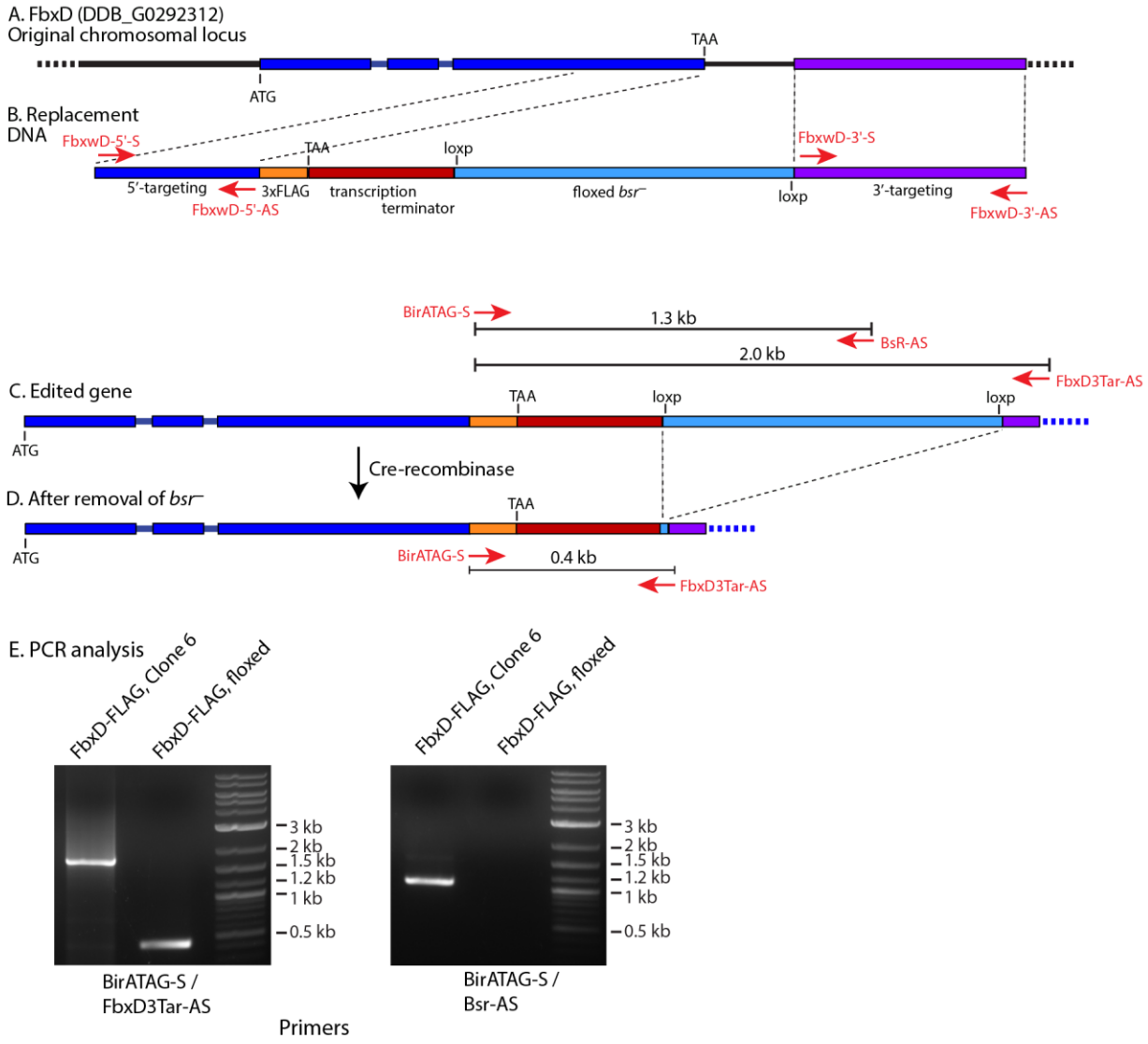

Fig. 2.13. Tagging the *fbxwD* gene locus. A, the 3-exon chromosomal locus of fbxwD. B, the DNA fragment encoding a C-terminal 3×FLAG tag and a floxed blasticidin S resistance (bsr) cassette, flanked by gene specific targeting sequences directing double cross-over homologous recombination. Primers used to amplify gene-specific DNA are shown in red. C, The expected edited gene, together with expected PCR amplicons, was verified by PCR. D, clone 6 from panel C was transiently transfected with Cre recombinase, resulting in removal of the floxed bsr cassette and leaving the FLAG tag coding region intact. Expected PCR product is diagrammed. E, confirmation of expected outcomes from panels C and D, based on agarose gel analyses of PCR experiments using the indicated primer pairs, in red.

Fig. 2.14. Tagging the jcdI gene locus.

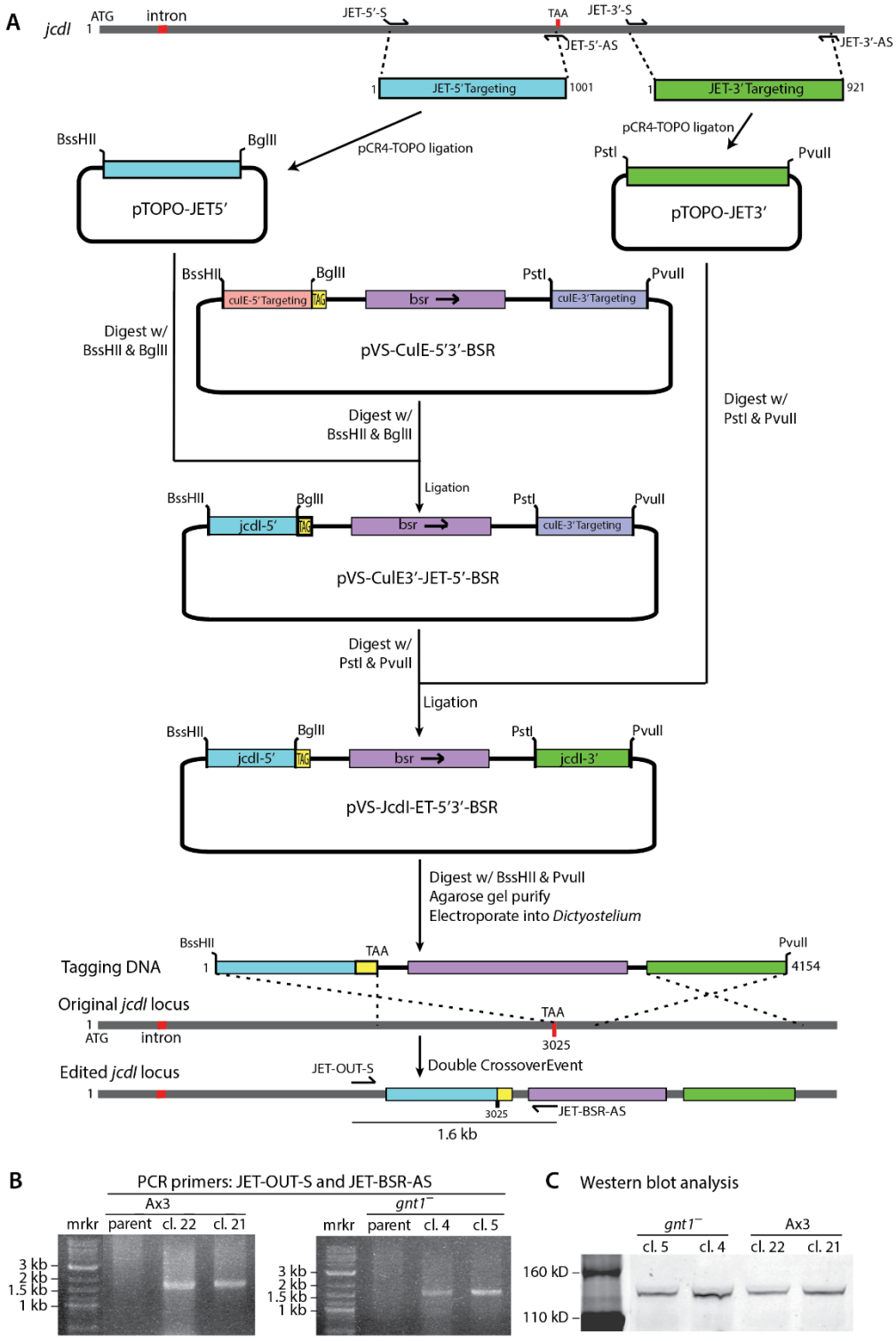

Fig. 2.14. Tagging the *jcdI* gene locus. A, the previously described tagging plasmid for Dictyostelium *culE* (14) was modified by replacement of its gene-specific 5'- and 3'-homology sequences with corresponding sequences from *jcdI,* as illustrated and described in detail in Methods. Oligonucleotides are described in Table 2.3. The linearized tagging DNA was electroporated into amoebae strains (Ax3 and gnt1–) and transformants, expected to uniquely edit the *jcdI* locus as depicted, were selected in the presence of blasticidin S. *B,* after selection, clones were screened by PCR with JET-OUT-S and JET-BSR-AS primers. *C,* screening by Western blot analysis using anti-FLAG (mAb M2) yielded clones with a band consistent with the expected Mr value of 116,000, and the expressed protein is referred to as JcdI-FLAG.

Expression of JcdI in E. coli

The coding sequence for JcdI from *D. discoideum* (DDB_G0270006 at dictyBase.org; Q55CL5 at UniProtKB) was codon optimized for *E.coli* expression, modified to include silent restriction sites to facilitate domain deletions, and synthesized and inserted into pUC57 by GenScript. pUC57-JcdI was digested with NdeI and BglII to release the coding region for a C-terminally truncated fragment of JcdI that retains its F-box and catalytic domains, and ligated into pET15TEVi that was digested with NdeI and BamHI. This resulted in the addition of an N-terminal His_6-tag; the construct was referred to as His_6-JcdIΔC. Transformation of *E. coli* resulted in expression of substantial amounts full-length protein, which was nearly all insoluble.

A Skp1A expression cassette (T7 promoter + cDNA) was amplified by PCR using p48-Skp1-for-dual-S and p48-Skp1-for-dual-AS from pET19b-Skp1A and ligated into the SpeI site of pET15TEV-JcdIΔC. The correct orientation of the insert was confirmed by dual digestion with XbaI and HindIII and agarose gel electrophoresis. Induction of *E. coli* transformed with this dual expression plasmid yielded a soluble His_6-JcdIΔC/Skp1 complex (see below), but breakdown products were observed on CBB gels and anti-His_6 Western blots. To allow future co-expression with other proteins, this double expression cassette was transferred from the pET15 backbone (*ampR*) to pET24 backbone (*kanR*), using BglII and HindIII.

To overcome apparent instability, His_6JcdIΔC was subjected to further truncations. To remove the N-terminal amino acids 2-42 (123 nucleotides), which included a poorly conserved poly-N tract, two primers, NtermJCDIdel-S and NtermJCDIdel-AS, that bridged the interval to be deleted, with 9 nucleotides on either side, and off-set from each other so that the 3'-end of each primer did not anneal to the 5'-end of the other, were used to amplify the deletion construct by

PCR. PCR conditions were: 2U Q5 DNA polymerase (NEB), 1 µM each primer, 0.2 mM dNTPs, plasmid template, 30 cycles with 70°C annealing temperature and 4 min extension time. The amplification product was treated with DpnI, reacted with T4 DNAse at 22°C for 1-2 min to create sticky ends, incubated at 75°C for 20 min, and allowed to self-anneal for 30 min at 55°C or 65°C. The final product was transformed into *E. coli* TOP10 cells yielding, after sequence confirmation, pET28a-ΔNJcdIΔC/Skp1A. Next, the C-terminal coding region was further truncated by 60 amino acids using the same method, using JCDI-N-ΔN-S and JCDI-N-ΔN-AS as primers, except that DNAse treatment was not done, resulting in expression plasmid pET28a-ΔNJcdIΔCΔC/Skp1A.

This plasmid was transformed into *E. coli* strain ER2566 and protein expression was induced using 0.5 mM isopropyl β-D-1-thiogalactopyranoside in 100 µg/ml ampicillin in Luria Broth. Cells were harvested by centrifugation, resuspended in ice-cold 20 mM Tris-HCl, pH 7.5, spun again, and frozen at -80°C. The cell pellet was thawed in 20 ml/culture liter of 0.1 M Tris-HCl, pH 7.5, 5 mM benzamidine, 0.5 µg/ml pepstatin A, 10 µg/ml aprotinin, 10 µg/ml leupeptin, 1 mg/ml lysozyme, and 1 mM PMSF, subjected to Dounce homogenization with 4 strokes on ice, and probe-sonicated with a 1/2 inch probe, 60% amplitude, 1 sec on, 3 off, for 5 minutes, in an ice-water bath. The suspension was supplemented to achieve 5 mM $MgCl_2$, 50 µg/ml RNaseA, and 10 µg/ml DNaseI. A supernatant was generated by centrifugation at 22,000 × *g* for 30 min at 4°C, and adjusted to 0.5 M NaCl and 5 mM imidazole before loading onto a pre-equilibrated 1 ml His-Trap column (Pharmacia). The column was washed with the same buffer and step-eluted with increasing concentrations of imidazole in the same buffer. The majority of ΔNJcdIΔCΔC co-eluted with Skp1A at 250 mM imidazole, and was concentrated by centrifugal ultrafiltration and further

purified over a Superdex200 16/60 column equilibrated in 50 mM HEPES-NaOH, pH 7.4, 50 mM NaCl, 10% (v/v) glycerol, 2 mM DTT, 10 µg/ml aprotinin and 10 µg/ml leupeptin.

JcdI enzyme activity

Reaction cocktails consisting of 100 µM α-ketoglutarate, 1 mM ascorbate, 5 µM $FeSO_4$, 0. 1% Tween-20, 50 mM Tris-HCl (pH 7.5), 25 mM NaCl, 1 mM TCEP, 0.5 M betaine, 5% (v/v) glycerol,10 µg/ml aprotinin, and 10 µg/ml leupeptin, were pre-equilibrated in 1-ml sealed conical reactivials (Pierce) through which flowed, via needles piercing the Teflon seal, humidified premixed gas mixtures of O_2 and N_2. The reaction was initiated by the introduction, via a gas tight syringe, of highly purified and degassed JcdI (ΔNJcdINShort + Dd-Skp1A), to a final volume of 50 µl. Following incubation at 22°C, 10 µl was withdrawn with a syringe and divided over 2 wells of a white 384-well plate each containing 5 µl of freshly prepared SDR-1 (according to manufacturer's directions for Succinate-Glo kit, Promega). Following mixing for 30 seconds and incubation for 1 h at 22°C, 10 µl of SDR-II was added. After 30 seconds of mixing and 10 min of incubation at 22ºC, luminescence was recorded at 1 mm height for 1 second by a Synergy H4 plate reader (Bio-Tek). Pilot studies established incubation times and protein concentrations for which activity was linearly dependent.

Ectopic expression of JcdI in D. discoideum

Exon 1 of JcdI was amplified from *D. discoideum* gDNA (80) by PCR using primers JcdI-Ex1-S and JcdI-Ex1-AS, and Exon 2 was similarly amplified using JcdI-Ex2-S and JcdI-Ex2-AS. The PCR product bands were purified by electrophoresis and separately cloned into pCR4-TOPO (Invitrogen), resulting in pCR4-TOPO-JcdI-Ex1 and pCR4-TOPO-JcdI-Ex2. Their sequences were confirmed using primers M13F and M13R. Exon 2 was released using BspEI and SacI and cloned

into similarly digested and Antarctic phosphatase (NEB) treated pCR4-TOPO-JcdI-Ex1. The predicted F-box domain was modified by the introduction of 3 point mutations by site-directed mutagenesis of pCR4-TOPO-JcdI using JcdI-SDM-F-box ARA-S and JcdI-SDM-F-box ARA-AS as previously described (46), yielding pCR4-TOPO-JcdI(ARA). The *jcdI* cDNAs were released using NcoI and SacI and cloned into similarly digested and Antarctic phosphatase treated pV3D (pVS3). The pV3D-JcdI plasmid was used as a template to generate a FLAG-JcdI(H319A) expression plasmid through site-directed mutagenesis. The FLAG-ΔNJcdIΔCΔC expression construct was achieved by PCR deletion on the pV3D JcdI plasmid with overlapping homology regions in the 5' portion of primers. All sequences were verified. Native pV3D-JcdI and the mutant constructs were electroporated into strains Ax3 (*phyA*$^{+}$) or HW288 (*phyA*$^{-}$) and transformants were selected in the presence of 10 µM G418 (77). Clones were recovered from plaques growing on lawns of *Klebsiella aerogenes*, and screened by Western blotting with an anti-FLAG mAb M2. Clones expressing similar levels of FLAG-JcdI, FLAG-JcdI-ARA, and FLAG-JcdI(H319A) during vegetative growth were chosen for further analysis. High levels of FLAG-ΔNJcdIΔCΔC expression were not found. None of the stains showed proliferation defects in HL-5 medium.

Disruption of jcdI and jcdH loci

The coding region of the *jcdI* locus was disrupted by double cross-over homologous recombination as previously described (77. Briefly, a 1033-nt 5'-targeting region was amplified from the 5'-end of the coding region with JCDI-5'-S and JCDI-5'-AS, using gDNA (80) as a template, and cloned into pCR4-TOPO. An 860-nt 3'-targeting region was amplified from the middle of the coding region using JcdI-3'-S-Stop and JcdI-3'-AS, and cloned into pCR4-TOPO. The 5'-targeting region was excised using BssHII and BamHI cloned into pVSCulE-BsR (see above) pre-digested

with BssHII and BglII. The 3’-targeting region was next excised with PstI and PvuII and cloned into similarly digested pVS-JcdI-5’-BsR, yielding pVS-JcdI-5’-BsR-3’. This construct was designed to replace the JmjC domain with a floxed *bsr* cassette, and introduced stop codons at the intersections to minimize possible of read-through translation of remaining coding DNA. The *jcdI* disruption DNA was released using BssHII and PvuII and electroporated into Ax3 cells. Clones were screened by PCR using JcdI-KO-5’UpS, which anneals upstream of the 5’-targeting sequence, and JET-BSR-AS, which anneals within the introduced bsr cassette, and with JcdI-KO-3’Scr-AS, which anneals downstream of the 3’-targeting DNA, and JcdI-KO-BSR3’Scr-S, which anneals within the bsr cassette. The floxed bsr cassette was then excised as above, and successfully deleted clones were screened based on sensitivity to bsr, and confirmed by PCR using primer pairs p5 and p9, and p8 and p6.

JcdH (DDB_G0280485; protein model: DDB0238368, at dictyBase.org; Q54VA7 at UniProtKB) was disrupted in the *jcdI*$^{-}$ strain. As for *jcdI*, a 739-bp 5’-targeting DNA was PCR-amplified from gDNA using 5'-targeting forward (p1) and 5'-targeting reverse (p2) oligonucleotides and cloned into pCR4-TOPO. A 665-bp 3’-targeting DNA was PCR amplified from within the coding region using 3'-targeting forward (p3) and 3'-targeting reverse (p4) oligonucleotides, and cloned into pCR4-TOPO. These fragments were assembled into pVSCulE-BsR as above to generate pVS-JcdH-5’-BsR-3’. This construct is designed to replace JcdH amino acids 24-347, which include the F-box domain and a portion of the JmjC domain, with the *bsr* cassette. PCR screening of transfected clones was performed using pVS_tag_non-c_seq_F-v2, which anneals within the bsr cassette, and JcdH3'UTRScrR(p6) or p12/JcdH-3'ext-AS, which anneal downstream from the 3’-targeting DNA.

Phylogenetic analyses

Sequences related to *Dictyostelium* JcdI were analyzed as described previously (81). In brief, the sequence of the JmjC domain (147 amino acid residues) from XP_646466.1 was used as query for BLASTp searches against sequence databases (NCBI, DOE JGI, EUPATHDB, and Broad Institute). The 74 best hit sequences were aligned and trimmed of highly gapped insert regions. The phylogenetic tree was built using IQ-Tree (82) with the following options: -m MFP -bb 10000, and used the LG+R5 substitution model. ModelFinder (83), implemented in IQ-Tree, was used to find the best fit model. Bootstrap support values were obtained using UltraFast bootstrap approximation (UFBoot) (84) implemented in IQ-Tree, and the tree was visualized in iTOL (85). The overall topology of the tree was robust as an independent tree generated using MEGA had a similar topology.

Fig. 2.15. Disruption of the *jcdI* and *jcdH* gene loci.

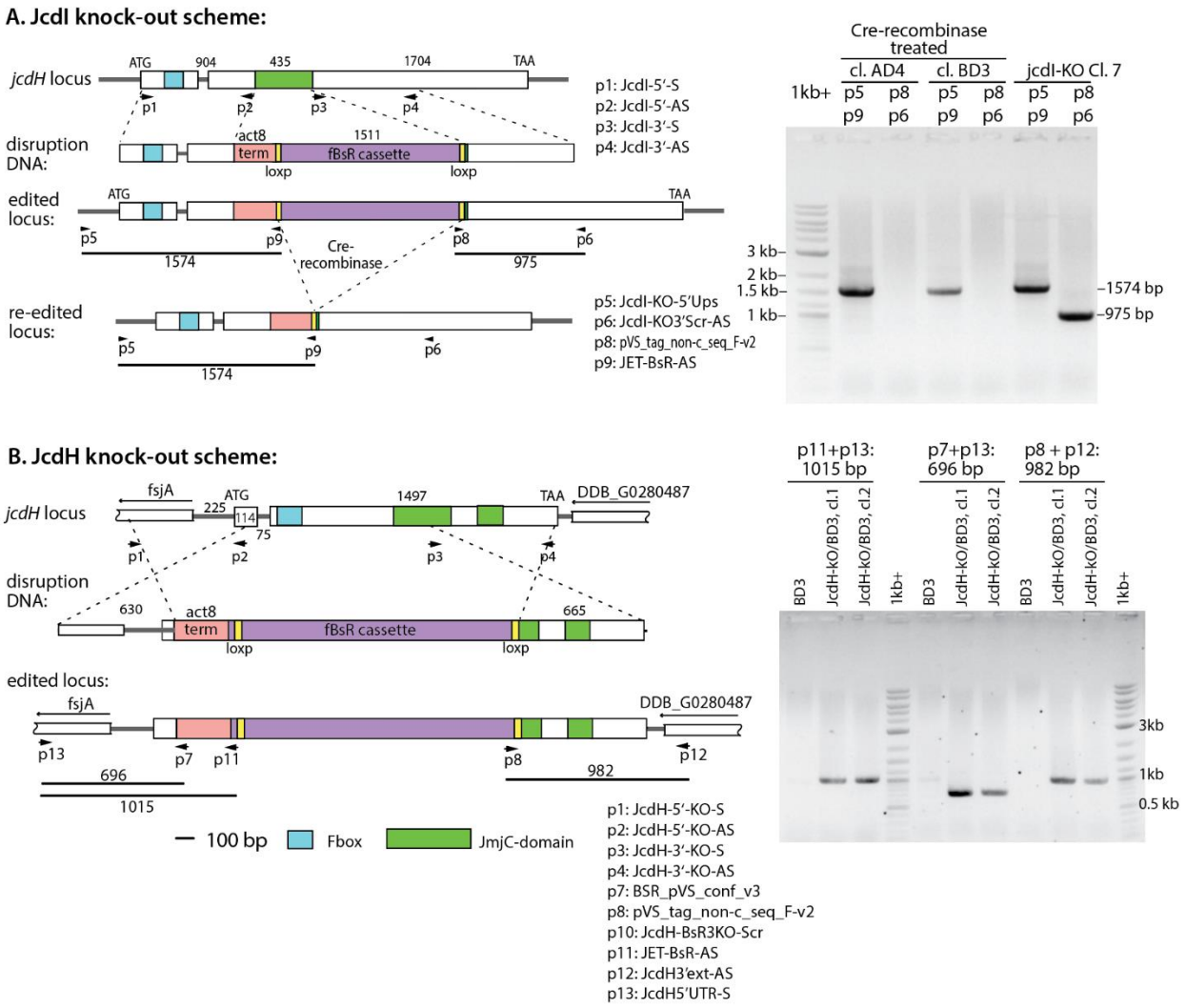

Fig. 2.15. Disruption of the *jcdI* and *jcdH* gene loci. Replacement DNAs were designed to integrate into their target loci via double cross-over homologous recombination, thereby replacing a region of the coding region with a floxed blasticidin S resistance cassette (bsr). PCR reactions with pairs of oligonucleotide primers residing either within the cassette or flanking the targeting DNA sequences were performed to assess the expected editing events. Expected products are shown at the left, and results are at the right. *A,* strategy for *jcdI*. In addition, a replacement clone (cl. 7) was transiently transfected with a Cre-recombinase expressing vector to remove the floxed bsr cassette, enabling its reuse for replacing jcdH. *B,* strategy for replacing *jcdH* in a *jcdI*$^{-}$ strain (cl. BD3) from panel A.

Chapter 2 References

1. Willems, A. R., Schwab, M., and Tyers, M. (2004) A hitchhiker's guide to the cullin ubiquitin ligases: SCF and its kin. *Biochim. Biophys. Acta - Molecular Cell Research* **1695**, 133-170
2. Harper, J. W., and Schulman, B. A. (2021) Cullin-RING ubiquitin ligase regulatory circuits: A quarter century beyond the F-Box hypothesis. *Annu. Rev. Biochem.* **90**, 403-429
3. Reitsma, J. M., Liu, X., Reichermeier, K. M., Moradian, A., Sweredoski, M. J., Hess, S., and Deshaies, R. J. (2017) Composition and regulation of the cellular repertoire of SCF ubiquitin ligases. *Cell* **171**, 1326-1339
4. Wang, K., Deshaies, R. J., and Liu, X. (2020) Assembly and regulation of CRL ubiquitin ligases. *Adv. Exp. Med. Biol.* **1217**, 33-46
5. Cavadini, S., Fischer, E. S., Bunker, R. D., Potenza, A., Lingaraju, G. M., Goldie, K. N., Mohamed, W. I., Faty, M., Petzold, G., Beckwith, R. E., Tichkule, R. B., Hassiepen, U., Abdulrahman, W., Pantelic, R. S., Matsumoto, S., Sugasawa, K., Stahlberg, H., and Thomä, N. H. (2016) Cullin-RING ubiquitin E3 ligase regulation by the COP9 signalosome. *Nature* **531**, 598-603
6. de Bie, P., and Ciechanover, A. (2011) Ubiquitination of E3 ligases: self-regulation of the ubiquitin system via proteolytic and non-proteolytic mechanisms. *Cell Death & Differentiation* **18**, 1393-1402
7. Schulman, B. A., Carrano, A. C., Jeffrey, P. D., Bowen, Z., Kinnucan, E. R., Finnin, M. S., Elledge, S. J., Harper, J. W., Pagano, M., and Pavletich, N. P. (2000) Insights into SCF ubiquitin ligases from the structure of the Skp1-Skp2 complex. *Nature* **408**, 381-386
8. Skaar, J. R., Pagan, J. K., and Pagano, M. (2013) Mechanisms and function of substrate recruitment by F-box proteins. *Nat. Rev. Mol. Cell Biol.* **14**, 369-381
9. Baptista, C. G., Lis, A., Deng, B., Gas-Pascual, E., Dittmar, A., Sigurdson, W., West, C. M., and Blader, I. J. (2019) *Toxoplasma* F-box protein 1 is required for daughter cell scaffold function during parasite replication. *PLoS Pathog.* **15**, e1007946
10. Teng-umnuay, P., Morris, H. R., Dell, A., Panico, M., Paxton, T., and West, C. M. (1998) The cytoplasmic F-box binding protein SKP1 contains a novel pentasaccharide linked to hydroxyproline in *Dictyostelium*. *J. Biol. Chem.* **273**, 18242-18249
11. Xu, Y., Brown, K. M., Wang, Z. A., van der Wel, H., Teygong, C., Zhang, D., Blader, I. J., and West, C. M. (2012) The Skp1 protein from *Toxoplasma* is modified by a cytoplasmic prolyl 4-hydroxylase associated with oxygen sensing in the social amoeba *Dictyostelium*. *J. Biol. Chem.* **287**, 25098-25110
12. Rahman, K., Zhao, P., Mandalasi, M., van der Wel, H., Wells, L., Blader, I. J., and West, C. M. (2016) The E3 ubiquitin ligase adaptor protein Skp1 Is glycosylated by an evolutionarily conserved pathway that regulates protist growth and development. *J. Biol. Chem.* **291**, 4268-4280
13. West, C. M., and Blader, I. J. (2015) Oxygen sensing by protozoans: How they catch their breath. *Curr. Opin. Microbiol.* **26**, 41-47
14. van der Wel, H., Gas-Pascual, E., and West, C. M. (2019) Skp1 isoforms are differentially modified by a dual function prolyl 4-hydroxylase/N-acetylglucosaminyltransferase in a plant pathogen. *Glycobiology* **29**, 705-714

15. Cochet-Escartin, O., Demircigil, M., Hirose, S., Allais, B., Gonzalo, P., Mikaelian, I., Funamoto, K., Anjard, C., Calvez, V., and Rieu, J.-P. (2021) Hypoxia triggers collective aerotactic migration in *Dictyostelium discoideum*. *eLife* **10**, e64731
16. Pugh, C. W., and Ratcliffe, P. J. (2017) New horizons in hypoxia signaling pathways. *Exp. Cell Res.* **356**, 116-121
17. Islam, M. S., Leissing, T. M., Chowdhury, R., Hopkinson, R. J., and Schofield, C. J. (2018) 2-oxoglutarate-dependent oxygenases. *Annu. Rev. Biochem.* **87**, 585-620
18. van der Wel, H., Ercan, A., and West, C. M. (2005) The Skp1 prolyl hydroxylase from *Dictyostelium* is related to the hypoxia-inducible factor-alpha class of animal prolyl 4-hydroxylases. *J. Biol. Chem.* **280**, 14645-14655
19. Liu, T., Abboud, M. I., Chowdhury, R., Tumber, A., Hardy, A. P., Lippl, K., Lohans, C. T., Pires, E., Wickens, J., McDonough, M. A., West, C. M., and Schofield, C. J. (2020) Biochemical and biophysical analyses of hypoxia sensing prolyl hydroxylases from *Dictyostelium discoideum* and *Toxoplasma gondii*. *J. Biol. Chem.* **29**, 16545–16561
20. Sheikh, M. O., Xu, Y., van der Wel, H., Walden, P., Hartson, S. D., and West, C. M. (2015) Glycosylation of Skp1 promotes formation of Skp1-Cullin-1-F-box protein complexes in *Dictyostelium*. *Mol. Cell. Proteomics* **14**, 66-80
21. Xu, Y., Wang, Z. A., Green, R. S., and West, C. M. (2012) Role of the Skp1 prolyl-hydroxylation/glycosylation pathway in oxygen dependent submerged development of *Dictyostelium*. *BMC Devel. Biol.* **12**, 31-31
22. Wang, Z. A., Singh, D., van der Wel, H., and West, C. M. (2011) Prolyl hydroxylation- and glycosylation-dependent functions of Skp1 in O_2-regulated development of *Dictyostelium*. *Dev. Biol.* **349**, 283-295
23. Mandalasi, M., Kim, H. W., Thieker, D., Sheikh, M. O., Gas-Pascual, E., Rahman, K., Zhao, P., Daniel, N. G., van der Wel, H., Ichikawa, H. T., Glushka, J. N., Wells, L., Woods, R. J., Wood, Z. A., and West, C. M. (2020) A terminal α3-galactose modification regulates an E3 ubiquitin ligase subunit in *Toxoplasma gondii*. *J. Biol. Chem.* **295**, 9223-9243
24. Sheikh, M. O., Thieker, D., Chalmers, G., Schafer, C. M., Ishihara, M., Azadi, P., Woods, R. J., Glushka, J. N., Bendiak, B., Prestegard, J. H., and West, C. M. (2017) O_2 sensing-associated glycosylation exposes the F-box-combining site of the *Dictyostelium* Skp1 subunit in E3 ubiquitin ligases. *J. Biol. Chem.* **292**, 18897-18915
25. Sheikh, M. O., Schafer, C. M., Powell, J. T., Rodgers, K. K., Mooers, B. H., and West, C. M. (2014) Glycosylation of Skp1 affects its conformation and promotes binding to a model F-box protein. *Biochemistry* **53**, 1657-1669
26. Xu, X., Eletsky, A., Sheikh, M. O., Prestegard, J. H., and West, C. M. (2018) Glycosylation promotes the random coil to helix transition in a region of a protist Skp1 associated with F-box binding. *Biochemistry* **57**, 511-515
27. Kim, H. W., Eletsky, A., Gonzalez, K. J., van der Wel, H., Strauch, E. M., Prestegard, J. H., and West, C. M. (2020) Skp1 dimerization conceals its F-box protein binding site. *Biochemistry* **59**, 1527-1536
29. Mantri, M., Krojer, T., Bagg, E. A., Webby, C. A., Butler, D. S., Kochan, G., Kavanagh, K. L., Oppermann, U., McDonough, M. A., and Schofield, C. J. (2010) Crystal structure of the 2-oxoglutarate- and Fe(II)-dependent lysyl hydroxylase JMJD6. *J. Mol. Biol.* **401**, 211-222

30. Böttger, A., Islam, M. S., Chowdhury, R., Schofield, C. J., and Wolf, A. (2015) The oxygenase Jmjd6--a case study in conflicting assignments. *Biochem. J.* **468**, 191-202
31. Wong, M., Sun, Y., Xi, Z., Milazzo, G., Poulos, R. C., Bartenhagen, C., Bell, J. L., Mayoh, C., Ho, N., Tee, A. E., Chen, X., Li, Y., Ciaccio, R., Liu, P. Y., Jiang, C. C., Lan, Q., Jayatilleke, N., Cheung, B. B., Haber, M., Norris, M. D., Zhang, X. D., Marshall, G. M., Wang, J. Y., Hüttelmaier, S., Fischer, M., Wong, J. W. H., Xu, H., Perini, G., Dong, Q., George, R. E., and Liu, T. (2019) JMJD6 is a tumorigenic factor and therapeutic target in neuroblastoma. *Nat. Commun.* **10**, 3319
32. Early, A. E., Gaskell, M. J., Traynor, D., and Williams, J. G. (1993) Two distinct populations of prestalk cells within the tip of the migratory *Dictyostelium* slug with differing fates at culmination. *Development* **118**, 353-362
33. Kelly, B., Carrizo, G. E., Edwards-Hicks, J., Sanin, D. E., Stanczak, M. A., Priesnitz, C., Flachsmann, L. J., Curtis, J. D., Mittler, G., Musa, Y., Becker, T., Buescher, J. M., and Pearce, E. L. (2021) Sulfur sequestration promotes multicellularity during nutrient limitation. *Nature* **591**, 471-476
34. Lee, D. H., and Goldberg, A. L. (1998) Proteasome inhibitors: valuable new tools for cell biologists. *Tr. Cell Biol.* **8**, 397-403
35. Adams, J., Behnke, M., Chen, S., Cruickshank, A. A., Dick, L. R., Grenier, L., Klunder, J. M., Ma, Y.-T., Plamondon, L., and Stein, R. L. (1998) Potent and selective inhibitors of the proteasome: Dipeptidyl boronic acids. *Bioorganic & Medicinal Chemistry Letters* **8**, 333-338
36. Demo, S. D., Kirk, C. J., Aujay, M. A., Buchholz, T. J., Dajee, M., Ho, M. N., Jiang, J., Laidig, G. J., Lewis, E. R., Parlati, F., Shenk, K. D., Smyth, M. S., Sun, C. M., Vallone, M. K., Woo, T. M., Molineaux, C. J., and Bennett, M. K. (2007) Antitumor activity of PR-171, a novel irreversible inhibitor of the proteasome. *Cancer Res.* **67**, 6383-6391
37. Stein, M. L., Cui, H., Beck, P., Dubiella, C., Voss, C., Krüger, A., Schmidt, B., and Groll, M. (2014) Systematic comparison of peptidic proteasome inhibitors highlights the α-ketoamide electrophile as an auspicious reversible lead motif. *Angew Chem. Int. Ed. Engl.* **53**, 1679-1683
38. Ercan, A., Panico, M., Sutton-Smith, M., Dell, A., Morris, H. R., Matta, K. L., Gay, D. F., and West, C. M. (2006) Molecular characterization of a novel UDP-galactose:fucoside alpha3-galactosyltransferase that modifies Skp1 in the cytoplasm of *Dictyostelium*. *J. Biol. Chem.* **281**, 12713-12721
39. Sassi, S., Sweetinburgh, M., Erogul, J., Zhang, P., Teng-Umnuay, P., and West, C. M. (2001) Analysis of Skp1 glycosylation and nuclear enrichment in *Dictyostelium*. *Glycobiology* **11**, 283-295
40. Lundgren, D. H., Hwang, S. I., Wu, L., and Han, D. K. (2010) Role of spectral counting in quantitative proteomics. *Expert Rev. Proteomics* **7**, 39-53
41. Mohanty, S., Lee, S., Yadava, N., Dealy, M. J., Johnson, R. S., and Firtel, R. A. (2001) Regulated protein degradation controls PKA function and cell-type differentiation in *Dictyostelium*. *Genes Dev.* **15**, 1435-1448
42. Geneious Prime 2019.2.3. (https://www.geneious.com).
43. O'Day, D. H., Suhre, K., Myre, M. A., Chatterjee-Chakraborty, M., and Chavez, S. E. (2006) Isolation, characterization, and bioinformatic analysis of calmodulin-binding protein cmbB

reveals a novel tandem IP22 repeat common to many *Dictyostelium* and Mimivirus proteins. *Biochem. Biophys. Res. Comm.* **346**, 879-888
44. Zhang, D., van der Wel, H., Johnson, J. M., and West, C. M. (2012) Skp1 prolyl 4-hydroxylase of *Dictyostelium* mediates glycosylation-independent and -dependent responses to O_2 without affecting Skp1 stability. *J. Biol. Chem.* **287**, 2006-2016
45. Russell, I. D., Grancell, A. S., and Sorger, P. K. (1999) The unstable F-box protein p58-Ctf13 forms the structural core of the CBF3 kinetochore complex. *J. Cell Biol.* **145**, 933-950
46. West, C. M., van der Wel, H., and Wang, Z. A. (2007) Prolyl 4-hydroxylase-1 mediates O_2 signaling during development of *Dictyostelium*. *Development* **134**, 3349-3358
47. Chang, B., Chen, Y., Zhao, Y., and Bruick, R. K. (2007) JMJD6 is a histone arginine demethylase. *Science* **318**, 444-447
48. Liu, W., Ma, Q., Wong, K., Li, W., Ohgi, K., Zhang, J., Aggarwal, A., and Rosenfeld, M. G. (2013) Brd4 and JMJD6-associated anti-pause enhancers in regulation of transcriptional pause release. *Cell* **155**, 1581-1595
49. Heim, A., Grimm, C., Müller, U., Häußler, S., Mackeen, M. M., Merl, J., Hauck, S. M., Kessler, B. M., Schofield, C. J., Wolf, A., and Böttger, A. (2014) Jumonji domain containing protein 6 (Jmjd6) modulates splicing and specifically interacts with arginine-serine-rich (RS) domains of SR- and SR-like proteins. *Nuc. Ac. Res.* **42**, 7833-7850
50. Sternfeld, J., and David, C. N. (1981) Oxygen gradients cause pattern orientation in *Dictyostelium* cell clumps. *J. Cell. Sci.* **50**, 9-17
51. Kwok, J., O'Shea, M., Hume, D. A., and Lengeling, A. (2017) Jmjd6, a JmjC dioxygenase with many interaction partners and pleiotropic functions. *Front. Genet.* **8**, 32
52. Reiterer, V., Figueras-Puig, C., Le Guerroue, F., Confalonieri, S., Vecchi, M., Jalapothu, D., Kanse, S. M., Deshaies, R. J., Di Fiore, P. P., Behrends, C., and Farhan, H. (2018) The pseudophosphatase STYX targets the F-box of FBXW7 and inhibits SCF(FBXW)(7) function. *EMBO J.* **37**, e99170
53. Nelson, D. E., and Laman, H. (2011) A Competitive binding mechanism between Skp1 and exportin 1 (CRM1) controls the localization of a subset of F-box proteins. *J. Biol. Chem.* **286**, 19804-19815
54. Yam, A. Y., Xia, Y., Lin, H. T., Burlingame, A., Gerstein, M., and Frydman, J. (2008) Defining the TRiC/CCT interactome links chaperonin function to stabilization of newly made proteins with complex topologies. *Nat. Struct. Mol. Biol.* **15**, 1255-1262
55. Yu, H., Zhang, Y., Moss, B. L., Bargmann, B. O., Wang, R., Prigge, M., Nemhauser, J. L., and Estelle, M. (2015) Untethering the TIR1 auxin receptor from the SCF complex increases its stability and inhibits auxin response. *Nat Plants* **1**:pii:14030.
56. Lauinger, L., Flick, K., Yen, J. L., Mathur, R., and Kaiser, P. (2020) Cdc48 cofactor Shp1 regulates signal-induced SCF(Met30) disassembly. *Proc. Natl. Acad. Sci. USA* **117**, 21319-21327
57. Beltrao, P., Albanèse, V., Kenner, L. R., Swaney, D. L., Burlingame, A., Villén, J., Lim, W. A., Fraser, J. S., Frydman, J., and Krogan, N. J. (2012) Systematic functional prioritization of protein posttranslational modifications. *Cell* **150**, 413-425
58. Rosengarten, R. D., Santhanam, B., Fuller, D., Katoh-Kurasawa, M., Loomis, W. F., Zupan, B., and Shaulsky, G. (2015) Leaps and lulls in the developmental transcriptome of *Dictyostelium discoideum*. *BMC Genomics* **16**, 294

59. Nguyen, K. M., and Busino, L. (2020) The biology of F-box proteins: The SCF family of E3 ubiquitin ligases. *Adv. Exp. Med. Biol.* **1217**, 111-122
60. Willhoft, O., Kerr, R., Patel, D., Zhang, W., Al-Jassar, C., Daviter, T., Millson, S. H., Thalassinos, K., and Vaughan, C. K. (2017) The crystal structure of the Sgt1-Skp1 complex: the link between Hsp90 and both SCF E3 ubiquitin ligases and kinetochores. *Sci. Rep.* **7**, 41626
61. Rayon, T., Stamataki, D., Perez-Carrasco, R., Garcia-Perez, L., Barrington, C., Melchionda, M., Exelby, K., Lazaro, J., Tybulewicz, V. L. J., Fisher, E. M. C., and Briscoe, J. (2020) Species-specific pace of development is associated with differences in protein stability. *Science* **369**, eaba7667
62. Das, O. P., and Henderson, E. J. (1983) A novel technique for gentle lysis of eucaryotic cells Isolation of plasma membranes from *Dictyostelium discoideum*. *Biochim. Biophys. Acta - Biomembranes* **736**, 45-56
63. Müller, T., and Winter, D. (2017) Systematic evaluation of protein reduction and alkylation reveals massive unspecific side effects by iodine-containing reagents. *Molec. Cell. Prot.* **16**, 1173-1187
64. Eichinger, L., Pachebat, J. A., Glöckner, G., Rajandream, M. A., Sucgang, R., Berriman, M., Song, J., Olsen, R., Szafranski, K., Xu, Q., Tunggal, B., Kummerfeld, S., Madera, M., Konfortov, B. A., Rivero, F., Bankier, A. T., Lehmann, R., Hamlin, N., Davies, R., Gaudet, P., Fey, P., Pilcher, K., Chen, G., Saunders, D., Sodergren, E., Davis, P., Kerhornou, A., Nie, X., Hall, N., Anjard, C., Hemphill, L., Bason, N., Farbrother, P., Desany, B., Just, E., Morio, T., Rost, R., Churcher, C., Cooper, J., Haydock, S., van Driessche, N., Cronin, A., Goodhead, I., Muzny, D., Mourier, T., Pain, A., Lu, M., Harper, D., Lindsay, R., Hauser, H., James, K., Quiles, M., Madan Babu, M., Saito, T., Buchrieser, C., Wardroper, A., Felder, M., Thangavelu, M., Johnson, D., Knights, A., Loulseged, H., Mungall, K., Oliver, K., Price, C., Quail, M. A., Urushihara, H., Hernandez, J., Rabbinowitsch, E., Steffen, D., Sanders, M., Ma, J., Kohara, Y., Sharp, S., Simmonds, M., Spiegler, S., Tivey, A., Sugano, S., White, B., Walker, D., Woodward, J., Winckler, T., Tanaka, Y., Shaulsky, G., Schleicher, M., Weinstock, G., Rosenthal, A., Cox, E. C., Chisholm, R. L., Gibbs, R., Loomis, W. F., Platzer, M., Kay, R. R., Williams, J., Dear, P. H., Noegel, A. A., Barrell, B., and Kuspa, A. (2005) The genome of the social amoeba *Dictyostelium discoideum*. *Nature* **435**, 43-57
65. Weber, R. J. M., Li, E., Bruty, J., He, S., and Viant, M. R. (2012) MaConDa: a publicly accessible mass spectrometry contaminants database. *Bioinformatics* **28**, 2856-2857
66. Wilson, J., Palmeri, J., and Pappin, D. (2020) SimpliFi: a data-to-meaning analytics engine to bring omics understanding to all. *J. Biomol. Tech.* **31(Suppl)**, S1–S2 (abstract)
67. Perez-Riverol, Y., Csordas, A., Bai, J., Bernal-Llinares, M., Hewapathirana, S., Kundu, D. J., Inuganti, A., Griss, J., Mayer, G., Eisenacher, M., Pérez, E., Uszkoreit, J., Pfeuffer, J., Sachsenberg, T., Yilmaz, S., Tiwary, S., Cox, J., Audain, E., Walzer, M., Jarnuczak, A. F., Ternent, T., Brazma, A., and Vizcaíno, J. A. (2019). The PRIDE database and related tools and resources in 2019: improving support for quantification data. *Nuc. Ac. Res.* **47**(D1), D442-D450
68. Altschul, S. F., Wootton, J. C., Gertz, E. M., Agarwala, R., Morgulis, A., Schäffer, A. A., and Yu,Y. K. (2005) Protein database searches using compositionally adjusted substitution matrices. *FEBS J*. **272**, 5101-5109

69. Parikh, A., Miranda, E. R., Katoh-Kurasawa, M., Fuller, D., Rot, G., Zagar, L., Curk, T., Sucgang, R., Chen, R., Zupan, B., Loomis, W. F., Kuspa, A., and Shaulsky, G. (2010) Conserved developmental transcriptomes in evolutionarily divergent species. *Genome Biol.* **11**, R35
70. Yan, K., Zhang, Z., Yang, J., McLaughlin, S. H., and Barford, D. (2018) Architecture of the CBF3-centromere complex of the budding yeast kinetochore. *Nat. Struct. Mol. Biol.* **25**, 1103-1110
71. Waterhouse, A., Bertoni, M., Bienert, S., Studer, G., Tauriello, G., Gumienny, R., Heer, F. T., de Beer, T. A. P., Rempfer, C., Bordoli, L., Lepore, R., and Schwede, T. (2018) SWISS-MODEL: homology modelling of protein structures and complexes. *Nuc. Ac. Res.* **46**, W296-W303
72. Bienert, S., Waterhouse, A., de Beer, T. A., Tauriello, G., Studer, G., Bordoli, L., and Schwede, T. (2017) The SWISS-MODEL Repository-new features and functionality. *Nuc. Ac. Res.* **45**, D313-D319
73. Guex, N., Peitsch, M. C., and Schwede, T. (2009) Automated comparative protein structure modeling with SWISS-MODEL and Swiss-PdbViewer: a historical perspective. *Electrophoresis* **30 Suppl 1**, S162-173
74. Studer, G., Rempfer, C., Waterhouse, A. M., Gumienny, R., Haas, J., and Schwede, T. (2020) QMEANDisCo-distance constraints applied on model quality estimation. *Bioinformatics* **36**, 2647
75. Bertoni, M., Kiefer, F., Biasini, M., Bordoli, L., and Schwede, T. (2017) Modeling protein quaternary structure of homo- and hetero-oligomers beyond binary interactions by homology. *Sci. Rep.* **7**, 10480
76. Ercan, A., Panico, M., Sutton-Smith, M., Dell, A., Morris, H. R., Matta, K. L., Gay, D. F., and West, C. M. (2006) Molecular characterization of a novel UDP-galactose:fucoside alpha3-galactosyltransferase that modifies Skp1 in the cytoplasm of *Dictyostelium*. *J. Biol. Chem.* **281**, 12713-12721
77. Pang, K. M., Lynes, M. A., and Knecht, D. A. (1999) Variables controlling the expression level of exogenous genes in *Dictyostelium*. *Plasmid* **41**, 187-197
78. Zhang, Y., Zhang, P., and West, C. M. (1999) A linking function for the cellulose-binding protein SP85 in the spore coat of *Dictyostelium discoideum*. *J. Cell Sci.* **112 (Pt 23)**, 4367-4377
79. Faix, J., Linkner, J., Nordholz, B., Platt, J. L., Liao, X. H., and Kimmel, A. R. (2013) The application of the Cre-loxP system for generating multiple knock-out and knock-in targeted loci. *Meth. Mol. Biol.* **983**, 249-267
80. Charette, S. J., and Cosson, P. (2004) Preparation of genomic DNA from *Dictyostelium discoideum* for PCR analysis. *Biotechniques* **36**, 574-575
81. Taujale, R., Venkat, A., Huang, L. C., Zhou, Z., Yeung, W., Rasheed, K. M., Li, S., Edison, A. S., Moremen, K. W., and Kannan, N. (2020) Deep evolutionary analysis reveals the design principles of fold A glycosyltransferases. *Elife* **9**, e54532
82. Nguyen, L.-T., Schmidt, H. A., von Haeseler, A., and Minh, B. Q. (2015) IQ-TREE: A fast and effective stochastic algorithm for estimating maximum-likelihood phylogenies. *Molec. Biol. Evol.* **32**, 268-274

83. Kalyaanamoorthy, S., Minh, B. Q., Wong, T. K. F., von Haeseler, A., and Jermiin, L. S. (2017) ModelFinder: fast model selection for accurate phylogenetic estimates. *Nature Meth.* **14**, 587-589
84. Hoang, D. T., Chernomor, O., von Haeseler, A., Minh, B. Q., and Vinh, L. S. (2018) UFBoot2: Improving the ultrafast bootstrap approximation. *Molec. Biol. Evol.* **35**, 518-522
85. Letunic, I., and Bork, P. (2021) Interactive Tree Of Life (iTOL) v5: an online tool for phylogenetic tree display and annotation. *Nuc. Ac. Res.* **49**, W293-W296
86. Loomis, W. F. (1971) Sensitivity of *Dictyostelium discoideum* to nucleic acid analogues. *Exp. Cell Res.* **64**, 484-486
87. Gruenheit, N., Baldwin, A., Stewart, B., Jaques, S., Keller, T., Parkinson, K., Salvidge, W., Baines, R., Brimson, C., Wolf, J. B., Chisholm, R., Harwood, A. J., and Thompson, C. R. L. (2021) Mutant resources for functional genomics in *Dictyostelium discoideum* using REMI-seq technology. *BMC Biol.* **19**, 172
88. West, C. M., van der Wel, H., and Gaucher, E. A. (2002) Complex glycosylation of Skp1 in *Dictyostelium*: implications for the modification of other eukaryotic cytoplasmic and nuclear proteins. *Glycobiology* **12,** 17R-27R

CHAPTER 3

A CYTOPLASMIC VIT/vWFA PROTEIN SYNERGIZES WITH A WD40-REPEAT F-BOX PROTEIN TO CONTROL DEVELOPMENT IN *DICTYOSTELIUM*

A. W. Boland, E. Gas-Pascual, H. van der Wel, C. M. West. To be submitted to *Journal of Biological Chemistry*

Abstract

Like most eukaryotes, the pre-metazoan social amoeba *Dictyostelium* depends on the SCF (Skp1/cullin-1/F-box protein) family of E3 ubiquitin ligases to regulate its proteome. In *Dictyostelium*, starvation induces a transition from unicellular feeding to a multicellular slug that responds to external signals to culminate into a fruiting body containing terminally differentiated stalk and spore cells. These transitions are subject to regulation by F-box proteins and O_2-dependent posttranslational modifications of Skp1. Here we examine in greater depth the essential role of FbxW2 and Vwa1, which was found in the FbxWD interactome by co-immunoprecipitation and is classified as a vault protein inter-alpha- trypsin (VIT) and von Willebrand factor-A (vWFA) domain containing protein. Reciprocal co-IPs using gene-tagged strains confirmed the interaction and their similar changes in protein levels during multicellular development suggesting they function together. FbxWD overexpression and proteasome inhibitors did not affect Vwa1 levels suggesting a non-substrate relationship. Forced FbxwD overexpression in slug tip cells where it is enriched during development blocked culmination by a mechanism that depended on its F-box and RING domains, and on Vwa1 expression itself. However, *vwa1*-disruption alone did not affect development. In contrast, overexpression of either of its three conserved domains arrested development but the effect depended on Vwa1 expression. Based on structure predictions, we propose that the Vwa1 domains exert their negative effect by artificially activating Vwa1 which in turn imbalances its synergistic function with FbxWD. Autoinhibition or homodimerization might be relevant to the poorly understood tumor suppressor role of the evolutionarily related VWA5A/BCSC-1 in humans.

Introduction

As cells grow, replicate, and differentiate, their proteomes must be remodeled to meet their needs. The ubiquitin proteasome system helps address these needs using highly regulated assemblies of poly-ubiquitin ligases to target proteins for degradation by the 26S proteasome. Cullin-1 Ring Ub ligases, also known as Skp1/Cullin-1/Fbox protein (SCF) complexes, comprise a major family that is highly evolutionarily conserved. They utilize a cullin (Cul1) scaffold and Rbx1 to bind Ub-charged E2 subunits in proximity to the Skp1 adaptor and substrate binding F-box protein (FBP) (1,2). Canonical FBPs have a substrate binding domain located C-terminal to the ~40 amino acid Skp1 interfacing F-box domain. These substrate receptor (SR) domains, which include WD40 repeat propellers, Leucine-rich repeats (LRR), Armadillo-repeats, and others, confer specificity to the SCF (3). While many FBPs and their substrates have been characterized in humans, yeast, and *Arabidopsis*, the majority of FBP substrates are yet to be elucidated. Furthermore, the evolutionary diversity of FBPs complicates their characterization in unrelated organisms. Thus, the role of the SCF in the vast kingdom of protists, which includes many pathogens that seriously impact human and animal health, as well as agriculture, remains unknown.

The amoebozoan are a broad group of protists that lie near the base of the branch of eukaryotic evolution that gave rise to fungi, yeast, and animals (4-6). *Dictyostelium discoideum* is well-studied representative and prior work establishes that the SCF complex actively regulates its development (7). *D. discoideum* lives freely in the soil as a unicellular organism when nutrients are plentiful. Upon nutrient depletion, the cells aggregate into motile slugs that differentiate into prespore cells, prestalk cells, and anterior-like cells. These slugs will follow environmental cues

and ultimately culminate into fruiting bodies consisting of terminally differentiated spore and stalk cells with cellulose-rich cell walls (8). This process is highly dependent on concerted transcriptional (9-11) and proteomic (12-14) changes. The significance of proteomic changes is emphasized by the effects of mutations in FBPs and enzymes that modify Skp1 (15-17).

A novel form of regulation of the SCF has been discovered in *Dictyostelium*. Its Skp1 subunit is post translationally modified by hydroxylation of a proline in an oxygen dependent manner and subsequent glycosylation with a pentasaccharide (18). Loss of the prolyl hydroxylase responsible for generating the anchor point for the Skp1-glycan modifies the O2-setpoint for permitting its transition from the motile slug stage of development to mature fruiting bodies (19), by a mechanism that involves the proteasome (20). The addition of the glycan has been shown to increase Skp1's level of interaction with several F-box proteins, including the WD40 domain containing FBP FbxWD (20,21). *Dictyostelium* is a favorable model organism for investigation of SCF regulation, since this Skp1 modification is found in numerous other unicellular organisms including the human parasite *Toxoplasma gondii* (22,23), the plant pathogen *Pythium ultimum* (24), and pathogenic fungi (24).

FbxWD is of particular interest not only because the level of interaction is dependent on Skp1 modification but also because it is selectively expressed in the tip organizer cells that govern slug behavior and its ectopic overexpression delays development (21). In addition to the canonical WD40 propellor substrate receptor domain, FbxWD contains an N-terminal RING domain. While not unprecedented (25-27), RING domains are unusual on F-box proteins and their role in SCF activity is unknown. Here we find that the *fbxwd* gene resists deletion, and its overexpression in tip organizer cells has dramatic inhibitory effects on development. Examination

of the interactome of endogenously tagged FbxWD by analysis of co-immunoprecipitations by mass spectrometry yielded an uncharacterized protein, named Vwa1 evolutionarily related to the nucleocytoplasmic VWA5A/BCSC-1 clade of VIT (Vault Inter-alpha Tryspin) and VWFA (von Willebrand Factor A) domain containing proteins (28). Domain overexpression and gene disruption studies reported here indicate a synergistic relationship between FbxWD and Vwa1.

The VIT domain is found in a subset of the wide variety of intra- and extra-cellular proteins that contain vWFA domains. The VIT-vWFA domain arrangement is characteristic of the protein family containing extracellular ITIH (28,29), intracellular PARP4's (poly ADP-Ribose Polymerases) (30,31), and tumor suppressing (32-34) VWA5A/BCSC-1. The crystal structure of ITIH1 shows that the VIT domain exists as a hybrid β-sandwich atop the characteristic Rossman-fold of the vWFA domain, with a connecting hybrid domain that consists of two parts that are separated by the vWFA, and a C-terminal domain on a flexible linker that wraps back around to contact the VIT domain (35). As we describe here, examples of these VIT-vWFA proteins are found throughout prokaryotic and eukaryotic phylogeny. Their functions are unknown but their modular associations with functional domains in some proteins suggests a role in protein-protein interactions. *Dictyostelium* Vwa1 has highest homology to intracellular nucleocytoplasmic protein, VWA5A/BCSC-1 (34). VWA5A/BCSC-1 has been previously reported to inhibit tumor metastasis (32-34) and is down-regulated in a schizophrenia model (36). Interestingly, VWA5A has been reported to interact with the SPRY domain containing SOCS-box protein, SPSB1 (37,38), which is a component of the elongin B/C, Rbx2 and Cullin5 E3 ligase (39). Our findings in *Dictyostelium* describing synergistic action with an E3 ubiquitin ligase through a WD40-containing

FBP that is essential for developmental progression provides new clues for the roles of its mammalian counterparts.

Results

FbxwD interacts with VIT-vWFA domain containing proteins

Previous studies identified several dozen FBP candidates in *Dictyostelium*, and many of these have predicted substrate receptor (SR) domains (40,41). However, their SR sequences are so unrelated to those of known FBPs that further analysis of their roles will depend on experimental approaches to identify their substrates. FbxwD was chosen for further analysis because it is an abundant validated WD40 repeat FBP that interacts directly with Skp1 in a way that is enhanced when Skp1 is prolyl hydroxylated and glycosylated (21). A previously described strain in which the endogenous *fbxD* locus was edited to modify the C-terminus of FbxwD with a 3×-FLAG or a 3x-FLAG+2xUBA (ubiquitin associated domain (42)) tag was used to probe the FbxwD-FLAG interactome where FbxwD was presumably expressed at its native level and in its normal cell type specific pattern of expression. FbxwD-FLAG was IP'd from the soluble (S21) fraction of cell lysates using bead-bound anti-FLAG Ab (mAb M2). Proteins were eluted at high pH and analyzed using nLC MS/MS. Proteins that satisfied the following criteria were examined further: present at a peptide FDR <1%, detected with ≥2 peptides, present at ≥4-fold higher levels in tagged strains vs. untagged strains, predicted nucleocytoplasmic localization. FbxwD-FLAG and FbxwD-2UBA were treated as biological replicates as the interactomes of the two were indiscernible. Identified proteins detected in vegetative or slug stage extracts included the SCF components Skp1 and CulE (Fig. 3.1A, B), indicating that at fraction of the FbxD-FLAG was engaged in SCF complexes. Six additional proteins were detected in vegetative cells. Three have

been named Vwa1, Vwa2, and Vwa3 due to the presence of sequences predicting the presence of an N-terminal VIT (vault-vault protein inter-alpha- trypsin) domain followed by a VWA (von Willebrand type-A) domain. Three other homologues of Vwa1-3 are predicted in the *Dictyostelium* genome (Fig. 3.2). These VIT/vWFA interactors are specific to FbxwD as they were not found in a similar analysis of the interactome of FbxwA, a previously characterized WD40-type FBP that regulates development (7). Vwa1, Vwa2, and Vwa3 were previously identified as interactors of FbxwD in a strain that overexpressed FLAG-FbxwD under control of the *cotB* promoter, which drives FLAG-FbxwD expression in prespore cells, a cell type in which it is normally not well expressed (43). Thus, the interaction is supported under physiological conditions. Vwa1 was also detected in co-IPs from strains in which the *culE* gene was edited to encode C-terminally FLAG-tagged CulE, indicating its occurrence in SCF complexes (21). Furthermore, this interaction was enhanced in wild-type vs. phyA-KO cells, in correspondence with the effect on FbxwD, and consistent with the interaction between Vwa1 and FbxwD. The gene loci for Vwa1 and Vwa2, which were more abundant than Vwa3, were separately endogenously tagged with a C-terminal 3×-FLAG tag (Fig. 3.17), and over expressed with an N-terminal 3×-FLAG tag under control of the semi-constitutive discoidin promotor (Fig. 3.9). co-IPs of overexpressed FLAG-Vwa1 or FLAG-Vwa2 confirmed their interactions with not only FbxwD but also CulE (Fig. 3.1C), whereas the interactions were not observed at native levels of Vwa1 or Vwa2 expression, possibly due to lower level of sensitivity of this approach. A summary of the observed interactions is shown in Fig. 1D.

Fig. 3.1. Interactomes of FbxwD co-IP and reciprocal co-IP of Vwa1.

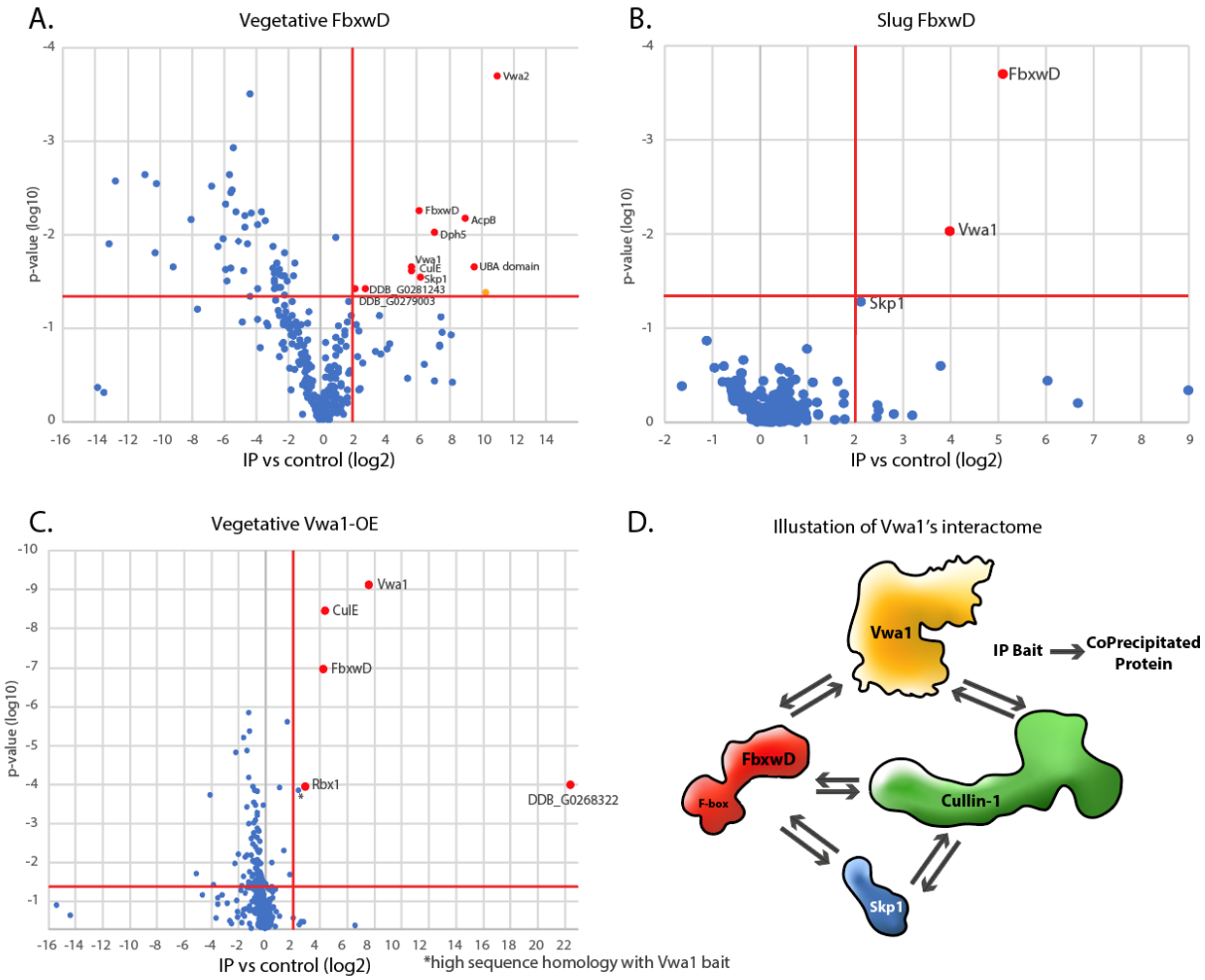

Fig. 3.1. Interactomes of FbxwD co-IP and reciprocal co-IP of Vwa1. Co-immunoprecipitations from cells solubilized with non-ionic detergent were analyzed via nLC MS/MS and the immunoprecipitated protein IDs were plotted as volcano plot comparing control vs. FbxwD or Vwa1 bait. Interaction candidates (red) were determined as proteins that were 4-fold higher in tagged vs. control strains with a p value<0.05, as indicated by the red lines. *A,* Endogenous FbwxD-3x FLAG IP reveals a number of vegetative interactors with known SCF proteins as well as the uncharacterized Vwa1 and Vwa2. Timm10 was excluded from the list of interactors (orange) as it is a mitochondrial protein. *B,* Slug cell FbxwD IP (n=3) confirmed Vwa1 as significant interactor. *C,* Reciprocal co-IPs of Vwa1-FLAG from tagged vegetative cells. *D,* A visual summary of the FbxwD SCF interactome as observed experimentally. See Table S2 for further descriptions.

Fig. 3.2. Dictyostelium discoideum VIT/vWFA/Hybrid domain containing proteins.

Vwa1
http://dictybase.org/gene/DDB_G0292016
https://www.uniprot.org/uniprot/Q54DV3

FASTA
>DDB0306747|DDB_G0292016 |Protein|gene: DDB_G0292016 on chromosome: 6
position 1027245 to 1030001
MFSSITSKLSAISGGSSKNDYKEANYYNYFRILEKKQTEEIARKRCGLYSLKNHNNVFVL *Dd* homology
KEFSIETEINDCSSTSIWTQSYSNDSNTPVEAKYQLPLHPTSVVSNFQIEYQGKVIQGKI VIT
KEKEKALEKYNDAIASGGQAFMATKSDDGYFNLTLGNLPPKENVKVRVVISSELGTHTDG
QLHYCLHRYMF*PSYA*FNFNYNVVLKFSIPIKSIDCDGFDVNVNYKENSSKKEAKITSKSQ
HTSGVK*KNIILIIQPVELNEPKSMIE*YIGGGDDKSYATAINFYPSFKNVNPDEVYQKSEF hybrid-1
IFLIDCSGSMSGQSINKARRAMEIIIRSLNEQHKVNIYCFGSSFNKVFDKSRVYNDETLE VWFA
IAGSFVEKISANLGGTELLPPMVDILSSPNDPEYPRQVFILTDGEISERDKLIDYVAKEA
NTTRIFTYGIGASVDQELVIGLSKACKGYYEMIKETTNMEKQVMKLLNVAFEPMLSNIKL D3
DWSSCGLVDVIQAPSHIRPLFNQERMMIYSMIPSNQTNQDIINASIETSKPLIITLTGDG hybrid-2
PKGNVLSFPITLDFKNDLSTNSNQIHTLAAFKHIQDLEESERKEKKDNKDKIVELGKKYG 3xαHelices
LVSKHTSYIVTADSDNVTEETMKTVDIMNQSPPIRPGGRIVSRGGGRSGASGALSSSILS VIT pt2
RKRSSSPSTATKRSSSSSFSSSYLSLSSSSQKKKKEVSRSDDDDDDEKIENCVESYESDG
GDQSSEQDEEEEDDCDDFHEDLDEDLGATAMDVDKKECEKECKKKDSSKVDLKVKPSKVP
LPSRSPSVSKPTTTSLLSPSPKSAPSAPSQQKSVKSTGDLLIDLLKIQKSNGSWTKSSID
QLKIPTDKAPAELSTTELNDIWVTIIVIAKIVKFFSSEKAQYELAIQKSTRWVKLQLSKL D4
NLPENTFDKFLSNAKSLV*

Vwa2
http://dictybase.org/gene/DDB_G0292740
https://www.uniprot.org/uniprot/Q54CQ8

FASTA
>DDB0238133|DDB_G0292740 |Protein|gene: DDB_G0292740 on chromosome: 6
position 2078010 to 2080742
MIKNLISAFSQGVGIQKKELPSTIILNKDDYKEANYYNYYRNLELNKPDEVLARRIAGLA *Dd* homology
PIAYQYYNVSSFDNNQFKIVDFSIDSKLNDTCLTCVWTQTYKNESKTPVEAVYRIPLSPL VIT
STVSAFSVQFNGKTLHGKIKDSTKAQEKYDDAIASGGQAFLAEKSKDDDNYFNFKLGNIP
PTESSITIHITMISEIGSHLNSLHYLLHRYCFPQSSNYNFSLSLSVNLSNSIKSIFFDGD
KSHSLQYENKEKTKCIIQYKKSLGFNTQPNILIVFELDDLNKPQSFIEKLSINKEDIKNN
PHSDSDSDSDDEENKKENEKSSYAIALNFFPKFESINKEDIYQKGEFIFLIDCSGSMSGN hybrid-1
PIDSARRALEIIIRSLNEQCKFNIYCFGSGFNKAFQEGSRKYDDDSLAVVNRYVSNISAN VWFA
LGGTELLQPIKDILSKEIDPEYPRQIFILTDGAVSDRSKLIEFVSKESKTTRIFTYGIGS
SVDVELVVGLSKACKGYYTLIRNSSDMETEVMKLLSIAFEPTLSNVSFDWSQLLDLSNGK D3
STTIIQSPTQIRPIFNNERMMVYATIELDNDISNNIENHGQPVIVTMNADGPLGDRLSYH hybrid-2
VELDFKNYSQSNSIHTLAAFKRIQDLEEIERKSSKETEKLEIIKLGKKYNLVSKHTSLVV 3xαHelices
TSDSDSPTEDTMKVINILPNNSQHPIIVDRCHTFAVNFNSPLQYQQQQQQQQQNFNSGFA VIT pt2
PPPPPMMSSGPPPPPGSSFGAPPPPPPGGAFPTSSISEKKSSSQSSSSYLPPTMSLSRKS
SLSPSSPSKNYPSPKLSSPSLSYGSTQSESTPSNDPLISLLAKQKANGSWSKSSIQDQFS D4
SAISKIPNELSAVEDVWATLLVISKIMKTFASQKSKWELSVQKSNKWVKQQLLKLNLSFD
QFLELAKSNV*

Vwa3
http://dictybase.org/gene/DDB_G0292028
https://www.uniprot.org/uniprot/Q54DU5

FASTA
>DDB0306748|DDB_G0292028 |Protein|gene: DDB_G0292028 on chromosome: 6 position 1046109 to 1048990
MNFIKKVIGGGSSKSKTDIKIEDEQHEQQHEQQHEKQQIPDKISTSKVNSPCVPPTCTYI
SKENVRSDLSLIKDFNSAYYYNYYRTLEKNSTNLLTSPGLNTKVVSNQFTLKEFNIVSEM *Dd homology*
TDSCIVSVWTQKYSNLSLTPVEAVYQIPLAPYATVSDFSVILKDKVLKGKIKENEKAKEK VIT
YNDAIASGGQAFLAEKVEGFFKLQIGNLPPQEDVTVNITITSEIGTHLESLHFCLHRFIF
PKSAFKFNYTLNASLSTPIETIEMDHFQPTITYKDESKTNATVTISTENGVSNNIIAIIV
PKYSEKPESFIEYSPIDKSYALAINFYPKFSVGLDEVDQKSEFIFVLDC**SG**SM**S**GKPIEK hybrid-1
SKMALEICMRSLNENSKFNIVCFGSNFNKLFETSKHYNDETLQKASEYINRIDANLGGTE VWFA
LLEPIVDILSKESDPEFPRQVFILTDGEISNRDKLIDYVGKEANTTRIFTYGIGSYVDKE
LIVGVSKACKGYYEMIVDNSDMEEKVMKLISIAMQPTLSNIKVDWGVLSNVVQSPAQIRP D3
LFNQERMMIYATLDKEPTEKQVTVILSGNGPLSERISFPVDLDFSKANQSTSHIHTLSAF hybrid-2
KHIQDLEESERKEKKDNKDKIV**KLGKRFGLVSKHTSYIVT**ADSDKVTEETMKTVQVLEPT 3xαHelices
QQINTSPGSGSGFIPTTRVQGSSSVFPSSPTPLSGPSPYTVCAPPPPPPTSSPYTNCAPP VIT pt2
PPQFSRCIAPQPYQSAPAPPAPPAPSRLSQAQSQMDYCDQELLCESLEGDLLVEEEELEC
KEIECSPPQKLSYITPFAPTSQISQSSRECRSKKSSSPTIQKSSSLPSRPSTSSSSLIEI
IRQQKANGSFTKSSVSSFINVDTPPPSSDIPEDVWTTLLIIANFILNFDSQKSQWELVSQ D4
KATKFVKQQIIKSSIASTFETLLESAKKSISN*

Vwa4
http://dictybase.org/gene/DDB_G0285975
https://www.uniprot.org/uniprot/Q54MG4

FASTA
>DDB0307857|DDB_G0285975 |Protein|gene: DDB_G0285975 on chromosome: 4 position 3896573 to 3899326
MLQSLKNVFFSDTTTTTTPTTPTTPTTPTTTTPTTTTPTTTTTSTTPISNLSIKRD
IGNINDYKNANYFNYYRILENKYNYLRYNTGLKNISNNETFKLIDFTIDSEMNNTCITSN *Dd homology*
WNQKYSNNSSTPVEGVYKIPLAPYSVVSGFTVEYQDKVFIGKIKSKEKAQNQYSDSIASG VIT
GQAFLAEKTQDGQFSFRIGNLPPNENVTIHLTIISEVCPHLSSLQNCFHRFLFPNYSFNF
QFNLNIKLTLPIKTIELLYYPNKDIKFKENSNNKEATLTFSSNNGIDDDIVCIVEPENDI
ERPQSIIEHSKLNNTYAVSVNFTPSFSHLTSDDVNQKSEFIFLIDCSGSMSGEPIKKAKR hybrid-1
ALEIIIRSLNENCKFNIYCFGSRFTKAFDNSKMYNDETLKEISGYVEKIDADLGGTELLP VWFA
PIRDILSTESDFEYPRQLFILTDGEVSERDSLINYVATESNNTRIFTYGIGNSVDTELVI D3
GLSKACKGYYEMIKDNSNFEEQVMKLVSIAFEPTLSNIKVDWGTELQIEQGPTKIRPLYS hybrid-2
GETLIVYALLKDNKIPQSTVQVSLIGDGPTGSKLEFPITLDFSKTIDYENNSVHTLAAFN 3xαHelices
IIKDLEEVERKGNHSNNRDRIEELGKNYGLISKYTSYIVTAASEQVTEETMKTLNIIQIP VIT pt2
TTTTTSHTNFETEEDSDDLFSSENRNQTLANISNDMEKIKDIFDDISRLISEQSCMLNEI tSNAREcoiledcoil
GDANIEASTLGINSIPQKSNIFSKITSFFSSPSEVSTSKSNFDSDIGSEERRNNNNNNNN
NNININNNNNNNNNNNNNNNNNNNNNNNNNNNNNNNNNNSDNSDSLLKLIRLQKANGSWSS
PFSEFKIDLSKKPSNIDNDDIWITLIVINKILNDYPTQQSQYDLVIQKASKWVKQQLTRL D4
NIPNQYGSLLATSKLYI*

Vwa5
http://dictybase.org/gene/DDB_G0267758
https://www.uniprot.org/uniprot/Q55G98

FASTA
>DDB0305054|DDB_G0267758 |Protein|gene: DDB_G0267758 on chromosome: 1 position 789209 to 791845
MSSDNNDNNNNHSYKEANYYNYYRLLENNLKKKSRGLFLTENNKKKSKVFKLTKFSIDTE *Dd* homology
INDCSSTSKWTQIYSNDSKTPIEARYKIPLHPTWIITDFRVESQDKVVVLIGKIKEHEKA VIT
LNNYNDTIANGGQSFLASKSSIEDLDFFNLNIGNLPPNETVKITLTITSEIGTHINGQLH
YYLHHSLFPTYNFNFNLNIIIKLSNSIESIINWYGNSKRILNINSSNTGCGSDDGDDDVI
KVLYNNSNNKEIKIKSNDKLNSIEDSLVLIIQPSIINDEPKSMIEYNKIENSLAVSINYY hybrid-1
SSFKDIKIEDMNQKSEFIFLIDCSGSMVGEPMRKVKRAMEIIIRSLNENQHRVNVVCFGS
SFKKVFKVSRDYNDETLECLSKYIQSIEANLGGTELLTPIKNILSSPPNPEYPRQLFILT
DGEAPHRDKIIHYLSKESNTTRIFTYGIGDSVDIDLIIGLSNACKGHYEFITDNDNFEKQ VWFA
VMKLLNISLKPMFSNIKLDLSTLFSNNKNKNKNNNNCKEDIIIQSPSQIRPLFYQERMIV D3
YLMIESLSTRLKDIINDSIENSKPLIITMTCDGPKGDKLSIPIELDLKNNCIISSSSSSS hybrid-2
SSSSSSSSSSSSSSSSSSSSSSTTTATTNQNQIHRLSAYHQIKDLEEKERKKKKDNKTR αHelices
IVELSKKYGILSKHTSFIVKCESTKPTLESMDFIDIIDQFSFENQVSATKNKSQCLLTKS VIT pt2
KKSKTAAPTTTTTTTITKKRFSDVDEDISRQSVKKSKKSETKEETTKTTSSKTKSSSSFD
LIDLLRIQRANGSWTKSTISQMGISIGNAPVELSSDQLYNIWVTLIVISKIIKLFPNEKI D4
EYEFAIQKSKKWVKLELSKLNLPNTTFDKFSLKANSLC*

Vwa6
http://dictybase.org/gene/DDB_G0285981
https://www.uniprot.org/uniprot/Q54MG1

FASTA
>DDB0232083|DDB_G0285981 |Protein|gene: DDB_G0285981 on chromosome: 4 position 3901446 to 3903941
MLQSLKNVFFSETTTTTTTSTTTPVSNSAIKRYIGNINDYKNANYFNYYRILENKYDYLR *Dd* homology
DTFGLKTFSNNETFKLIDFTIDSEMNNTCITSIWNQKYSNNSSIPVEGIYKIPLAPYSVI VIT
SGFTVEYQDKVFIGKIKSKEKAQNQYSDSIASGGQAFLAEKTQDGQFSFRIGNLPPNENV
TIHLTIISGVCPHLSSLQNCFHRFLFPNYSFNFQFNLNIKLTLPIKTIELLYYPNREIKF
KENSNNKEATLTFSSKNGIDSDIVCIVEPENDIERPQSIIEHSKLNNTYAVSVNFTPSFS hybrid-1
HLTSDDVNQKSEFIFLIDCSGSMSGEPIKKAKRALEIIIRSLNENCKFNIYCFGSRFTKA
FDNSKMYNDETLAQISGYVEKIDADLGGTELLPPIRDILSTESDFEYPRQLFILTDGEVS VWFA
ERDSLINYVATESNNTRIFTYGIGNSVDTELVIGLSKACKGYYEMIKDNSNFEEQVMKLV D3
SIAFEPTLSNIKVDWGTELQIEQGPTKIRPLYSGETLIVYALLKDNKIPQSTVQVSLIGD hybrid-2
GPTGSKLEFPITLDFSKTIDYENNSVHTLAAFNIIKDLEEVERKGNHSNNRDRIEELGKS 3xαHelices
YGLISKYTSYIVTAASEQVTEETMKTLNIIQTPTTTTTTSHSNRRREEADHTMNQTLLKN VIT pt2
CAVVDDLFESCEMLSETSIKFECNRVYKKIPSSLSKIFSFFSSLSTSSSVRSEVVSNFDN
DIESEEKKNNSINNNSDSLLKLIKLQKANGSWSSPFSEFKIDLSKKPSNIDSDDIWITLI D4
VINKILNDYPTQQSQYDLVIQKASKWVKQQLTRLNIPNQYGSLLATSKLHI*

PARP-4
http://dictybase.org/gene/DDB_G0286613/feature/DDB0187042
https://www.uniprot.org/uniprot/Q54LJ4

FASTA
>DDB0232950|DDB_G0286613 |Protein|gene: DDB_G0286613 on chromosome: 4 position 4708744 to 4716594
MVVNKNSVLNNLTFYLDCGNSGLKSKKVLQSYVESHGGNVSMILNQKINYYIFSGDFNDL
IKVDEKNNNNNSYQDEEEKKNINLETLSSNIKKAIKLNIPIVSKRYLEDSISNGNLLSPN
EYSLVSLYNIKEYHYKSLDFSNLLEDPSSSSSSSTNGEQQQQQYERIKYNNKVENDKFPT
ESKYHVVKHNVLISPKAESFICLELHVAGKILELIKTGNSDNSGGSGDQTQSYYRVFLNY
GSLDANKINDSVKEWIPFTNLENSLDQYNEIFKDHLINKKYSKFQLGSTLIGSNKLQELC
YNKLFDDTTITTTNNIDDSNNINNEIPKPIHELIKILYDEAISTLGNKFGNGSKLHLSPE
GSIKTSMGDITLMQVDKAELSLFQLSTVLRGNGGKIDSKESTDLIDEIFRSLPQLKPPGG
KFNNSYELLNDIQESVQLMKDILSVGESLSGVSKTLTSASSGEMAKYRALRCQINQLDKS PARP
SKDFKRITDQIKGGTKIEGLTQPQQSIKKSNGNDNNNNNENCIDNNNNNNNLIKIKNIFK
IIRKEEDNYNFEVGNLKTLYHGSNPSNILGILSRGLLTPNVSTSIGAGRRDIGYLGSGIY
FGVKPSTSIQYCKASTKTLSKYMFICSVALGQIKKYTTHQTQLSKPPKGFDSVQGVGSSS
SSSSSSSSSNNTVKQSDFIDDEIVIYDSKQQKIQYLIEFDDLNSLTIPPILKSSLSSNND
KLLEISKESVKPTIESEKVPNSLPQKSLIDDSNDDDDNQEIGLISKNGGGDNAIPLKSVH
VKGKILDLIGEVTIYQHYQNNSKNMIEAKYVFPLDEMGAVCGFEAYVNGKHIIGECKEKE
KAQREYREAVAAGHGAYLMDEDKPDVFTVSVGNLPPNCDVLIKIVYVTELSIDGLDISFV VIT
LPRSITPKQRLQSSSSNTQSVTSTVQVTELAQKQSDLSISVGIEMPYNIVKLISPTHDVR
IKRTHTKATIELNNQDNQYLDKNFQLLIGLEEPYSPRMWVEVDEKGHHASMLAFYPKLDI hybrid-1
DNTMKDSHTMVTLLIDLSSSMAGDAFEDLLRAVRITISNLRGMQKVLFDVVCFGDTFDWL
FGIGVPPTESNLQIAWSHINHLKTSYGGTLLHQPLQSLYLLAEKAKPTNPHNILLFTDGN VWFA
VANEELVQMLVKKASPYCRMFAFGIGEHCSRHFVKSICRLGGGYPEFIQTNKRPNPKKII D3
DQLQRLTQPAMSNISVKFDSSDTNSIVQSPATITSIFKKERQVMYAFSGICTRATLICQA hybrid-2
PGGGLITNVVHTPEIGFIKGNLIHRLAARSMIREYQDGTYSQNKHEHDLIKLKKKNDVID 3xαHelices
LSIKYSIVTPFTSFVAVEKREKHETFSKLPPIQSIISQTIVDSLPYIAWEDKSQGIDQDP VIT pt2
NDPILLNKRDQLSKLIEQYHSNSKFSDTINVFHQISDTFGEFSMKELNLLSDTINNLISK
RVDKLSINDDSTTTTTTTPTTPSKLLREKKKLKEDIIYQGKGLLRLLESSTNHSNNEEAI 14-3-3
ISLMNNQCTVYKSLLNCDDNKYSKKQWCEKFESTLKSALQRSENSLSPTNPILLQLSLLS
ANYYKENGDFEKSIQISKNTFDKAISELDTLSEDSYKDTTLLLQLIRDSTTECLQFIEDE
QEINEFNLDQRHQHQPENNVDNEPKDEPQIESTISSKQWSITPKKLGIKKATTTYKPIVV
NQIVSNNNNTDIDYEGGVSENQSESGSDSESDSFSNEVSLRGISFDKYRCVTRSRSPSPE
GNIRSNNSSRGEVSLRGISIDKYRCVTRSRSPSPEGNIRSNNSSRGRGGSSRGGSIGSSR
GGRGGNIGTAFGRGAPPPPQPPPPPSTSLGRGAPPPSLFFQASQPYSPTSPFYIPTSPSY
SPTSPSYSPTSPSYSPTSPSYSPTSPSYSTSPLYASTSQSYSPVSPSYTPTSLLYAPTIP
SYSPVSPSYAPTKPSKLPVLTSYSPSSPSFSKSKAKEESTLSEINLPSKPMVAGYSRMST
VSFSSTPTPTPTPTPPPLPNAPRPSVSTNVFSPAPPAPQVFGGMMRRSSAHIGYSPEKEN
LQEERNISKKSDGMPRFKRTTLPPQPSSSGPPPPPPPSSSTSKNNSIEANSLKSDEGSLL
NSIKRGYSLKAVPEKLKEEAKTIDNLSAQLINSLSRRRVAIDCIENDEDDDDDDAWSDEP
VKKGGSGGGGSGSSYSFGGVPNAITSLVTASSTPASYLAAKSQPKDEEEEWGDEDMGFDL
FGDYPTSSTTTTKAAATTTVSKPTSLPKKKESYDEDEDMGFGLFGDEEDYQLQRVLSQSL
YESKQIQPQQPKSGPQKEQEESDGEGDCGFGLFGEYDDYCPPPPKSQPQPQLQSQKQQER
KEKEQEESDEEEYCGFGLFDDNEDYVSPPPKYLSSSSSSSSSLSLSKDGSRSKLSKSKNE
DIFNSSSSIIGKSWALETEKEEKEKKKKSKKEDKSNDIMKQKQQQLFEKEIVTLYSDLLM
IVNSPTSYETVKKVSLALGVSRSSLIKFDSTLGGQLSDNFRFFILELIKIFVKLLKPSTT D4
VSFEVIISKCNSTTGGSVLKSFGIKDDVITGIVKLSKKSHLFK*

von Willebrand factor A domain-containing protein
http://dictybase.org/gene/DDB_G0286969
https://www.uniprot.org/uniprot/C7G046

FASTA
>DDB0252861|DDB_G0286969 |Protein|gene: DDB_G0286969 on chromosome: 4 position 5063512 to 5069942

MYSGLWTKNGEQILPSFISINAKVVDLAAQIVFTKTYSDINKYFATMNKMNSSNEEDATF
KAFLNTSMGVLCGFEINLDGKKITSQVVSQADAMRLFEKNQISTADDIVKEAEFNNSDPH
IEEDFFLCKVNNLSQYKELEIIITYSTEMSTQGDYLFMEFPTSLTTIRSSQFFETLDNEN VIT
STTNTNTQTQPQSVNTTTTTTPSTTTATNITNINNNIQNIGSSTTGGLTHSTSSNKLSLS
SSSIQVNQKQGLLIEMNLDMPSKISEIISPSHSGLIDVEYKGETGKVTYKDSRSIDVVNQ
SDLVVLIKLDNPHEPYGFIEENENGSRALMIAFYPQLSSAAIAASATTPVVESELIFLVD
VSESMEGYNMKHAKKALHRFLHSLSKDTYFNIISFASSHRKLFAQSVKYNDENLKAATAY VWFA
VESLKAISHGETNLLEPLKDIYSVDATCPRKIFLLTDGRVNNIGPIVDLVRQNAHNTSVF
PIGMGEFVSRQLVEYIANAGSGVAELVIENETIESKVMRQLKRALQPAMSNIKVDWGSLS D3
SKSQAPRDLRTLFFGDRLTIYNILGKDEKIDGTTVKLIANGPTGPVSFPVTIKSEETKKG hybrid-2
NLVHSLAAYTLIQDLQDQIYENNLVDPKDIDPIRQKIIDLGIKYGLASNYTSFCSVEQPD 3xαHelices
QFNELLNNNKQSEQAQETTTTTTTATTVDDNVVIEENKQPEPIVEEQPPVLNGNINLQNL VIT pt2
TINHDGKSNDNGLFKSNDRLKTHHQGESAMISLRGSASGIPTTLSGSGIPFYNPSSPNHD
RNINTTQQPTPTQSTPLKTPLKTPLTPLSKSGLKVSSPEFVPKNTLSAKAAPFVPSPNKL
PTTTTSAPATTPITTPAPTTTTTEVKPTVAEPVKPVVAEPTKPVVAEPTIPAVAEPIKPV
VTEPTKPVVEEPAKPAVKPTLFEMIKIAEAKAAAEQKAAAEQKAIADAKAAAEQAAKPVE
PAVVQQQQPQQTKPKADKQSKQNAKDNKQSNKPVVVEQKPPVVTETKPTVATESATPTKP
TFAQAAAAAAAAAQQAAQQAAATTPVKQQPTKQTTPNKSTPAVETKSVVAETKPAVEQPK
PVETKPVVEQPKPVETKPVEQTKPVETKPVEVKPTVEQPKPVEVKPTVEQPKPIETKPTV
NSIASTLANFGFQTNEPAKQATPTPAPTPVQSNESNNNNNNNNNNNNNNNNNNNNNIV
SSTPIKKPAVTNILPTQAVILSSGGRRVYNNDFLLSFKDSNTKAPDSLKTTPIFSNGPQG
ISPSSGNGSNKSHFGKKRGDRGGRGGRDRNADAEPSTPIIVKKVFSQDVQGTHQELLKKF
KFNLNRITMDTYSSLIKNIDELKVPDEEALKSISKILFEKAIIDQKYSAVYAILAGHLDT
TFPKFAELSLKRAILDNCQTEFSAVVDKSKFEGLSKEDLEEQEFIIKRRVLGNIKFIGEL MIF4G
YKHGVLGEKVAKAIVVQLITKCEERLDEESIEPLVKILNTIGKKLDEVDKANTDLYFSKV
TNISNNPVVTSRGRFILLDLIDLRANKWQPKNSTQTKTKKDESDKEERFIAKHGGPQKRE
NDSRRDGGRDSRGDDRRGGGGRDSRGDDRRGGRDSRDAPRSAFGGKSSKDGWETVGAKGG
NNRDKGGRGGDRSGGKQSPSGKKDSGFGPSSGGSSLFGSRRGDDRRDGGGNSSPYRPGQG
FGRKDDQSSSIPSIPNRSNAFSALEDDDYQPSTSPQPPSVFGNRSNDRDSRGPSKPDNRK
QPAQPPAPVEPVKPKINFEKIEDDISMTLDEYAETQDIDEAIECIKEINEPTVLGKQFNI
FIMKSLERKEKEKQLIIELFSGILTAQLFNAEQIKEGLKEIIDTIEDIEIDLPFSGVFVA
TIVGICIESEIFPLNYLEEAYAHLVDSDKAEEMIVNTFNSIVKVSDKDRLVEIYENTKGL
DILKLFALKNRKVAYLEEFYQTHFPYLSHEKAVEGSNESALNEQPDLIEHLLLLQSADGY
WQLDKKLAGILGISLNILEEVDSSDSCVITTHPEVWATCLAITFVNLNNVSDPDDEDDLE D4
LVLSKSHKWLASQYQSDKPPKQSQDDVLLKAKRLLSEVL*

Developmental regulation of FbxwD, Vwa1 and Vwa2 expression

The significance of the interactions were examined by assessing whether they were co-expressed during development. An examination of previously presented transcriptomic data (9-11,43) suggested that, for bacterially grown cells (44), FbxwD, Vwa1, and VwA2 were expressed in two waves: one during growth and the other after aggregation (8-12 h) as the cells organize into slugs (Fig. 3.3A). Analysis of axenically grown cells shaken in nutrient rich media (10), showed an induction of expression an hour after starvation, followed by a decline in expression (Fig. 3.3B). These trends were confirmed in another trial of axenically grown cells that tracked expression with higher resolution and further through development (9). A peak in expression of FbxwD and Vwa1-3 did occur 12-16hours (Fig. 3.3C). Analysis of protein expression, based on Western blot analysis of the strains where the endogenous protein loci were FLAG-tagged, showed that the highest expression levels occurred in growing cells. During starvation induced development, the levels of all 3 proteins decreased, but the trends varied (Fig. 3.3E-H). Vwa1 and Vwa2 declined rapidly over the first 6 h, after which they plateaued for a few hr, possibly corresponding to the second wave suggested by mRNA levels, before declining further. In contrast, FbxwD protein levels declined monotonically throughout development. Significantly, the transcriptome analysis of separated prestalk and prespore cells indicated that FbxwD is approximately 16-fold enriched in prestalk compared to prespore cells (Fig. 3.3D). In contrast, Vwa1 and Vwa2 appear to be expressed at similar levels between the two cell types, i.e., <2-fold difference p-value >0.05 (43). The general correlation in expression levels is consistent with the evidence for the physical interactions, and the differences in cell type expression suggest a possible role for FbxwD in developmental regulation despite the relatively low level of transcript and protein expression.

Fig. 3.3. Changes in FbxwD, Vwa1 and Vwa2 protein and expression levels throughout development.

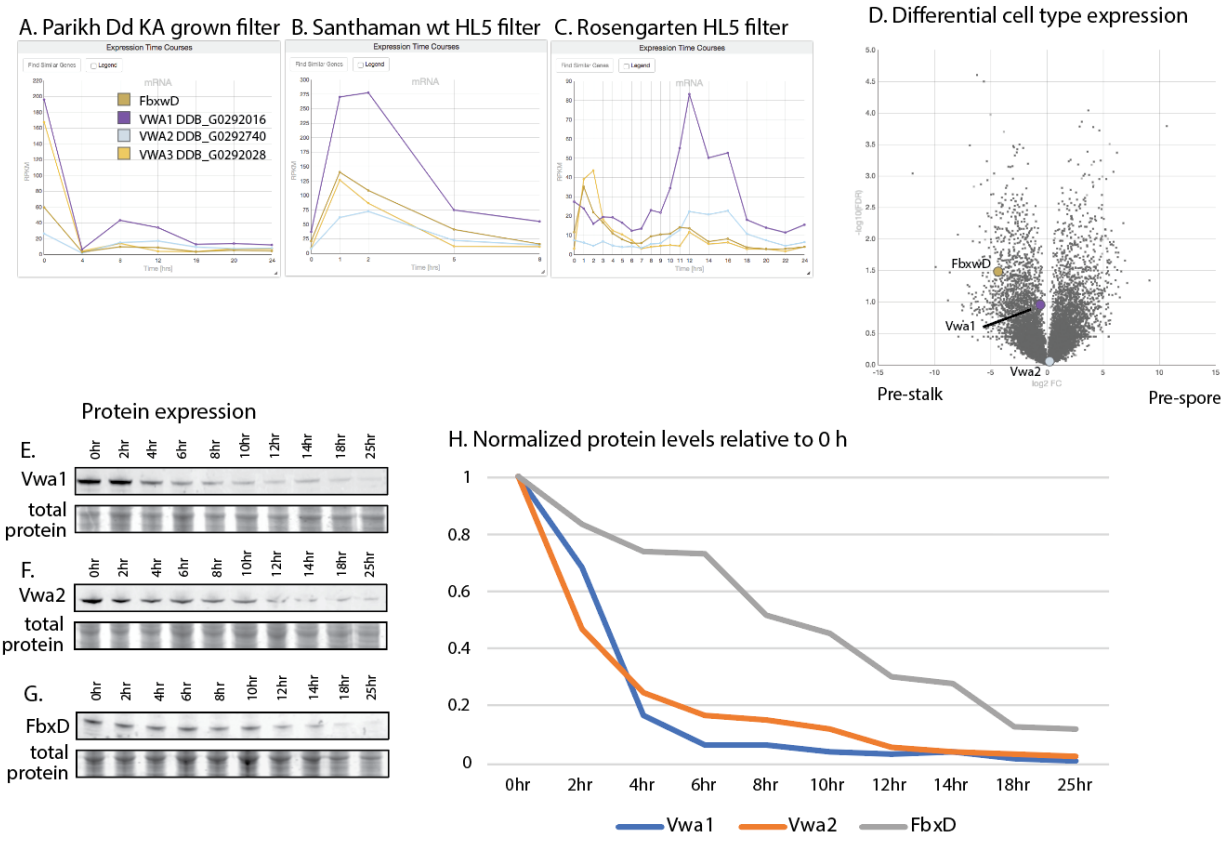

Fig. 3.3. Changes in FbxwD, Vwa1 and Vwa2 protein and expression levels throughout development. *A-D,* mRNA levels of Vwa1, Vwa2, FbxwD and Vwa3 (a low level FbxwD interacting Vwa1 paralogue) throughout *Dictyostelium* development as previously reported (43). *E-G,* Strains expressing endogenously FLAG-tagged Vwa1, Vwa2 and FbxwD were plated on nitrocellulose filters and allowed to develop and blotted to track changes in protein levels from the growth stage (0 h) through differentiation to slugs (14 h) and fruiting bodies (21 h). *H,* Band densitometry of Vwa1, Vwa2, and FbxwD normalized to Coomassie blue and scaled to 0 hr levels.

FbxwD does not affect Vwa1 stability

To address the possibility that Vwa1 is a substrate of Fbxwd, its level was examined in strains expressing different levels of wild-type or mutant FbxD. Since *fbxwd* has resisted disruption and therefore may be essential, a previously described strain in which FLAG-FbxD was overexpressed in prespore cells under the control of the *cotB* promoter, and a variant in which the F-box sequence was mutated (LPAA) to reduce interaction with Skp1 and therefore the SCF complex (21), were examined. In addition, 2 new corresponding strains in which FbxwD were expressed under control of the *ecmA* promotor, which directs expression in prestalk cells, were analyzed. Levels of Vwa1 were monitored using an antiserum that was developed against recombinant full-length Vwa1 (Fig. 3.4). Expression of FbxwD-FLAG was confirmed (Fig. 3.6B). Slugs over-expressing either FbxwD or FbxwD(LPAA) under control of the *ecmA* promotor showed similar levels of Vwa1 as in parental cells (Fig. 3.6C), which did not support the idea that Vwa1 is a substrate. In additional experiments, vegetative cells in nutrient-free aggregation buffer were incubated in the proteasome inhibitor bortezomib or the protein synthesis inhibitor cycloheximide for 2 h, but no reproducible differences in accumulation of Vwa1 or Vwa2 were observed (Fig. 3.7).

FbxwD overexpression inhibits development in a RING and F-box dependent manner

FbwxD overexpression was previously reported to inhibit developmental rate and prevent successful sporulation when induced under control of the prespore cell-specific *cotB* promotor (21). See Fig. 3.8A for a schematic of *Dictyostelium* development. This inhibition of development was dependent on an intact F-box domain as the F-box-mutant (LPAA) expressors sporulated similarly to the parentals. As previously mentioned FbxwD is prestalk cell enriched (43), the cells

Fig. 3.4. Validation of Vwa1 anti-sera.

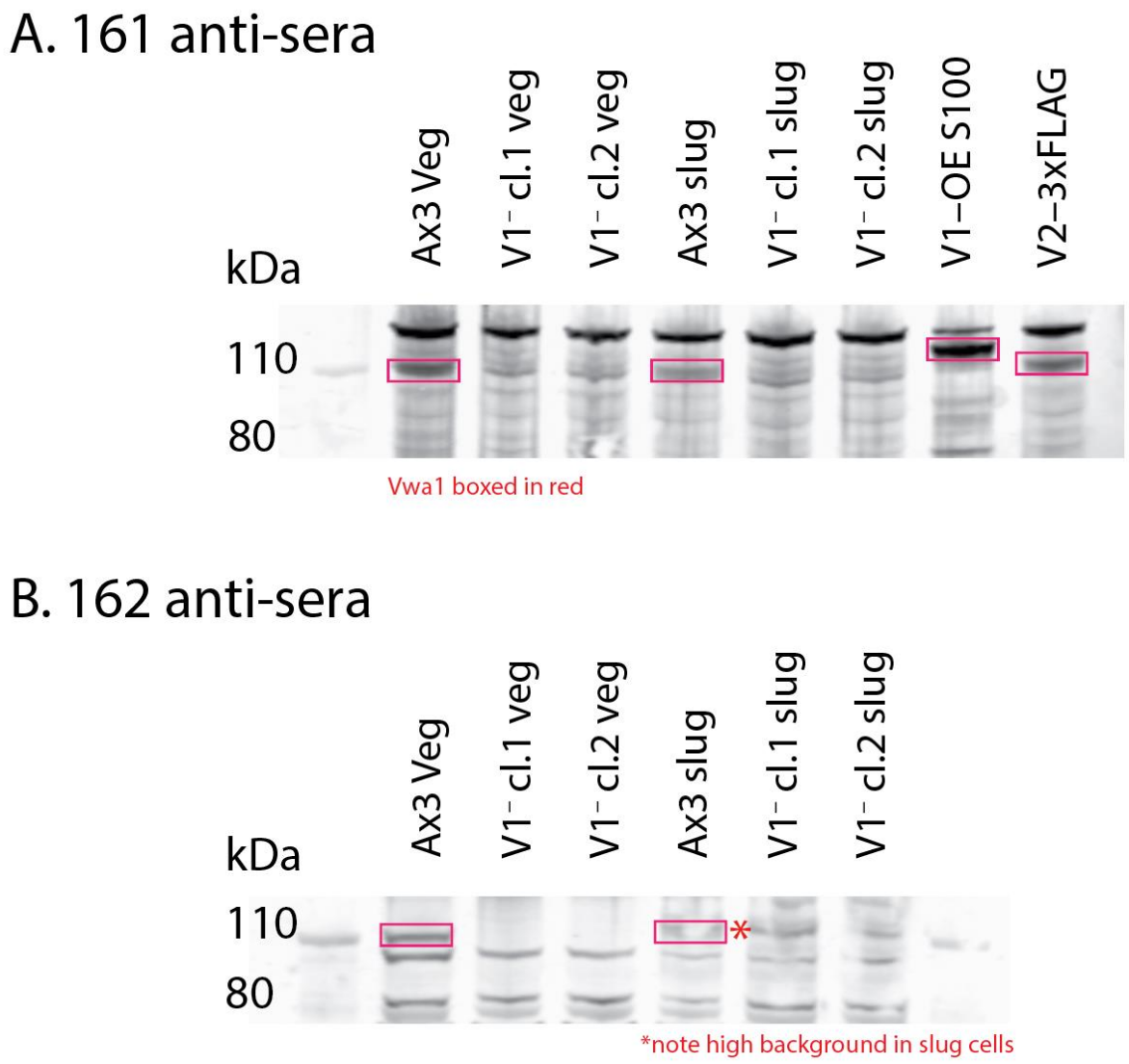

Fig. 3.4. Validation of Vwa1 anti-sera. Vwa1 rabbit exsang. anti-sera 1:200 was used to probe whole cell lysates of parental (Ax3), two orthogonal Vwa1-trunc clones, a Vwa1 over-expressor, and a Vwa2 over-expressor to validate that there was no cross-reactivity with a homologous protein with an identical 3xFLAG tag. Vegetative and slug lysates of parental and Vwa1 truncation cells to assess differences in background between the two cell types. *A,* Vwa1 anti-sera 161 demonstrates high background but strong reactivity to Vwa1 in all strains that contain and intact copy of the gene, including the Vwa2 over-expressor. *B,* Vwa1 anti-sera shows responsiveness to Vwa1and low background in vegetative cells. Unfortunately, a strong background bad at the same molecular weight as Vwa1 limited its usefulness to vegetative cells.

Figure 3.5. FbxwD expression construct validation.

A. FbxwD RING domain aligned with mutation locations marked

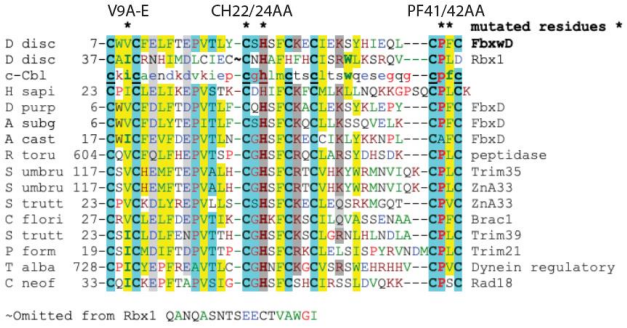

B. Western blot validation of FbxwD RING mutant expression in slug lysates

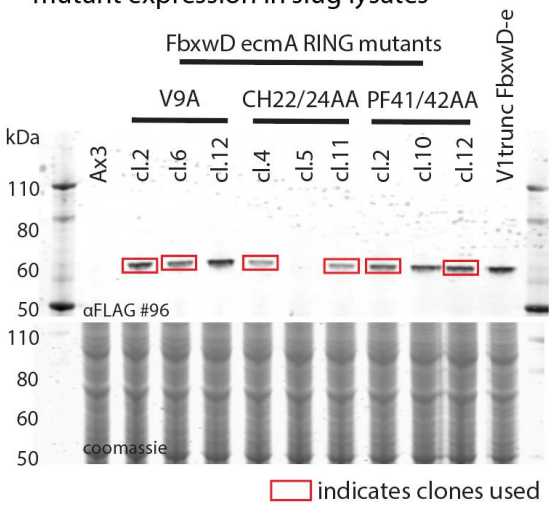

C. Western blot validation slug FbxwD overexpression expression in Vwa1-truncation background

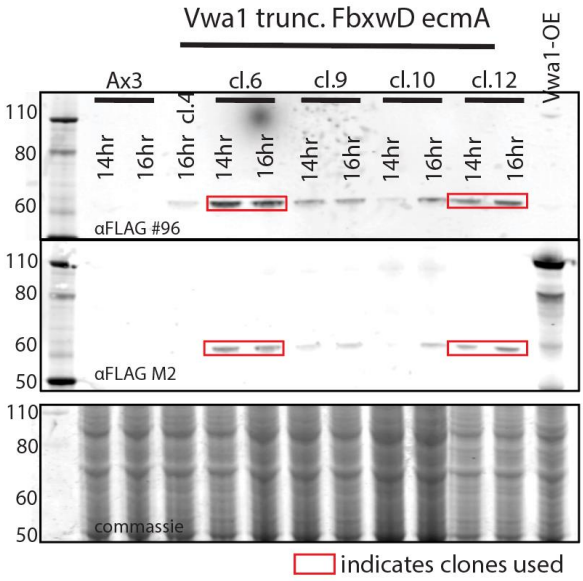

Figure 3.5. FbxwD expression construct validation. *A,* FbxwD RING domain aligned with representative examples of RING domains with the mutated residues marked with asterisks. *B,* Western blot validation of expression of the three RING-mutating FbxwD constructs. *C,* Western blot validation of FbxwD expression in Vwa1-truncated parental backgrounds. Blot was probed with commercial M2 αFLAG mouse monoclonal antibody as well as UGA96 αFLAG mouse monoclonal which recognizes the single FLAG more effectively. Clones that were selected for experimentation have the bands boxed in red.

Fig. 3.6. Vwa1's stability relative to FbxwD levels.

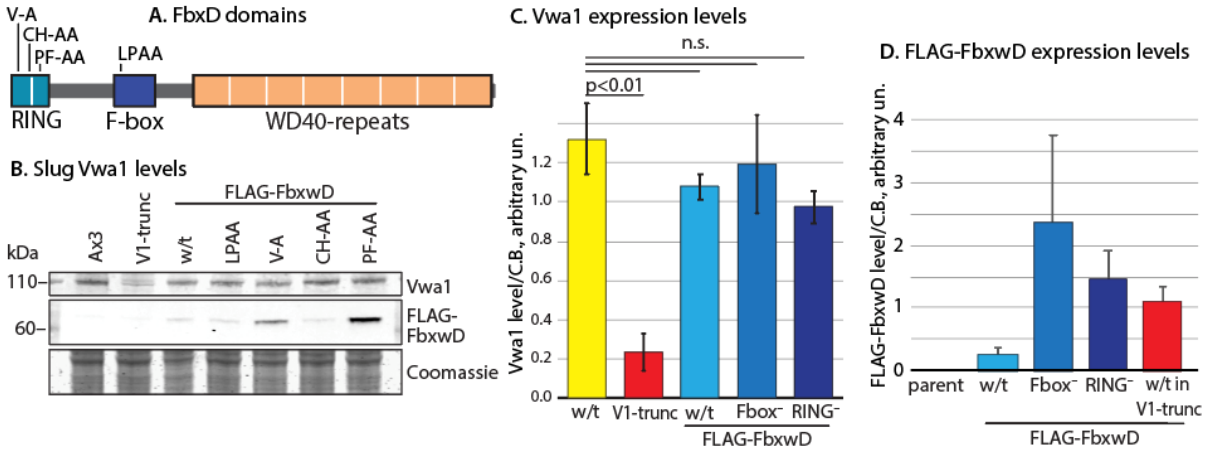

Fig. 3.6. Vwa1's stability relative to FbxwD levels. *A.* Domain diagram of FbxwD and point mutations. *B*. Cells expressing FbxwD and its F-box-null form (LPAA) on the inducible pre-spore, *cotB*, and pre-stalk, *ecmA*, promotors were developed on nitrocellulose filters and lysed to determine if Vwa1 levels based on Western blots probed with pAB UOK162. FbxwD expressing cells were lysed at 14 h and 17h as the w/t FbxwD constructs were developmentally delayed. *B*. RING-mutant FbxwD expressors from the *ecmA* pre-stalk promotor were developed and lysed as in A to determine if the RING domain in FbxwD affected Vwa1 levels. *C.* Vwa1 levels normalized to total protein stained by Coomassie blue reveal that there is no significant difference in Vwa1 level upon induction of w/t FbxwD or various mutants. *D,* Average normalized levels of protein for all FLAG-FbxwD^{OE} constructs used for tracking Vwa1 level changes or lack thereof.

Fig. 3.7. Vwa1 and Vwa2 blots tracking stability.

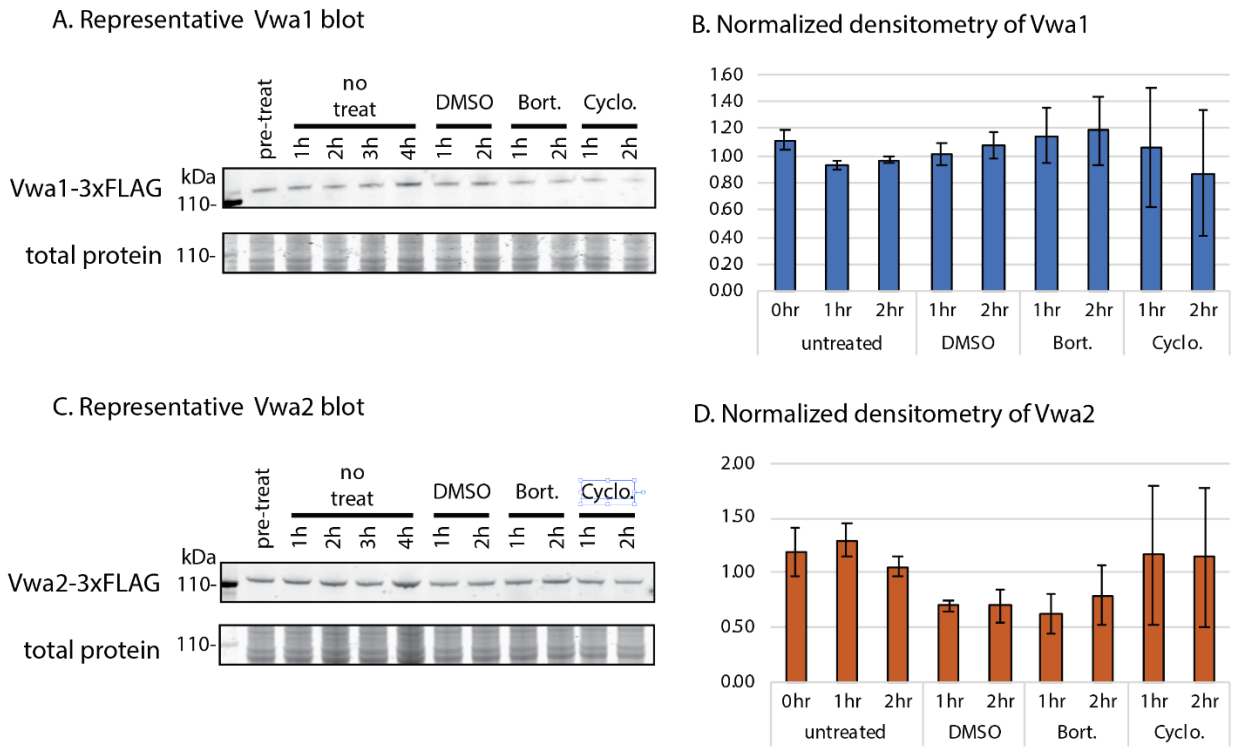

Fig. 3.7. Vwa1 and Vwa2 blots tracking stability. To determine if Vwa1 and Vwa2 levels were affected by traditional drugs used to assess protein stability, vegetative cells shaken in HL5 expressing tagged endogenous genes were treated with 1 µM Bortezomib or 1 mM cycloheximide. Representative blot of cells post treatment for Vwa1 (A) and Vwa2 (B) are shown. Average normalized densitometry (n=3) for both proteins (B and D) reveals that neither proteasome nor translation inhibitor significantly affect protein levels relative to the DMSO carrier.

expressing FbxwD or FbxwD(LPAA) were developed in parallel with the *cotB*::FbxwD cells (Fig. 3.8B). As for *cotB*::FbxwD, *ecmA*::FbxwD inhibited terminal morphogenesis and sporulation. Phase-contrast and calcofluor staining of cellulose showed that while the cells made fruiting body like structures, there were several differences from parental (Fig. 3.8B). The stalks were enlarged and lacked the regular cylindrical structure and the sorus of the *ecmA*::FbxwD fruiting body contained immature pre-spore cells that lacked the elongated shape and cellulose staining of a mature spore coat. While the FbxwD(LPAA) mutant expressing cells expressed the protein at a much higher level (Fig. 3.6D), there was no observable inhibition effect on development. This directly tied FbxwD's developmental inhibition to its role as an FBP.

The role of the RING-like domain of FbxwD was also probed. The V9A and PF41/42AA were designed to abrogate the protein-protein contact function of the RING and the CH22/24AA mutation served to eliminate potential Zn-binding (Fig. 3.6A, 3.5A) (45-48). Cells expressing these FbxwD-RING mutants were confirmed to express the mutant protein in slugs by Western blotting (Fig. 3.5B, C), and did not affect Vwa1 expression levels (Fig. 3.6B). To determine whether the RING-like domain contributes to FbxwD's role in development, the FbxwD RING mutants were expressed under the *ecmA* prestalk promotor as above. Significantly, none of the 3 RING mutants had an observable effect on sporulation (Fig. 3.8D). This implicated the RING domain as an essential feature of FbxwD function.

Expression and interactome of individual Vwa1 domains

To explore the basis for the interaction between FbxwD and Vwa1 or Vwa2, recombinant expression of FbxwD in *E. coli* was attempted. However, FbxwD was found only in inclusion bodies, as frequently occurs for FBPs. Similar results were obtained for constructs N-terminally

Fig. 3.8. Effects of w/t and mutant FbxwD on development.

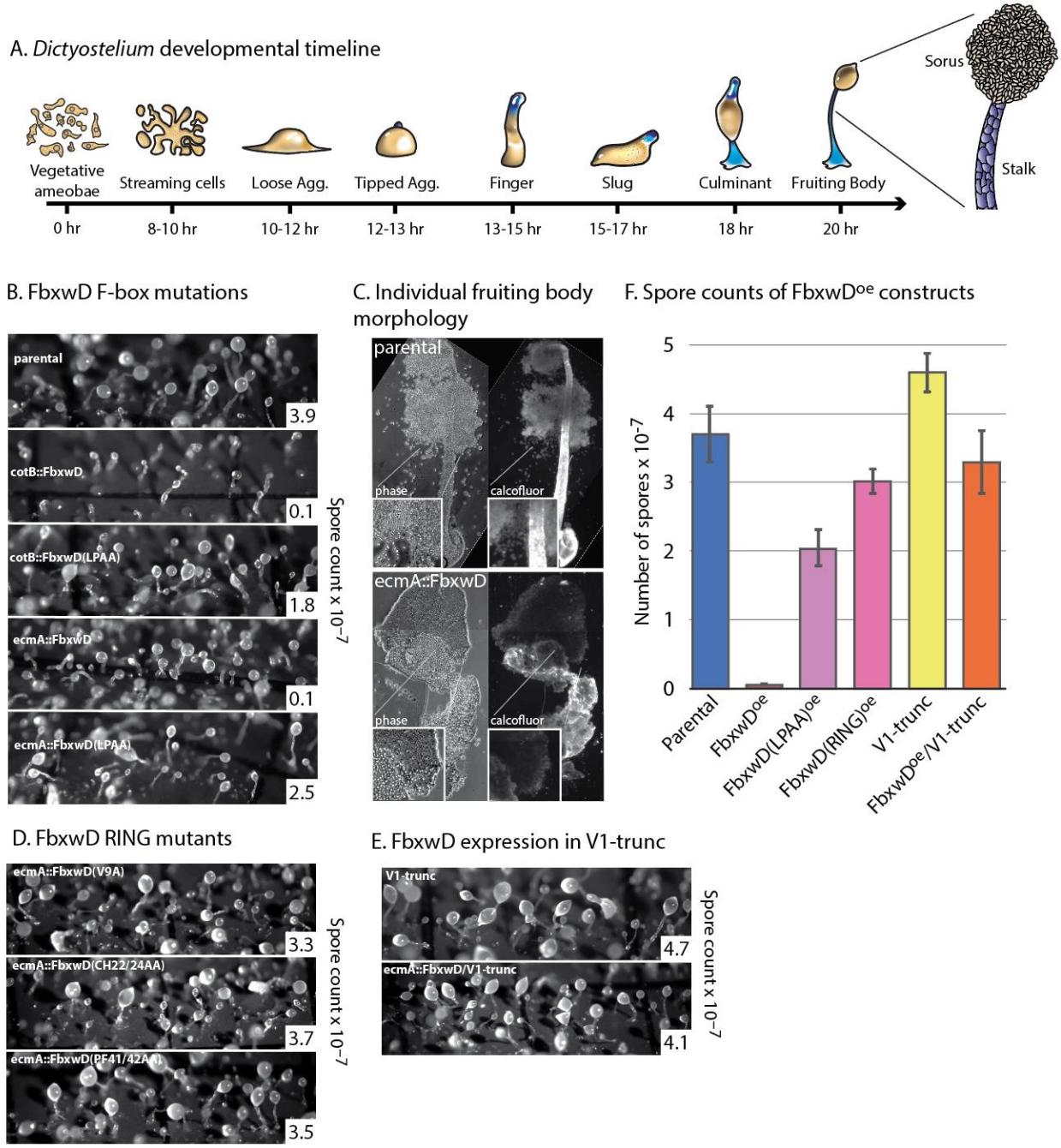

Fig. 3.8. Effects of w/t and mutant FbxwD on development. *A,* schematic illustration of the starvation-induced developmental cycle of *Dictyostelium discoideum*. Pre-stalk cells and anterior-like cells are labeled blue. The life cycle is renewed when spores from a fruiting body germinate to become feeding amoebae (77). *B*, Cells expressing w/t or F-box-mutant (LPAA) FbxwD under the *cotB* or *ecmA* promotors were developed on filters and photographed at their terminal developmental morphology before spores were harvested. Final spore counts are listed in the lower right corners. *C.* Representative fruiting bodies were squashed under a coverslip in Calcofluor White ST and visualized under phase contrast and UV illumination to image stalk cellulose structure and spores between parental and mutant cells. *D.* Morphology of terminally developed cells expressing RING mutant FbxwDs on the *ecmA* promotor. *E.* Representative morphologies of *ecmA*::FbxwD expressing cells in V1-trunc cells. *F*. Average spore counts of FbxwD expression constructs from these and other independent experiments (n≥3). RING mutants were pooled together.

deleted of the RING domain. Thus, an indirect approach was attempted in which individual domains of Vwa1 were separately expressed in *Dictyostelium* (Fig. 3.9C). Three truncated constructs were designed based on Vwa1's homology with ITIH1 and its crystal structure (35), with domains color coded (Fig. 3.9B) as they correspond to the color coding in ITIH1 (Fig. 3.9A). The constructs were the VIT (vault inter-alpha trypsin) domain, vWFA (von Willebrand factor-A) domain, and the C-terminus. All truncations were tagged with an N-terminal 3xFLAG tag. The VIT and C-terminus constructs expressed robustly but all vWFA constructs appeared to express at similar levels to the full-length construct (Fig. 3.9G). The truncated constructs were over expressed and immunoprecipitated as for full length Vwa1. The results of these immunoprecipitations show that in both vegetative and aggregate cells, no interactors were detected for the Vit or Vwa1 fragments (Fig. 3.10). The C-terminal Vwa1 fragment immunoprecipitated several heat-shock proteins suggesting that the truncated protein was misfolded and was triggering an unfolded stress response (Fig. 3.10A). These data suggest that the full-length Vwa1 is necessary to bind to FbxwD or other SCF proteins.

Transdominant effects of Vwa1 domain overexpression

To examine the role of Vwa1 in development, a strain that was reported to have an interrupted the *vwa1* locus in a genome-wide screen as analyzed (49,50). This strain was sporulation-negative; however, this defect was not rescued by complementation of the gene (Fig. 3.11). Therefore, a new disruption was prepared which inserted an in-frame 3xFLAG epitope tag followed by a stop codon within the VIT domain (Fig. 3.9B, 3.19). This strain, V1-trunc, developed normally (Fig. 3.9F). Therefore, we examined strains that overexpressed Vwa1 and its separate domains (Fig. 3.9D-F).

Fig. 3.9. Effects of truncated Vwa1 over-expression on development.

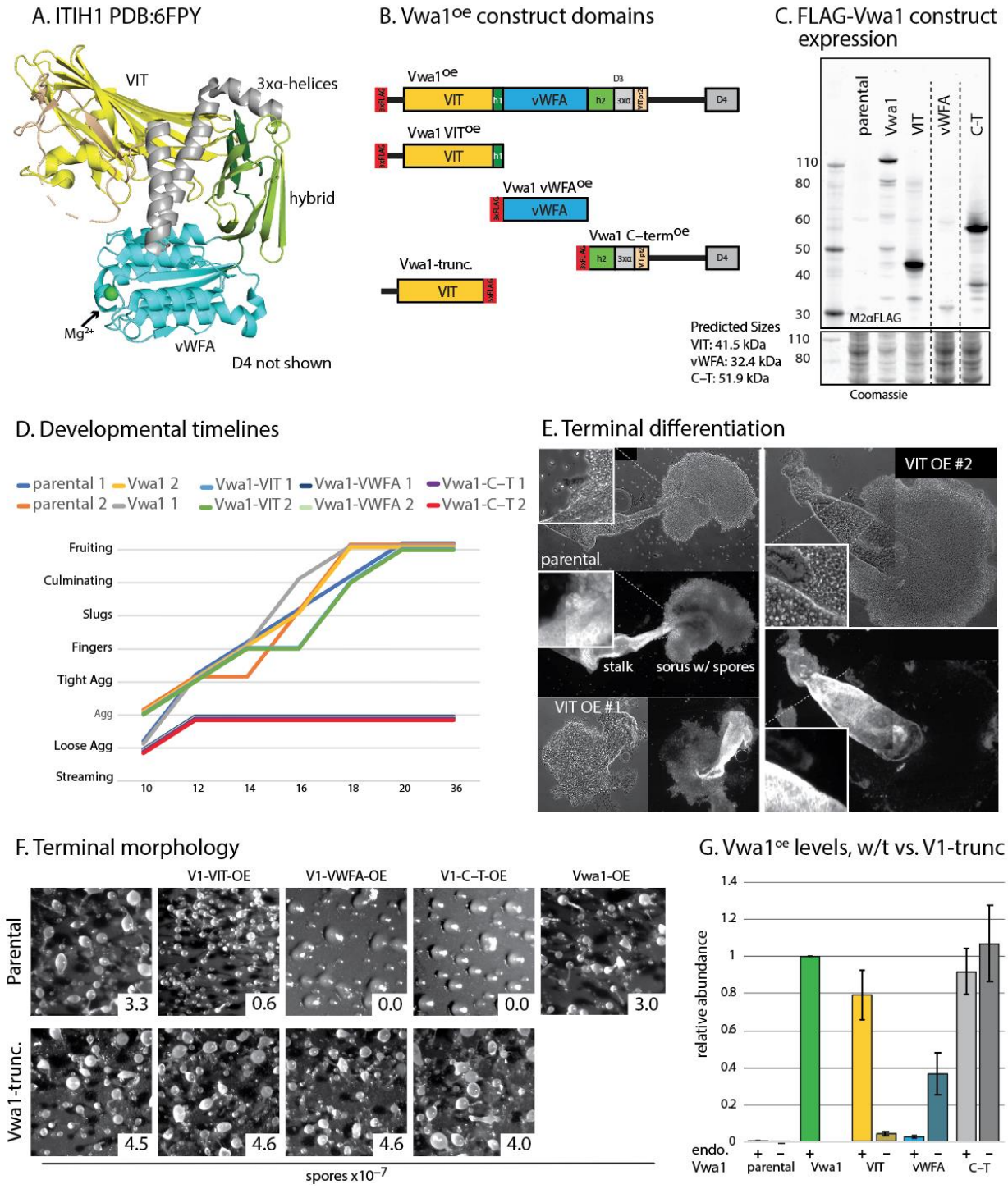

Fig. 3.9. Effects of truncated Vwa1 over-expression on development. *A,* A color coded visualization of the crystal structure of ITIH1 PDB:6FPY (35) used to inform truncated construct generation. *B,* Domain diagram of Vwa1 constructs. *C,* Western blot analysis of domain expression. *D,* Shaken media grown *Dictyostelium* cells were plated (n=2 per strain) on nitrocellulose filters and their morphology was tracked every 2 hours from 10hrs to 20hrs and at 36hrs. Development is represented graphically as morphology over time. *E,* Representative images of fruiting bodies from Ax3/parental and Vwa1-VIT domain only over expressing cells. Fruiting bodies were stained with 0.2% calcofluor to stain cellulose on mature stalk cells and spores. Images taken in phase brightfield as well as UV. *F,* Representative morphologies of wildtype/Ax3 and endogenous Vwa1-truncation strains over-expressing truncated and full length Vwa1 before spore harvest as well as total spore counts. *G,* Average levels of $Vwa1^{OE}$ relative to w/t $Vwa1^{OE}$ in Ax3 and Vwa1-trunc. parental strains.

Fig. 3.10. Scatter plots of truncated Vwa1 domain over-expression construct immunoprecipitation.

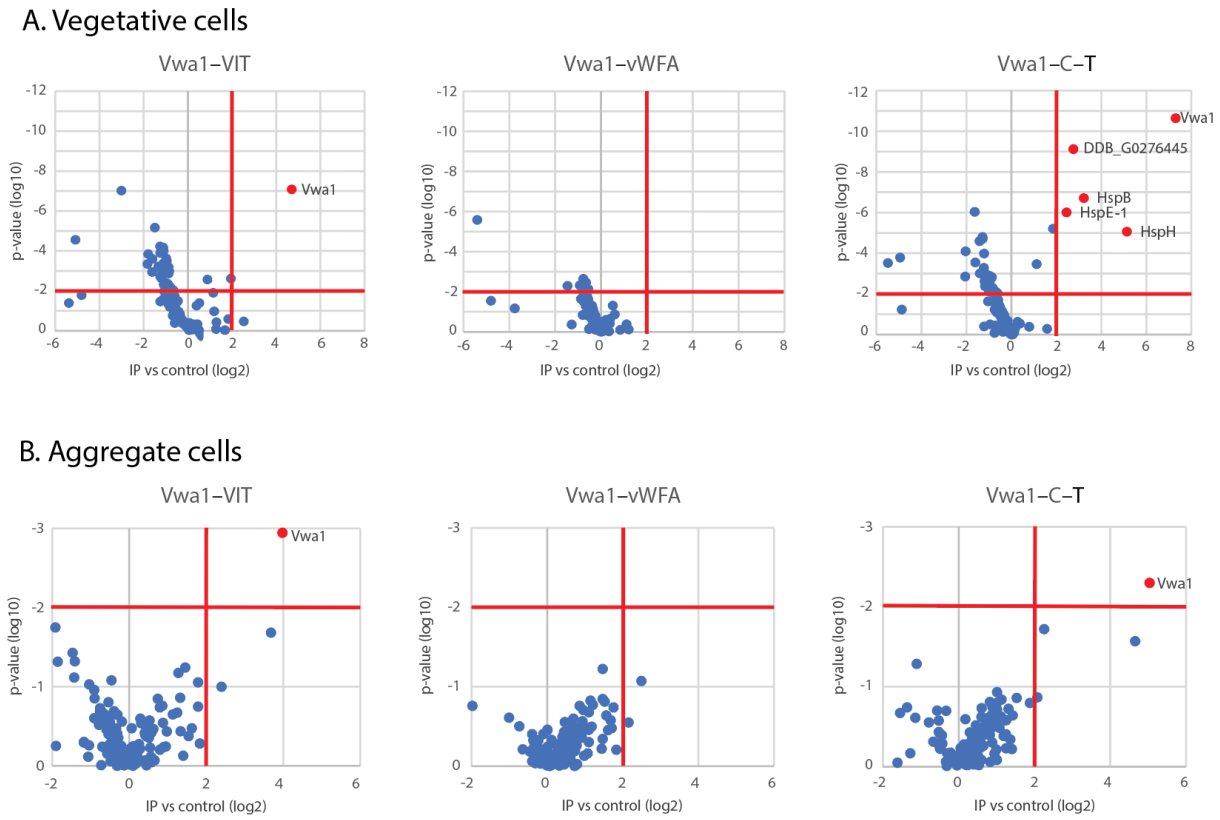

Fig. 3.10. Scatter plots of truncated Vwa1 domain over-expression construct immunoprecipitation. Scatter plots of IP vs control for Vwa1 VIT, vWFA, and C-terminus constructs are presented for vegetative (A) and slug (B) immunoprecipitations. Proteins 4fold higher than control with a p-value<0.01 were considered significant. Largely the Vwa1 bait was the only protein that met that criterion. Vwa1-vWFA was not significantly identified in experimental vs control due to very low expression levels of the construct. Vwa1 C-terminus IP in vegetative cells pulled down a number of Hsp70 homologues indicating an unfolded protein.

Fig. 3.11 Complementation of GWDI generated Vwa1-KO cells.

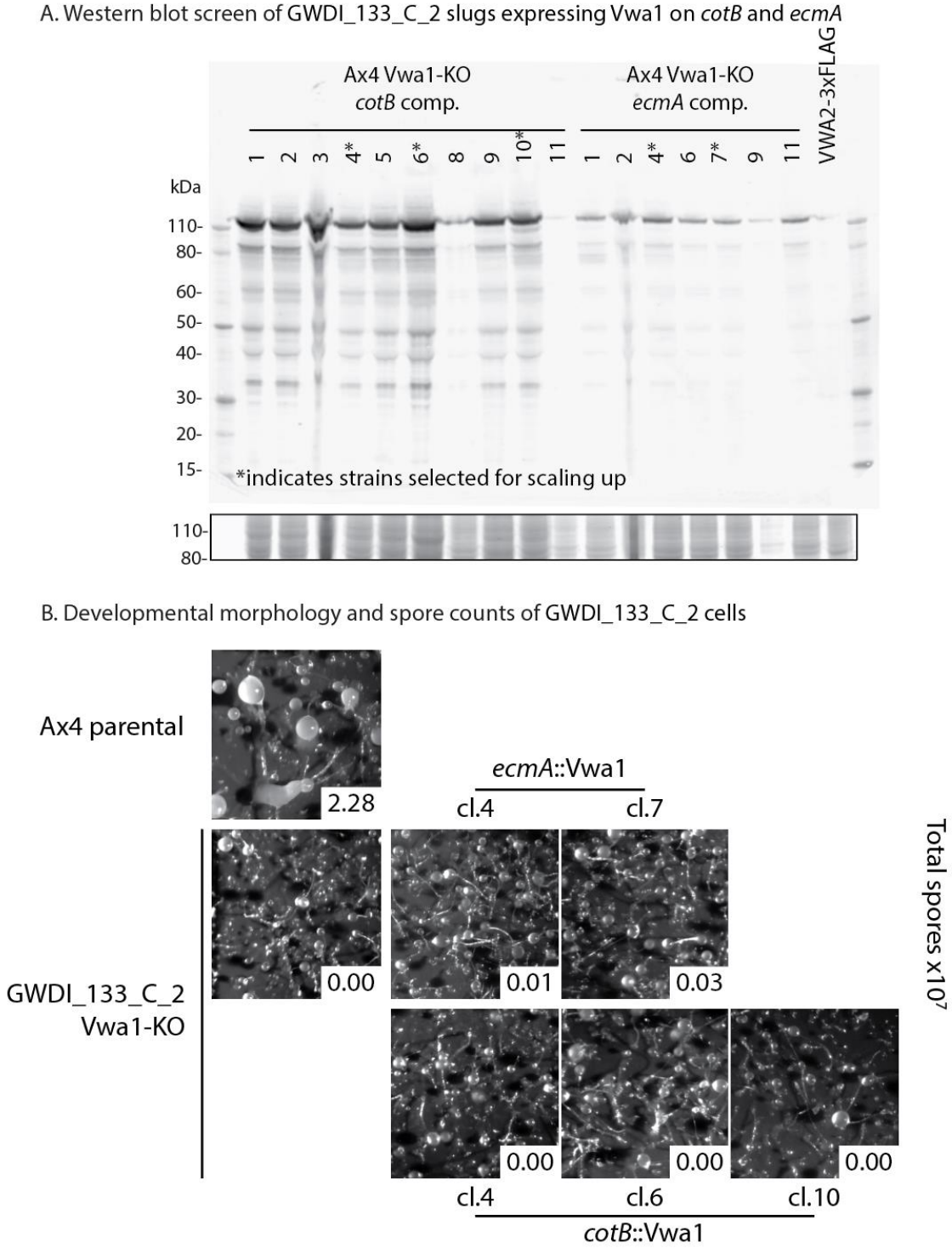

Fig. 3.11 Complementation of GWDI generated Vwa1-KO cells. *A,* Western blot screening of prespore *cotB*::3xFLAG-Vwa1 and prestalk *ecmA*::3xFLAG-Vwa1 in GWDI_133_C_2 Vwa1^{KO} Ax4 slugs (49,50). Clones used for subsequent developmental assays are marked with an asterisk. B, developmental assays of Ax4 Vwa1^{KO} cells and to screen for rescue of spore production via developmentally induced complementation of Vwa1. Ax4 from the Thompson lab was used as a control. Spore counts in the boxes in the lower right-hand corner at x10^{7}. Despite high levels of Vwa1 over-expression on prespore and prestalk promotors, Vwa1 over-expression failed to rescue the low spore mutant phenotype.

Fig. 3.12 Development of Cells Expressing Truncated VWA1 constructs.

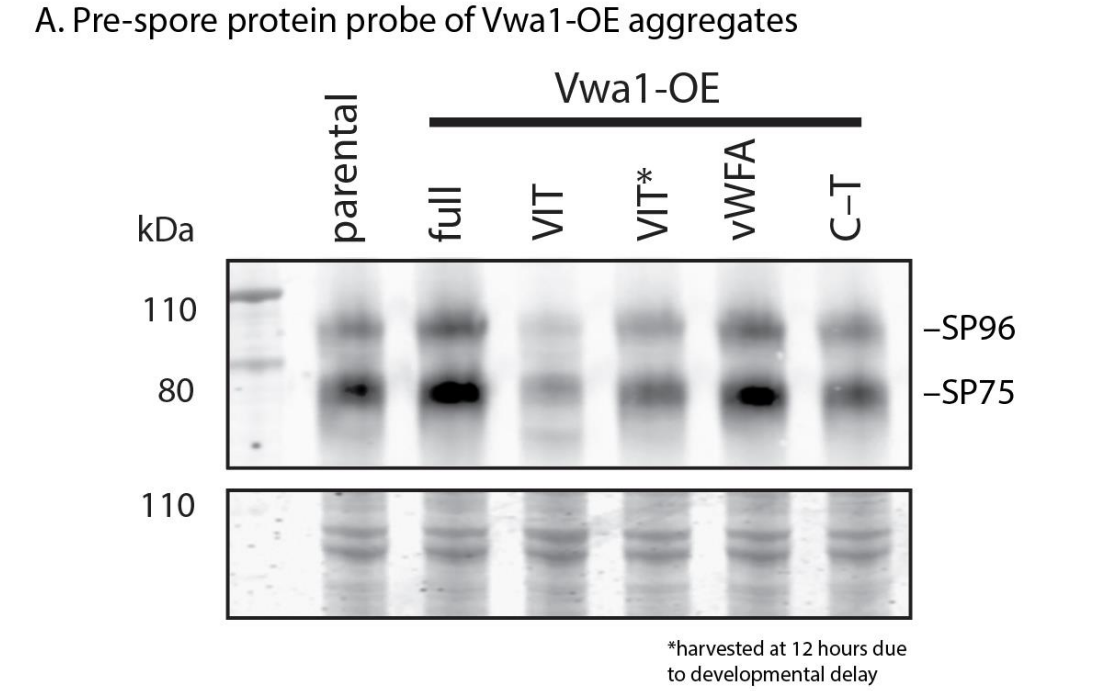

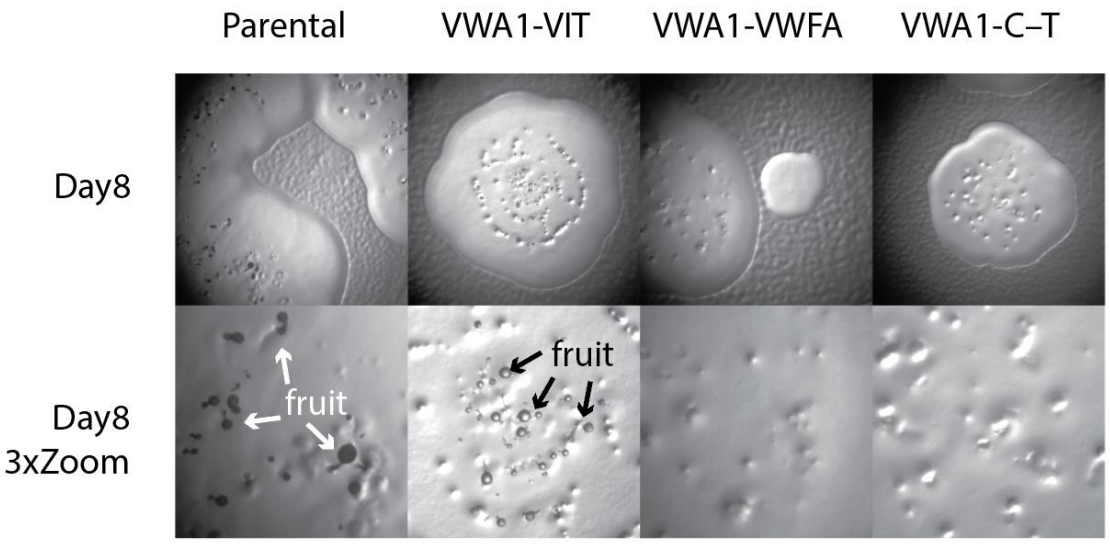

Fig. 3.12 Development of Cells Expressing Truncated VWA1 constructs. *A,* A probe of aggregate lysates of Vwa1 overexpression constructs for the fucosylated prespore protein, SP75, as a metric for developmental progression. *B,* The following strains were plated and grown on a bacterial lawn, Ax3(parental), Vwa1-VIT, Vwa1-VWFA, Vwa1-C–T. All four strains grew and produced plaques in the bacterial lawns at a normal rate. Parental and Vwa1-VIT cells developed and produced fruiting bodies with the parental randomly distributing fruit and the Vwa1-VIT produced fruit in more organized ring patterns. Vwa1-VWFA and Vwa1-C–T failed to produce any organized structures beyond loose aggregate mounds.

Fig. 3.13. FbxD-ecmA^{OE} Vwa1-trunc western blot validation.

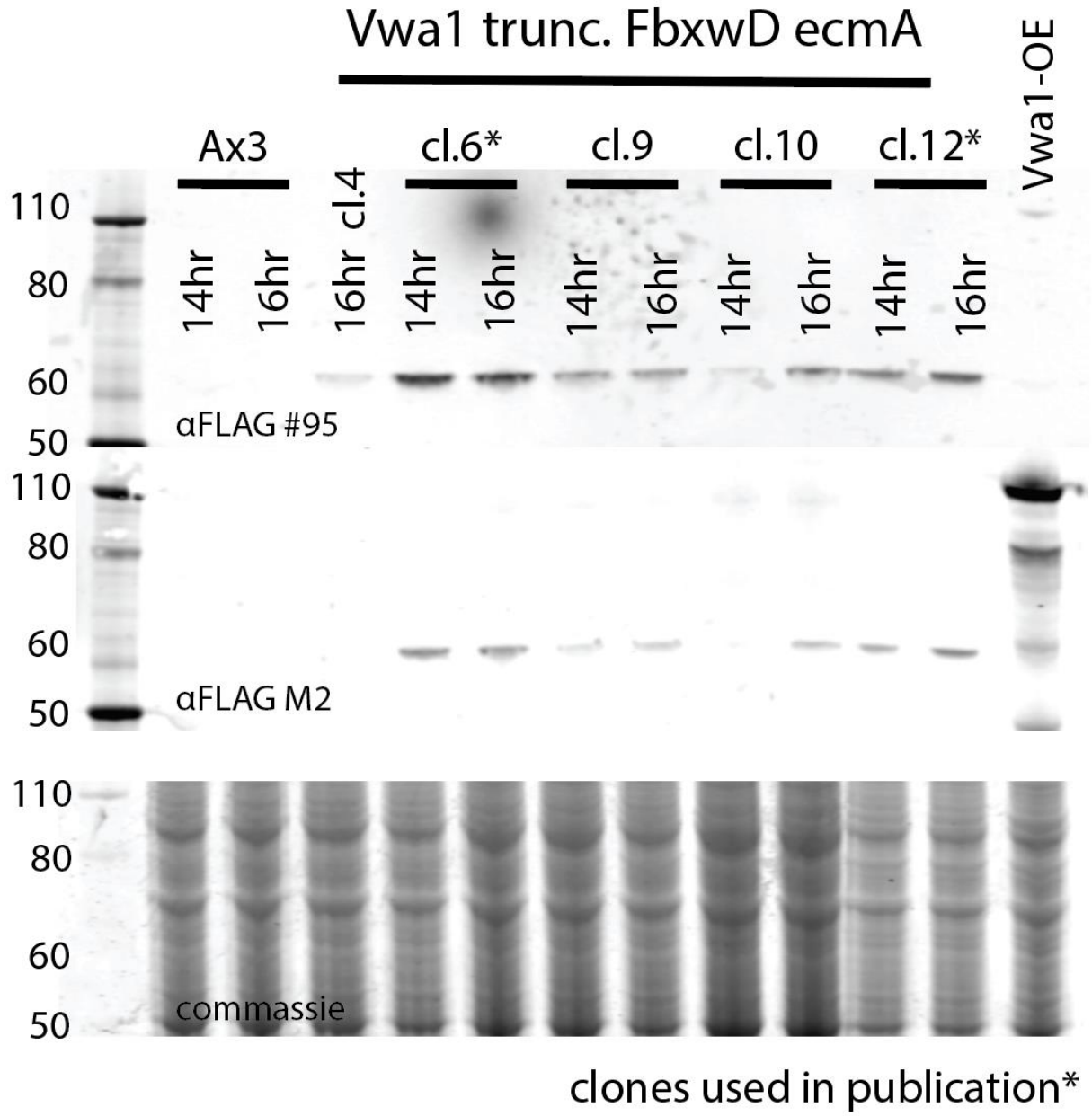

Fig. 3.13. FbxD-ecmA^{OE} Vwa1-trunc western blot validation. Western blot validation of FLAG-FbxwD expression on the *ecmA* pre-stalk promotor in *Vwa1-trunc.* background slugs.

Full-length Vwa1 expression under control of the semi-constitutive discoidin 1γ promoter had no effect on developmental timing relative to the parental (Fig. 5D, F), nor on morphology or spore count (Fig. 3.9F, G). In contrast, VIT-domain overexpression resulted in a 2-h delay in culmination (Fig. 3.9D) and an 80% reduction in spore production whereas the morphology of fruiting bodies was not obviously different (Fig. 3.9F). However, when developed on bacterial lawns, VIT-domain overexpression led to a range of fruiting body morphologies with predominantly immature prespore cells and misshapen spores (Fig. 3.9E). Most dramatically, the vWFA- and CT-domain overexpressors were not only initially delayed relative to parental cells during development (Fig. 3.9D), but they failed to develop beyond the tight aggregate stage (Fig. 3.9D, F). To address whether gene expression was similarly blocked, extracts were probed with mAb 83.5, which recognizes a fucose-dependent epitope on several spore coat proteins that are expressed in prespore cells. Cells that were blocked at the tight aggregate did express the prespore markers, but the VIT-domain expressors had a greatly reduced level indicating a dysregulation of the developmental program that may be the source of the reduced spore counts and abnormal morphology on bacterial lawns (Fig. 3.12A). Observations of cells developing on bacterial lawns were consistent with findings from cells developed on nitrocellulose on filters (Fig. 3.12B). These effects were specific to development because overexpression of the single domain constructs of Vwa1 had no significant effect on growth rate of cells.

To determine if these trans-dominant negative phenotypes were dependent on full-length Vwa1, the 3 domain constructs were expressed in the V1-trunc strain. Strikingly, despite similar levels of expression (Fig. 3.9G), development was normal in these strains (Fig. 5F).

Additionally, the spore reduction seen in VIT over expression cell, was not replicated when the truncated protein was expressed in the endogenous truncation background.

To further explore a functional interaction between FbxwD and Vwa1, the *ecmA*::FbxwD construct was transfected into V1-trunc cells. Strikingly, overexpression of FbxwD, as documented by Western blotting (Fig. 3.13), exerted no developmental phenotype (Fig. 3.8E). Thus, the detrimental effects of both FbxwD overexpression and overexpression of Vwa1 domains depend on the presence of endogenous full-length Vwa1, even though Vwa1 is dispensable for development.

Evolution of VIT/vWFA containing proteins

Homologs of Vwa1 are present throughout eukaryotic phylogeny. To assess the evolutionary relationship of the Dictyostelium paralogs to these proteins, initially, BLASTp (51) was implemented to search throughout phylogeny for vWFA-like domains with Expect value <0.05. The sequences of these proteins were aligned, and additional proteins that were annotated as containing vWFA domains (52) but did not meet the Expect threshold were included. The great majority of proteins found by BLASTp also contained hybrid domains and VIT domains. These VIT/hybrid/vWFA domain containing proteins were found throughout but not all Eukarya. For example, none were found in the model organism *Saccharomyces cerevisiae*, but 5 homologs of Vwa1 were found in *Dictyostelium*. The domain boundaries of the alignment were refined using reference to the crystal structure of ITIH1 (Fig. 3.9A), and further refined as needed using AlphaFold structural predictions (53,54). The relationship of the sequences was examined using a maximum likelihood method. Representatives of the large number of proteins containing only vWFA domains were clustered at the base of the tree and are proposed to be the progenitor

(Fig. 3.15A). Many of these proteins contain additional functional domains such as kinases (55), suggesting that their vWFA domains mediate targeting. The acquisition of the VIT domain appeared to occur more recently, and no proteins with VIT sequences without a vWFA sequence were found indicating that VIT domain evolved in co-dependence with vWFA domains. Based on the evolution of the vWFA domain, the VIT/hybrid/vWFA domain containing proteins then diversified into 5 clades each with distinctive domains: a) a minimal sequence with no additional domains; b) C-terminal D3/D4 domains; c) signal peptide directing the protein to the secretory pathway with D3/D4; d) signal peptide with C-terminal D3/D5 domain; and e) poly-ADP-ribose transfer domain with D3. The tree suggests that all sequences of each group are clustered with, in all cases except one, significant bootstrap values. This suggests single originating events presumably via gene duplication and subsequent specialization. However, the order of events suggested by the topology of the tree did not show a convergence of domain acquisition with vWFA sequence evolution. Thus, a new analysis was performed for the sequence of the combined VIT/hybrid/vWFA domains (Fig. 3.14).

In the combined domain evolutionary tree the same cades of VWA5A, PARP4, ITIH, and plant specific VIT/hybrid/vWFA proteins, confirming their independent singular appearance and potential shared functions. However, the sequence of appearance was distinct. For example, ITIH emerged well before the differentiation of VWA5A-like and PARP4s whereas and VWA5B emerged as a vertebrate specific duplication of VWA5A followed by a rapid evolution of the VIT domain as seen in Fig. 3.15B. This indicates two events for secretory proteins with different functions. A cytoplasmic protein with C-terminal D4 domain emerged early in protists and PARPs appear to have derived from the protist gene, followed by subsequent radiation of the D4 version

Fig. 3.14. Evolutionary Trees of VIT/Hybrid/vWFA domains.

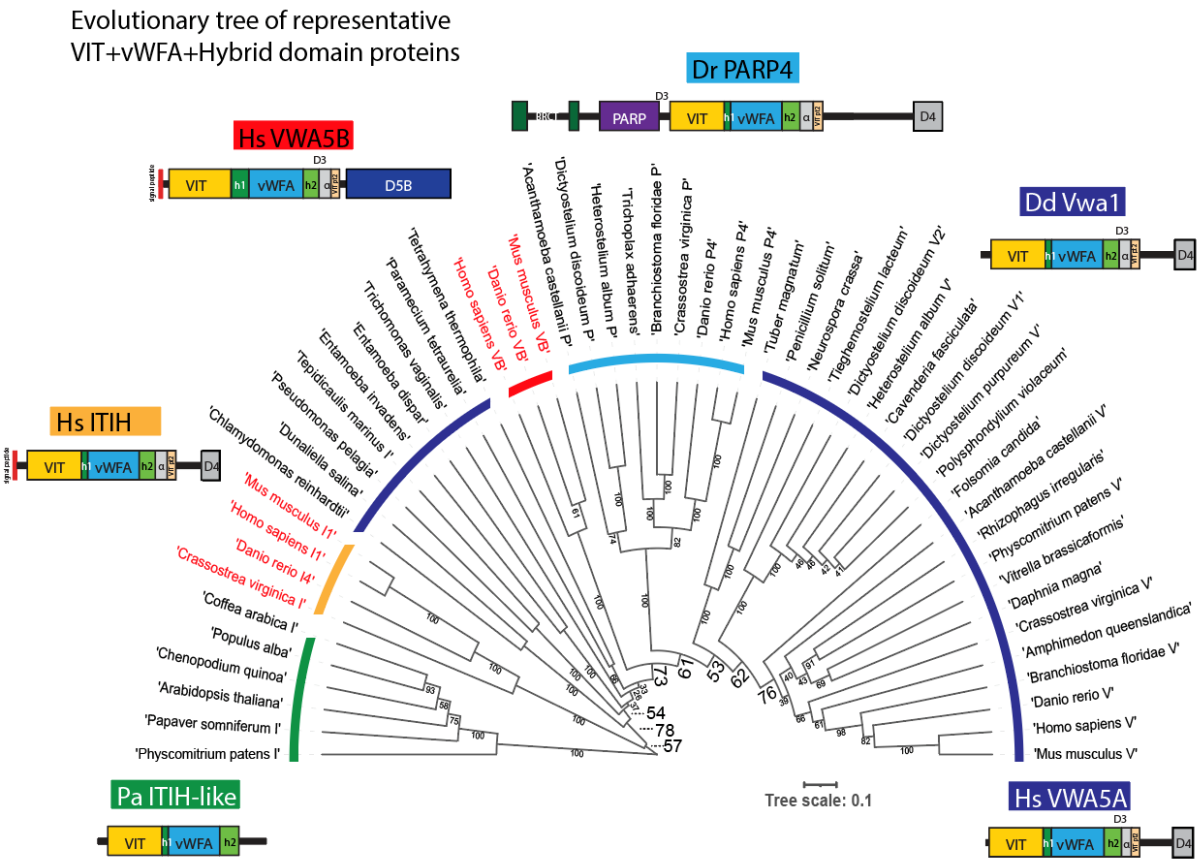

Fig. 3.14. Evolutionary Trees of VIT/Hybrid/vWFA domains. VIT+VWFA alignments in which all amino acids between the N-termini of the annotated VITs to the C-termini of the VWFA domain were aligned. All protein clades have representative examples of domain structures displayed by their branches. Extra-cellular lineages are in red.

Fig. 3.15. Evolutionary Trees of vWFA and VIT domains.

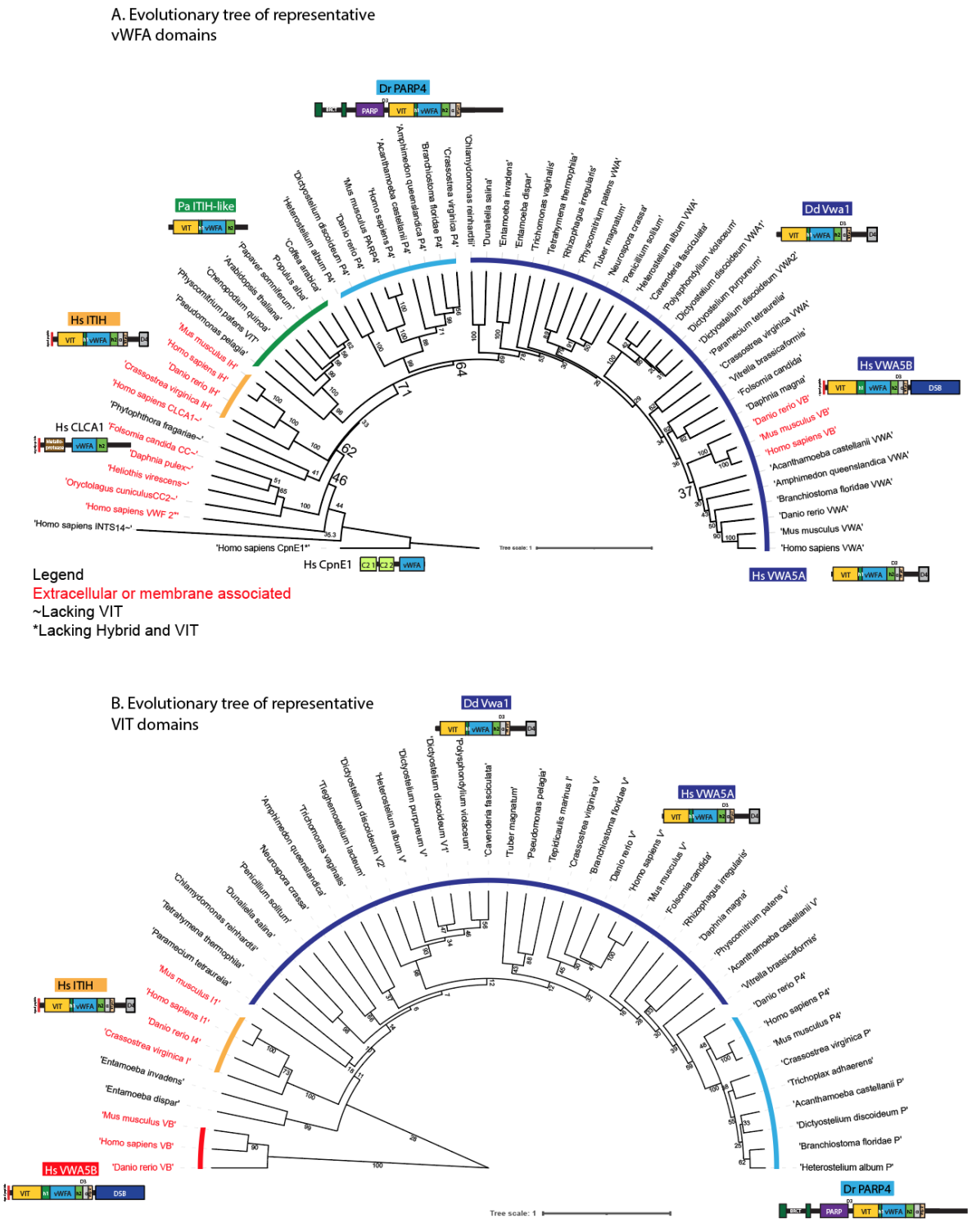

Fig. 3.15. Evolutionary Trees of vWFA and VIT domains. *A,* A tree built from the alignment of vWFA domains from representative proteins found through amino acid or predicted structural homology to the vWFA domain of VWA1. Representative examples of each clade are displayed with domains color coded in a manner to correspond to the color-coded domains on the ITIH1 structure 6FPY. *B,* Alignment of representative curated VIT domains. All protein clades have representative examples of domain structures displayed by their branches. Extra-cellular lineages are in red.

across phylogeny including humans. According to both trees, the Dictyostelium Vwa1 is orthologous to human VWA5A, and all 5 Dictyostelium paralogs are more closely related to each other than to VWA5 and other animal homologs.

Discussion

Vwa1 is a highly conserved intracellular multi-domain protein that is broadly expressed across eukaryotes, but whose cellular functions are poorly understood. Three homologs in Dictyostelium were found in the interactome of FbxwD, a previously characterized F-box protein that is expected to be a receptor for substrates that are subject to polyubiquitination and degradation in the proteasome. The functional importance of Vwa1 was established by finding that forced overexpression of discrete domains of Vwa1 exerted dominant negative effects on morphogenesis and terminal spore differentiation. However, inhibition depended on expression of intact Vwa1, suggesting a perturbation of Vwa1 function despite Vwa1 being dispensable for development. The functional significance of FbxwD is indicated by negative effects of its forced overexpression and its resistance to genetic deletion. Remarkably, the dominant negative effect of its forced overexpression also depended on the expression of intact Vwa1. These findings suggest that Vwa1 modulates FbxwD activity in cells via physical interaction. While the biochemical basis by which these two proteins interact remains unclear, it has been previously shown that Vwa1 interacts with FbxwD in an F-box domain independent manner (21). Cellular differentiation is a highly concerted process involving dramatic transcriptomic and proteomic changes even in the simplest of systems such as Dictyostelium. Among the factors involved in this process, the SCF and ubiquitin-proteasome system act as a targeted downstream sculptor of the proteome. SCF assembly and activity is increasingly understood to be regulated by a number of

factors from Cand1, chaperones, localization factors, post translational modification, etc. (56). Here we present evidence that a homologue of the tumor-suppressing VWA5A interacts primarily with the developmentally regulated F-box protein, FbxWD. Our evidence that FbxwD does not negatively regulate Vwa1 levels and that Vwa1 is necessary for FbxwD to inhibit development suggests that Vwa1's interaction with FbxwD is that of a synergistic binding partner and not that of an SCF substrate. Vwa1's evolutionary similarity to VWA5A suggests that the homologous proteins may be orthologues with retained function. The model of Vwa1 as an SCF cofactor or component may explain VWA5A's role as a tumor suppressor with the knowledge that deregulation of the SCF is characteristic of several cancer types (32-34).

FbxwD's Fbox and RING domain necessary for its role in the cell

FbxwD is highly expressed in growing cells and during early development, and its levels gradually taper off during development such that, during the slug stage, it is highly overexpressed in prestalk compared to prespore cells (43). Thus, FbxwD has the potential to control terminal differentiation especially considering that prestalk cells occupy the anterior tip of the slug which is thought to be the origin of controlling morphogenetic signals. Interestingly, overexpression in either prestalk or prespore cells has similarly strong inhibitory effects on terminal spore differentiation, and both led to abnormal stalk morphology.

FbxwD has sequence characteristics of a classical WD40 type FBP except for the presence of a RING domain sequence N-terminal to its F-box domain. RING domains are characteristic of RING type E3 Ub ligases, suggesting potential dual activities for FbxwD in protein degradation. To test these roles, the activity of overexpressed FbxwD proteins with point mutations expected to inactivate the RING function, or known to inactivate the F-box function, were investigated. Either

type of mutation abrogated the inhibitory effect of FbxwD overexpression, indicating a role for both domains in FbxwD activity. FbxwD appears capable of acting in SCF complexes based on the detection of CulE and Rbx1 in the FbxwD interactome, and the presence of FbxwD in the CulE interactome. However, no evidence could be obtained that Vwa1 acts as a target substrate based on effects of proteasome inhibitors, though our inability to knock out FbxwD limited our approaches to test this hypothesis. However, the abundance of Vwa1 in the FbxwD interactome and the abundance of FbxwD in the Vwa1 interactome raises the possibility that they are in a more stable complex that modulates the activity of FbxwD. There is precedent for FBPs that depend on protein co-factors for targeting certain substrates (57,58). A related Zn-finger domain, with its potential to mediate protein-protein interactions, is found in human Emi1/Fbx05 where its zinc-finger has been implicated in controlling the rate of polyubiquitination (59), though the mechanism is unknown.

Vwa1 interacts with FbxWD and may be essential for its function

Vwa1 is a multi-domain protein, and based on currently available information, it appears that the vWFA domain sequentially acquired flanking Hybrid and then upstream VIT and downstream D4 domains during evolution. Though it appeared to evolve as a cytoplasmic protein, variants acquired motifs at least twice that directed the protein to the cell surface – an extracellular space. A crystal structure of ITIH1, an extracellular example that possesses all characteristic domains, suggests that for Vwa1, the flanking Hybrid sequences assemble to create a domain adjacent to the vWFA domain, with the VIT domain nestled on the opposite side. An alpha fold analysis of the full-length protein suggests that the C-terminal D4 domain, which was not included in the ITIH1 sample analyzed by crystallography, folds back and potentially masks

the VIT domain (53,54). In addition, evidence indicates that ITIH1 can occur in a homodimer state (35). This organization suggests that individual domains have the potential to disturb these intramolecular interactions or dissociate the dimer. Alternatively, the expressed domains have the potential to interfere, by competitive binding, with interactions with other proteins. For example, one clade of the Vwa lineage acquired a PARP enzyme domain, a feature that supports the idea that one or more of these domains mediates protein-protein interactions that direct the enzyme to appropriate locations or even substrates. However, our attempts to detect interactors with the expressed domains by co-IP methods failed to identify significant candidates. A possible explanation is that, in the cell, the interactions are transient or become so upon extract preparation. Alternatively, Vwa1 may need to be post-translationally modified via proteolytic cleavage as is the case with the C-terminus of ITIH (60).

A developmental role for Vwa1 was not evident from the disruption of its genetic locus. Although a full deletion of its coding region was not achieved, its interruption within the VIT domain was expected, based on inspection of the VIT structure, to yield an unfolded and therefore non-functional polypeptide suggesting that this interrupted strain was an effective Vwa1-knockout. However, forced overexpression of individual domains of Vwa1 throughout development exerted substantial negative effects on the developmental program. There is adequate precedent for trans-dominant negative effects for numerous proteins (61,62). Most severe were effects of overexpressing the vWFA and Hybrid 2/D4 domains, which interrupted development at the tight aggregate stage before slugs appeared, which was much earlier than the effect of FbxwD overexpression. The timing of this effect coincided approximately with an uptick of Vwa1 and FbxwD expression at the transcriptional level (Fig. 3.3). In comparison, VIT

domain overexpression had a relatively mild effect by permitting fruiting body formation but inhibiting terminal spore differentiation and interfering with normal stalk morphogenesis; these effects were more similar to the effect of FbxwD overexpression. Strikingly, overexpression of the entire Vwa1 protein rendered no obvious developmental deficiency. These effects on development did not correlate in an obvious way with expression levels of the constructs. These findings suggest that the effects of the domains were due to inhibition rather than activation of a process. The target of this inhibition might be Vwa1 itself, because, remarkably, they did not occur in the V1-trunc strain. The modular organization of Vwa1 would allow for possible interference of its function by discrete domains. This result furthermore indicates that the lack of a phenotype for the V1-trunc strain was not due to compensation by any of the other Vwa proteins, including Vwa2 and Vwa3 that were found in the FbxwD interactome.

The parallel dependence of FbxwD overexpression and Vwa1 domain overexpression on the presence of Vwa1 indicates a functional interdependence and based on the interactome studies, this interdependence is mostly like based on a biochemical interaction. However, we have not obtained evidence for a stable stoichiometric complex, suggesting that the functional interactions are in equilibrium with dissociated states. Vwa1 may be an adaptor or scaffold protein necessary for FbxwD to function in addition to Skp1. The serine and aspartate residues from the Mg^{2+} coordinating MIDAS (metal ion dependent adhesion site) motif (52,63) in ITIH1 are conserved in Vwa1 suggesting that it may engage in protein-protein contacts via a coordinated metal ion as for other vWFA domain containing proteins, though FbxwD lacks a canonical RGD domain or any of the functional derivatives (64) expected to interface with the MIDAS ion. Examples of vWFA proteins that use the MIDAS domain to bind to specific ligands include Hs

CLCA1 (65) featured in Fig.7B, but other MIDAS domains lend themselves to more promiscuous binding to other proteins by coordinating with an aspartic or glutamic acid on the ligand protein (66). Alternatively, it may interface with the large β-sandwich of the VIT or the smaller hybrid domain. ITIH1's hybrid domain has been shown to bind to the integrin substrate, vitronectin, in a MIDAS independent manner (35). Biophysical studies have also shown that in proteins such as integrins that contain vWFA and hybrid domains, ligand binding allosterically affected the conformation and binding affinity of the hybrid domains via MIDAS (66). Individual truncated domains might interfere with allosteric regulation. In addition, the C-terminal D4 domain may act to autoregulate the other domains as suggested by the structure prediction in Fig. 3.16B, consistent with precedent in other studies that illustrate protein auto-inhibition through domain masking (67-69). When comparing the AphaFold prediction (53,54) of the structure and location of D4 between ITIH1 and Vwa1, D4 is predicted to mask the functional VIT (78) in ITIH1 (Fig. 7A) and a portion of the vWFA in Vwa1 (Fig. 7B). This potential auto-inhibition by D4 in ITIH1 would be abrogated by the proteolysis that takes place before mature ITIH1 is covalently bound to the hyaluronic acid in the extracellular matrix (60). Similar proteolysis of D4 to activate Vwa1may take place before it is capable of binding FbxwD which would explain the non-stoichiometric levels of interaction seen in reciprocal IP.

The non-essentiality of Vwa1 contrasts with the possible essentiality of FbxwD which leads to the hypothesis that Vwa1 primarily acts via modulation of FbxwD. This mechanism must allow for normal FbxwD activity in the absence of Vwa1 but abnormal activity in the presence of Vwa1 whose function is perturbed by the domain constructs. We suggest that the domains generate an overactive positive activity or underactive inhibitory activity that balances an

unknown opposite regulatory activity of FbxwD, as frequently occurring during developmental or physiological regulation. Both proteins are expressed throughout development allowing for multiple roles, presumably in protein turnover. Although FbxwD overexpression did not render an apparent effect prior to culmination whereas overexpression of vWFA and D4 domains interrupted slug formation, this is likely because FbxwD overexpression was not induced until the slug stage. Interestingly, FbxwD was active when overexpressed in either prestalk or prespore cells, by inhibiting the terminal differentiation of both stalk and spore cells. This is not surprising given the inter-coordination of these two processes in the formation of the fruiting body. It is expected that selective protein turnover would be required to coordinate the numerous parallel processes required for terminal differentiation, which has been described for the assembly of the spore coat (70,71).

VWA5, which sequence alignments suggest is orthologous to Vwa1, is tumor suppressing (32-34) and schizophrenia associated (36). These findings may shed insight into the poorly understood roles of human VWA5. We speculate that VWA5A influences E3 ubiquitin ligase activity through its interaction with SPSB1 (37,38). Vwa1's interaction with FbxwD could give insight into how VWA5A and SPSB1 function within the cell. Ubiquitin ligase dysregulation is a characteristic of many cancer types and, furthermore, reduced VWA5A levels were significantly correlated to poor cellular differentiation in breast cancers (34), a characteristic of cells with the capacity for metastasis.

Fig. 3.16. Model of Vwa1's potential mechanism of autoregulation and its synergistic relationship with FbxwD in development.

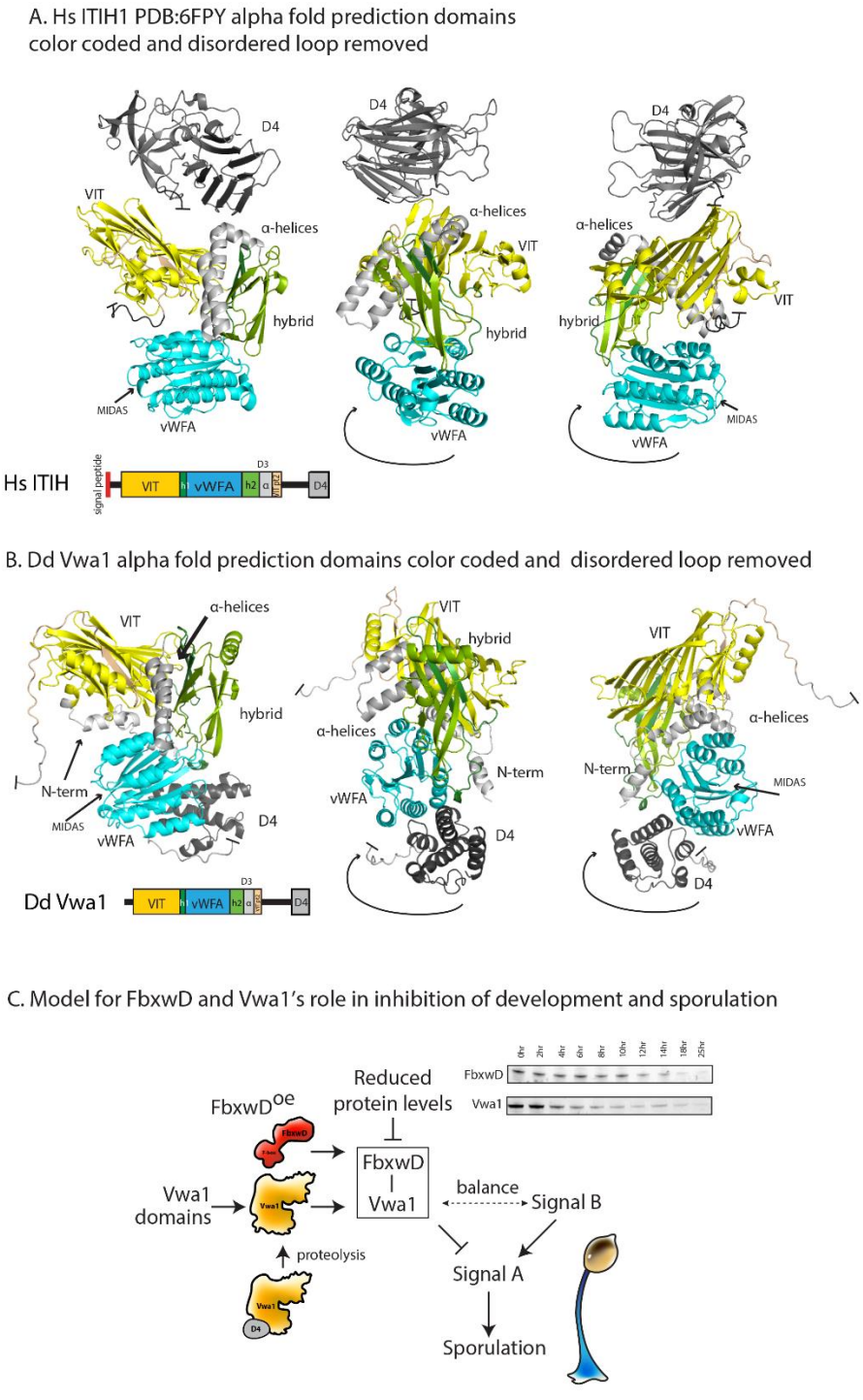

Fig. 3.16. Model of Vwa1's potential mechanism of autoregulation and its synergistic relationship with FbxwD in development. *A,* The ITIH1 model with domains color coded according to the literature's description of domains (35) with a corresponding domain diagram. Multiple conformations are displayed to emphasize a potential site of autoinhibition by D4 which was not featured in the crystal structure. *B,* The AlphaFold model of Vwa1, PRO_0000389207, is color coded according to homology with ITIH1 and multiple poses mirroring the ITIH model are presented to show the predicted position of the D4 domain. Disordered portions of the C-terminus are not shown as the predicted structure is of low statistical likelihood. *C,* The genetic model of FbxwD and Vwa1's cooperative role in inhibiting a hypothetical Signal A and subsequently sporulation. Expression of FbxwD and Vwa1-domains shift the balance from hypothetical Signal B to FbxwD–Vwa1. Endogenous transcription trends during development contribute to lower levels of Vwa1 and FbxwD thus inhibiting the complex. Vwa1 require post-translational proteolysis of D4 to activate it and allow it to functionally complex with FbxwD.

Table 3.1. Strains used in this study.

Strains	parental	genotype	resistance	ref.
Ax3	NC-4	axenic	none	
Ax4	Ax3	axenic	none	
HW540	Ax3	fbxwD-FLAG	blasticidin-S	(21)
HW542	Ax3	fbxWD-FLAG-3UBA	blasticidin-S	this pub.
HW548	Ax3	*cotB*::FLAG-FbxwD	G418	(21)
HW552	Ax3	*cotB*::FLAG-FbxwD(LP-AA)	G418	(21)
HW553	Ax3	*ecmA*::FLAG-fbxWD	G418	this pub.
HW554	Ax3	*ecmA*::FLAG-fbxWD(LP-AA)	G418	this pub.
HW556	Ax3	*ecmA*::FLAG-fbxWD(V9A)	G418	this pub.
HW557	Ax3	*ecmA*::FLAG-fbxWD(CH22/24AA)	G418	this pub.
HW558	Ax3	*ecmA*::FLAG-fbxWD(PF41/42AA)	G418	this pub.
HW601	Ax3	VWA1-3xFLAG endogenous	blasticidin-S	this pub.
HW602	Ax3	VWA2-3xFLAG endogenous	blasticidin-S	this pub.
HW603	Ax3	Vwa1-truncation	blasticidin-S	this pub.
GWDI_133_C_2	Ax4	Vwa1 insertion at position 82	blasticidin	(50)
HW604	HW603	dscC:: 3xFLAG-VWA1–VIT; V1-trunc.	blast/G418	this pub.
HW605	HW603	dscC:: 3xFLAG-VWA1–vWFA; V1-trunc.	blast/G418	this pub.
HW606	HW603	dscC:: 3xFLAG-VWA1–C–T; V1-trunc.	blast/G418	this pub.
HW609	HW603	*ecmA*::FLAG-fbxWD; V1-trunc.	blast/G418	this pub.
HW611	Ax3	dscC:: 3xFLAG-VWA1 medium	G418	this pub.
HW612	Ax3	dscC:: 3xFLAG-VWA1 high	G418	this pub.
HW622	Ax3	dscC:: 3xFLAG-VWA2	G418	this pub.
HW624	Ax3	dscC:: 3xFLAG-VWA1–VIT	G418	this pub.
HW626	Ax3	dscC:: 3xFLAG-VWA1–vWFA	G418	this pub.
HW628	Ax3	dscC:: 3xFLAG-VWA1–C–T	G418	this pub.

Methods

Cell culture and developmental assays

Dictyostelium discoideum cells derived from Ax3, axenic-3, were grown primarily in HL-5 (72) shaken media at 22°C. Cells were passaged every 3-4 days by 1000-fold dilution to maintain thriving cultures. All vegetative cell collections were taken during logarithmic growth phase (2.5-7.5x10^6 cells/ml). Culture density was determined by hemocytometer. All developmental assays were performed using cells collected at the same logarithmic growth phase for consistent behavior across developmental assays. Developmental assays on nutrient free nitrocellulose filters and nutrient free agar as previously described (5) using 4x10^7 cells per filter. Slug cells were typically scraped at 14hours unless developmental delay required a later scraping to ensure uniform morphology upon harvest.

For spore collection to measure fruiting success, after 36 hours of development filters were rinsed in 0.2% v/v Triton x100, vortexed for 30 seconds, probe sonicated at 20% in five intervals of one second on, three seconds off and finally vortexed again for 30 seconds before counting on a hemocytometer.

Endogenous tagging

Endogenous C-terminal 3x-FLAG tagging constructs of *Vwa1* and *Vwa2* were constructed in a similar manner as previously described for CulE (21). Using genomic DNA as a template, targeting fragments ranging from 500-1000 bp were generated by PCR using appropriate oligonucleotide primers (Table 3.2, Fig. 3.17, Fig. 3.18A-B) and proofreading polymerase (Q5 NEB). These targeting sequences, derived from the 3'-end of the coding sequence and 3' non-coding sequences (see Fig. 3.18A-B), were used to replace the CulE targeting sequences in the

pVS_CulE-3xFLAG plasmid (ref 1) via two step standard restriction enzyme digestions and ligations. The tagging plasmid was linearized with BssHII and gel purified. $7.5x10^6$ cells at a growth density of $2.5\text{-}7x10^6$ cells/ml were transformed as described in (73) using a BioRad Genepulser with 2x pulses of 850 V and 25 µF capacitance separated by 5 seconds. Cells were allowed to recover for 10 min before being rinsed from the cuvette and added to petri dishes containing 10 ml of HL5+ (10 g/l Dextrose, 5 g/l Proteose Peptone 3, 5 g/l thionine peptone E, 5 g/l Yeast Extract, 3.84 ml/l 400X Phosphate stock, Ampicillin 100 ug/ml, Streptomycin 100 ug/ml, Vitamin B12 5 ng/ml, Folic acid 2 ug/ml) and incubated in the dark at 22°C. Blasticidin S was added the next day to 10 µg/ml. Cells were grown to confluence and cloned out as described (73). The expected modifications are shown in Fig. 3.18C and D, and confirmed western blotting using mouse M2 anti-FLAG antibody (Sigma-Aldrich), and subsequently by immunoprecipitation and subsequent analysis by nLC MS/MS. Strains are listed in Table 1.

Overexpression Constructs

Overexpression of epitope-tagged versions of Vwa1, Vwa2, and FbxwD was accomplished essentially as described (21). The entire ORF of *Vwa1* was amplified via PCR and inserted into pCR4-TOPO (Invitrogen) vectors, using oligonucleotides described in Table 3.2 and Fig. 3.17. The amplified DNA fragments were trimmed by digestion with NcoI and BamHI, gel purified, and cloned into similarly digested and gel-purified pV3d (discoidin 1γ semi-constitutive promotor), pV3c (*cotB* pre-spore cell specific promotor), and pV3e (*ecmA* pre-stalk cell specific promotor) (ref). Circular plasmids were electroporated into cells and transformants were selected for by growth in the presence of 20 µg/ml G418. The precise sequence of the N-terminally tagged FLAG3-Vwa1 is shown in Fig. 3.17. Overexpression was validated via western blotting mouse with

Table 3.2. Oligonucleotides employed in this study.

Primer Name	Sequence
FbxwD-V9A RING point mutations	
DdFbxD-V9A-S	5'-GGGCATGCTTTGAATTGTTCACTGAACCAG
DdFbxD-V9A-AS	5'-AGCATGCCCAACAGTTATAGTCATATGACAT
FbxwD-CH22/24AA RING point mutations	
DdFbxD-CH22/24AA-S	5'-TATGCATCAGCTTCATTTTGTAAAGAATGTATAGAGAAATCATATCATATCG
DdFbxD-CH22/24AA-AS	5'-TGAAGCTGATGCATATAATGTCACTGGTTCAGTGAACAATTCAAAG
FbxwD-PF41/42AA RING point mutations	
DdFbx-DPF41/42AA-S	5'-TATGCGCAGCTTGCAGAAAAGAAATTCAAATGCCACTAC
DdFbxD-PF41/42AA-AS	5'-CAAGCTGCGCATAATTGTTCGATATGATATGATTTCTCTATAC
Vwa1 endogenous tagging	
endo_pVS 3_	5'-TTATTGTTGTTGTTGTTTTAAAATTTGTTGTTGAGTATATTCCCATATTACAATT GAACCAGATACATGAACATTTAAAC
endo_pVS c_term	5'-GAGAGTTTCAGCATCCTCACTTGCAG
5_VWF1_c_t 2	5'-tgcaagtgaggatgctgaaactctcGTGTTGAAAGTTATGAAAGTGACG
3_VWF1_c_t 2	5'-GCTGCCGCTGCCAACTAATGATTTAGCGTTTGATAAAAATTTATCGATAC
VwF_FLAG_BSR	5'-taaatcattagttGGCAGCGGCAGCAGATCT
3_BSR_VWF_non	5'-aaactgaattattCTGCAGGAATTAACCATGCG
5_VWF non_code_b	5'-ttaattcctgcagAATAATTCAGTTTATGAAAAAGAAAAGG
5_VWF n_c_v	5'-tttaaaacaacaacaacaacaataaGGAAGTGGTATAATTTCAAAAG
Vwa1 endogenous tagging confirmation	
VWA1 3.UTR con_sq	5'-CAAGGTTTATAGAATTACCAAAATAATTTGTACATTTACCGA
pVS tag non-c seq F V2	5'-CCGAAAGCTCGGATCTGATATCATAACTTC
pVS tag C-t seq R V2	5'-GTGCTTCAAAAATATCATTTAAACCACCACCG
VWA1 c_t conf_seq	5'-CATCTTCATCCCAAAAGAAGAAAAAAGAAGTTAGTAG

Vwa1-disruption

VWA1_KO_PvuI_F	5'-atacgatcgTTTAGTAGTATAACAAGTAAATTATCAGC
VWA1_KO_PvuI_R	5'-ttcgatcgTTAAACTAATGATTTAGCGTTTG
VWA1_KO_FGBSR	5'-atatgttcccatcttatgcaGGCAGCGGCAGCAGATCT
VWA1_KO_BSR_R	5'-tatagttgaaattgaatgcaCTGCAGGAATTAACCATGCGGC

Vwa1-disruption Screening

pMini sequencing S	5'-ACCTGCCAACCAAAGCGAGAAC
pMiniT sequencing AS	5'-TCAGGGTTATTGTCTCATGAGCG
pVS tag C-t seq R V2	5'-GTGCTTCAAAAATATCATTTAAACCACCACCG
VWA1_FLAG_KO_val1_F	5'-GAGCTCGAAATTTATTTCAAGCATTTTCTTTTTTTTTCCC

Vwa1 expression

VWA1_OE_NcoI	5'-TACCATGGaTTTAGTAGTATAACAAGTAAATTATCAGC
VWA1_OE_BamHI	5'-TAGGATCCTTAAACTAATGATTTAGCGTTTG
VWA1_vitOE_F	5'-ttGGATCCTTTAGTAGTATAACAAGTAAATTATCAGCAATTTCAGG
VWA1_vitOE_R	5'ACTAGGATCCACTCTTTTGATAAACTTCATCTGGATTAACATTCTTG
VWA1_vwaOE_F	5'-AGGGGATccGAATTTATTTTCTTAATTGATTGTTCTGGTTCAATGAGTGG
VWA1_vwaOE_R	5'-GAAggatccATTTGATGGTATCATTGAATAGATCATCATTCTCTCTTG
VWA1_ctermOE_F	5'-GCAAGGATCCCAAACCAATCAAGATATCATCAATGCC

Vwa1 expression plasmid sequencing

pV3 Sequencing Pimer S	5'-GGTACCAAAAAAATGTCTGATCA
pV3 Sequencing Pimer AS	5'-GAGCTCTGATCATTAGGATCC
Vwa1_OE_seq_F	5'-CAATTACATTATTGTCTTCATCGTTATATGTTCCC
VWA1_OE_seq_R	5'-CGTTTAGTAGCAGTAGATGGGGAGG
VWA1_OE_seq_R2	5'-CACCAATACCATAGGTGAAGATACGAGTTG
VWA1 c_t conf_seq	5'-CATCTTCATCCCAAAAGAAGAAAAAAGAAGTTAGTAG
pVS_bamHI_Val	5'-GGTTTAAATGATATTTTTGAAGCACAAAAAATTGAATGG
pVS_V1vit_conR	5'-CGATGAAGACAATAATGTAATTGACCATCGG

Vwa2 expression

VWA2_OE_NcoI	5'-ACCCATGGaATAAAAAATTTAATTTCAGCATTTTCACAAGG
VWA2_OE_BamHI	5'-ATGGATCCTTATACATTTGATTTTGCAAGTTCTAAAAATTGATC

Vwa2 expression plasmid sequencing

pV3 Sequencing Pimer S	5'-GGTACCAAAAAAATGTCTGATCA
pV3 Sequencing Pimer AS	5'-GAGCTCTGATCATTAGGATCC
VWA2_OE_seq_F	5'-CTATTACATCGTTACTGTTTTCCACAATCGTCA
VWA2_OE_seq_R2	5'-CAGAGACAGCACCATCAGTAAGAATG
VWA2 c_term conf_seq V2	5'-GAACCAACACTTTCAAATGTATCTTTTGATTGGAGTC
VWA2_OE_seq_R	5'-CTGAAGTGGTGAATTAAAATTAACAGCAAAAG

Vwa2 endogenous tagging

endo_pVS 3_	5'-TTATTGTTGTTGTTGTTTTAAAATTTGTTGTTGAGTATATTCCCATATTACAA TTGAACCAGATACATGAACATTTAAAC
endo_pVS c_term	5'-GAGAGTTTCAGCATCCTCACTTGCAG
VWF2 3_c_t	5'-ataatcagatctTACATTTGATTTTGCAAGTTCTA
VWF2 5_c_t	5'-gaggatgctgaaactctcGAACTCGATAATGATATTTCTAATAAC
V2_FG_BSR	5'-cttgcaaaatcaaatgtaAGATCTGATTATAAGGATGATGA
3_BSR V2_non	5'-cttattctcaaaccCTGCAGGAATTAACCATG
5_V2 non_code_b	5'-gttaattcctgcagGGTTTGAGAATAAGAAATATTATTTATC
3_V2 n_c_v	5'-taaaacaacaacaacaacaataaCCAATACCATTACCTGCTG

Vwa2 endogenous tagging confirmation and sequencing

pVS tag C-term seq F	5'-CTTTACGGATGATCCCTGTAATCCGGG
pVS tag C-term seq R	5'-GCTCTGATCATTAGGATCC
VWA2 c_term conf_seq	5'-GCAATGGTAAAAGTACAACTATAATTCAATCACCTACTC
VWA2 3.UTR conf_seq	5'-CATCCAATAATATATTTACTGCAGCTTCAGCCATATC

Fig. 3.17. *Dictyostelium discoideum* Vwa1 master sequence.

http://dictybase.org/gene/DDB_G0292016
https://www.uniprot.org/uniprot/Q54DV3

```
FASTA
>DDB0306747|DDB_G0292016 |DNA coding sequence|gene: DDB_G0292016 on chromosome: 6
position 1027245 to 1030001
TGTGATTATTAAATCTTTTGTAATCTAAAACCTTTTATTTAATAGATAATTTTTTATAAA
AATCTAAAATATTATTAAATATTTTCAATCGATTTTGATCATCGATCATTATTAGATTTT
GGGTCTTTATTTTTATTATTAATTTTTGTTTCTTTTTATTTAATTTAATTTAATATTTAT
TTTATTTTATTTTAAAAGCCAGTGATTTAAAGAAATTATTTCAAAAAAAAAAGATAAAAA
ATTAATAAAAAAAAAAAAAAAACTATATTAACAACTTCATGAAATTAGTAAAGATAAAGG
TTTTTTTCATTGAAAATTTTAATTTTAAATTTTTTTTTATTTTTACTTTCAATTCAAATA
AATCAATTTTATCTAGAAATATTTTTTTAAAAATTATTTTATTTTAATTTGACAAGATAA
AATAATAATAAAAAAAAAAAAAAAAAAAAAAAAAATTATAATTTAATAAAAAAAGAAAA
TAAAAGAAAATTAAATTAAAAAAAATAAAAGAAAATAAAAGAAAAATAAATAGTATAAGA
TAATTCATTAATACTTGAGAGAATGAACAATTGGTTGTTTTTTTTTTTTTTCTCTAAATC
AACAATGATAACAATTTAAAAAAAAAAAAATAAAGAATTTAAAATTTATTTTATTTTGTA
TCTTAATAAATTAATTTAGTATTTTTTTTTTGCTATAAAGAAATTTAAAGATGTAACTAT
CATTTCCAAAAAAATTTGAAAGTATAAACACAATCAAAGAAAAACAATTTTTTTTTTTTT
TTTTTTTTTCAAGGAAATTTTTTCAAAAAATAAAAAATATCTTTTTAATGAGCTCGAAAT
TTATTTCAAGCATTTTCTTTTTTTTTTCCCATCTAATTTTTTATTTAAAATCAAAAATAA
TTTTTTTTTTTTTTTTTTTTATAATCTCATTTTTTTTATTTTTTTTTAAAAACAAATAAA
AAACAAATATATAAATATAAAAAAAAAAAAAAAAAAAAA
5'-taccat
aggTTTAGTAGTATAACAAGTAAATTATCAGC-3'                                    VWA1_OE_NcoI
ATGTTTAGTAGTATAACAAGTAAATTATCAGCAATTTCAGGTGGATCAAGTAAAAATGAT          Dicty domain?
M  F  S  S  I  T  S  K  L  S  A  I  S  G  G  S  S  K  N  D
TATAAAGAAGCAAATTATTATAATTATTTTAGAATTTTAGAAAAGAAACAAACTGAAGAG
Y  K  E  A  N  Y  Y  N  Y  F  R  I  L  E  K  K  Q  T  E  E
ATTGCAAGAAAAAGATGTGGTTTATATAGTTTAAAAAATCATAATAATGTATTTGTTTTA                VIT
I  A  R  K  R  C  G  L  Y  S  L  K  N  H  N  N  V  F  V  L
AAAGAGTTTTCAATTGAAACTGAAATTAATGATTGTAGTTCAACATCAATTTGGACACAA
K  E  F  S  I  E  T  E  I  N  D  C  S  S  T  S  I  W  T  Q
AGCTATTCAAATGATTCAAATACACCAGTCGAGGCAAAGTATCAATTACCATTACATCCA
S  Y  S  N  D  S  N  T  P  V  E  A  K  Y  Q  L  P  L  H  P
ACATCGGTTGTATCAAATTTTCAAATTGAATATCAAGGTAAAGTAATTCAAGGTAAAATC
T  S  V  V  S  N  F  Q  I  E  Y  Q  G  K  V  I  Q  G  K  I
AAAGAGAAAGAGAAAGCATTAGAGAAATACAATGATGCAATTGCAAGTGGTGGTCAAGCA
K  E  K  E  K  A  L  E  K  Y  N  D  A  I  A  S  G  G  Q  A
TTTATGGCAACAAAATCAGATGACGGTTATTTCAATTTAACACTTGGTAATTTACCACCA
F  M  A  T  K  S  D  D  G  Y  F  N  L  T  L  G  N  L  P  P
AAAGAGAATGTTAAAGTTAGAGTTGTAATCTCATCAGAGTTGGGTACACATACCGATGGT
K  E  N  V  K  V  R  V  V  I  S  S  E  L  G  T  H  T  D  G
                        5'-atatgttcccatcttatgcaGGCAGCGGCAGCAGATCT-3'VWA1_KO_FGBSR
                  3'-CGGCGTACCAATTAAGGACGTCacgtaagttaaagttgata
                                                NsiI digest site for truncation insertion
CAATTACATTATTGTCTTCATCGTTATATGTTCCCATCTTATGCATTCAATTTCAACTAT
Q  L  H  Y  C  L  H  R  Y  M  F  P  S  Y  A   F  N  F  N  Y
t-5'
         VWA1_KO_BSR_R
AATGTAGTTTTAAAATTTTCAATTCCAATTAAATCGATTGATTGTGATGGTTTTGATGTA
N  V  V  L  K  F  S  I  P  I  K  S  I  D  C  D  G  F  D  V
AATGTAAATTATAAAGAGAATTCAAGTAAAAAAGAAGCAAAAATCACATCAAAATCACAG
N  V  N  Y  K  E  N  S  S  K  K  E  A  K  I  T  S  K  S  Q
CATACAAGTGGTGTTAAAAAGAATATAATTTTAATTATTCAACCTGTTGAGCTAAATGAA
H  T  S  G  V  K  K  N  I  I  L  I  I  Q  P  V  E  L  N  E
CCAAAATCCATGATTGAATATATTGGTGGTGGCGATGATAAATCTTATGCAACAGCAATT
P  K  S  M  I  E  Y  I  G  G  G  D  D  K  S  Y  A  T  A  I hybrid part 1
               3'-GTTCTTACAATTAGGTCTACTTCAAATAGTTTTCTCACctaggatca-5' VWA1_vitOE_R
```

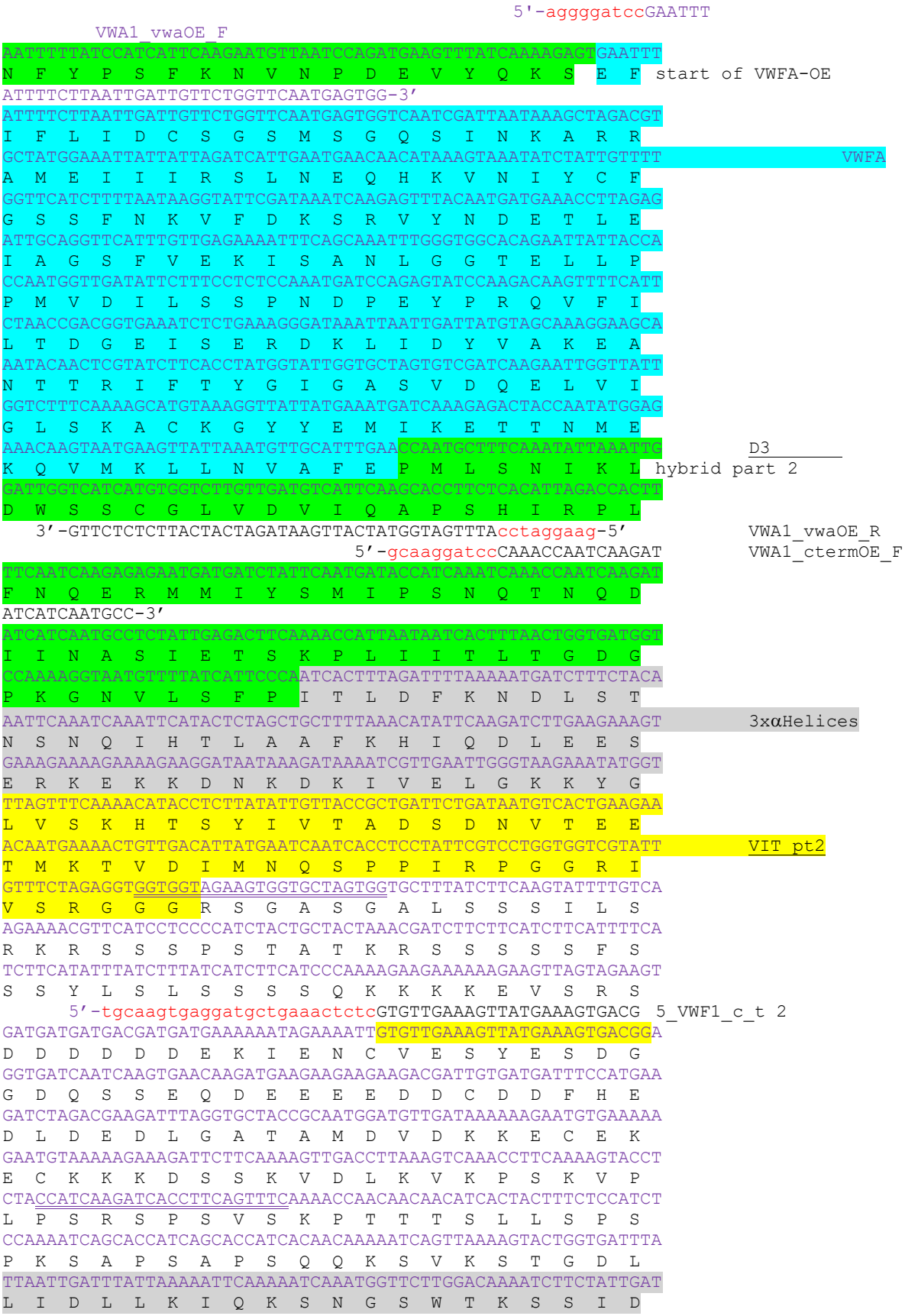
5'-aggggatccGAATTT
VWA1_vwaOE_F
start of VWFA-OE
VWFA
D3
hybrid part 2
VWA1_vwaOE_R
VWA1_ctermOE_F
3xαHelices
VIT pt2
5_VWF1_c_t 2

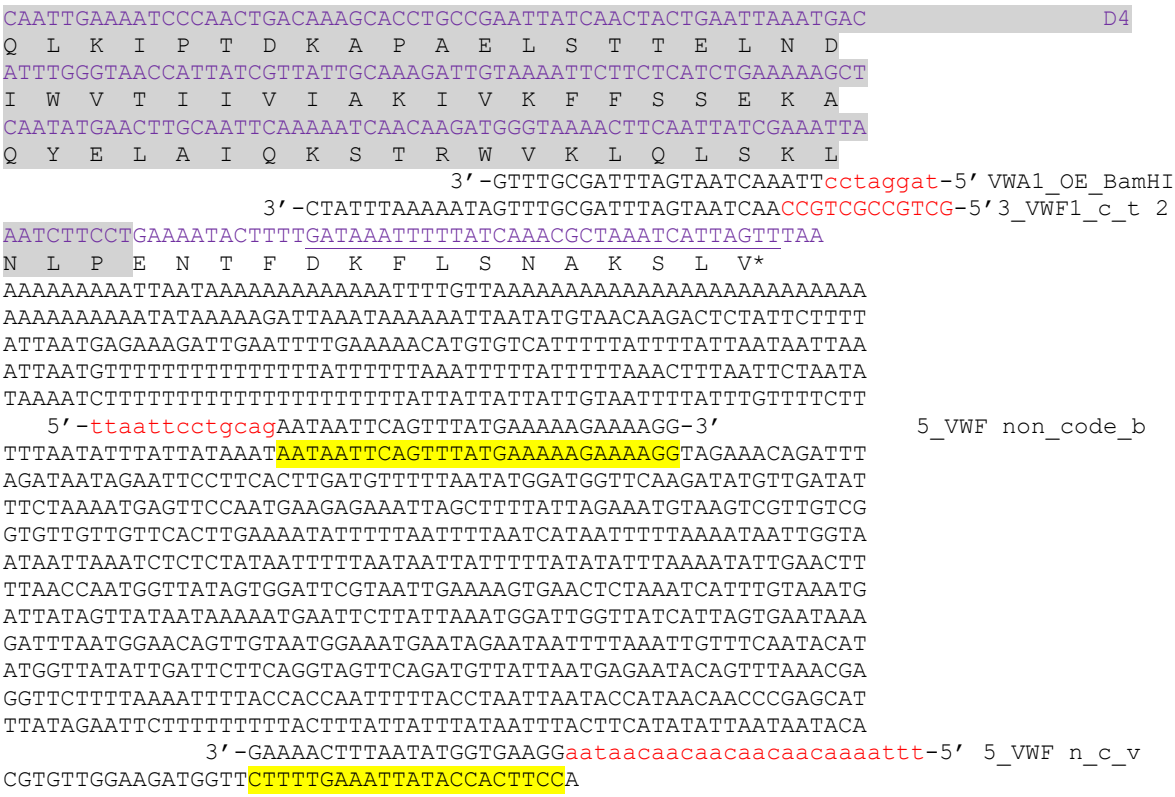
CAATTGAAAATCCCAACTGACAAAGCACCTGCCGAATTATCAACTACTGAATTAAATGAC D4
Q L K I P T D K A P A E L S T T E L N D
ATTTGGGTAACCATTATCGTTATTGCAAAGATTGTAAAATTCTTCTCATCTGAAAAAGCT
I W V T I I V I A K I V K F F S S E K A
CAATATGAACTTGCAATTCAAAAATCAACAAGATGGGTAAAACTTCAATTATCGAAATTA
Q Y E L A I Q K S T R W V K L Q L S K L
3'-GTTTGCGATTTAGTAATCAAATTcctaggat-5' VWA1_OE_BamHI
3'-CTATTTAAAAATAGTTTGCGATTTAGTAATCAACCGTCGCCGTCG-5'3_VWF1_c_t 2
AATCTTCCTGAAAATACTTTTGATAAATTTTTATCAAACGCTAAATCATTAGTTTAA
N L P E N T F D K F L S N A K S L V*
AAAAAAAAATTAATAAAAAAAAAAAAATTTTGTTAAAAAAAAAAAAAAAAAAAAAAAAA
AAAAAAAAAATATAAAAAGATTAAATAAAAAATTAATATGTAACAAGACTCTATTCTTTT
ATTAATGAGAAAGATTGAATTTTGAAAAACATGTGTCATTTTTATTTTATTAATAATTAA
ATTAATGTTTTTTTTTTTTTTTATTTTTTAAATTTTTATTTTTAAACTTTAATTCTAATA
TAAAATCTTTTTTTTTTTTTTTTTTTTTATTATTATTATTGTAATTTTATTTGTTTTCTT
5'-ttaattcctgcagAATAATTCAGTTTATGAAAAAGAAAAGG-3' 5_VWF non_code_b
TTTAATATTTATTATAAATAATAATTCAGTTTATGAAAAAGAAAAGGTAGAAACAGATTT
AGATAATAGAATTCCTTCACTTGATGTTTTTAATATGGATGGTTCAAGATATGTTGATAT
TTCTAAAATGAGTTCCAATGAAGAGAAATTAGCTTTTATTAGAAATGTAAGTCGTTGTCG
GTGTTGTTGTTCACTTGAAAATATTTTTAATTTTAATCATAATTTTTAAAATAATTGGTA
ATAATTAAATCTCTCTATAATTTTTAATAATTATTTTTATATATTTAAAATATTGAACTT
TTAACCAATGGTTATAGTGGATTCGTAATTGAAAAGTGAACTCTAAATCATTTGTAAATG
ATTATAGTTATAATAAAAATGAATTCTTATTAAATGGATTGGTTATCATTAGTGAATAAA
GATTTAATGGAACAGTTGTAATGGAAATGAATAGAATAATTTTAAATTGTTTCAATACAT
ATGGTTATATTGATTCTTCAGGTAGTTCAGATGTTATTAATGAGAATACAGTTTAAACGA
GGTTCTTTTAAAATTTTACCACCAATTTTTACCTAATTAATACCATAACAACCCGAGCAT
TTATAGAATTCTTTTTTTTTACTTTATTATTTATAATTTACTTCATATATTAATAATACA
3'-GAAAACTTTAATATGGTGAAGGaataacaacaacaacaacaaaattt-5' 5_VWF n_c_v
CGTGTTGGAAGATGGTTCTTTTGAAATTATACCACTTCCA

Fig. 3.17. *Dictyostelium discoideum* Vwa1 master sequence. Genomic sequence of Vwa1, DDB_G0292016, with 1000 base pairs of non-coding DNA before and after the ORF. Peptide sequence is aligned to the corresponding codons. Amino acids and DNA are colored to correspond with predicted domains. All primers used for construct generation and gene truncation are aligned to the genomic sequence with base pairs that do not bind colored in red.

Fig. 3.18. *vwa1* and *vwa2* gene tagging strategy and Western blot validation.

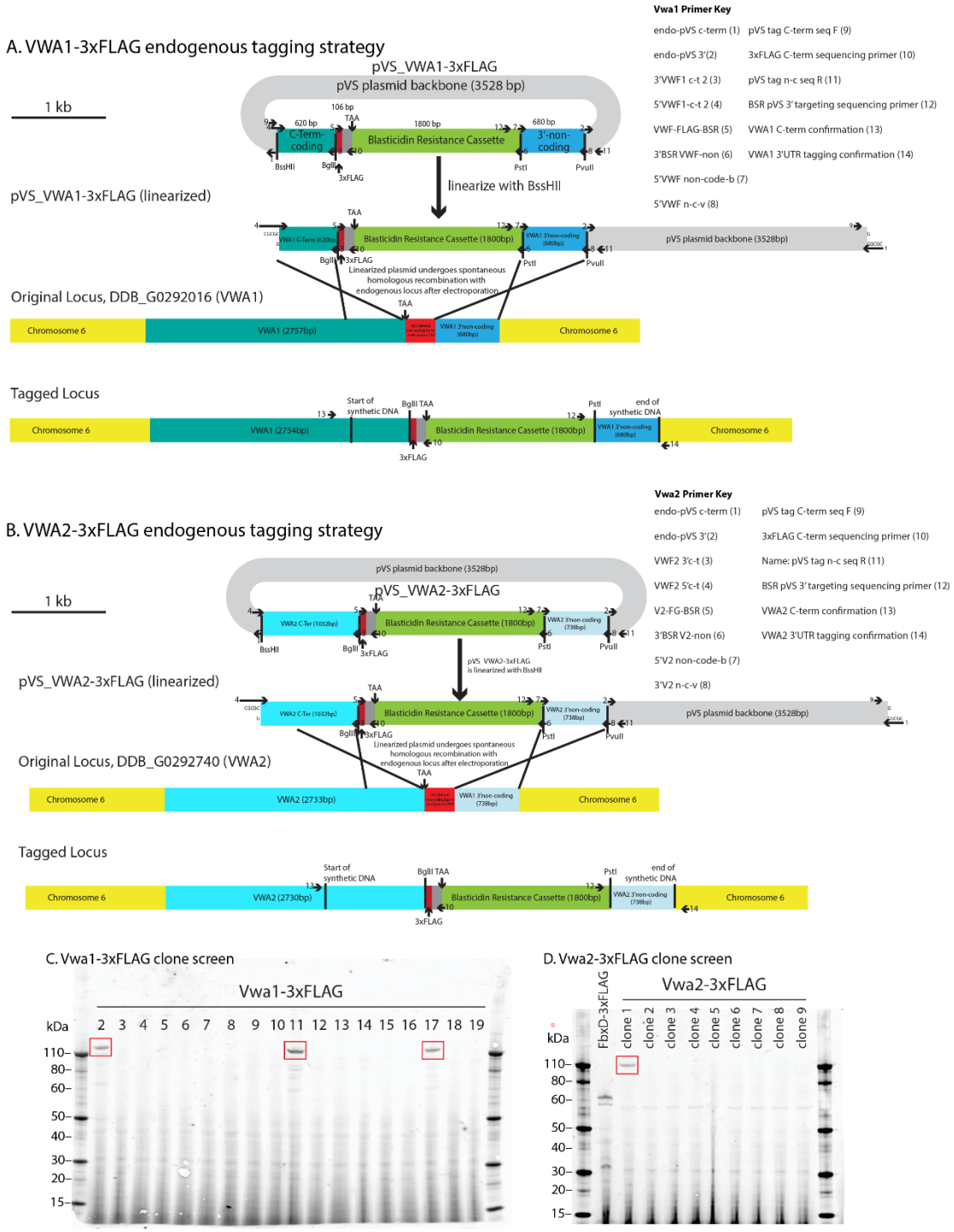

Fig. 3.18. *vwa1* and *vwa2* gene tagging strategy and Western blot validation. Vwa1 (A) and Vwa2 (B) editing plasmids were designed to insert sequences encoding a 3xFLAG/6xHis epitope tag, a stop codon, and blacticidin S deaminase upstream of their native stop codons. The tagging cassettes are flanked by C-terminal coding and 3'-UTR regions to direct spontaneous double cross-over homologous recombination. *C&D*, Western blot screening of transformed clones with anti-FLAG antibody. Positive clones used for experimentation are boxed in red.

Fig. 3.19. Vwa1 truncation strategy.

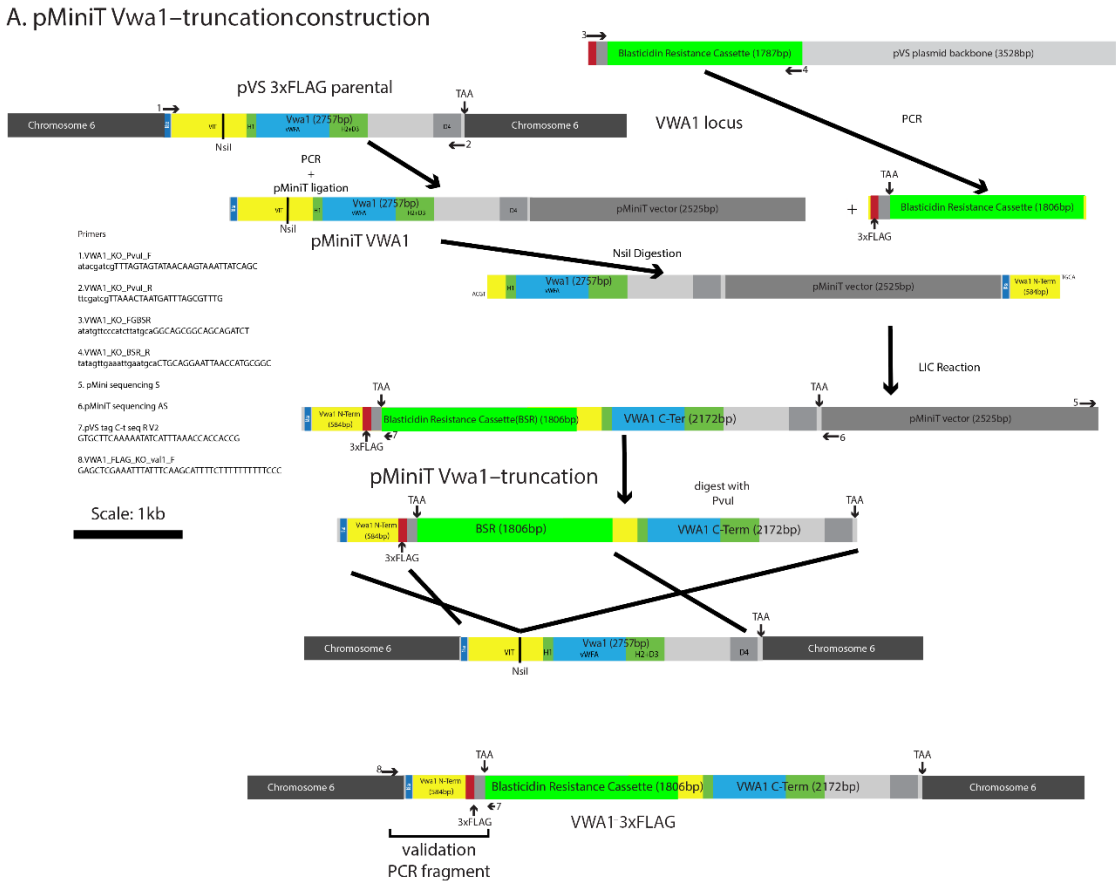

Fig. 3.19. Vwa1 truncation strategy. *A,* An illustrated workflow of the stepwise ligation independent strategy for assembling the double homologous recombination construct for truncating the Vwa1 endogenous locus. Insertion of a blasticidin resistance cassette and artificial stop codons in the VIT domain served to truncate the locus. *B,* DNA gel of PCR validation of insertion into the *Dictyostelium* genome. Note the band at 1 kbp is a nonspecific PCR product and the band for positive truncation of the *vwa1* locus is boxed in red at 883 bp. *C,* Anti-Vwa1 Western blot validation Vwa1 locus disruption.

M2 anti-FLAG antibody (Sigma-Aldrich) (Fig. 3.5, 6, 9, 11, and 13). Strains are listed in Table 3.1.

Filter Lysis and Creation of S100 for vegetative and slug cells

Before lysis, vegetative cells were rinsed twice in 17mM KH_2PO_4 pH 6.5 buffer and pelleted. Slug cells were scraped from nitrocellulose filters and dissociated in dissociation buffer (20mM EDTA and 50 Tris HCl pH 7.4) by pulling the slug cells through a 26-gauge syringe. When slug cells were dissociated from each other, they were rinsed twice in 17mM KH_2PO_4 pH 6.5 buffer and pelleted. After rinsing, cells were suspended in filter lysis buffer (250mM sucrose, 50mM Tris HCl pH 7.4) with leupeptin and aprotinin) and pressed through a 3µm filter to lyse the cells. Lysates were centrifuged at 100,000g for 1 hour to pellet out the insoluble fraction and produce a soluble S100 supernatant. The S100 would then be subsequently used for Western blotting for the levels of soluble proteins such as Vwa1.

Western blotting

Cell lysates and pellets were solubilized in Laemmli Sample Buffer containing 50 mM dithiothreitol and boiled for 5 minutes before running on SDS page gels. Approximately $4x10^5$ vegetative cells and $8x10^5$ slug cells or cell equivalents were loaded in each well in the 1mm 4-12% Bis/Tris NuPage polyacrylamide SDS. Gels were run in MOPS for higher molecular weight separation for approximately 45 minutes at 200V. Blots were transfer to nitrocellulose using iBlot 2 (Invitrogen) dry blotting system for 7min at 10V or 14min at 10V for visualization of higher molecular weight species such as Vwa1. Blots were blocked in 5% (w/v) nonfat dry milk in Tris-buffered saline (TBS) 100 mM NaCl, 50 mM Tris-HCl, pH 7.5, proved overnight with primary antibody diluted in the above-mentioned TBS/milk blocking solution, washed in TBS and then reprobed with Alexa Flour-680.

Densitometry analysis

Western blot band intensities were quantitated by densitometry using NIH ImageJ. Uncalibrated OD was used for the densitometry scale on gray-scale images of blots. Values were corrected by systematic subtraction of an adjacent blank area and normalized to similar densitometric analysis of the same lane (80-100 kDa range) of the Coomassie blue stained gel after blotting.

Immunoprecipitation

For interactome studies, cells were lysed for 15 min on ice in Lysis buffer (250 mM NaCl, 50 mM Tris-HCl (pH 8.0), 0.2% (v/v) NP-40, 10 µg/ml leupeptin, 10 µg/ml aprotinin) at a final concentration of 1.2-1.5 × 10^5 cells/µl for vegetative cells and 2.4×10^5 cells/µl for slugs. Lysates were spun at 21,000 × *g* for 15 min to remove the insoluble material. 10^7 cell equivalents of the supernatant (S21) were added to 5 µl packed volume of M2 anti-FLAG magnetic Sepharose beads (Sigma-Aldrich M8823). Lysate and beads were rotated for 1 hour at 4°C at a rate that kept the beads evenly suspended in the lysate. The beads were collected magnetically, rinsed three times in 20 bead vol of Lysis buffer, three times in detergent-free Lysis buffer, and once more in 20 vol of unbuffered salt solution (250 mM NaCl, 10 µg/ml leupeptin, 10 µg/ml aprotinin). For Western blot analysis, beads were boiled in 10 vol 2% SDS for 5 min. For mass spectrometric analysis, beads were eluted with 10 bead vol of 133 mM triethanolamine for 15 min and neutralized with acetic acid. Samples were dried by vacuum centrifugation and resolubilized in 8M urea in 50 mM Tris-HCl (pH 8.0). The efficiency of IP capture was routinely evaluated by Western blot analysis of the S21, IP supernatant, and eluted fractions.

Mass spectrometric analysis

Dried eluates from were solubilized in 8 M urea, reduced at room temperature with 10 mM dithiothreitol, and alkylated with 50 mM chloroacetamide (74). After addition of 1 µg of endo-LysC/trypsin (Pierce, A40009), the sample was incubated at 22°C for 2 h, and then diluted with the same buffer to a final concentration of 2 M urea for continued overnight digestion.

The peptide samples were amended with heptafluorobutyric acid to a final concentration of 0.1% (v/v) and aspirated 5 times through a pre-equilibrated C18 Zip-Tip (Agilent Bond Elut Omix), which was then rinsed twice with 0.1% heptafluorobutyric acid. Peptides were eluted with 50% (v/v) acetonitrile, 0.1% formic acid, followed by 75% acetonitrile, 0.1% formic acid. The eluants were pooled, dried in a vacuum centrifuge, and dissolved in 5% acetonitrile, 0.05% trifluoroacetic acid.

The peptide solution was loaded onto a C18 trap column (Thermo Acclaim™ PepMap™ 100 C18 series) in a Thermo Fisher UltiMate 3000 nano-HPLC, and eluted from the trap column onto a C18 nano-column (Thermo Acclaim™ PepMap™ 100 C18 series) in a 5%-90% acetonitrile gradient in 0.1% formic acid over 3 h. The eluent was directly introduced via a nano-electrospray source into a Thermo-Fischer Q-Exactive Plus and analyzed by MS and MS/MS. Full MS scans were acquired from *m*/*z* 350 to 2000 at 70,000 resolution. Peptides were selected for fragmentation in the C-trap via higher energy collision-induced dissociation for MS/MS analysis using a Top 10 method and a 30 sec fragmentation exclusion window.

Samples were analyzed in Proteome Discoverer 2.5, using its two step Protein Search method with label free quantification and Consensus workflow with parameters specific to the MS1 and MS2 fragmentation and mass tolerances of the Thermo-Fischer Q Exactive Plus. A

modified *D. discoideum* protein database containing 12,428 unique proteins (73), modified to include a 179-protein exclusion list of common ectopic contaminants (57), was used for peptide identification. Sequest HT search parameters were 10 ppm parent ion mass tolerance, 0.02 Da fragment ion tolerance, and up to 2 missed tryptic cleavages; variable modifications: oxidation of Met, formylation or acetylation of the protein N terminus; fixed modification: carbamidomethylation of Cys. False Discovery Rate (FDR) was determined via Target/Decoy in the Proteome Discoverer processing workflow. Protein identifications were ranked by protein FDR confidence intervals of High (X<1%), Medium (1%<X<5%) and Low (5%<X<10%). Candidates assigned as mitochondrial, ribosomal or secretory proteins (see listing in database referenced below) were filtered as before (25). Protein quantifications were derived from reconstructed ion chromatograms of all peptides assigned to a protein at the MS1 level. Comparisons of protein abundance were done after setting total abundance of each sample within a single analysis equal to the highest value within the experiment in Proteome Discoverer. Normalized abundance values of proteins were analyzed for statistically significant differences between groups using the SimpliFi algorithm (https://simplifi.protifi.com/) (75). Since Simplifi can use nonparametric statistics that assume only that data model themselves, we used this to perform tests on normalized abundances, with 1 added to all spectral counts to avoid zero values, rather than on logarithmic transformations. Proteins whose abundances were >4-fold higher in experimental vs. control samples with a Wilcoxon test p-value <0.01 and a t-test p-value <0.01 were classified as Skp1 interactors. Proteins whose values were ≥1.5-fold higher in *phyA*$^{+}$ vs. *phyA*$^{-}$ samples, with t-test and Wilcoxon test p-values <0.05, were classified as enriched in the *phyA*$^{+}$ Skp1 interactome. The mass spectrometry proteomics data are deposited in the ProteomeXchange

Consortium via the PRIDE (The PRIDE database and related tools and resources in 2019: improving support for quantification data) partner repository with the dataset identifiers for all FbxwD IP's Project accession: PXD035633 and Project DOI: 10.6019/PXD035633 and the identifiers for Vwa1 IP's Project accession: PXD035634 and Project DOI: 10.6019/PXD035634.

Generation of Vwa1 anti-sera

$7x10^{10}$ *Dictyostelium* expressing Vwa1-3xFLAG-6xHis on the discoidin promotor were lysed by passing cells suspended in 50 mM Tris, pH 7.4, 0.25 M sucrose, 10µg/ml aprotinin and leupeptin through 5µm nitrocellulose filters. Lysate was then spun at 3000g and 100,000g to produce an S100 soluble fraction. This fraction was loaded and eluted off a 200ml DEAE column using a salt gradient. Fractions containing intact Vwa1 were subsequently purified on a 1ml His-trap with stepwise imidazole elution. The purified Vwa1 was concentrated using spin columns and 1.2-1.5mg of purified protein was run on a gradient slab gel. After coomassie staining, the Vwa1 band was excised and detained. The detained gel slice was sent to Cocalico Biologicals, Inc. where it was used to immunized two rabbits with one initial dose and two boosters. Pre-bleeds, post-boost, and exsanguination bleeds were screen against lysates of Ax3, Vwa1-trunc, Vwa1-OE, Vwa2-OE cells to determine that the anti-sera were specific to Vwa1. Exsang. sera 161 and 162 were used to visualize Vwa1 in slug and vegetative cells respectively due to different properties of the background (Fig. 3.4).

Alignment and tree building

Boundaries of the VIT, vWFA, AND D3 for Vwa1 and Vwa2 (see Fig. 3.2, 3) were based on sequence conservation with the ITIH1 crystal structure (35) that clearly defines the unique structural components of the VIT β-sandwich, vWFA Rossman fold, and D3 β-sheet (Fig. 3.17).

The less thoroughly conserved D4 was determined through sequence homology. The vWFA and vWFA domains were BLASTed to find orthologous proteins with the default expect threshold of <0.05. VIT domain alone was not used for homology searches as all VIT domains were found were accompanied by a C-terminal vWFA domain. For the vWFA only tree, representative vWFA domains from distantly related (expect >0.05) representative proteins such as von Willebrand Factor were added to the alignment to provide an outgroup for the ITIH/VWA5A like proteins. All preliminary alignments were done with a Global alignment with a PAM250 cost matrix in Geneious Prime 2019.1.3 with the following penalties Gap open penalty of 20, Gap extension penalty of 10. Extensive manual refinement of alignment was done to improve quality and accuracy. The trees were assembled using the previously mentioned alignment with the UPGMA tree building method and 1000 bootstrapping iterations and no %bootstrap cutoff. Tree files were exported as .newick files and visualized in iTOL (76). Branches with less than 25% bootstrap support were collapsed for the vWFA tree and a 50% bootstrap support cutoff was used for the VIT+vWFA tree as the sequences included were inherently more closely related.

Model Generation

AlphaFold model, PRO_0000389207, (42,43) was used to generate the model of full length Vwa1. Domains were colored according to homology with Hs ITIH1in PyMOL v2.0.

Chapter 3 References

1. Willems, A. R., Schwab, M., and Tyers, M. (2004) A hitchhiker's guide to the cullin ubiquitin ligases: SCF and its kin. *Biochim Biophys Acta* **1695**, 133-170
2. Harper, J. W., and Schulman, B. A. (2021) Cullin-RING Ubiquitin Ligase Regulatory Circuits: A Quarter Century Beyond the F-Box Hypothesis. *Annu Rev Biochem* **90**, 403-429
3. Skaar, J. R., Pagan, J. K., and Pagano, M. (2013) Mechanisms and function of substrate recruitment by F-box proteins. *Nat Rev Mol Cell Biol* **14**, 369-381
4. Baldauf, S. L., and Doolittle, W. F. (1997) Origin and evolution of the slime molds (Mycetozoa). *Proceedings of the National Academy of Sciences* **94**, 12007
5. Xu, Y., Wang, Z. A., Green, R. S., and West, C. M. (2012) Role of the Skp1 prolyl-hydroxylation/glycosylation pathway in oxygen dependent submerged development of Dictyostelium. *BMC Developmental Biology* **12**, 31-31
6. West, C. M., and Blader, I. J. (2015) Oxygen Sensing by Protozoans: How They Catch Their Breath. *Current opinion in microbiology* **26**, 41-47
7. Mohanty, S., Lee, S., Yadava, N., Dealy, M. J., Johnson, R. S., and Firtel, R. A. (2001) Regulated protein degradation controls PKA function and cell-type differentiation in Dictyostelium. *Genes Dev* **15**, 1435-1448
8. Bonner, J. T., and Lamont, D. S. (2005) Behavior of cellular slime molds in the soil. *Mycologia* **97**, 178-184
9. Rosengarten, R. D., Santhanam, B., Fuller, D., Katoh-Kurasawa, M., Loomis, W. F., Zupan, B., and Shaulsky, G. (2015) Leaps and lulls in the developmental transcriptome of Dictyostelium discoideum. *BMC Genomics* **16**, 294
10. Santhanam, B., Cai, H., Devreotes, P. N., Shaulsky, G., and Katoh-Kurasawa, M. (2015) The GATA transcription factor GtaC regulates early developmental gene expression dynamics in Dictyostelium. *Nature Communications* **6**, 7551
11. Palecek, S. P., Parikh, A. S., and Kron, S. J. (2000) Genetic analysis reveals that FLO11 upregulation and cell polarization independently regulate invasive growth in Saccharomyces cerevisiae. *Genetics* **156**, 1005-1023
12. Bakthavatsalam, D., and Gomer, R. H. (2010) The secreted proteome profile of developing Dictyostelium discoideum cells. *Proteomics* **10**, 2556-2559
13. Czarna, M., Mathy, G., Mac'Cord, A., Dobson, R., Jarmuszkiewicz, W., Sluse-Goffart, C. M., Leprince, P., De Pauw, E., and Sluse, F. E. (2010) Dynamics of the Dictyostelium discoideum mitochondrial proteome during vegetative growth, starvation and early stages of development. *Proteomics* **10**, 6-22
14. Journet, A., Klein, G., Brugière, S., Vandenbrouck, Y., Chapel, A., Kieffer, S., Bruley, C., Masselon, C., and Aubry, L. (2012) Investigating the macropinocytic proteome of Dictyostelium amoebae by high-resolution mass spectrometry. *Proteomics* **12**, 241-245
15. Wang, Z. A., van der Wel, H., Vohra, Y., Buskas, T., Boons, G. J., and West, C. M. (2009) Role of a cytoplasmic dual-function glycosyltransferase in O2 regulation of development in Dictyostelium. *J Biol Chem* **284**, 28896-28904

16. Schafer, C. M., Sheikh, M. O., Zhang, D., and West, C. M. (2014) Novel Regulation of Skp1 by the Dictyostelium AgtA α-Galactosyltransferase Involves the Skp1-binding Activity of Its WD40 Repeat Domain*. *Journal of Biological Chemistry* **289**, 9076-9088
17. Ennis, H. L., Dao, D. N., Pukatzki, S. U., and Kessin, R. H. (2000) Dictyostelium amoebae lacking an F-box protein form spores rather than stalk in chimeras with wild type. *Proc Natl Acad Sci U S A* **97**, 3292-3297
18. Teng-umnuay, P., Morris, H. R., Dell, A., Panico, M., Paxton, T., and West, C. M. (1998) The cytoplasmic F-box binding protein SKP1 contains a novel pentasaccharide linked to hydroxyproline in Dictyostelium. *J Biol Chem* **273**, 18242-18249
19. West, C. M., van der Wel, H., and Wang, Z. A. (2007) Prolyl 4-hydroxylase-1 mediates O2 signaling during development of Dictyostelium. *Development* **134**, 3349-3358
20. Boland, A., Gas-Pascual, E., Nottingham, B., van der Wel, H., Sheikh, M. O., Schafer, C. M., and West, C. M. (2022) Oxygen-dependent regulation of E3(SCF)ubiquitin ligases and a Skp1-associated JmjD6 homolog in Dictyostelium development. *Journal of Biological Chemistry*
21. Sheikh, M. O., Xu, Y., van der Wel, H., Walden, P., Hartson, S. D., and West, C. M. (2015) Glycosylation of Skp1 promotes formation of Skp1-Cullin-1-F-box protein complexes in Dictyostelium. *Mol Cell Proteomics* **14**, 66-80
22. Xu, Y., Brown, K. M., Wang, Z. A., van der Wel, H., Teygong, C., Zhang, D., Blader, I. J., and West, C. M. (2012) The Skp1 protein from Toxoplasma is modified by a cytoplasmic prolyl 4-hydroxylase associated with oxygen sensing in the social amoeba Dictyostelium. *J Biol Chem* **287**, 25098-25110
23. Rahman, K., Zhao, P., Mandalasi, M., van der Wel, H., Wells, L., Blader, I. J., and West, C. M. (2016) The E3 Ubiquitin Ligase Adaptor Protein Skp1 Is Glycosylated by an Evolutionarily Conserved Pathway That Regulates Protist Growth and Development. *J Biol Chem* **291**, 4268-4280
24. van der Wel, H., Gas-Pascual, E., and West, C. M. (2019) Skp1 isoforms are differentially modified by a dual function prolyl 4-hydroxylase/N-acety lglucosaminyltransferase in a plant pathogen. *Glycobiology* **29**, 705-714
25. Kuroda, H., Takahashi, N., Shimada, H., Seki, M., Shinozaki, K., and Matsui, M. (2002) Classification and Expression Analysis of Arabidopsis F-Box-Containing Protein Genes. *Plant and Cell Physiology* **43**, 1073-1085
26. Zielke, N., Querings, S., Grosskortenhaus, R., Reis, T., and Sprenger, F. (2006) Molecular dissection of the APC/C inhibitor Rca1 shows a novel F-box-dependent function. *EMBO Rep* **7**, 1266-1272
27. Cenciarelli, C., Chiaur, D. S., Guardavaccaro, D., Parks, W., Vidal, M., and Pagano, M. (1999) Identification of a family of human F-box proteins. *Curr Biol* **9**, 1177-1179
28. Himmelfarb, M., Klopocki, E., Grube, S., Staub, E., Klaman, I., Hinzmann, B., Kristiansen, G., Rosenthal, A., Durst, M., and Dahl, E. (2004) ITIH5, a novel member of the inter-alpha-trypsin inhibitor heavy chain family is downregulated in breast cancer. *Cancer Lett* **204**, 69-77
29. Zhuo, L., Hascall, V. C., and Kimata, K. (2004) Inter-α-trypsin Inhibitor, a Covalent Protein-Glycosaminoglycan-Protein Complex*. *Journal of Biological Chemistry* **279**, 38079-38082

30. Perina, D., Mikoč, A., Ahel, J., Ćetković, H., Žaja, R., and Ahel, I. (2014) Distribution of protein poly(ADP-ribosyl)ation systems across all domains of life. *DNA Repair (Amst)* **23**, 4-16
31. van Zon, A., Mossink, M. H., Schoester, M., Scheffer, G. L., Scheper, R. J., Sonneveld, P., and Wiemer, E. A. C. (2002) Structural Domains of Vault Proteins: A Role for the Coiled Coil Domain in Vault Assembly. *Biochemical and Biophysical Research Communications* **291**, 535-541
32. Martin, E. S., Cesari, R., Pentimalli, F., Yoder, K., Fishel, R., Himelstein, A. L., Martin, S. E., Godwin, A. K., Negrini, M., and Croce, C. M. (2003) The BCSC-1 locus at chromosome 11q23-q24 is a candidate tumor suppressor gene. *Proceedings of the National Academy of Sciences of the United States of America* **100**, 11517-11522
33. Anghel, S. I., Correa-Rocha, R., Budinska, E., Boligan, K. F., Abraham, S., Colombetti, S., Fontao, L., Mariotti, A., Rimoldi, D., Ghanem, G. E., Fisher, D. E., Lévy, F., Delorenzi, M., and Piguet, V. (2012) Breast cancer suppressor candidate-1 (BCSC-1) is a melanoma tumor suppressor that down regulates MITF. *Pigment Cell Melanoma Res* **25**, 482-487
34. Di, D., Chen, L., Guo, Y., Wang, L., Wang, H., and Ju, J. (2018) Association of BCSC-1 and MMP-14 with human breast cancer. *Oncol Lett* **15**, 5020-5026
35. Briggs, D. C., Langford-Smith, A. W. W., Birchenough, H. L., Jowitt, T. A., Kielty, C. M., Enghild, J. J., Baldock, C., Milner, C. M., and Day, A. J. (2020) Inter-α-inhibitor heavy chain-1 has an integrin-like 3D structure mediating immune regulatory activities and matrix stabilization during ovulation. *J Biol Chem* **295**, 5278-5291
36. Szabo, A., Akkouh, I. A., Vandenberghe, M., Osete, J. R., Hughes, T., Heine, V., Smeland, O. B., Glover, J. C., Andreassen, O. A., and Djurovic, S. (2021) A human iPSC-astroglia neurodevelopmental model reveals divergent transcriptomic patterns in schizophrenia. *Translational Psychiatry* **11**, 554
37. Kamura, T., Maenaka, K., Kotoshiba, S., Matsumoto, M., Kohda, D., Conaway, R. C., Conaway, J. W., and Nakayama, K. I. (2004) VHL-box and SOCS-box domains determine binding specificity for Cul2-Rbx1 and Cul5-Rbx2 modules of ubiquitin ligases. *Genes Dev* **18**, 3055-3065
38. Nishiya, T., Matsumoto, K., Maekawa, S., Kajita, E., Horinouchi, T., Fujimuro, M., Ogasawara, K., Uehara, T., and Miwa, S. (2011) Regulation of inducible nitric-oxide synthase by the SPRY domain- and SOCS box-containing proteins. *J Biol Chem* **286**, 9009-9019
39. Linossi, E. M., and Nicholson, S. E. (2012) The SOCS box-adapting proteins for ubiquitination and proteasomal degradation. *IUBMB Life* **64**, 316-323
40. Jones, P., Binns, D., Chang, H. Y., Fraser, M., Li, W., McAnulla, C., McWilliam, H., Maslen, J., Mitchell, A., Nuka, G., Pesseat, S., Quinn, A. F., Sangrador-Vegas, A., Scheremetjew, M., Yong, S. Y., Lopez, R., and Hunter, S. (2014) InterProScan 5: genome-scale protein function classification. *Bioinformatics* **30**, 1236-1240
41. Blum, M., Chang, H. Y., Chuguransky, S., Grego, T., Kandasaamy, S., Mitchell, A., Nuka, G., Paysan-Lafosse, T., Qureshi, M., Raj, S., Richardson, L., Salazar, G. A., Williams, L., Bork, P., Bridge, A., Gough, J., Haft, D. H., Letunic, I., Marchler-Bauer, A., Mi, H., Natale, D. A., Necci, M., Orengo, C. A., Pandurangan, A. P., Rivoire, C., Sigrist, C. J. A., Sillitoe, I., Thanki, N., Thomas, P. D., Tosatto, S. C. E., Wu, C. H., Bateman, A., and Finn, R. D. (2021)

The InterPro protein families and domains database: 20 years on. *Nucleic Acids Res* **49**, D344-d354
42. Tan, M. K., Lim, H. J., Bennett, E. J., Shi, Y., and Harper, J. W. (2013) Parallel SCF adaptor capture proteomics reveals a role for SCFFBXL17 in NRF2 activation via BACH1 repressor turnover. *Mol Cell* **52**, 9-24
43. Stajdohar M, J. L., Kokosar J, Blenkus D, Janez T, Kuspa A, Shaulsky G, Zupan B. (2015) dictyExpress: visual analytics of NGS gene expression in Dictyostelium.
44. Parikh, A., Miranda, E. R., Katoh-Kurasawa, M., Fuller, D., Rot, G., Zagar, L., Curk, T., Sucgang, R., Chen, R., Zupan, B., Loomis, W. F., Kuspa, A., and Shaulsky, G. (2010) Conserved developmental transcriptomes in evolutionarily divergent species. *Genome Biology* **11**, R35
45. Kosztyu, P., Slaninová, I., Valčíková, B., Verlande, A., Müller, P., Paleček, J. J., and Uldrijan, S. (2019) A Single Conserved Amino Acid Residue as a Critical Context-Specific Determinant of the Differential Ability of Mdm2 and MdmX RING Domains to Dimerize. *Front Physiol* **10**, 390
46. Deshaies, R. J., and Joazeiro, C. A. P. (2009) RING Domain E3 Ubiquitin Ligases. *Annual Review of Biochemistry* **78**, 399-434
47. Zheng, N., Wang, P., Jeffrey, P. D., and Pavletich, N. P. (2000) Structure of a c-Cbl-UbcH7 complex: RING domain function in ubiquitin-protein ligases. *Cell* **102**, 533-539
48. Garcia-Barcena, C., Osinalde, N., Ramirez, J., and Mayor, U. (2020) How to Inactivate Human Ubiquitin E3 Ligases by Mutation. *Front Cell Dev Biol* **8**, 39
49. Fey, P., Dodson, R. J., Basu, S., Hartline, E. C., and Chisholm, R. L. (2019) dictyBase and the Dicty Stock Center (version 2.0) - a progress report. *Int J Dev Biol* **63**, 563-572
50. Gruenheit, N., Baldwin, A., Stewart, B., Jaques, S., Keller, T., Parkinson, K., Salvidge, W., Baines, R., Brimson, C., Wolf, J. B., Chisholm, R., Harwood, A. J., and Thompson, C. R. L. (2021) Mutant resources for functional genomics in Dictyostelium discoideum using REMI-seq technology. *BMC Biology* **19**, 172
51. Coordinators, N. R. (2016) Database resources of the National Center for Biotechnology Information. *Nucleic acids research* **44**, D7-D19
52. Whittaker, C. A., and Hynes, R. O. (2002) Distribution and Evolution of von Willebrand/Integrin A Domains: Widely Dispersed Domains with Roles in Cell Adhesion and Elsewhere. *Molecular Biology of the Cell* **13**, 3369-3387
53. Jumper, J., Evans, R., Pritzel, A., Green, T., Figurnov, M., Ronneberger, O., Tunyasuvunakool, K., Bates, R., Žídek, A., Potapenko, A., Bridgland, A., Meyer, C., Kohl, S. A. A., Ballard, A. J., Cowie, A., Romera-Paredes, B., Nikolov, S., Jain, R., Adler, J., Back, T., Petersen, S., Reiman, D., Clancy, E., Zielinski, M., Steinegger, M., Pacholska, M., Berghammer, T., Bodenstein, S., Silver, D., Vinyals, O., Senior, A. W., Kavukcuoglu, K., Kohli, P., and Hassabis, D. (2021) Highly accurate protein structure prediction with AlphaFold. *Nature* **596**, 583-589
54. Varadi, M., Anyango, S., Deshpande, M., Nair, S., Natassia, C., Yordanova, G., Yuan, D., Stroe, O., Wood, G., Laydon, A., Žídek, A., Green, T., Tunyasuvunakool, K., Petersen, S., Jumper, J., Clancy, E., Green, R., Vora, A., Lutfi, M., Figurnov, M., Cowie, A., Hobbs, N., Kohli, P., Kleywegt, G., Birney, E., Hassabis, D., and Velankar, S. (2021) AlphaFold Protein

Structure Database: massively expanding the structural coverage of protein-sequence space with high-accuracy models. *Nucleic Acids Research* **50**, D439-D444
55. Betapudi, V., and Egelhoff, T. T. (2009) Roles of an unconventional protein kinase and myosin II in amoeba osmotic shock responses. *Traffic* **10**, 1773-1784
56. Wang, K., Deshaies, R. J., and Liu, X. (2020) Assembly and Regulation of CRL Ubiquitin Ligases. *Adv Exp Med Biol* **1217**, 33-46
57. Hao, B., Zheng, N., Schulman, B. A., Wu, G., Miller, J. J., Pagano, M., and Pavletich, N. P. (2005) Structural basis of the Cks1-dependent recognition of p27(Kip1) by the SCF(Skp2) ubiquitin ligase. *Mol Cell* **20**, 9-19
58. Correia, S. P., Chan, A. B., Vaughan, M., Zolboot, N., Perea, V., Huber, A.-L., Kriebs, A., Moresco, J. J., Yates, J. R., and Lamia, K. A. (2019) The circadian E3 ligase complex SCFFBXL3+CRY targets TLK2. *Scientific Reports* **9**, 198
59. Wang, W., and Kirschner, M. W. (2013) Emi1 preferentially inhibits ubiquitin chain elongation by the anaphase-promoting complex. *Nat Cell Biol* **15**, 797-806
60. Salier, J. P., Rouet, P., Raguenez, G., and Daveau, M. (1996) The inter-alpha-inhibitor family: from structure to regulation. *Biochem J* **315 (Pt 1)**, 1-9
61. Rine, J., Hansen, W., Hardeman, E., and Davis, R. W. (1983) Targeted selection of recombinant clones through gene dosage effects. *Proc Natl Acad Sci U S A* **80**, 6750-6754
62. Herskowitz, I. (1987) Functional inactivation of genes by dominant negative mutations. *Nature* **329**, 219-222
63. Springer, T. A. (2006) Complement and the Multifaceted Functions of VWA and Integrin I Domains. *Structure* **14**, 1611-1616
64. Mateu, M. G., Valero, M. L., Andreu, D., and Domingo, E. (1996) Systematic replacement of amino acid residues within an Arg-Gly-Asp-containing loop of foot-and-mouth disease virus and effect on cell recognition. *J Biol Chem* **271**, 12814-12819
65. Berry, K. N., and Brett, T. J. (2020) Structural and Biophysical Analysis of the CLCA1 VWA Domain Suggests Mode of TMEM16A Engagement. *Cell Rep* **30**, 1141-1151.e1143
66. Luo, B.-H., Carman, C. V., and Springer, T. A. (2007) Structural Basis of Integrin Regulation and Signaling. *Annual Review of Immunology* **25**, 619-647
67. Pearson, M. A., Reczek, D., Bretscher, A., and Karplus, P. A. (2000) Structure of the ERM Protein Moesin Reveals the FERM Domain Fold Masked by an Extended Actin Binding Tail Domain. *Cell* **101**, 259-270
68. Simaan, H., Lev, S., and Horwitz, B. A. (2019) Oxidant-Sensing Pathways in the Responses of Fungal Pathogens to Chemical Stress Signals. *Frontiers in Microbiology* **10**
69. Niggli, V., and Rossy, J. (2008) Ezrin/radixin/moesin: Versatile controllers of signaling molecules and of the cortical cytoskeleton. *The International Journal of Biochemistry & Cell Biology* **40**, 344-349
70. West, C. (2003) Comparative analysis of spore coat Formation, structure, and function in Dictyostelium. *International review of cytology* **222**, 237-293
71. Alexander, S., Srinivasan, S., and Alexander, H. (2003) Proteomics opens doors to the mechanisms of developmentally regulated secretion. *Mol Cell Proteomics* **2**, 1156-1163
72. Ashworth, J. M., and Watts, D. J. (1970) Metabolism of the cellular slime mould Dictyostelium discoideum grown in axenic culture. *Biochem J* **119**, 175-182

73. Pang, K. M., Lynes, M. A., and Knecht, D. A. (1999) Variables controlling the expression level of exogenous genes in Dictyostelium. *Plasmid* **41**, 187-197
74. Hains, P. G., and Robinson, P. J. (2017) The Impact of Commonly Used Alkylating Agents on Artifactual Peptide Modification. *J Proteome Res* **16**, 3443-3447
75. Wilson, J., Palmeri, J., and Pappin, D. (2020) SimpliFi: a data-to-meaning analytics engine to bring omics understanding to all. *J Biomol Tech* **31**, S1-S2
76. Letunic, I., and Bork, P. (2021) Interactive Tree Of Life (iTOL) v5: an online tool for phylogenetic tree display and annotation. *Nucleic Acids Research* **49**, W293-W296
77. Early, A. E., Gaskell, M. J., Traynor, D., and Williams, J. G. (1993) Two distinct populations of prestalk cells within the tip of the migratory Dictyostelium slug with differing fates at culmination. *Development* **118**, 353-362
78. Rose, M., Huth, S., Wiesehöfer, M., Ehling, J., Henkel, C., Steitz, J., Lammers, T., Kistermann, J., Klaas, O., Koch, M., Rushrush, S., Knüchel, R., and Dahl, E. (2022) ITIH5-Derived Polypeptides Covering the VIT Domain Suppress the Growth of Human Cancer Cells In Vitro. *Cancers (Basel)* **14**

CHAPTER 4

FUTURE DIRECTIONS

The previous chapters have expanded our knowledge of *Dictyostelium*'s Skp1 interactome and increased our understanding of an important FbxwD interacting protein, Vwa1. Here, I propose additional experiments to elucidate the effects of the Skp1 glycan on *Dictyostelium*'s proteome and to more thoroughly characterize Vwa1's physical properties and its role interacting with FbxwD.

PhyA's and Skp1 glycosylation's role in sculpting the proteome of Dictyostelium

Concerted protein degradation is of elevated importance during the rapid differentiation from vegetative cells to specialized spore and stalk cells. It is here during strong pressure for proteomic remodeling, any disruption in the UPS would most likely manifest phenotypically. This is when many SCF/UPS mutations themselves such as *phyA*$^{-}$ (94), *fbxA*$^{-}$ (29), and the delayed development and abnormal fruiting bodies of *culE-3xFLAG* manifest morphologically. How exactly does the *phyA*$^{-}$ disrupt the proteome of developing cells?

Within the scope of our investigation, Skp1 glycosylation enhances levels of interaction with a number of proteins predominantly with F-box character. On top of that reciprocal co-immunoprecipitations of two FBPs confirmed that their interaction with Skp1 is enhanced in the presence of the glycan. We hypothesize that most if not all Skp1-FBP interactions are stabilized by the glycosylation of Skp1. Despite this, evidence does not suggest that SCF activity is enhanced by the presence of the glycan as based on side-by-side comparisons of K-48 linked ubiquitin blots before and after proteasome inhibitor treatments. It could serve to reinforce self-regulation of

FBPs. Previous publications have demonstrated that in absence of substrates, SCF complexed FBPs may be subsequently auto-ubiquitinated and degraded via the proteasome (95). The Skp1 glycan's ability to stabilize these SCF assemblies may increase that efficiency of this self-regulatory mechanism. In the case of JcdI where the SCF appears to be a source of its degradation, the glycan could serve to increase the efficiency of this FBP level regulation. In slug cells there is evidence that it may be taking place as JcdI levels are significantly reduced when Skp1 is glycosylated.

Emerging research is elucidating novel mechanisms by which the SCF is assembled to meet the needs of the cells such as the competitive relationship between CAND1 and NEDD8 (9,96). It can be inferred from observed differences in *Dictyostelium's* Skp1 interactomes between life stages in Chapter 2 that assemblies are regulated between life stages via cryptic mechanisms beyond transcription. With the weakened Skp1-F-box protein interface in unmodified Skp1, it is possible that this system of SCF assembly may be dysregulated with F-box proteins. A weakened interface could result in spontaneous dissociation and reassociation of Skp1 and FBPs. This would result in aberrant turnover of proteins necessary for the slugs to culminate and successfully sporulate. This hypothesis of dysregulated protein turnover is supported by the evidence that the proteasome inhibitors delayed but ultimately rescued the development of *phyA*$^{-}$ cells.

To test the above-mentioned hypotheses that *phyA*$^{-}$ results in dysregulated FBP turnover or Skp1-FBP interactions at ambient oxygen akin to low oxygen signaling, several fundamental questions must be asked. What is the effect of PhyA on the ubiquitinome/proteome of the cell?

What FBP substrates contribute to culmination and sporulation? Does SKp1 glycosylation prevent exchange of F-box proteins?

Characterization of the phyA$^+$ and phyA$^-$ interactomes

Investigation of the ubiquitinome of *Dictyostelium* can be done via immunoprecipitation and LC MS/MS using the PTMScan® Ubiquitin Remnant Motif (K-ε-GG) Kit #5562. This kit's antibodies recognize the di-glycine PTM indicative of ubiquitination on peptides post trypsin digest and the protocol avoids exposing the ubiquitinated proteins to fast acting de-ubiquitinates (DUBs) by lysing cells in denaturing urea concentrations. An optimized protocol from the Seyfried lab at Emory titled 'Digly Ubiquitin Enrichment Protocol Abreha.docx' contains details on how to execute this experiment successfully (97). The protocol elaborates on the manufacture's methods with an emphasis on lyophilization per instructions for workable levels of peptide recovery. We hypothesize that di-Gly immunoprecipitations will provide a list of proteins that are significantly different between *phyA*$^+$ and *phyA*$^-$ cells though little difference in total abundances of ubiquitinated peptides recovered. It is hypothesized that the variation between the two genetic backgrounds will come down to a number of specific proteins affected by modified Skp1. K48 ubiquitination via the SCF only represents a fraction of the ubiquitination that takes place for degradation, signaling etc. Proteasome inhibitor treatments such as 1 µM Bortezomib or 80 µM MG132 pre lysis will help enrich for these K48-ubiquitinated proteins. While not all factors that contribute to development are characterized, several proteins and their effectors are well known and one or more direct or indirect effectors may be identified as ubiquitinated at higher levels in the *phyA*$^-$ background. Excessive ubiquitination and degradation of a promotor of fruiting would explain the *phyA*$^-$ mutant phenotype and the ability to rescue the mutant with proteasome

inhibitor. Additionally, this study would be of value as the first snapshots of *Dictyostelium*'s ubiquitinome.

BioID for F-box protein substrate identification

Analysis of the ubiquitinome may yield SCF substrates affected by PhyA agnostic of the F-box protein by which they are targeted. To fully understand the role of PhyA and Skp1 glycosylation, the role of affected FBP's must be elucidated. Up to this point, true substrates for two developmentally relevant substrate receptor type FBPs, FbxwD and FbxA, have remained elusive with eh exception of RegA (98). Traditional immunoprecipitation of tagged constructs and of tagged constructs with ubiquitin trapping constructs (99) failed to yield confident candidate substrates but tag interference was an uncertainty. This may also be due to the transient nature of FPB-substrate interactions. Traditional IP lacks the ability to preserve and observe transient interactions through the strenuous lysis, incubation, and washes. BioID addresses these problems through proximity labeling using a promiscuous biotin ligase attached to the protein of interest. Treatment of transiently transfected cells with excess biotin activates the biotin-ligase which proceeds to label proteins within a 10 nm radius of the tagged protein of interest (100,101). The FBPs of interest could be tagged endogenously or for lower abundance candidates, over-expressed with a *Dictyostelium* codon optimized BioID or BioID2 tag. The location of the tag/BioID would need to be evaluated based on the structure of the FBP of interest. This would allow for induced proximity labeling of proteins around the FBP and presumably some relevant substrates. FbxwD and FbxA could be used as controls for one another in addition to another non-SCF cytoplasmic protein to control for background labeling such as actin, discoidin, and other commonly seen non-specific interactors. There is a possibility that the WD40-type FBPs may have

overlapping substrates. This technique has proven effective in identifying transient substrate candidates of many proteins including OGT (102).

In vitro Skp1-FBP swap assays

The Skp1 glycan may play a role in stabilizing the Skp1-F-box interface resulting in higher levels of certain FBPs co-precipitating with Skp1 (20,103). Stabilization of the interface would prevent or reduce the rate of spontaneous swapping of F-box proteins, a potential phenomenon that could be determined in vitro. Using glycosylated and unmodified recombinant Skp1, the Skp1 could be incubated for an amount of time in presence of a soluble recombinant FBP, guinea pig Ocp1/Fbs1 (104). After a fixed incubation period, another soluble Fbs1, Fbs1-2 with an alternative epitope tag or additional mass to differentiate it from Fbs1-1 would be added to the mix. After a set amount of time, the Skp1 would be immunoprecipitated and the co-precipitating FBPs would be blotted for to determine if Skp1 glycosylation affected the proportion of Fbs1-1 to Fbs1-2 bound to Skp1. It is very likely that glycosylated Skp1 would immunoprecipitate more total FBP based on previous work (20), but it would be the ratio of #1 to #2 that would be important. If glycosylated Skp1 had a higher ratio of Fbs1-1 : Fbs1-2, then it would mean that the glycan not only increase levels of interaction with FBPs but it also would mean that the glycan helps prevent spontaneous, unregulated swapping of FBPs.

Vwa1's biophysical properties and how that affects FbxwD

In Chapter 3, evidence was provided for an interaction between Vwa1, FbxwD and CulE. No other FBPs were present in Vwa1's interactome suggesting that its role in the cell is specifically involved with its binding to FbxwD. This binding cannot be accomplished by single domain expression. This is likely due to the fact that at least the VIT, vWFA and hybrid domain may work

in concert to modulate binding affinity (77). Is this interaction directly or indirectly due to the divalent ion coordinating MIDAS domain or through interaction with the β-sandwiches of the VIT or hybrid? The first could be investigated through in vivo or in vitro pulldowns in the presence and absence of chelators to strip any ions from the protein. Preliminary LC-MS/MS IP's of 3xFLAG-Vwa1 in present or absence of Mg^{2+} indicated that mere absence of added divalent ions in the lysis buffer was not enough to abrogate Vwa1's binding to FbxwD.

Investigating Vwa1 homodimer and potential disruption by truncated protein fragments

Crystallographic data on ITIH1, a paralogue of Vwa1, presents a homodimer of the protein that may be biologically relevant (17) (Fig.4.1). The MIDAS domains of the homodimer are positioned with 19.8 angstroms between the two Mg^{2+} ions. AUC of ITIH has shown that Mg^{2+} and the MIDAS site are necessary for homodimerization (17). A model of regulation proposed for Vwa1 is a homo-dimer model sequestering excess protein until activation by a cryptic signal. In this model, over expressed Vwa1 has no effect on the cell as itself regulates, but over-expression of domains may disrupt the self-sequestering homodimers of Vwa1 and allow it to act within the cell.

This could be solved with gel filtration assays using a column that allows for separation of Vwa1 homodimers as well as AUC. The homodimer may be disrupted or weakened by chelation of the divalent ion from is MIDAS site as was the case with ITIH. In addition to exploring the role of Mg^{2+} on Vwa1 potential dimerization, the role of individual domains on Vwa1 dimerization should be investigated. Experimental conditions would include running pure full length Vwa1 compared to full length Vwa1 incubated with individual Vwa1 domains and/or naturally truncated protein. The natural proteolysis patterns of Vwa1 may be a result of similar activation

Fig. 4.1. ITIH dimer structure

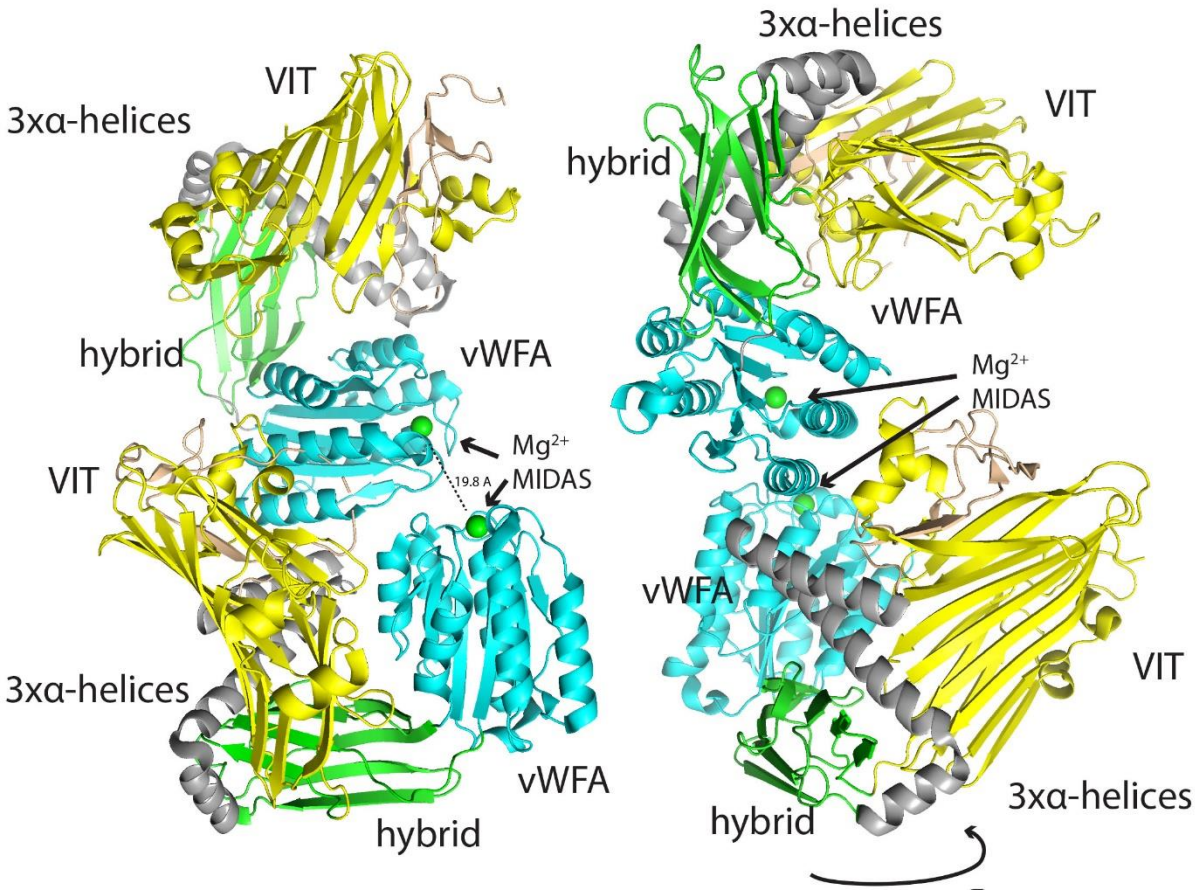

Fig. 4.1. ITIH dimer structure. Two different views of the ITIH crystallographic dimer (17) with domains color coded and labeled in colors corresponding to the model in Fig 3.9 Crystalized protein was the proteolytically truncated and mature form of ITIH (105). Distance between Mg^{2+} ions is noted as 19.8 angstroms.

patterns seen in ITIH. ITIH must have its C-terminus cleaved to become covalently bound to the extracellular matrix (105) and its VIT domain has been shown to be active despite lacking the ability to ancho to the ECM (106). Elimination of the Vwa1 dimer peak upon incubation with excess truncated domains and/or chelators would support the hypothesis that Vwa1 self regulates through dimerization in an ion dependent manner.

Investigating Vwa1's interactome using orthogonal methods

The observed interactome of Vwa1 was very small compared to say, Skp1. It only included FbxwD and CulE. If other interactions exist, they may be transient. As mentioned earlier, BioID is a powerful tool for investigating weaker interactions than traditional co-immunoprecipitations. This would necessitate the construction of additional strains. An alternative method would involve a gentle in vivo crosslinking with glutaraldehyde on ice (107). A mild crosslink would hypothetically enhance the number of in vivo interactors without destroying the lysine rich 3xFLAG epitope and over crosslinking the lysate and overly complicating the mass spectrometric analysis. With some intact epitope as in in the pilot experiment (Fig.4.2), successful immunoprecipitations could be performed on the Vwa1 bait protein as intact 3xFLAG epitope remains while maintaining the possibility that transient interactor were crosslinked to a pool of protein that are below the detection threshold of Western blot due to the heterogeneity of crosslinked Vwa1.

Vwa1 subcellular localization and its role on FbxwD

Vwa1's role in complex with FbxwD may be to target FbxwD to its location of action. Immuno-fluorescence (IMF) microscopy could be sued to determine if there are changes in subcellular localization of FbxwD with and without and intact Vwa1 gene. Any proteins that are

Fig. 4.2. Glutaraldehyde crosslinking of FLAG-Vwa1-OE cl14H.

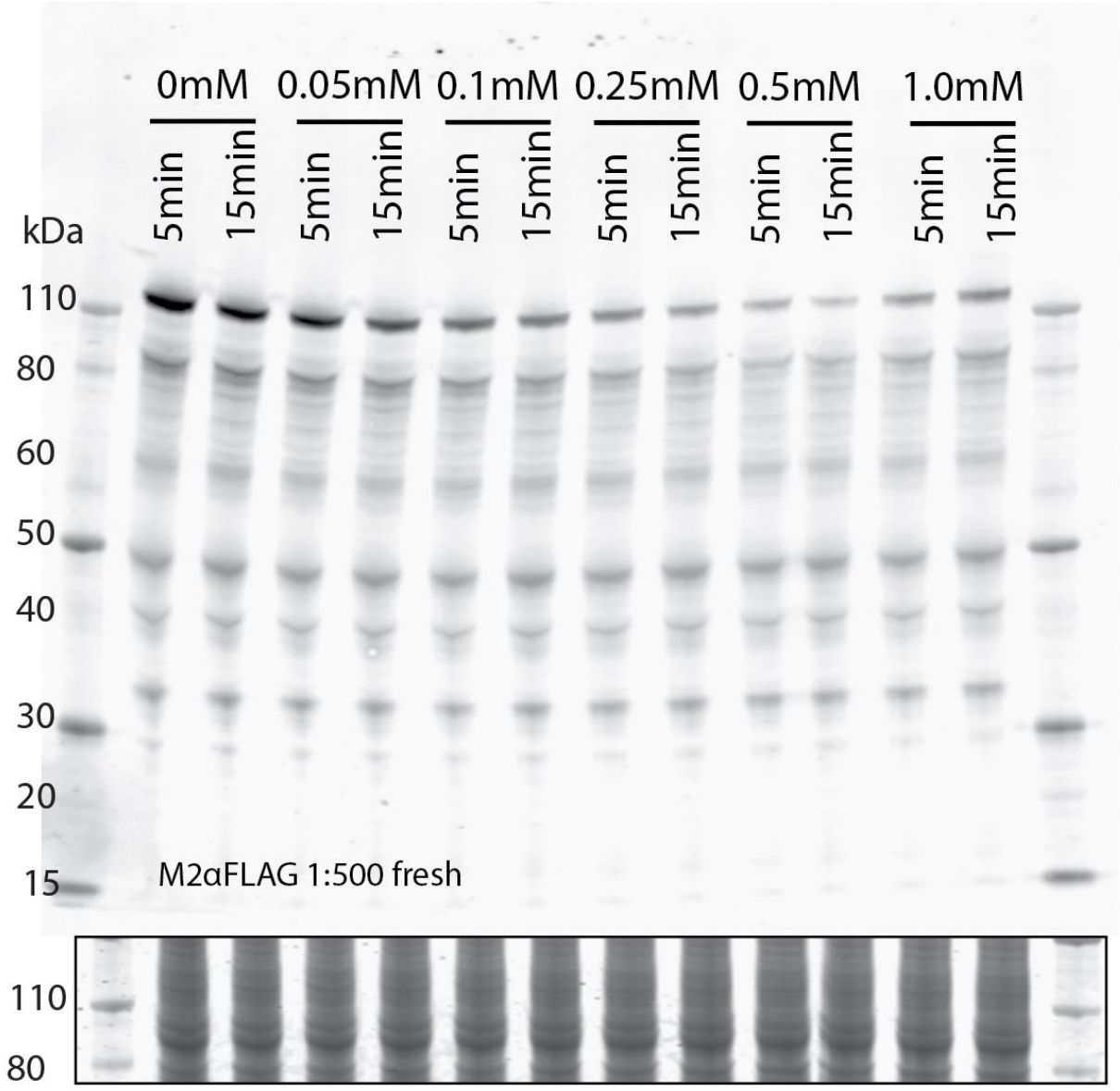

Fig. 4.2. Glutaraldehyde crosslinking of FLAG-Vwa1-OE cl14H. A pilot gentle crosslinking experiment on vegetative cells expressing FLAG-Vwa1 under the constitutive discoidin promotor at a high-level resuspended in buffer and glutaraldehyde to test different glutaraldehyde concentrations and different lengths of crosslinking incubations on ice. Destruction of the lysine rich FLAG epitope for full length Vwa1 >110 kDa was used as a metric for crosslinking efficacy.

to be visualized by IFA may need to be performed on over expressed as the basal levels of endogenously tagged Vwa1 and FbxwD are near the threshold for detection via Western blot. Additionally, fully length Vwa1 alone should investigated via IFA to determine if it is cytoplasmic or nuclear. The latter is the predicted location of the homolog VWA5A/BCSC-1 (108). Co-localization of Vwa1 and FbxwD would give strong indication of cooperative action but lack of evidence of colocalization may be due to the proteins predominantly being sequestered apart from each other until they form active complexes.

Mutagenesis and additional truncation constructs of Vwa1

It would be worthwhile investigating if Vwa1's VIT+vWFA+hybrid domain is capable of interacting with FbwxD and if it is infact the active form of Vwa1. The construct should be informed by AphaFold's structural prediction (109,110) and homology to the known ITIH1 structure. In addition, Vwa1 constructs with the MIDAS' DxSxS (amino acids 305-309) disrupted should be investigated for changes in interacting partners. In ITIH1, mutation of the aspartic acid (D) to an alanine (A) abolished binding to Mg^{2+} ion (17), but the protein was able to still bind to its ligands. If as the literature suggests, helix α-1 and α-6 may engage in conformational changes upon binding to Vwa1's MIDAS domain to a ligand such as FbxwD (77). Mutagenesis to add rigidity to these helices may result in a loss of function. What specific mutations that would be useful will need to be investigated. Previous studies on integrins utilized artificial disulfide bonds within the hybrid domain to lock the protein in open or closed orientations. This method would not be useful for a cytoplasmic protein.

CHAPTER 5

CONCLUSIONS

Expansion of the Skp1 interactome and comparison of vegetative vs. slug Skp1 interactomes

The *Dictyostelium discoideum* Skp1 interactome in developing slug cells had been previously reported with 15 interactors using polyclonal anti-Skp1 co-immunoprecipitation (20). When compared to other organisms, this was less than the 16 predicted substrate-receptor type F-box proteins predicted in the yeast *Saccharomyces cerevisiae* (111,112) and a fraction of what has been predicted in an extreme example, *Arabidopsis thaliana,* which is predicted to contain over 500 F-box proteins (65). The BLASTp search reported in Chapter 2 even predicted 54 F-box proteins in *Dictyostelium's* genome. To get a more comprehensive picture or Skp1's interactome, an orthogonal immunoprecipitation strategy using anti-myc beads against Skp1-myc expressed at approximately the same level as endogenous Skp1 was employed during vegetative growth and at the slug stage of development. Additionally, endogenous Skp1 was immunoprecipitated from vegetative cells using the polyclonal anti-Skp1 as in ref. 20. This search for Skp1 interactors in vegetative cells and slug cells expanded the pool of observed Skp1 interactors from 15 to 92 (Fig.2.7). As predicted, the vastly different proteomic requirements of free-living vegetative cells and developing slug cells were reflected in differences in the Skp1 interactome. Only 23 proteins were shared between life stages. While differences in transcript and protein levels between the two stages may have some impact on this, as a whole there is little correlation between transcript

levels and identification in the Skp1 interactome (Fig.2.4). This suggests that there is specificity to the mechanism of interacting partner selection between vegetative and slug life stages.

***Dictyostelium* F-box proteins**

The BLASTp search found 54 proteins with F-box like sequences, one of which was JcdI. These appear to each be conserved in a comparison of the genomes of 5 different cellular slime molds. A manual alignment search of the 92 Skp1 interaction candidates using a training set of 17 predicted SR-type F-box domains, revealed 28 novel F-box-like sequences. Between the BLASTp search, targeted alignment, and 5 previously annotated FBPs, the total number of putative *Dictyostelium* F-box domain containing proteins currently stands at 88. Of these 88, 38 were observed interacting with Skp1 thus strengthening their identification as putative FBPs (Table 2.1).

Role of the Skp1 glycosylation in F-box protein binding

The Skp1 glycan through modeling (54) has been proposed to increase the amount of time Skp1 remains in an open conformation and thus available to bind F-box domains. Consistent with the model of increased Skp1 availability to F-box domains, the Skp1 glycan enhanced interaction with predominantly F-box protein-like interactors (Fig.2.7D,G). Many factors may have influenced these enhanced interactions such as transcriptional changes, changes in Skp1+FBP interface stability or changes in FBP stability in the presence of glycosylated Skp1. Reciprocal pulldowns of two representative FBP's, FbxwD and JcdI, confirm that glycosylation increases the amount of Skp1 observed binding to the FBPs (Fig.2.8, 2.9), supporting the hypothesis the increased Skp1+FBP interaction is a result of glycosylated Skp1's receptive conformation (54). It remains unclear whether or not these FBPs are interacting with other proteins to a greater extent

when Skp1 is unmodified. The possibility remains that FBPs interact with Skp1 to the same extent when it is modified or unmodified, but the interaction may be more fragile without the glycan, thus less likely to survive the harsh conditions of an immunoprecipitation. Regardless of whether the Skp1 glycan causes high levels of interaction or higher stability of the interface, Skp1 glycosylation results in result in lower JcdI levels during development potentially due to increased turnover via the SCF (Fig.2.9G).

JcdI as an oxygen-sensing non-heme dioxygenase containing F-box protein

In Chapter 2, JcdI has been shown to be an oxygen-sensing JmjC containing F-box protein. Homologues in different subclades of JcdI have been identified in protists including *Toxoplasma gondii*, plants, and some fungi (Fig.2.11). It was subsequently validated as a true F-box protein via mutagenesis of conserved residues abolishing Skp1 binding (Fig.2.9C). JcdI's enzymatic activity as a non-heme dioxygenase has been validated by succinate glow assays. With a K_M of 22±5% atmospheric O_2 (Fig.2.10), JcdI functions optimally when *Dictyostelium* are above ground and most likely engaging in sporulation as opposed to the lower oxygen percentages experienced within their soil habitat. This suggests it is likely a mechanism for sensing higher oxygen levels within the cells.

JcdI/JcdH knockout had no evident impact on *Dictyostelium* under conditions tested, but over expression of the full-length protein modestly reduced the oxygen percentage needed for successful fruiting and sporulation from 15% down to 10% O_2. Abundance of protein could have helped amplify the oxygen signal within the cell to thresholds that permitted fruiting. Although JcdI is an F-box protein, its mechanism of action is likely outside of the context of the SCF and the F-box may act to control degradation and regulate protein abundance (93). As JcdI binds at a

higher level to Skp1 in cells capable of sensing oxygen through PhyA, JcdI levels may be regulated during development through the SCF and PhyA dependent oxygen sensing. This was concluded as the reduced fruiting threshold was observed even when the over-expressed mutant protein lacked the ability to bind Skp1. The other uncharacterized domains appear to be necessary for JcdI's role in oxygen sensing but not its ability to transfer an O-atom to α-ketoglutarate.

FbxwD's domains are required for full functionality

FbxwD has been shown to dramatically inhibit development and sporulation when overexpressed under the direction of pre-stalk or pre-spore promotors. Using this inhibition as a metric for observing FbxwD functionality, it was shown that an intact F-box domain that can reliably interact with Skp1 is necessary for full functionality, unlike JcdI. FbxwD is a canonical substrate receptor type WD40 repeat containing protein except for its N-terminal RING domain. The function of this RING domain remains cryptic, but it does appear to be necessary for its suppressing role when overexpressed. Over-expression constructs with conserved residues mutated in the RING domain fail to inhibit development and sporulation despite elevated levels of over-expression relative to wild-type FbxwD. The RING domain may serve a role in ubiquitination outside of the scope of the traditional SCF ubiquitination (113-115). Mono-ubiquitination by FbxwD may prime substrates for polyubiquitination or allow FbxwD to serve as a non-SCF E3 ligase. Along these lines the uncharacterized protein, DDB_G0279003, found in the endogenous vegetative IP's has predicted homology to the known E3 ligase, Retinoblastoma-binding protein 6 (116). Preliminary evidence is not clear as to whether an observable difference in the interactome is seem without an intact RING domain.

Vwa1 multi domain FbxwD cofactor

Vwa1 was found in pilot immunoprecipitations of FbxwD. It is one of six VIT-vWFA-hybrid domain containing proteins found in *Dictyostelium's* genome. Two others, Vwa2 and Vwa3, were found in FbxwD co-immunoprecipitations but at lower levels and inconsistently across development. Vwa1 follows a similar transcriptional trend across development as FbxwD with a marked decrease in RPKM (23,57,58) and protein levels upon initiation of development (Fig.3.2). Vwa1 truncation was likely a full knockout of the protein as the in frame 3xFLAG included in the antibiotic resistance marker was undetectable by Western blotting. Over-expression of Vwa1 and the truncation of the endogenous locus don't have any noticeable effect on *Dictyostelium* proliferation or development. In contrast, constitutive expression under the discoidin promotor of the VIT, vWFA or C-terminus domains alone causes significant disruption in development and sporulation with the vWFA and C-terminus arresting development in early aggregation. This phenomenon is dependent on an intact endogenous Vwa1 locus suggesting a dominant negative interaction between the endogenous protein and truncated constructs. The mechanism of this dominant-negative effect is unknown, but it may be due to disruption of a regulatory checkpoint for the activation of full length Vwa1. Interestingly, an intact Vwa1 domain is also necessary for FbxwD over-expression to inhibit development (Fig.3.4). This suggests that FbxwD requires Vwa1 to function as an F-box protein.

Vwa1 can serve as a model for studying other VIT-vWFA-hybrid domain proteins

Phylogenetic analysis of the vWFA domain of Vwa1 confirmed that Vwa1 is part of a clade of proteins related to the human tumor suppressor VWA5A/BCSC-1. These VWA5A-like proteins are part of a super family containing the more thoroughly investigated ITIH's and PARP4/vPARPs.

Sequence homology with the crystalized ITIH suggests that Vwa1 and other VWA5A-like proteins likely have a similar structure to ITIH with the variability existing in the loosely conserved C-terminus. Reinforcing the idea that Vwa1's interaction with an E3 ubiquitin ligase can serve as a model for understanding VWA5A, interactome data shows that VWA5A also interacts with an SOCS-box type ubiquitin ligase receptor, SPRY (82,83) that acts through the Elongin B and C, Rbx2 and Cullin5 E3 ligase (117). Thus both proteins may serve an important role in targeted protein degradation through their respective E3 ligases.

Introduction, Future Directions and Conclusions references

1. Sun, Y. (2020) Introduction. *Adv Exp Med Biol* **1217**, 1-8
2. Willems, A. R., Schwab, M., and Tyers, M. (2004) A hitchhiker's guide to the cullin ubiquitin ligases: SCF and its kin. *Biochimica et Biophysica Acta (BBA) - Molecular Cell Research* **1695**, 133-170
3. Zheng, N., and Shabek, N. (2017) Ubiquitin Ligases: Structure, Function, and Regulation. *Annu Rev Biochem* **86**, 129-157
4. Rusnac, D. V., and Zheng, N. (2020) Structural Biology of CRL Ubiquitin Ligases. *Adv Exp Med Biol* **1217**, 9-31
5. Zimmerman, E. S., Schulman, B. A., and Zheng, N. (2010) Structural assembly of cullin-RING ubiquitin ligase complexes. *Current Opinion in Structural Biology* **20**, 714-721
6. Kamura, T., Koepp, D. M., Conrad, M. N., Skowyra, D., Moreland, R. J., Iliopoulos, O., Lane, W. S., Kaelin, W. G., Jr., Elledge, S. J., Conaway, R. C., Harper, J. W., and Conaway, J. W. (1999) Rbx1, a component of the VHL tumor suppressor complex and SCF ubiquitin ligase. *Science* **284**, 657-661
7. Deshaies, R. J., and Joazeiro, C. A. P. (2009) RING Domain E3 Ubiquitin Ligases. *Annual Review of Biochemistry* **78**, 399-434
8. Reitsma, J. M., Liu, X., Reichermeier, K. M., Moradian, A., Sweredoski, M. J., Hess, S., and Deshaies, R. J. (2017) Composition and Regulation of the Cellular Repertoire of SCF Ubiquitin Ligases. *Cell* **171**, 1326-1339 e1314
9. Wang, K., Deshaies, R. J., and Liu, X. (2020) Assembly and Regulation of CRL Ubiquitin Ligases. *Adv Exp Med Biol* **1217**, 33-46
10. Bohnsack, R. N., and Haas, A. L. (2003) Conservation in the mechanism of Nedd8 activation by the human AppBp1-Uba3 heterodimer. *J Biol Chem* **278**, 26823-26830
11. Hori, T., Osaka, F., Chiba, T., Miyamoto, C., Okabayashi, K., Shimbara, N., Kato, S., and Tanaka, K. (1999) Covalent modification of all members of human cullin family proteins by NEDD8. *Oncogene* **18**, 6829-6834
12. Cavadini, S., Fischer, E. S., Bunker, R. D., Potenza, A., Lingaraju, G. M., Goldie, K. N., Mohamed, W. I., Faty, M., Petzold, G., Beckwith, R. E., Tichkule, R. B., Hassiepen, U., Abdulrahman, W., Pantelic, R. S., Matsumoto, S., Sugasawa, K., Stahlberg, H., and Thomä, N. H. (2016) Cullin-RING ubiquitin E3 ligase regulation by the COP9 signalosome. *Nature* **531**, 598-603
13. Enchev, R. I., Scott, D. C., da Fonseca, P. C., Schreiber, A., Monda, J. K., Schulman, B. A., Peter, M., and Morris, E. P. (2012) Structural basis for a reciprocal regulation between SCF and CSN. *Cell Rep* **2**, 616-627
14. Skaar, J. R., Pagan, J. K., and Pagano, M. (2013) Mechanisms and function of substrate recruitment by F-box proteins. *Nature Reviews Molecular Cell Biology* **14**, 369-381
15. Liu, Y., Pan, B., Qu, W., Cao, Y., Li, J., and Zhao, H. (2021) Systematic analysis of the expression and prognosis relevance of FBXO family reveals the significance of FBXO1 in human breast cancer. *Cancer Cell International* **21**, 130
16. Bai, C., Sen, P., Hofmann, K., Ma, L., Goebl, M., Harper, J. W., and Elledge, S. J. (1996) SKP1 connects cell cycle regulators to the ubiquitin proteolysis machinery through a novel motif, the F-box. *Cell* **86**, 263-274
17. Briggs, D. C., Langford-Smith, A. W. W., Birchenough, H. L., Jowitt, T. A., Kielty, C. M., Enghild, J. J., Baldock, C., Milner, C. M., and Day, A. J. (2020) Inter-α-inhibitor heavy chain-1 has an integrin-like 3D structure mediating immune regulatory activities and matrix stabilization during ovulation. *J Biol Chem* **295**, 5278-5291
18. West, C. M., and Blader, I. J. (2015) Oxygen Sensing by Protozoans: How They Catch Their Breath. *Current opinion in microbiology* **26**, 41-47

19. Sheikh, M. O., Schafer, C. M., Powell, J. T., Rodgers, K. K., Mooers, B. H., and West, C. M. (2014) Glycosylation of Skp1 affects its conformation and promotes binding to a model f-box protein. *Biochemistry* **53**, 1657-1669
20. Sheikh, M. O., Xu, Y., van der Wel, H., Walden, P., Hartson, S. D., and West, C. M. (2015) Glycosylation of Skp1 promotes formation of Skp1-Cullin-1-F-box protein complexes in Dictyostelium. *Mol Cell Proteomics* **14**, 66-80
21. Bonner, J. T., and Lamont, D. S. (2005) Behavior of cellular slime molds in the soil. *Mycologia* **97**, 178-184
22. Xu, Y., Wang, Z. A., Green, R. S., and West, C. M. (2012) Role of the Skp1 prolyl-hydroxylation/glycosylation pathway in oxygen dependent submerged development of Dictyostelium. *BMC Developmental Biology* **12**, 31-31
23. Rosengarten, R. D., Santhanam, B., Fuller, D., Katoh-Kurasawa, M., Loomis, W. F., Zupan, B., and Shaulsky, G. (2015) Leaps and lulls in the developmental transcriptome of Dictyostelium discoideum. *BMC Genomics* **16**, 294
24. González-Velasco, Ó., De Las Rivas, J., and Lacal, J. (2019) Proteomic and Transcriptomic Profiling Identifies Early Developmentally Regulated Proteins in Dictyostelium Discoideum. *Cells* **8**
25. Annesley, S. J., and Fisher, P. R. (2009) Dictyostelium discoideum--a model for many reasons. *Mol Cell Biochem* **329**, 73-91
26. Lozanne, A. D. (1987) Chapter 27 Homologous Recombination in Dictyostelium as a Tool for the Study of Developmental Genes. in *Methods in Cell Biology* (Spudich, J. A. ed.), Academic Press. pp 489-495
27. Faix, J., Linkner, J., Nordholz, B., Platt, J. L., Liao, X. H., and Kimmel, A. R. (2013) The application of the Cre-loxP system for generating multiple knock-out and knock-in targeted loci. *Methods Mol Biol* **983**, 249-267
28. Ashworth, J. M., and Watts, D. J. (1970) Metabolism of the cellular slime mould Dictyostelium discoideum grown in axenic culture. *Biochem J* **119**, 175-182
29. Ennis, H. L., Dao, D. N., Pukatzki, S. U., and Kessin, R. H. (2000) Dictyostelium amoebae lacking an F-box protein form spores rather than stalk in chimeras with wild type. *Proc Natl Acad Sci U S A* **97**, 3292-3297
30. Newell, P. C., and Ross, F. M. (1982) Genetic Analysis of the Slug Stage of Dictyostelium discoideum. *Microbiology* **128**, 1639-1652
31. Mohanty, S., Lee, S., Yadava, N., Dealy, M. J., Johnson, R. S., and Firtel, R. A. (2001) Regulated protein degradation controls PKA function and cell-type differentiation in Dictyostelium. *Genes Dev* **15**, 1435-1448
32. Reymond, C. D., Schaap, P., Véron, M., and Williams, J. G. (1995) Dual role of cAMP during Dictyostelium development. *Experientia* **51**, 1166-1174
33. Sassi, S., Sweetinburgh, M., Erogul, J., Zhang, P., Teng-Umnuay, P., and West, C. M. (2001) Analysis of Skp1 glycosylation and nuclear enrichment in Dictyostelium. *Glycobiology* **11**, 283-295
34. van der Wel, H., Ercan, A., and West, C. M. (2005) The Skp1 prolyl hydroxylase from Dictyostelium is related to the hypoxia-inducible factor-alpha class of animal prolyl 4-hydroxylases. *J Biol Chem* **280**, 14645-14655
35. West, C. M., Wang, Z. A., and van der Wel, H. (2010) A cytoplasmic prolyl hydroxylation and glycosylation pathway modifies Skp1 and regulates O2-dependent development in Dictyostelium. *Biochim Biophys Acta* **1800**, 160-171
36. Wang, Z. A., Singh, D., van der Wel, H., and West, C. M. (2011) Prolyl hydroxylation- and glycosylation-dependent functions of Skp1 in O2-regulated development of Dictyostelium. *Dev Biol* **349**, 283-295

37. Sternfeld, J., and David, C. N. (1981) Oxygen gradients cause pattern orientation in Dictyostelium cell clumps. *J Cell Sci* **50**, 9-17
38. Xu, Y., Brown, K. M., Wang, Z. A., van der Wel, H., Teygong, C., Zhang, D., Blader, I. J., and West, C. M. (2012) The Skp1 protein from Toxoplasma is modified by a cytoplasmic prolyl 4-hydroxylase associated with oxygen sensing in the social amoeba Dictyostelium. *J Biol Chem* **287**, 25098-25110
39. Rahman, K., Zhao, P., Mandalasi, M., van der Wel, H., Wells, L., Blader, I. J., and West, C. M. (2016) The E3 Ubiquitin Ligase Adaptor Protein Skp1 Is Glycosylated by an Evolutionarily Conserved Pathway That Regulates Protist Growth and Development. *J Biol Chem* **291**, 4268-4280
40. Stanley, P. (2011) Golgi glycosylation. *Cold Spring Harb Perspect Biol* **3**, a005199
41. Schoberer, J., Shin, Y. J., Vavra, U., Veit, C., and Strasser, R. (2018) Analysis of Protein Glycosylation in the ER. *Methods Mol Biol* **1691**, 205-222
42. West, C. M., and Kim, H. W. (2019) Nucleocytoplasmic O-glycosylation in protists. *Current Opinion in Structural Biology* **56**, 204-212
43. Mannino, M. P., and Hart, G. W. (2022) The Beginner's Guide to O-GlcNAc: From Nutrient Sensitive Pathway Regulation to Its Impact on the Immune System. *Front Immunol* **13**, 828648
44. Torres, C. R., and Hart, G. W. (1984) Topography and polypeptide distribution of terminal N-acetylglucosamine residues on the surfaces of intact lymphocytes. Evidence for O-linked GlcNAc. *J Biol Chem* **259**, 3308-3317
45. Zentella, R., Sui, N., Barnhill, B., Hsieh, W.-P., Hu, J., Shabanowitz, J., Boyce, M., Olszewski, N. E., Zhou, P., Hunt, D. F., and Sun, T.-P. (2017) The Arabidopsis O-fucosyltransferase SPINDLY activates nuclear growth repressor DELLA. *Nat Chem Biol* **13**, 479-485
46. Bandini, G., Agop-Nersesian, C., van der Wel, H., Mandalasi, M., Kim, H. W., West, C. M., and Samuelson, J. (2021) The nucleocytosolic O-fucosyltransferase SPINDLY affects protein expression and virulence in Toxoplasma gondii. *J Biol Chem* **296**, 100039
47. Lassak, J., Keilhauer, E. C., Fürst, M., Wuichet, K., Gödeke, J., Starosta, A. L., Chen, J.-M., Søgaard-Andersen, L., Rohr, J., Wilson, D. N., Häussler, S., Mann, M., and Jung, K. (2015) Arginine-rhamnosylation as new strategy to activate translation elongation factor P. *Nat Chem Biol* **11**, 266-270
48. Fredriksen, L., Moen, A., Adzhubei, A. A., Mathiesen, G., Eijsink, V. G., and Egge-Jacobsen, W. (2013) Lactobacillus plantarum WCFS1 O-linked protein glycosylation: An extended spectrum of target proteins and modification sites detected by mass spectrometry. *Glycobiology* **23**, 1439-1451
49. van der Wel, H., Johnson, J. M., Xu, Y., Karunaratne, C. V., Wilson, K. D., Vohra, Y., Boons, G. J., Taylor, C. M., Bendiak, B., and West, C. M. (2011) Requirements for Skp1 processing by cytosolic prolyl 4(trans)-hydroxylase and α-N-acetylglucosaminyltransferase enzymes involved in O_2 signaling in dictyostelium. *Biochemistry* **50**, 1700-1713
50. Wang, Z. A., van der Wel, H., Vohra, Y., Buskas, T., Boons, G. J., and West, C. M. (2009) Role of a cytoplasmic dual-function glycosyltransferase in O2 regulation of development in Dictyostelium. *J Biol Chem* **284**, 28896-28904
51. Schafer, C. M., Sheikh, M. O., Zhang, D., and West, C. M. (2014) Novel Regulation of Skp1 by the Dictyostelium AgtA α-Galactosyltransferase Involves the Skp1-binding Activity of Its WD40 Repeat Domain*. *Journal of Biological Chemistry* **289**, 9076-9088
52. Rahman, K., Mandalasi, M., Zhao, P., Sheikh, M. O., Taujale, R., Kim, H. W., van der Wel, H., Matta, K., Kannan, N., Glushka, J. N., Wells, L., and West, C. M. (2017) Characterization of a cytoplasmic glucosyltransferase that extends the core trisaccharide of the Toxoplasma Skp1 E3 ubiquitin ligase subunit. *J Biol Chem* **292**, 18644-18659

53. Mandalasi, M., Kim, H. W., Thieker, D., Sheikh, M. O., Gas-Pascual, E., Rahman, K., Zhao, P., Daniel, N. G., van der Wel, H., Ichikawa, H. T., Glushka, J. N., Wells, L., Woods, R. J., Wood, Z. A., and West, C. M. (2020) A terminal α3-galactose modification regulates an E3 ubiquitin ligase subunit in Toxoplasma gondii. *J Biol Chem* **295**, 9223-9243
54. Sheikh, M. O., Thieker, D., Chalmers, G., Schafer, C. M., Ishihara, M., Azadi, P., Woods, R. J., Glushka, J. N., Bendiak, B., Prestegard, J. H., and West, C. M. (2017) O(2) sensing-associated glycosylation exposes the F-box-combining site of the Dictyostelium Skp1 subunit in E3 ubiquitin ligases. *J Biol Chem* **292**, 18897-18915
55. Henzl, M. T., Thalmann, I., and Thalmann, R. (1998) OCP2 exists as a dimer in the organ of Corti. *Hear Res* **126**, 37-46
56. Kim, H. W., Eletsky, A., Gonzalez, K. J., van der Wel, H., Strauch, E. M., Prestegard, J. H., and West, C. M. (2020) Skp1 Dimerization Conceals Its F-Box Protein Binding Site. *Biochemistry* **59**, 1527-1536
57. Parikh, A., Miranda, E. R., Katoh-Kurasawa, M., Fuller, D., Rot, G., Zagar, L., Curk, T., Sucgang, R., Chen, R., Zupan, B., Loomis, W. F., Kuspa, A., and Shaulsky, G. (2010) Conserved developmental transcriptomes in evolutionarily divergent species. *Genome Biology* **11**, R35
58. Santhanam, B., Cai, H., Devreotes, P. N., Shaulsky, G., and Katoh-Kurasawa, M. (2015) The GATA transcription factor GtaC regulates early developmental gene expression dynamics in Dictyostelium. *Nature Communications* **6**, 7551
59. Stajdohar M, J. L., Kokosar J, Blenkus D, Janez T, Kuspa A, Shaulsky G, Zupan B. (2015) dictyExpress: visual analytics of NGS gene expression in Dictyostelium.
60. Zheng, N., Schulman, B. A., Song, L., Miller, J. J., Jeffrey, P. D., Wang, P., Chu, C., Koepp, D. M., Elledge, S. J., Pagano, M., Conaway, R. C., Conaway, J. W., Harper, J. W., and Pavletich, N. P. (2002) Structure of the Cul1–Rbx1–Skp1–F boxSkp2 SCF ubiquitin ligase complex. *Nature* **416**, 703-709
61. Kondo-Okamoto, N., Ohkuni, K., Kitagawa, K., McCaffery, J. M., Shaw, J. M., and Okamoto, K. (2006) The Novel F-Box Protein Mfb1p Regulates Mitochondrial Connectivity and Exhibits Asymmetric Localization in Yeast. *Molecular Biology of the Cell* **17**, 3756-3767
62. Price, C. T., Al-Quadan, T., Santic, M., Rosenshine, I., and Abu Kwaik, Y. (2011) Host proteasomal degradation generates amino acids essential for intracellular bacterial growth. *Science* **334**, 1553-1557
63. Russell, I. D., Grancell, A. S., and Sorger, P. K. (1999) The unstable F-box protein p58-Ctf13 forms the structural core of the CBF3 kinetochore complex. *J Cell Biol* **145**, 933-950
64. Joazeiro, C. A., and Weissman, A. M. (2000) RING finger proteins: mediators of ubiquitin ligase activity. *Cell* **102**, 549-552
65. Kuroda, H., Takahashi, N., Shimada, H., Seki, M., Shinozaki, K., and Matsui, M. (2002) Classification and Expression Analysis of Arabidopsis F-Box-Containing Protein Genes. *Plant and Cell Physiology* **43**, 1073-1085
66. Zielke, N., Querings, S., Grosskortenhaus, R., Reis, T., and Sprenger, F. (2006) Molecular dissection of the APC/C inhibitor Rca1 shows a novel F-box-dependent function. *EMBO Rep* **7**, 1266-1272
67. Cenciarelli, C., Chiaur, D. S., Guardavaccaro, D., Parks, W., Vidal, M., and Pagano, M. (1999) Identification of a family of human F-box proteins. *Curr Biol* **9**, 1177-1179
68. Stajdohar M, J. L., Kokosar J, Blenkus D, Janez T, Kuspa A, Shaulsky G, Zupan B. (2015) dictyExpress: visual analytics of NGS gene expression in Dictyostelium.
69. Pang, K. M., Lynes, M. A., and Knecht, D. A. (1999) Variables controlling the expression level of exogenous genes in Dictyostelium. *Plasmid* **41**, 187-197

70. Himmelfarb, M., Klopocki, E., Grube, S., Staub, E., Klaman, I., Hinzmann, B., Kristiansen, G., Rosenthal, A., Durst, M., and Dahl, E. (2004) ITIH5, a novel member of the inter-alpha-trypsin inhibitor heavy chain family is downregulated in breast cancer. *Cancer Lett* **204**, 69-77
71. Voorberg, J., Fontijn, R., van Mourik, J. A., and Pannekoek, H. (1990) Domains involved in multimer assembly of von willebrand factor (vWF): multimerization is independent of dimerization. *The EMBO journal* **9**, 797-803
72. Perkins, S. J., Smith, K. F., Williams, S. C., Haris, P. I., Chapman, D., and Sim, R. B. (1994) The secondary structure of the von Willebrand factor type A domain in factor B of human complement by Fourier transform infrared spectroscopy. Its occurrence in collagen types VI, VII, XII and XIV, the integrins and other proteins by averaged structure predictions. *J Mol Biol* **238**, 104-119
73. Lee, J. O., Rieu, P., Arnaout, M. A., and Liddington, R. (1995) Crystal structure of the A domain from the alpha subunit of integrin CR3 (CD11b/CD18). *Cell* **80**, 631-638
74. Whittaker, C. A., and Hynes, R. O. (2002) Distribution and Evolution of von Willebrand/Integrin A Domains: Widely Dispersed Domains with Roles in Cell Adhesion and Elsewhere. *Molecular Biology of the Cell* **13**, 3369-3387
75. Springer, T. A. (2006) Complement and the Multifaceted Functions of VWA and Integrin I Domains. *Structure* **14**, 1611-1616
76. Xiao, T., Takagi, J., Coller, B. S., Wang, J. H., and Springer, T. A. (2004) Structural basis for allostery in integrins and binding to fibrinogen-mimetic therapeutics. *Nature* **432**, 59-67
77. Luo, B.-H., Carman, C. V., and Springer, T. A. (2007) Structural Basis of Integrin Regulation and Signaling. *Annual Review of Immunology* **25**, 619-647
78. Monaco, C., Negrini, M., Sozzi, G., Veronese, M. L., Vorechovsky, I., Godwin, A. K., and Croce, C. M. (1997) Molecular cloning and characterization of LOH11CR2A, a new gene within a refined minimal region of LOH at 11q23. *Genomics* **46**, 217-222
79. Hamm, A., Veeck, J., Bektas, N., Wild, P. J., Hartmann, A., Heindrichs, U., Kristiansen, G., Werbowetski-Ogilvie, T., Del Maestro, R., Knuechel, R., and Dahl, E. (2008) Frequent expression loss of Inter-alpha-trypsin inhibitor heavy chain (ITIH) genes in multiple human solid tumors: a systematic expression analysis. *BMC Cancer* **8**, 25
80. Di, D., Chen, L., Guo, Y., Wang, L., Zhao, C., and Ju, J. (2018) BCSC-1 suppresses human breast cancer metastasis by inhibiting NF-κB signaling. *Int J Oncol* **52**, 1674-1684
81. Szabo, A., Akkouh, I. A., Vandenberghe, M., Osete, J. R., Hughes, T., Heine, V., Smeland, O. B., Glover, J. C., Andreassen, O. A., and Djurovic, S. (2021) A human iPSC-astroglia neurodevelopmental model reveals divergent transcriptomic patterns in schizophrenia. *Translational Psychiatry* **11**, 554
82. Kamura, T., Maenaka, K., Kotoshiba, S., Matsumoto, M., Kohda, D., Conaway, R. C., Conaway, J. W., and Nakayama, K. I. (2004) VHL-box and SOCS-box domains determine binding specificity for Cul2-Rbx1 and Cul5-Rbx2 modules of ubiquitin ligases. *Genes Dev* **18**, 3055-3065
83. Nishiya, T., Matsumoto, K., Maekawa, S., Kajita, E., Horinouchi, T., Fujimuro, M., Ogasawara, K., Uehara, T., and Miwa, S. (2011) Regulation of inducible nitric-oxide synthase by the SPRY domain- and SOCS box-containing proteins. *J Biol Chem* **286**, 9009-9019
84. Hao, B., Zheng, N., Schulman, B. A., Wu, G., Miller, J. J., Pagano, M., and Pavletich, N. P. (2005) Structural basis of the Cks1-dependent recognition of p27(Kip1) by the SCF(Skp2) ubiquitin ligase. *Mol Cell* **20**, 9-19
85. Correia, S. P., Chan, A. B., Vaughan, M., Zolboot, N., Perea, V., Huber, A.-L., Kriebs, A., Moresco, J. J., Yates, J. R., and Lamia, K. A. (2019) The circadian E3 ligase complex SCFFBXL3+CRY targets TLK2. *Scientific Reports* **9**, 198

86. Rieu, P., Turchi, L., Thévenon, E., Zarkadas, E., Nanao, M., Chahtane, H., Tichtinsky, G., Lucas, J., Blanc-Mathieu, R., Zubieta, C., Schoehn, G., and Parcy, F. (2022) The F-box cofactor UFO redirects the LEAFY floral regulator to novel cis-elements. *bioRxiv*, 2022.2006.2014.495942
87. Hausinger, R. P. (2004) FeII/alpha-ketoglutarate-dependent hydroxylases and related enzymes. *Crit Rev Biochem Mol Biol* **39**, 21-68
88. Teixeira, C. S. S., and Sousa, S. F. (2021) Current Status of the Use of Multifunctional Enzymes as Anti-Cancer Drug Targets. *Pharmaceutics* **14**
89. Yi, J., Shen, H. F., Qiu, J. S., Huang, M. F., Zhang, W. J., Ding, J. C., Zhu, X. Y., Zhou, Y., Fu, X. D., and Liu, W. (2017) JMJD6 and U2AF65 co-regulate alternative splicing in both JMJD6 enzymatic activity dependent and independent manner. *Nucleic Acids Res* **45**, 3503-3518
90. Yang, J., Chen, S., Yang, Y., Ma, X., Shao, B., Yang, S., Wei, Y., and Wei, X. (2020) Jumonji domain-containing protein 6 protein and its role in cancer. *Cell Prolif* **53**, e12747
91. Tikhanovich, I., Kuravi, S., Artigues, A., Villar, M. T., Dorko, K., Nawabi, A., Roberts, B., and Weinman, S. A. (2015) Dynamic Arginine Methylation of Tumor Necrosis Factor (TNF) Receptor-associated Factor 6 Regulates Toll-like Receptor Signaling. *J Biol Chem* **290**, 22236-22249
92. Lamadema, N., Burr, S., and Brewer, A. C. (2019) Dynamic regulation of epigenetic demethylation by oxygen availability and cellular redox. *Free Radical Biology and Medicine* **131**, 282-298
93. Galan, J. M., and Peter, M. (1999) Ubiquitin-dependent degradation of multiple F-box proteins by an autocatalytic mechanism. *Proceedings of the National Academy of Sciences of the United States of America* **96**, 9124-9129
94. West, C. M., van der Wel, H., and Wang, Z. A. (2007) Prolyl 4-hydroxylase-1 mediates O2 signaling during development of Dictyostelium. *Development* **134**, 3349-3358
95. de Bie, P., and Ciechanover, A. (2011) Ubiquitination of E3 ligases: self-regulation of the ubiquitin system via proteolytic and non-proteolytic mechanisms. *Cell Death & Differentiation* **18**, 1393-1402
96. Kim, W. D., Mathavarajah, S., and Huber, R. J. (2022) The Cellular and Developmental Roles of Cullins, Neddylation, and the COP9 Signalosome in Dictyostelium discoideum. *Front Physiol* **13**, 827435
97. Abreha, M. H., Dammer, E. B., Ping, L., Zhang, T., Duong, D. M., Gearing, M., Lah, J. J., Levey, A. I., and Seyfried, N. T. (2018) Quantitative Analysis of the Brain Ubiquitylome in Alzheimer's Disease. *Proteomics* **18**, e1800108
98. Tekinay, T., Ennis, H. L., Wu, M. Y., Nelson, M., Kessin, R. H., and Ratner, D. I. (2003) Genetic interactions of the E3 ubiquitin ligase component FbxA with cyclic AMP metabolism and a histidine kinase signaling pathway during Dictyostelium discoideum development. *Eukaryot Cell* **2**, 618-626
99. Mark, K. G., Loveless, T. B., and Toczyski, D. P. (2016) Isolation of ubiquitinated substrates by tandem affinity purification of E3 ligase-polyubiquitin-binding domain fusions (ligase traps). *Nat. Protocols* **11**, 291-301
100. Roux, K. J., Kim, D. I., Burke, B., and May, D. G. (2018) BioID: A Screen for Protein-Protein Interactions. *Curr Protoc Protein Sci* **91**, 19.23.11-19.23.15
101. Sears, R. M., May, D. G., and Roux, K. J. (2019) BioID as a Tool for Protein-Proximity Labeling in Living Cells. *Methods Mol Biol* **2012**, 299-313
102. Stephen, H. M., Praissman, J. L., and Wells, L. (2021) Generation of an Interactome for the Tetratricopeptide Repeat Domain of O-GlcNAc Transferase Indicates a Role for the Enzyme in Intellectual Disability. *Journal of Proteome Research* **20**, 1229-1242

103. Boland, A., Gas-Pascual, E., Nottingham, B., van der Wel, H., Sheikh, M. O., Schafer, C. M., and West, C. M. (2022) Oxygen-dependent regulation of E3(SCF)ubiquitin ligases and a Skp1-associated JmjD6 homolog in Dictyostelium development. *Journal of Biological Chemistry*
104. Tan, A., and Henzl, M. T. (2009) Conformational stabilities of guinea pig OCP1 and OCP2. *Biophys Chem* **144**, 108-118
105. Salier, J. P., Rouet, P., Raguenez, G., and Daveau, M. (1996) The inter-alpha-inhibitor family: from structure to regulation. *Biochem J* **315 (Pt 1)**, 1-9
106. Rose, M., Huth, S., Wiesehöfer, M., Ehling, J., Henkel, C., Steitz, J., Lammers, T., Kistermann, J., Klaas, O., Koch, M., Rushrush, S., Knüchel, R., and Dahl, E. (2022) ITIH5-Derived Polypeptides Covering the VIT Domain Suppress the Growth of Human Cancer Cells In Vitro. *Cancers (Basel)* **14**
107. Guerrero, C., Tagwerker, C., Kaiser, P., and Huang, L. (2006) An integrated mass spectrometry-based proteomic approach: quantitative analysis of tandem affinity-purified in vivo cross-linked protein complexes (QTAX) to decipher the 26 S proteasome-interacting network. *Mol Cell Proteomics* **5**, 366-378
108. Di, D., Chen, L., Guo, Y., Wang, L., Wang, H., and Ju, J. (2018) Association of BCSC-1 and MMP-14 with human breast cancer. *Oncol Lett* **15**, 5020-5026
109. Jumper, J., Evans, R., Pritzel, A., Green, T., Figurnov, M., Ronneberger, O., Tunyasuvunakool, K., Bates, R., Žídek, A., Potapenko, A., Bridgland, A., Meyer, C., Kohl, S. A. A., Ballard, A. J., Cowie, A., Romera-Paredes, B., Nikolov, S., Jain, R., Adler, J., Back, T., Petersen, S., Reiman, D., Clancy, E., Zielinski, M., Steinegger, M., Pacholska, M., Berghammer, T., Bodenstein, S., Silver, D., Vinyals, O., Senior, A. W., Kavukcuoglu, K., Kohli, P., and Hassabis, D. (2021) Highly accurate protein structure prediction with AlphaFold. *Nature* **596**, 583-589
110. Varadi, M., Anyango, S., Deshpande, M., Nair, S., Natassia, C., Yordanova, G., Yuan, D., Stroe, O., Wood, G., Laydon, A., Žídek, A., Green, T., Tunyasuvunakool, K., Petersen, S., Jumper, J., Clancy, E., Green, R., Vora, A., Lutfi, M., Figurnov, M., Cowie, A., Hobbs, N., Kohli, P., Kleywegt, G., Birney, E., Hassabis, D., and Velankar, S. (2021) AlphaFold Protein Structure Database: massively expanding the structural coverage of protein-sequence space with high-accuracy models. *Nucleic Acids Research* **50**, D439-D444
111. Kus, B. M., Caldon, C. E., Andorn-Broza, R., and Edwards, A. M. (2004) Functional interaction of 13 yeast SCF complexes with a set of yeast E2 enzymes in vitro. *Proteins* **54**, 455-467
112. Palecek, S. P., Parikh, A. S., and Kron, S. J. (2000) Genetic analysis reveals that FLO11 upregulation and cell polarization independently regulate invasive growth in Saccharomyces cerevisiae. *Genetics* **156**, 1005-1023
113. Park, Y. C., Lim, S. D., Moon, J. C., and Jang, C. S. (2019) A rice really interesting new gene H2-type E3 ligase, OsSIRH2-14, enhances salinity tolerance via ubiquitin/26S proteasome-mediated degradation of salt-related proteins. *Plant Cell Environ* **42**, 3061-3076
114. Kiss, L., Clift, D., Renner, N., Neuhaus, D., and James, L. C. (2021) RING domains act as both substrate and enzyme in a catalytic arrangement to drive self-anchored ubiquitination. *Nature Communications* **12**, 1220
115. Han, G., Qiao, Z., Li, Y., Yang, Z., Wang, C., Zhang, Y., Liu, L., and Wang, B. (2022) RING Zinc Finger Proteins in Plant Abiotic Stress Tolerance. *Front Plant Sci* **13**, 877011
116. Xiao, C., Wu, G., Zhou, Z., Zhang, X., Wang, Y., Song, G., Ding, E., Sun, X., Zhong, L., Li, S., Weng, J., Zhu, Z., Chen, J., and Wang, X. (2019) RBBP6, a RING finger-domain E3 ubiquitin ligase, induces epithelial–mesenchymal transition and promotes metastasis of colorectal cancer. *Cell Death & Disease* **10**, 833
117. Linossi, E. M., and Nicholson, S. E. (2012) The SOCS box-adapting proteins for ubiquitination and proteasomal degradation. *IUBMB Life* **64**, 316-323